Author:
Briggs, Sam

Title:
Bioinspired Materials and Systems towards Protocellular Communciation

Bioinspired materials and systems towards protocellular communication

By

Sam Briggs

School of Chemistry

University of Bristol

A dissertation submitted to the University of Bristol in accordance with the requirements of the degree of Doctor of Philosophy in the Faculty of Science.

March 2018

Word Count: 47000

Abstract

The work herein described aimed to create tools to investigate self-assembly of compartments and how these compartments might be used in concert to produce synergistic effects in a prebiotic setting, to further our understanding of the transition from non-living to living matter. This could be described as research into the Origins of Life, or could also be framed in understanding how building the complexity of soft matter systems and taking a population, or systems, -view can yield exciting emergent group behaviours.

The first tool in the box used to explore this topic was a novel coacervate system that comprises a polyelectrolyte and a fatty acid. The system produced fatty acid vesicles that could retain sequestered cargo molecules from the discrete coacervate phase, upon a change in pH in the continuous phase. This was investigated using slowly hydrolising acid, and the effects of varying polymer weight on this transition were investigated and characterised. At low molecular weights, high aspect ratio unilamellar vesicles were formed; at intermediate weights spherical multilamellar vesicles budded from the surface of the droplets; and at high molecular weights the system produced lamellar fatty acid shells around the entirety of the coacervate droplets. A series of cargoes were transferred from the droplets to the vesicles in the low molecular instance which would fission from the coacervate droplet and become distinct compartments. A fluorescent polymer analogue was synthesised and doped into the system and showed that the polyelectrolyte was also retained within the vesicles that grew from the coacervate droplets. Molecular dyes, carbon nanodots, oligomers, fluorescent proteins, and single stranded DNA was transferred in this manner. This system illustrated how simple stimuli, in this case pH, could transfer guest molecules from non-membrane bound to membrane bound systems, an integral step in moving from a continuous chemical world as might have been found on the early Earth to the discrete cellular world of today.

The second system was another novel coacervate system that comprises a polyelectrolyte and a nucleotide that upon exposure to an inorganic stimulus yielded microgel droplets. The presence

of silver in the continuous phase allowed for the guanosine monophosphate (GMP) in the coacervate microdroplets to form complexes, which through π-stacking, produced bundles of interconnected fibrils which trapped and sequestered water, forming hydrogels. As the GMP was localised within the coacervate droplets, the hydrogels formed were spatially confined to those regions and so the bulk properties of the suspension remained fluid but using quantitative nanomechanical atomic force microscopy, the droplets were found to possess an increased Young's modulus commensurate with the stiffness measured in the bulk hydrogel system, indicating successful localised hydrogelation. This system presented another compartment that responds to a stimulus, one that produces a localised physical rearrangement of the chemical components within itself to produce a change in the viscoelastic mechanical properties of the protocell, making them stiffer and more robust with respect to deformation and coalescence. The system could be considered in the contexts of molecular crowding, and how protocells might have produced cytoskeletons as a rudimentary defence mechanism against dissolution, or to adhere to surfaces that have chemical feedstock emanating from them, allowing for the improved harvesting of a source of fuel.

Finally, using these two tools that respond to stimuli, an investigation was undertaken to understand whether a stimulus could be produced by one of the systems to trigger a response in the other population of compartments, and thus indicate rudimentary signalling and sensing behaviour. Initially, a novel hybrid protocell was generated by combining the two systems, that preserved both sets of functionalities when exposed to stimuli; and subsequently the two original systems were kept spatially discrete, to investigate their ability to communicate. The system which responds to silver produces a drop in pH as the system liberates protons and thus triggers the evolution of vesicles from the first system that contains fatty acid. Thus, the initial signal of an inorganic stimulus triggers a cascade of responses: hydrogelation and subsequent evolution of cargo carrying vesicles. This was further facilitated by using a custom extracellular matrix analogue setup comprising a functionalised microscopy dish/agarose hydrogel bridge apparatus. The work is then concluded with an outlook as to how these materials and systems move the field

towards demonstrating protocellular communication and their applications in drug delivery and soft matter research.

Dedication and Acknowledgements

This undertaking would not have been possible without the opportunity, guidance, and inspiration given by Professor Steve Mann, my doctoral supervisor, to whom I owe a great debt and would like to thank for the time that I worked in his lab towards my doctoral thesis, his thoughts and provocative questions, and his drive towards ever more exciting avenues of research. Invaluable discussion and guidance for the direction of this work was also received from Dr Avinash Patil, Dr Mei Li, and Dr Sean Davis, to whom I thank for their patience, their mentorship, and their friendship.

My thanks also go to the many people who helped me run the experiments that I needed on the multitude of instruments that I worked with; my heartfelt thanks go to Professor Robert Richardson, Dr Robert Harniman, Dr Dominic Alibhai, Dr JC Eloi, Mr Matthew Mulvee, Mr Jonathan Furze and Ms. Maddy Nichols.

Work of this nature can only survive and persist if the human element of the worker is preserved in the face of the daily realities of research. I am forever indebted to my colleagues in the Centre for Organised Matter Chemistry for their support, discussion, and ultimately, their friendship. To those who came before: Dr Ravinash Krishna Kumar, Dr Dora Tang, Dr James Fothergill, Dr Alicja Dzieciol, Dr Khrongkhwan Akkarachaneeyakorn, and Dr Thomas Farrugia I thank you for your time and patience, your advice and your jokes; to those who were there from the beginning, Maddy Nichols, Matthew Mulvee, and Nicolette Moreau, I hope we shared the burden together, for the load certainly felt lighter to me in your company; to those who came later, Dr Nicolas Martin, Dr Pavan Bosukonda, Dr Liangfei Tian, Joanna Sparks, Noha Abu El Magd, Dr Pierangelo Gobbo, Angela Suriyakumaran, Rafael Moreno, and Mary Jenkinson-Finch, your ambition and energy helped reignite my passion and I can only hope I have been able to help you in return. Special mentions go to Alex Croot and Dr Edward Lucas, both, I feel, honorary members of the COMC, who were there with crosswords and homebrew in the case of Alex, and who was the most excellent, kind, endearing, and funny housemate that I have ever had the

pleasure of living with, in the case of Edward. And of course – chemical physics for life, or until death, whichever comes first, my undergraduate cohort remains some of the best friends I will ever have, who have also shared in this journey. And finally, to the ever present and most ineffable Jonny Furze, lab partner, course mate, colleague, housemate, travel companion, friend, through undergraduate *and* postgraduate life, to the beaches, cities and bars that await us, my thanks go tenfold. I'm sure we'll get those tax breaks soon from natural marriage laws soon - I'll send you the rebate in the post.

This work has afforded me the opportunity to travel and to find another passion in my life; not only will my love for science forever be topped off with this work, but my new-found joy in communicating this passion, through Science Outreach and Public Engagement will be the fresh lodestar for my career, for the foreseeable future. My thanks go to Dr Tim Harrison, Dr Alison Rivett, Simone Breckell, Vivienne Kuh, Ellie Cripps, and Beth Anderson, for their help, guidance, and support in the work that I undertook with them during my time at Bristol, and for encouraging me to pursue this further in the future.

Speaking of the future, the PhD certainly gave me a conversation starter (or finisher, depending on the crowd) at parties - one in Canterbury at the beginning of 2017 in particular; and I will look at the beginning of the final year of my doctoral work as the true beginning of when I started to look to the future in earnest. The final projects and chapters firmly in my sights, and that horizon beckoning, I was encouraged, uplifted, and rejuvenated throughout by Rebecca. I hope my squiggly green blobs weren't too much of a bore - let's see the world together.

All of this, of course, would not have been conceivable in the slightest, had it not been for the warm, patient, kind, unending encouragement, support and love of my family. To Jack, the brother who I will always hold dearest to my heart, thank you for your light heartedness, your joy and your jokes, your nostalgia and your hugs. To Mum and Dad – you are without a doubt, the best folks a boy could hope for; for giving me all that I am and showing me the pathways to all that is yet to be, for giving me the truest compass and the keenest keel, and strong sheets for the wind, I will forever be thanking you.

— Sam Briggs, *March 2018*

"Fairy tales are more than true: not because they tell us that dragons exist, but because they tell us that dragons can be beaten."

— Neil Gaiman, Coraline

Author's Declaration

I declare that the work in this dissertation was carried out in accordance with the requirements of the University's Regulations and Code of Practice for Research Degree Programmes and that it has not been submitted for any other academic award. Except where indicated by specific reference in the text, the work is the candidate's own work. Work done in collaboration with, or with the assistance of, others, is indicated as such. Any views expressed in the dissertation are those of the author.

SIGNED:

DATE:

Table of Contents

List of Abbreviations

AFM - atomic force microscopy

ALP - alkaline phosphotase

ATP - adeonisine triphosphate

ATPS - aqueous two pahse separation

CAC - critical aggregation concentration

CCC - critical coacervation concentration

CD - circular dichroism

CMC - critical micelle concentration

CM-dextran - carboxymethyl-dextran

CND - carbon nanodot

CVC - critical vesicle concentration

DA - decanoic acid

DAA - diallylamine

DADMAC - diallyldimethylammonium chloride

dGMP - deoxy-guanoise monophosphate

DLS - dynamic light scattering

DNA - deoxyribosenucleic acid

DSC - differential scanning calorimetry

ECM - extracellular matrix

EDX - energy dispersive x-ray spectroscopy

EM - elctromagnetic

FeM - Fe(III)-enriched montmorillonite

FITC - fluorescein isothiocyanate

FLIM - fluoresence lifetime imaging

FMOC-DAA - N-(fluorenyl-9-methoxycarbonyl)-D-alanine-D-alanine

FMOC-Tyr-P - N-fluorenylmethyloxycarbonyl tyrosine-(O)-phosphate

FOA - fluorescein o-acrylate

Ga - giga-annum

GDL - glucono-δ-lactone

GFP - green fluorescent protein

GMP - guanosine monophosphate

GOx - glucose oxidase

GUV - giant unilamellar vesicle

HDMS - hexamethyldisilizane

HOMO - highest occupied molecular orbital

HPTS - hydroxypyrenetrisulfonic acid

IC - internal conversion

ICS - intersystem crossing

LCST - lower critical solution temperature

LUMO - lowest unoccupied molecular orbital

LWMG - low-weight molceular gelators

MW - molecular weight

NMR - nucelar magentic resonance spectroscopy

PAH - poly(allylamine hydrochloride)

PDDA - poly(diallyldimethylammonium chlrodie)

PEG - poly(ethylene glycol)

PEG-DA - poly(ethylene glycol)-diacrylate

PIC - polyionic complex

PMMA - polymethylmethacrylate

PNIPAM – poly(N-isopropylacrylamide)

pNPP - 4-nitrophenyl phosphate

POM - polyoxometalate

POPC - 1-palmitoyl-2-oleyl-sn¬-glycerol-3-phosphocholine

ppm - parts per million

PYCA - 1-pyrenecarboxaldehyde

QNM-AFM - quantitative nanomechanical property mapping AFM

RITC - rhodamine isothiocyanate

RNP - ribonucleic protein

SANS - small angle neutron scattering

SAXS - small angle x-ray scattering

SSB - single strand breaks

TEM - transmission electron microscopy

TNP-ATP - 2',3'-O-(2,4,6-Trinitrophenyl)adenosine-5'-triphosphate

UV - ultra-violet

VAI - 3-oxo-N-(tetrahydro-2-oxo-3-furanyl)hexanamide

VR -vibrational relaxing

List of Figures

exothermic and so heat flow required to change the temperature of the sample uniformly with respect to the sample pan decreases. The T_c, the crystallisation phase transition, is endothermic, and thus more energy is required to uniformly change the temperature of the sample with respect to the reference. Thus, various phase transitions can easily be determined using this technique.

List of Equations

List of Tables

Chapter 1 : Introduction

1. Introduction

1.1 Thesis overview

Chapter One – Introduction

Herein, the overall motivation for the thesis is presented and the history of the field and the state of current research of the topics which this work explores is described, and the concepts required to understand the results presented in the later chapters are illustrated. These concepts include the context of the problem 'Where did life come from?' if we can create models for simple, robust, self-assembling chemical systems then could they have been a route that led to animate matter; prebiotic chemistry and the synthetic constructs it gives chemists to experiment with when trying to answer this problem; how life can be defined by the chemist and how various analogues can be drawn between modern chemical systems and plausible models for early, or proto-, life, including how discrete units of living matter, in effect the cell, could have come about, how structural complexity may have emerged within this compartments in the form of gelled networks that provide robust mechanical properties and how these systems might have begun to communicate using simple chemical signals that engender morphological responses.

Chapter Two - Materials and methods

Herein, the materials, methods, calculations etc. are described. This chapter is broken down into two gross sections, that of synthesis, and that of characterisation. Firstly, the synthesis of the molecules used to form the coacervates and polymers studied in later chapters is detailed. The synthesis of the coacervate systems that are explored in the following chapters, and of the polymer synthesised to trace its localisation within those coacervates. The characterisation section details a short overview of the techniques used and the general conditions for each experiment undertaken. Additionally materials and methods are presented at the start of each experimental chapter detailing the precise conditions for the experiments that were undertaken.

Chapter Three – Polymer mediated vesicle growth from coacervates

Herein, a novel coacervate system, comprised of a polyelectrolyte, of variable molecular weight, and a fatty acid, is synthesised and characterised. Its response to pH is carefully explored, as the system is capable of evolving membrane bound vesicles from the non-membrane bound coacervate microdroplet. An unusual morphology of vesicles was observed in low molecular weight formulations, this morphology varied with respect to polymer weight when altered between different coacervate formulations. The ability of the system to produce vesicles was further explored by the inclusion a of a variety of guest molecules into the coacervate microdroplets prior to pH adjustment and cargo transport was observed to understand if genetic information, in the form of DNA, could be transferred between the first and second-generation protocell models. This would be illustrative rudimentary replicative processes.

Chapter Four – Building complexity into coacervates *via* G-quartet self-assembly

Herein, a novel coacervate system comprising a polyelectrolyte and a nucleotide is locally restructured by the introduction of an inorganic stimulus, silver ions. The system undergoes hydrogelation via stabilisation of G-quartets of the nucleotide which undergo π-stacking to produce long entangled fibrils. These fibrils present hydrophilic moieties on their exposed edges which produce the entangle 3D self-supporting network which is resistant to flow and so the coacervate droplets have solid like rheology at low shear rates, but above a given threshold the liquid-like nature of the system becomes dominant as this fibrous network is disrupted. The system produces silver nanoparticles when exposed to UV light and the system responds to temperature by undergoing a gel-sol transition that can release the incarcerated silver NPs and any other guest molecules included in the coacervate phase prior to gelation. This system is likened to possessing characteristics akin to the cytoskeleton and control over the organisation of the chemical matter in these microcompartments is considered.

Chapter Five – Sequential stimuli: inroads to protocell communication

Herein, the process of combining the systems in chapters three and four is described, creating a hybrid system that retains the behaviour of both previous systems and a spatially localised system that exhibits a call and response like behaviour. When the hydrogelating coacervate system from chapter four undergoes gelation as the stimulus is added, the system undergoes a pH change, this pH change is communicated via a custom-made agarose hydrogel bridge to a neighbouring population of the fatty acid containing coacervate system described in chapter three. The fatty acid containing system then produces vesicles containing any payload sequestered within the coacervate phase prior to the signal transduction by the nucleotide containing coacervate system.

Chapter Six – Summary and conclusions

Herein, conclusions from the previous three experimental chapters are drawn and the future directions and applications of this work are discussed.

1.2 The origins of life

Humans have a preoccupation with narratives, and all good stories have a beginning, middle, and an end [1] [2]. Life, seen as a narrative, seems to be missing its beginning. We have extensive observations of the variety of life all around us and can see the effects of the inter-dependency of our lives on those within the biosphere and have fantastic records of life evolving through the aeons [3], the middle if you will. And we can imagine, through the inexorable march of time, one day our sun consuming the planet and destroying all forms of life, the end. However, as we trace this evolutionary tree to its root we find LUCA, the last universal common ancestor, the organism with which all life-forms on Earth share a common ancestry, and yet this does not constitute a beginning, so to speak [4]. LUCA likely comprised a genetic information system based on DNA, whose structure was maintained by enzymes, which were expressed using translation and

transcription processes, which are still seen today, using RNA, which would have been encapsulated within a lipid membrane [5]. This highly organised system is reliant on many intricate interconnecting pieces to allow for the system to exist in harmony. This complexity belies another evolutionary tree, the farthest of but one branch of which, terminates with LUCA. It seems as with all stories; an ending is just another beginning.

One possible, and persistent [6], hypothetical answer to where the complexity of LUCA could have arisen from is that of the RNA World. The original proponents of this theory were Alexander Rich and Walter Gilbert who first explored the concept, and coined the term RNA World, respectively [6] [7]. The importance of this theory was that RNA, like DNA, can be a store of genetic information, but that it also has the capacity to catalyse reactions, like enzymes, and although RNAs may be more fragile, evidence shows that ancient RNAs could methylate other RNAs to protect them, removing vulnerable reactive sites along their length [8] [9]. A series of evolutions along from this and we arrive at the ribonucleoprotein world (RNP world) which was thought capable of making longer proteins, which then paved the way for the deoxyribose nucleic acid world (DNA world) which would then lead to LUCA and Darwinian evolution after the fact [7].

However, what were the requirements for the abiogenesis, the transition from inanimate matter to living matter, the process by which the RNA world came to exist such that the RNP, could lead to DNA, to LUCA, to the domains of life, evolution and finally to the diversity we see today? Here chemical approaches step into the breach.

1.3 Prebiotic chemistry

Miller and Urey were some of the first chemists to investigate the chemistry that could have been possible on the prebiotic Earth [10]. Their assumptions hinged on key assumptions about the

environment they understood to have existed at the time and that their chemistry ought to produce the minimal building blocks for the RNA world hypothesis, amino acids. They set about producing organic compounds in a reducing atmosphere using electricity. Their discussion of the 'Primitive Atmosphere' indicates that relevant prebiotic chemistry should have initially started under reducing atmospheres which eventually became oxidising due to the loss of hydrogen over time. This atmosphere would have consisted of hydrogen, methane, nitrogen and ammonia, with small parts carbon dioxide and carbon monoxide with the possible existence of other hydrocarbons and hydrogen sulphide and phosphine present. Compounds available for synthesis, they believed, could have come from meteorites, and would have consisted of metallic iron, iron carbides (a source of carbon), phosphorous and phosphides. These compounds would not have existed in equilibrium and it is this imbalance they hypothesise would have thermodynamically driven the production of the new compounds, e.g. amino acids, that would go on to become essential to modern life. Using their reducing atmospheric-electrical discharge setup Miller and Urey managed to synthesise aldehydes, hydrogen, cyanide and ammonia, all key components in the Strecker synthesis [11], see Figure 1.1, to forming amino acids.

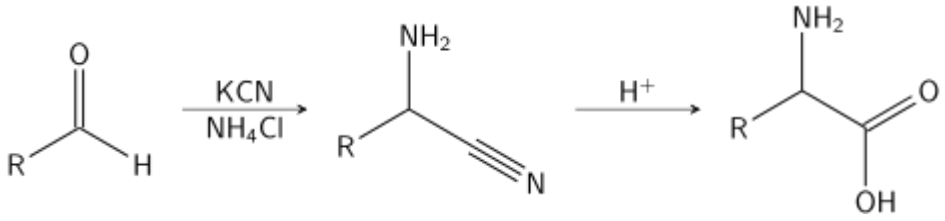

Figure 1.1: The Strecker synthesis, the aldehyde is condensed with ammonium chloride in the presence of potassium cyanide to form an α-aminonitrile which can be subsequently hydrolysed to form an amino acid.

Subsequent experiments that built upon the work of Miller and Urey produced even more components for prebiotic chemistry. Oro and Kimble [12] synthesised adenine without the addition of electric discharge adding further weight to the argument that these molecules could

have been present on the early Earth and why they are now so prevalent in modern living systems. Ferris, Sanchez and Orgel [13] showed that it was possible to use Miller and Urey's apparatus to produce pyrimidines and cyanoacetylene which could have been a reasonable source of the pyrimidine bases uracil and cytosine, vital components in the formation of RNA.

The concept of a reducing atmosphere is, however, not without its critics [14] [15], and as this was the underlying paradigm which allowed for the production of key precursor compounds on the prebiotic Earth according to Miller and Urey, this cast some doubts as to whether this was the only prebiotic chemistry available to chemists trying to understand the origins of the transition from non-living matter to living matter. Kasting [15] proposes that the Earth's early atmosphere could not have been as strongly reducing as previously thought. The period at which life is thought most likely to have emerged in is between 3.8 Ga (Giga-annum, 1 Billion years) and 3.5 Ga ago, the period after heavy bombardment of the Earth's crust by meteorites preventing any survival of proto-life, however, studies of volcanic plume content and analyses of corresponding atmospheric conditions indicating that the oxygen content of the atmosphere must have been much higher than previously thought. Cronin postulates that alternative routes for the relevant prebiotic chemicals could have been brought to earth on the meteorites during the bombardment of Earth 3.8 Ga ago [14]. The Murchison meteorite was thought to have contained many carbonaceous compounds which could have been vital to prebiotic chemistry becoming early biology.

1.4 Defining life

It is important when approaching the chemistry of life to have a good working definition for what life is so that the chemist, upon meeting these criteria, may know that they have produced what might be considered a living system, in addition to knowing the form of systems that they should be aiming to fashion. These criteria are hard to come by. The complexity of life and the variety of flora and fauna that have thus far been catalogued to generate a spectrum of ways in which

matter can be arranged to produce a variety of systems. Consequently, when designing chemical systems that utilise prebiotic chemistry that self-assemble in early solar system conditions, the chemist reaches for very broad definitions. These catch-all conditions lend themselves to four main areas of prebiotic research which can be neatly summarised as follows:

- Compartmentalisation
- Homeostasis
- Metabolism
- Replication

Compartmentalisation, the distinction between an interior and exterior of the system that is usually defined by a membrane and can be thought of as the minimal description of the cell, the unit building block of modern life. Homeostatic, the system must be able to maintain its current configuration and prevent large perturbations away from the desired temperature, salinity, acidity, etc. that would prevent the chemistry of the system from functioning, this can be thought of as a rudimentary form of communication between the information within the construct and its exterior. Metabolism, the ability of the system to consume fuel from its environment to maintain its current configuration and fuel any other processes that it performs. And finally, replication, it can produce copies of itself, if synthetic life is to qualify as a model for how natural systems evolved then there must be the ability for selection pressures to favour the reproduction of more successful systems. These processes together can be thought of as a set of heuristics for determining whether synthetic systems can be considered living. Moreover, these four areas allow for research to be focused in a productive fashion, consequently this thesis focuses primarily on compartmentalisation.

1.4.1 Compartmentalisation

The ability to generate compartments for reactions to occur within is of great importance to the chemist, biochemist, and biologist. Chemical reactions must be localised, be that within a reaction

vessel as large as a beaker on the bench top, or as small as the ribosomes within the cell. Understanding the origin of cellular compartmentalisation is one of the 'big unanswered questions'. In the case of micro-volume compartments, such as the cell, the presence of a permeable, semi-permeable, or impermeable boundary can generate distinct environments with molecularly crowded interiors which facilitate more rapid reactions and allows for the passive transfer of reactants.

1.4.1.1 Vesicles

Bi-layer lipids are amphiphilic molecules that consist of a hydrophilic 'head' group and a hydrophobic 'tail' group. Above a critical concentration, spontaneous self-assembly in aqueous media of these membrane molecules occurs to minimise the hydrophobic interactions of the alkyl chains and the water. Depending on the size, shape and concentration of the lipid, micelles or vesicles may form. These structures, which can be seen in Figure 1.2, creates a boundary between the two environments.

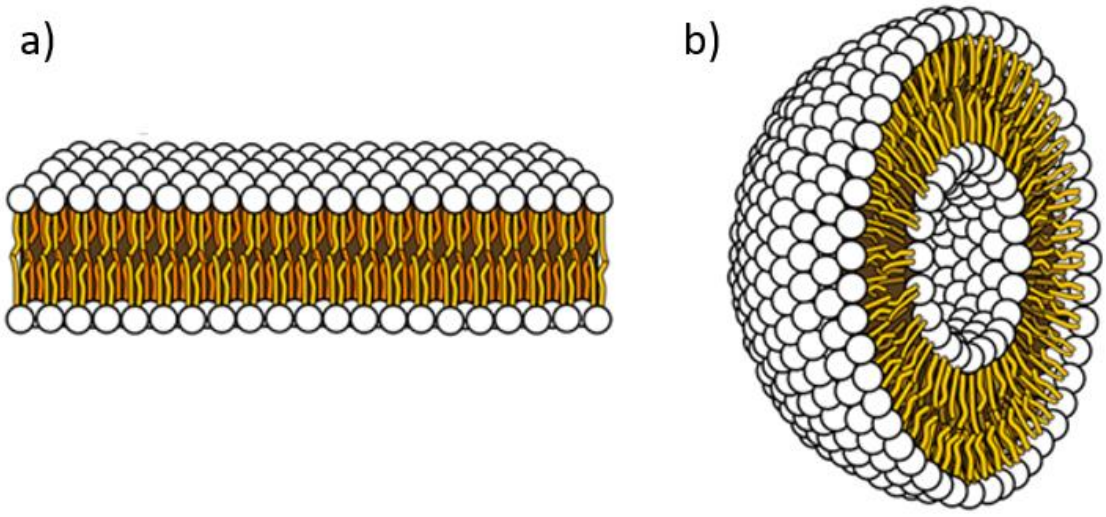

Figure 1.2: a) The arrangement of amphiphilic molecules within a bi-layer that forms the membrane of a vesicle. The yellow 'tails' are of a hydrophobic nature and the white 'head' groups separate them from the external polar solvent. b) The overall structure of a vesicle. Image courtesy of Mariana Ruiz Villarreal released under the creative commons license.

The micelle differs from the vesicle, in that the curvature of the membrane molecules spatial configuration is far greater than that of the vesicle. The configuration of the system is indicated by the packing parameter:

$$g = \frac{V}{a_0 l}$$

Equation 1.1: The packing parameter. Where g *is the packing parameter,* V *is the volume of the entire membrane molecule,* a_0 *is the area of the 'head' group and* l *is the length of the 'tail' group.*

For a vesicular configuration this value is equal to one half and for a micellar configuration, it is equal to one third. The micelle has a positive curvature and the vesicle no, or very small positive, curvature, locally. The materials from which vesicles are structured affects the aggregate's physical properties: their permeability, their stability etc., much like the cell.

One material that vesicles can be structured from is the phospholipid. The phospholipid is a class of molecules that possess the same structural elements: a double alkyl chain 'tail' group and a phosphate 'head' group (Figure 1.3). The shape of the phospholipid can be altered by the shifting the position and number of double bonds within the alkyl chain. Vesicle membranes are then formed by mixing phospholipids of various packing parameters to generate a bilayer that has the correct curvature to produce a vesicle.

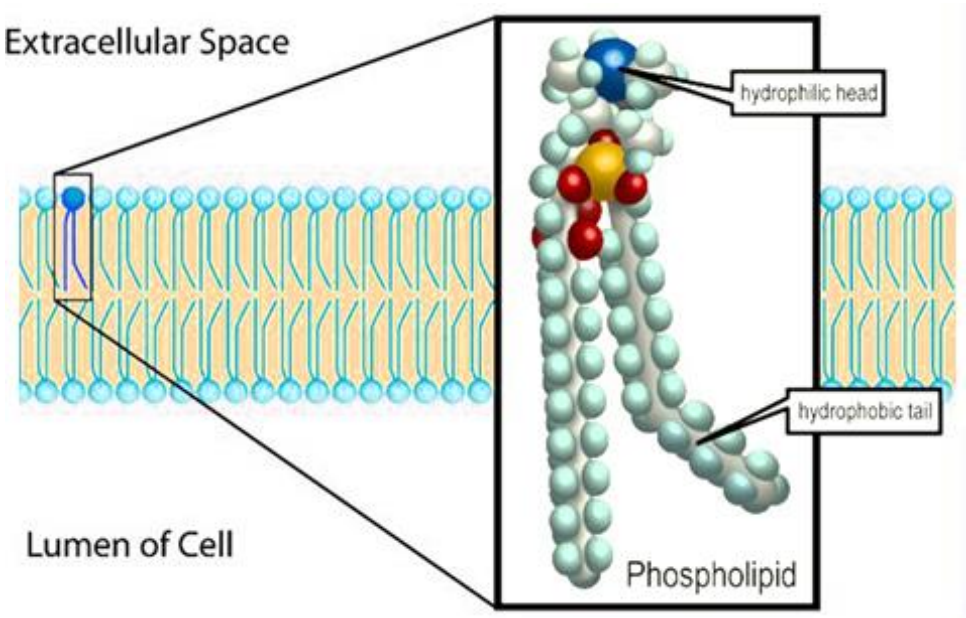

Figure 1.3: A cartoon illustrating the structure of a phospholipid and its orientation within a lipid bilayer functioning as the wall of a cell. Cartoon courtesy of Ties van Brussel released under the creative commons license.

Phospholipid vesicles produce membranes which are impermeable, due to the strong interactions between the head groups, and between the tail groups. The presence of transport proteins within the membrane are thus required to allow for mass transfer across the membrane. The complexity of phospholipids allows for a variety of vesicles sizes to be formed, however, in the context of origins of life research, this self-same complexity prevents phospholipids from being candidates for molecules that could have been present in prebiotic conditions. Origins of life research is a key example of chemical research that requires compartmentalisation and a more relevant molecule to that sphere of research is the fatty acid.

Vesicles can also be formed from fatty acids. Fatty acids are composed of a polar 'head' region, typically a carboxylic group, and non-polar saturated hydrocarbon chain or 'tail' region [16]. Fatty acids are similar in nature to the modern phospholipids that comprise the lipid bilayers observed in modern cells but are far simpler in chemical composition and as such present themselves as

plausible precursors to these molecules when considering early versions of cellular compartmentalisation.

The charge on the carboxylic group alters the packing parameter of the fatty acid molecule and thus affects the structures formed by the molecules after the critical aggregation concentration (CAC). The phases of decanoic acid (DA), Figure 1.4, illustrates the pH dependence of the system and the structures formed when the concentration of the fatty acid exceeds the CAC [17]. The critical micellar concentration (CMC) for DA is 60 mM [18] and the critical vesicular concentration (CVC) varies dependent on concentration and pH, for example at pH 7.6 the CVC is 26 mM and at pH 6.8 the CVC is 10 mM.

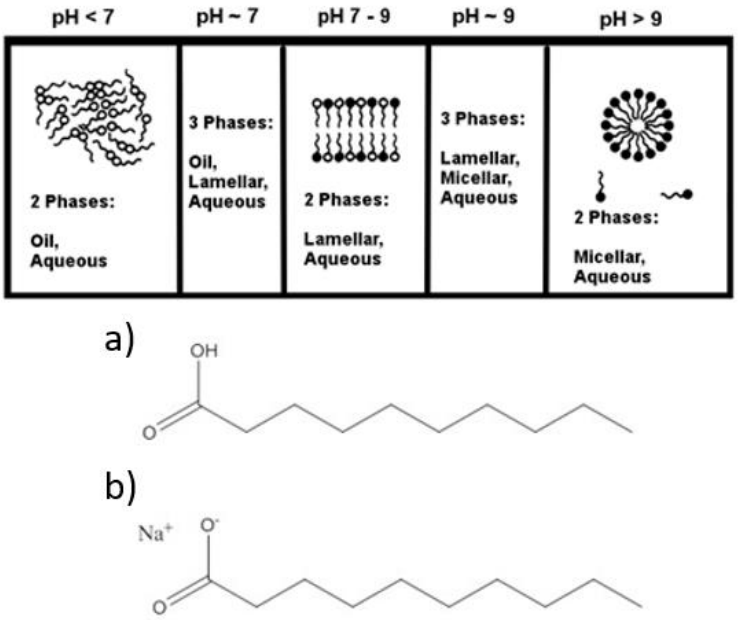

Figure 1.4: Fatty acids can form various states of matter dependent on the protonation state of the carboxylic group. In this schematic, the dark circles represent deprotonated carboxylic groups and the light circles, protonated groups, and curved lines indicate liquid hydrocarbons. The fatty acid is decanoic acid: a) the protonated acid state, and b), the deprotonated soap form. Cartoon adapted from [19].

The distinction between structures arises from another effect, hydrogen bonding, in addition to the alteration of packing parameter from the protonation state of the head group. At a pH equivalent to the pK_a of the carboxylic group on the decanoic acid molecule, fifty percent of the molecules will be protonated, in the acid form, and fifty percent will be deprotonated, in the soap form. Hydrogen bonds between these protonated and deprotonated forms and their 'head' groups, stabilise the lamellar structures required to form vesicles [20]. Therefore, if the decanoic acid solution is of a great enough concentration and prepared around pH 7.5 the formation of multi-lamellar vesicles is observed. When pH is equivalent to the pK_a, half of the carboxylic groups are deprotonated, this would imply that at pH 4.9 we would observe the formation of vesicles, as the bilayer membrane requires a mixture of protonated and non-protonated DA molecules to achieve the correct packing parameter to produce a low curvature. However, due to the length of the decanoic alkane chain, ten carbons, the hydrophobic effect drives aggregation of the DA molecules. This aggregation affects the number of molecules which possess a protonated carboxylic group and indeed for the protonated dimers. The result is that vesicles are observed at pH 7.5 and the precise value of pK_a between fatty acids varies depending on the chain length [21] [22]. These systems exist in equilibrium with monomers in solution molecules exchange with those within the membrane at a high rate [23]. Exchange of molecules between the two leaflets of the lamellar membrane is known as flip-flop and also plays a part in the transport of small molecules across the membrane [24]. Large molecules can also be embedded in these membranes if they comprise of a non-polar region of a size commensurate with the membrane width and polar regions which would be available to be solvated by water at the interface. Such molecules can act as transport channels between the interior environment and the external, such channels can be unidirectional and this gives rise to radically different environments separated by a fatty acid membrane [25].

The fatty acid vesicle has a distinct advantage over the phospholipid vesicle in that it can passively sequester small charged molecules through its membrane, rapid exchange of monomeric species between the bilayer leaflet and the surrounding environment allow for the association of charged

species with the deprotonated headgroup which can then rotate through the outer leaflet to the inner, thus facilitating trans-membrane transport. This allows for the accumulation of molecules to form a molecularly crowded interior without the use of additional membrane proteins to facilitate sequestration as shown by Deamer [26]. However, the fatty acid vesicle is limited in its comparison to the modern cell due to the lack of structuration within its interior. Current work on compartments as potential containers for pre-biotic chemistry are currently primarily being conducted by Lusisi, Whitesides, Szostak, Monnard [27] [24] [28].

1.4.1.2 Coacervates

Coacervates, first hypothesised by Oparin [28] as an essential step in the evolution of cellular complexity, and first reported by Tiebackx [29], present themselves as an attractive system for studying compartmentalisation. Unlike vesicles, coacervate microdroplets have no membrane and present a heterogeneous environment for guest molecules to be sequestered within. Coacervates, literally meaning ‘coming together’ [30], are a liquid-liquid phase separation. The first phase within the coacervate system consists of a polymer-rich liquid, and the second, is a polymer-poor liquid phase. Bungenberg de Jong investigated this phase separation in greater detail and made a distinction between two types of coacervation, simple and complex [31]. In the case of simple coacervation, the polyelectrolyte sequesters the solvent within its dense conformation, yielding the colloidal suspension of coacervate microdroplets in the bulk of the solvent solution. In the case of complex coacervation, it is achieved via the balance of interactions between a polyelectrolyte and an oppositely charged counter species, otherwise known as the charge screening effect. This phase separation generates a polymer rich droplet with no membrane as well. However, the dielectric constant of the droplet will vary with respect to the number of charges introduced by the counter species during coacervation. The system sequesters small molecules easily within the microdroplets due to the low dielectric constant of the interior of the compartments and the low energy barrier to overcome at the surface [32]. Coacervation makes use of the electrostatic interaction in conjunction with entropic effects [33], the polymer chain

can access a greater number of conformational states, after it has been partially desolvated during coacervation, than it can access when fully solvated in solution. This entropic force is the main thermodynamic driving force for coacervation, however as mentioned above, the electrostatic interactions of the compounds involved in coacervation can also affect the condensation of the polymer-rich phase, leaving coacervates with a susceptibility to ionic strength, pH, and temperature of solution, allowing for fine control of the parameters in which the system will form coacervate microdroplets.

Simple vs complex

The first system described above where the polyelectrolyte interacts with itself and the solvent is known as simple coacervation. It is also commonly known as aqueous two-phase separation (ATPS) [34]. The polymer must possess a sufficiently high molecular weight and high enough charge density to allow for the formation of the polymer dense phase to occur, in fact the ratio of these must be equal to 0.42 for phase separation to occur, thus opening up the field of chemical composition of these systems to include multi-valent polyelectrolytes of a low molecular weight and to systems which comprise larger monocharged moieties of a higher molecular weight. However, the macromolecule must not be so large as to undergo precipitation [35]. This precipitation can be exacerbated by temperature and the presence of salt ions, which can disrupt the interactions generating the microdroplets via shielding of the charged moieties along the polymer chain. In a study by Gupta and Bohidar [35] the process of simple coacervation is modelled as a combination of charge neutralisation and entropic conformational effects driving the formation of the coacervate microdroplets. The difference in osmotic pressure between the microdroplets and the polymer poor surrounding phase drives expulsion of the solvent thus completing the formation of the simple coacervate microdroplet, Figure 1.5**.**

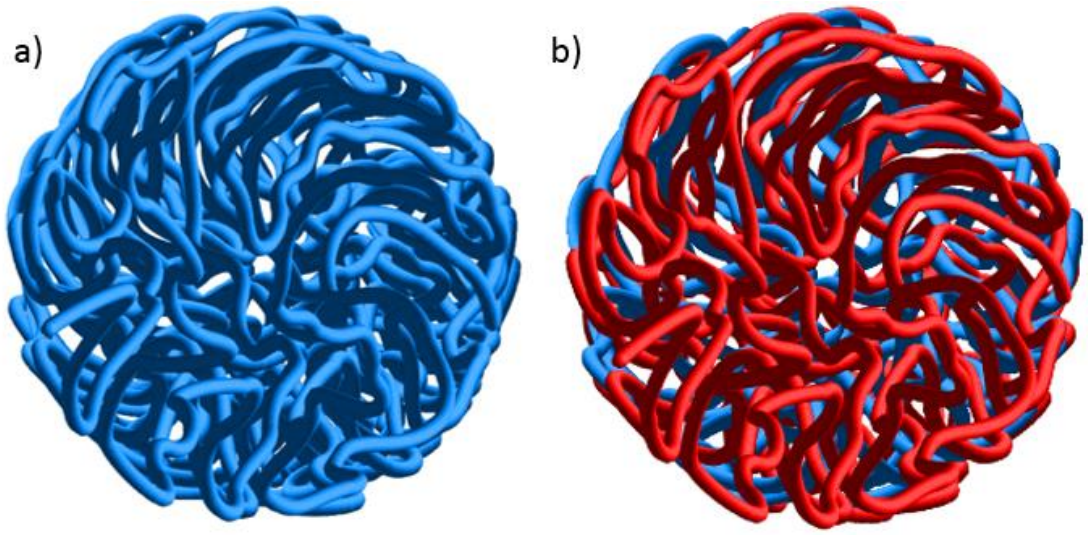

Figure 1.5: a) An illustration of a simple coacervate, the dark blue line represents the polymer that has undergone a conformational change to form the coacervate microdroplet. b) An illustration of a complex coacervate microdroplet. The red line represents the polymer, the blue line represents the counter species. In both systems solvent has been sequestered in the interstitial vacancies between the condensed polymer during coacervation, during this process guest molecules can also be incorporated into the microdroplets.

The second system involving a complementary charged species is known as complex coacervation [36], Figure 1.5. Electrostatic interactions allow the charged polymer and counter-species to form the dense colloidal polymer phase in addition to the increase in entropy from the new states accessible by the conformations of the polymer chain. However, as with salt, where the ions shield the charges along the length of polyelectrolyte preventing electrostatic interactions, if the molar ratio of the charges present between the polymer chain and the charged counter species are not balanced precipitation, or no coacervation, will occur. Both systems sequester complementarily charged guest species within the coacervate microdroplet and function as soft compartments that can aggregate molecules and generate a dense molecularly crowded environment for molecular machinery, such as cell–free protein expression kits, [37]. The lack of membrane and low surface tension of the coacervate allows for the coalescence of coacervate microdroplets. Indeed, this can be a problem and the stability of coacervates can be modulated by altering the molar ratio of the components which make up the coacervate [38]. This illustrates the

versatility of the coacervate system, as the charge ratios of the droplets can be tuned at a stoichiometric ratio level, thus adjusting the stability of the droplets formed [32]. The incorporation of different dyes or guest molecules allows for the study of coacervate suspensions as different populations that can undergo mixing and interactions with one another, in the case of micro-reactions and micro-volumes, or as individual coacervate microdroplets, as models for compartmentalised systems and as candidates for proto-life models.

Use in an origin of life setting

Recent work on coacervates has focused on their ability to be modelled as protocells, using biologically relevant molecules such as proteins (e.g. gelatin), polysaccharides (e.g. gum Arabic) [39] and as possessing biomedical applications [40] in addition to food and pharmaceutical uses [41]. Protocells are models that describe plausible routes for simple chemical systems to have become complex enough to be considered living. There is a consensus [42] [43], over the four core criteria that an organism should possess to qualify as living. These include:

- Compartmentalisation
- Replication
- Metabolism
- Homeostasis

The protocell then could have arisen first as a membrane-free coacervate microdroplet. Oparin thought that colloidal coacervate systems were important precursors to cellularity as they spontaneously formed via phase separation [28]. Coacervates as protocells provide reaction compartments for biologically relevant processes as shown by Crosby *et al*. [44], Figure 1.6. The system allowed for compartmentalisation of the minimal complex of actinorhodin polyketide synthase which produced elevated yields of the shunt products under various ionic strength conditions. This indicated that the coacervate microdroplet presented a preferential pathway for systems that utilised this reaction.

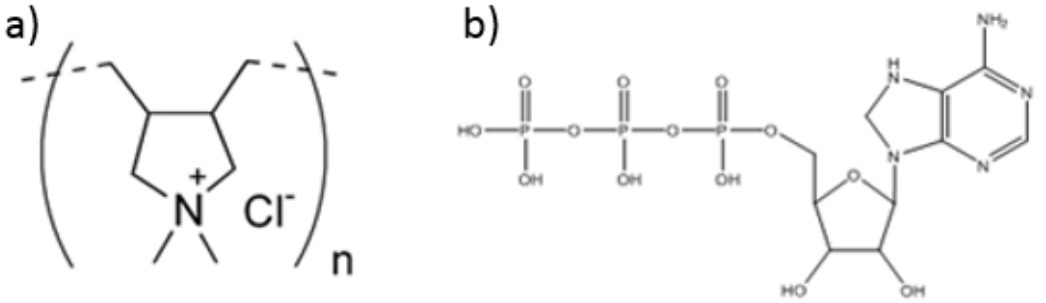

Figure 1.6: The chemical structures, a) of the polymer, poly(diallyldimethylammonium chloride), PDDA, b) the counter-ionic species adenosine triphosphate, ATP, that comprise the coacervate system used by Crosby et al. *[44]*.

Additionally, they have been utilised to encapsulate other compounds, in a facile manner, before being restructured, via the addition of further biologically relevant molecules, to form more complex protocell models. Inorganic components, phosphotungstate polyanionic clusters, were introduced to the PDDA/ATP coacervate to generate a novel three-tiered structure comprising a phosphotungstate/PDDA shell, a PDDA/ATP sub-membrane and an aqueous filled lumen that responded to osmotic pressure changes, as demonstrated by Williams *et al.* [45]. Organic, prebiotically relevant molecules have also been added to coacervate systems to generate new structures, PDDA/ATP and oligolysine/ATP coacervates were formed and oleic acid micelles

were added to form thin multilamellar vesicles at the surface of the coacervate microdroplets as shown by Tang *et al.* [46]. These systems make use of the polymer poly(diallyldimethylammonium chloride) (PDDA) and oligolysine, and various counter species, adenosine triphosphate (ATP) and carboxymethyl-dextran (CM-dextran) to generate the coacervate microdroplets as models for protocells. The molecular weight (MW) of the polymer is generally quite high, greater than one hundred kDa, as the length of the polymer has an influence on the size of the microdroplets formed, and encapsulation of other guest molecules was key to the investigations being conducted. Having discussed vesicles and their merits of possessing a membrane that can act as a barrier to unwanted molecules and aid in aggregation of desired molecules, and the facile manner in which coacervates sequester molecules into a molecularly crowded environment, it would be of great interest to investigate a system that could combine elements of both vesicles and coacervates and study how guest molecules behave in such a system.

1.4.2 Hydrogels

Cells have structure, strength, and motility [47]. These aspects of their character are derived from the structure known as the cytoskeleton, comprising of one of a series of three protein families which allow cells to be rigid, to undergo division and replication, and to translate themselves within in an environment to hunt for food or to hunt down invasive foreign bodies [48]. One example of the many structures found within the cytoskeleton is the microtubule, which maintains cellular structure by working in conjunction with a variety of other filaments in the cytoskeleton [49]. Its structure and composition can be seen in Figure 1.7.

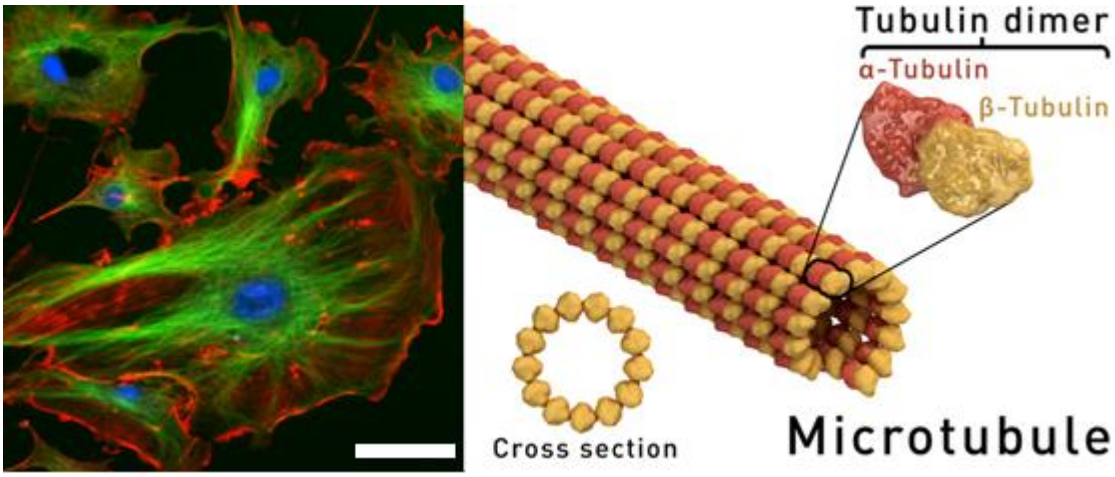

Figure 1.7: The image on the left is of a series of eukaryotic cells stained with various dyes to highlight the various components of the cell. The microtubule structures that comprise the cytoskeleton are stained green with a Fluorescein isothiocyanate bound to an antibody. Image Courtesy of ImageJ (public domain) scale bar = 10 µm. The cartoon on the right illustrates the alpha-beta-tubulin heterodimer that comprises the microtubules within the eukaryotic cell. Outer diameter of cross-section is 24 nm and the inner diameter is 12 nm. Image courtesy of Wikipedia user: Thomas Splettstoesser released under the creative commons licence.

In the context of Origins of Life studies, the cytoskeleton is an important aspect of a minimal system to investigate, as such structures, and the proteins that comprise them, are prevalent amongst the three domains of life we observe today. This requires that cytoskeletal genetic information and protein encoding must have evolved very early on, and that there is a common ancestor between eukaryotes, prokaryotes, and eubacteria [48]. The question then presents itself in the following form; could simple chemical systems emulating the cytoskeleton have formed that produced favourable evolutionary pathways that became incorporated into cellular make-up for the benefits that they provided?

The cytoskeleton in the modern eukaryote provides pathways for intracellular chemical transport [50] in conjunction with motor proteins such as kinesin and vesicle micro compartments [51]. The subsequent crowding of the interior of a microcompartment that is being used as a protocell

model, has the added effect of changing the ability of molecules to diffuse throughout the interior, generating the ability to sustain internal concentration gradients which could be used to drive other relevant reactions [52]. The nature of simple self-assembling systems is that they are often thermodynamically driven and as such are reversible, this allows for structuration of the interior after pre-requisite components have been sequestered within the protocell container and can then be released at a later time after 'sensing' a change in its environment a triggered response [53]. This allows the Synthetic Biologist to create rudimentary chemical or physical stimuli sensing mechanisms that can then be employed within systems that require the release of components at certain points within a reaction, pointing the way towards rudimentary metabolic pathways. Controlled release of molecules using nano-hydrogels has also been investigated as a method for targeted drug delivery and controlled release [54]. As such a proto-cytoskeletal model is one which could be employed in many other systems and will possess interesting and complicated chemistry and kinetic properties of its own, and as such merits investigation.

1.4.2.1 Characteristics and definitions

Gels are a "soft, solid or solid-like material of two or more components; one, which is a liquid, present in substantial quantity" [55]. This can be quantified using rheological measurements. Measuring frequency sweeps of the storage modulus, G′ and the loss modulus, G″ as a function of angular frequency (ω) one can illustrate the gels moduli independence for several decades with G′>G″ (G′: G″ > 10) over the range of frequencies scanned [56]. The storage modulus, G′ also known as elastic modulus, plateaus at low frequencies of shear allowing for the deformation in the gel to persist for a time on the scale of a few seconds [55]. This behaviour denotes the presence of a 'network' capable of storing energy imparted to the gel during deformation. A facile test for the formation of a gel is the 'vial-inversion' test, if the material supports its own weight upon turning the container it is in upside down, it can be considered a gel [57].

Hydrogels are three-dimensional networks of self-assembling chemical systems that swell with the addition of solute [58]. In the case of hydrogels, the solute is water. The supramolecular nature of many cross-linked chains, or fibres, allows the system to be resilient to dissolution. In addition to this, the hydrophilic functionality of the chains allows the hydrogel network to sequester and incorporate the additional water into the fibrous network that forms the gel. There are two commonly accepted and widely used routes for generation of hydrogels [59]: functionalisation of pre-existing polymers which entangle and cross-link via either physical or chemical bonds; and polymerisation of monomeric units with pre-requisite functionality via self-assembly into supramolecular gels. In the former case, Michael additions have been extensively used to cross-link polymers *in situ*. In the latter case, the hydrogels formed, consisting of a series of biomonomeric and/or low weight molecular gelator units with hydrophilic/hydrophobic functionality [60]. These units are then polymerised to form a fibrous network which sequesters water to generate a gel phase. This gel is known as a hydrogel due to the necessary presence of water to generate the gel. The gel phase is an interesting one in that it allows for the immobilisation of large molecules within it [61]. It can adhere to surfaces and possesses a higher viscosity than the solutions of its individual components. The hydrogel can be characterised through the use of calorimetric techniques to yield the gel-sol transition temperature, the point at which enough thermal energy has been inputted to the system that the entangled network begins to disassemble and produce a liquid solution of monomeric units.

1.4.2.2 Existing hydrogels

There are two examples of hydrogel systems that have been explored by the Mann group previously. Work conducted by Kumar et al. centred on a hydrogel system that consisted of an Alkaline Phosphatase (ALP)-mediated dephosphorylation of N-fluorenylmethyloxycarbonyl tyrosine-(O)-phosphate (FMOC-Tyr-P) [62]. The reaction scheme is illustrated in Figure 1.8.

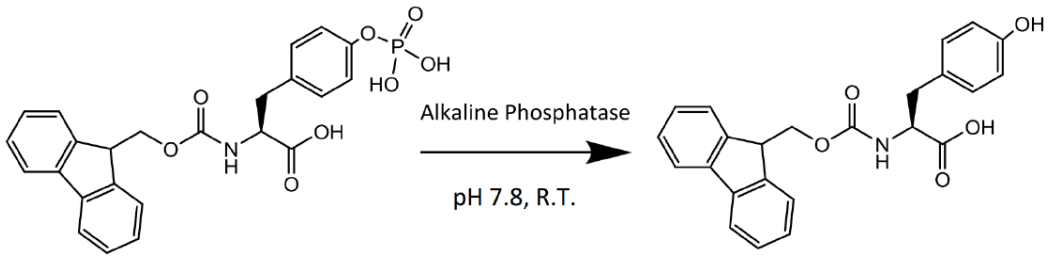

Figure 1.8: The ALP-mediated dephosphorylation of FMOC-Tyr-P. Schematic courtesy of [63].

Dephosphorylation leads to a change in amphiphilicity of the molecule, as a result, the product spontaneously self-assembles via π-stacking to form a one-dimensional structure; a nano-fibre. These highly entangled nano-fibres encapsulate water to form the gel phase.

Another system that has been explored in the Mann group utilised the same methodology of polymerisation of monomeric units to generate the hydrogel network. Guanosine Monophosphate (GMP) and silver nitrate were combined to generate a hydrogel [64]. Modified hydrogen bonding, as a result of ion-mediation, abstracts a proton from the N1 site and generates the enolate tautomer which ensures silver binding at the O6 and N7 sites which then form the GMP-Ag dimer seen in Figure 1.9. Through π-stacking, these dimers then form the fibrils which exhibit the pre-requisite hydrophilic structures required to sequester water and generate fibril cross-linking and water encapsulation, necessary for the generation of the gel phase.

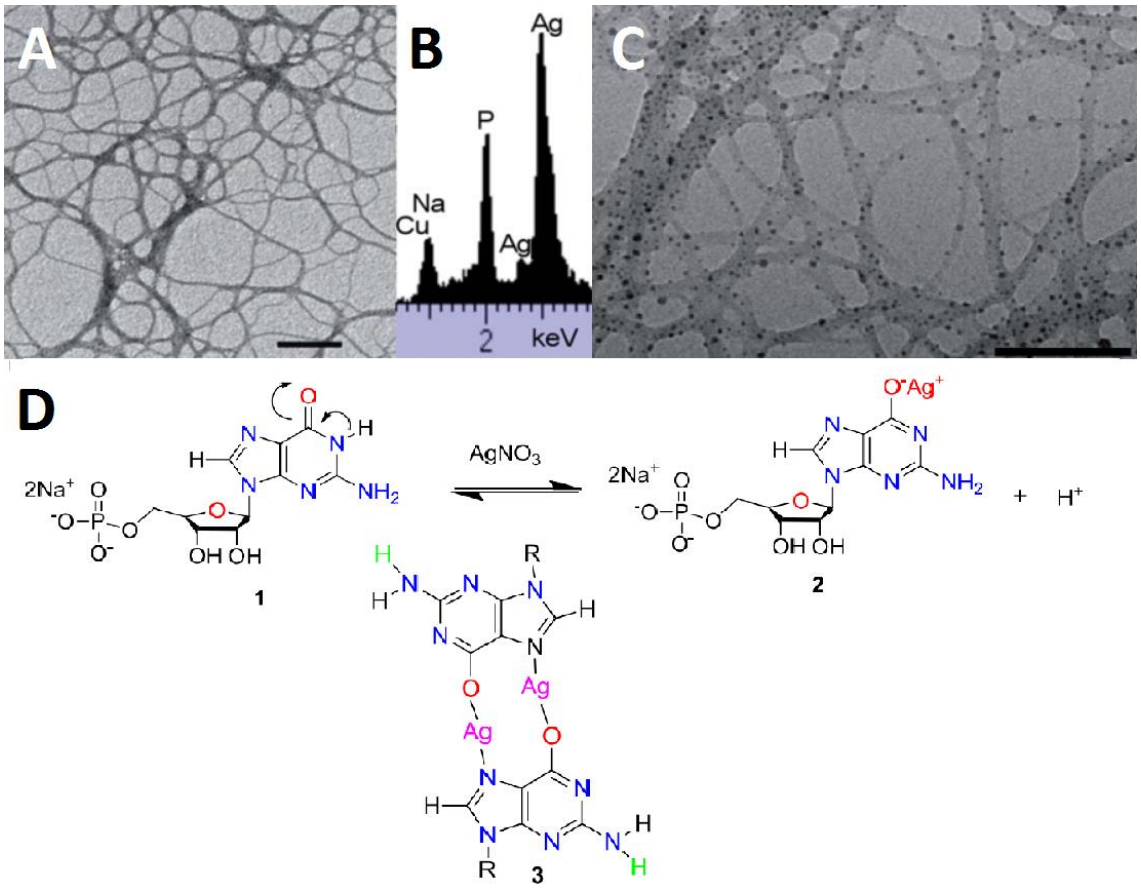

Figure 1.9: A) Transmission electron micrograph (TEM) of the fibrils formed in a 1:1 AG-GMP hydrogel, scale bar 200 nm, B) Corresponding energy dispersive x-ray spectrogram (EDX) of the micrograph, C) TEM micrograph of 1:2 hydrogel after 12 h prior exposure to light illustrating the presence of Ag nanoparticles, scale bar = 100 nm D) Reaction schematic illustrating the generation of an enolate tautomer by the addition of Ag^+ ions also produces the release of a proton at N1 and subsequently, due to binding at N7 and N6, a GMP-Ag dimer is formed. Image courtesy of [64].

Both of these examples of self-assembling hydrogel networks were couched within the framework of origins of life research as models for cytoskeletal networks as their rheological properties were analogous to the properties observed in modern cells and further molecular crowding and spatial confinement of bio-relevant reactions are favourable and can produce non-equilibrium behaviour [65] this was illustrated by Kumar et al. [63] where the fabrication of an enzymatically active bio-inorganic protocell was enabled by the self-assembly of an amino-acid supramolecular hydrogel. Comparisons are drawn between this self-assembled network and the viscosity of the cytoplasm

in natural cells, the viscosity within the protocell being measured as 0.41 ± 0.17 Pa.s compared to a viscosity within HeLa (the immortal Henrietta Lacks human cell line used as a standard human cell cell-line for biomedical research) of 0.05-0.2 Pa.s [66].

1.4.3 Communicating Systems

Another way of parsing the riddle of life is to circumvent the question of how to define it entirely. First postulated by Cronin *et al.,* drawing on the ideas of Turing, it was thought that by invoking a synthetic paradigm that could imitate natural systems to the point of fooling them into interacting with them as if they were fellow natural systems then such synthetic systems could be thought of as being alive – in effect, having played, and won, the imitation game [67]. Two-way chemical communication between artificial and natural cells was achieved by Lentini *et al.* using *V. fischeri, V. harveyi, E. coli,* and *P. aeruginosa* bacteria as the natural cells [68]. The activity of communication with the synthetic, or artificial cell, comprising various signalling pathways encoded by a cell-free genetic kit, were incarcerated within a phospholipid, 1-palmitoyl-2-oleyl-*sn*-glycerol-3-phosphocholine (POPC), vesicle, to determine whether quoracy determining molecules could diffuse across this membrane.

1.4.3.1 Modern cells

Modern cells possess a plethora of sensing pathways that they use to coordinate actions such as apoptosis, the process of programmed cell death which is considered vital to normal cell turnover and is distinct morphologically from other forms of cell death [69]. First defined by Kerr, Wyllie and Currie [70], apoptosis utilises many communication pathways between cells, these include but are not limited to, ligand binding, protein cross-linking, or decay pathway blocking by hormones or growth factors. Intercellular communication remains a key topic for today's researchers as it is thought that it plays a key role in the prevention and treatment of cancer [71].

To date, the most extensive studies of inter-cellular communication are on bacteria [72]. Bacteria are simple single-celled organisms that exhibit differentiated interiors from exteriors, possess a metabolism, have mechanisms for regulating their internal alkalinity and salinity, and of course replicate [73].

1.4.3.2 Signalling Compounds

The population density of bacteria can be self-determined using the autoinduction system [74]. The process of autoinduction, also known as quorum sensing, is regulated by the expression of diffusible compounds that are present in the environment in low concentrations when the population density is low but as this increases the concentration correspondingly increases. In the case of *V. fischeri*, the first system in which Quorum sensing was identified, the autoinducer is the compound 3-oxo-*N*-(tetrahydro-2-oxo-3-furanyl)hexanamide (*V.* fischeri autoinducer, VAI Figure 1.10), once it begins to accumulate in the cells of the bacteria due to high concentration in the exterior environment the transcription of the luminescence gene *lux* is initiated. *Lux* transcription, the process whereby the genetic information in the bacteria's plasmid, a simple DNA information ring, is replicated by mRNA, messenger RNA, and then read by ribosomes to express the corresponding protein encoded in the genes, the fluorescent protein is then expressed, and the system begins to fluoresce, as can be seen in Figure 1.10. These are commonly known as *N*-acyl homoserine lactones (AHLs) and are commonly associated with gram-negative bacteria for the functioning of their autoinduction systems [75].

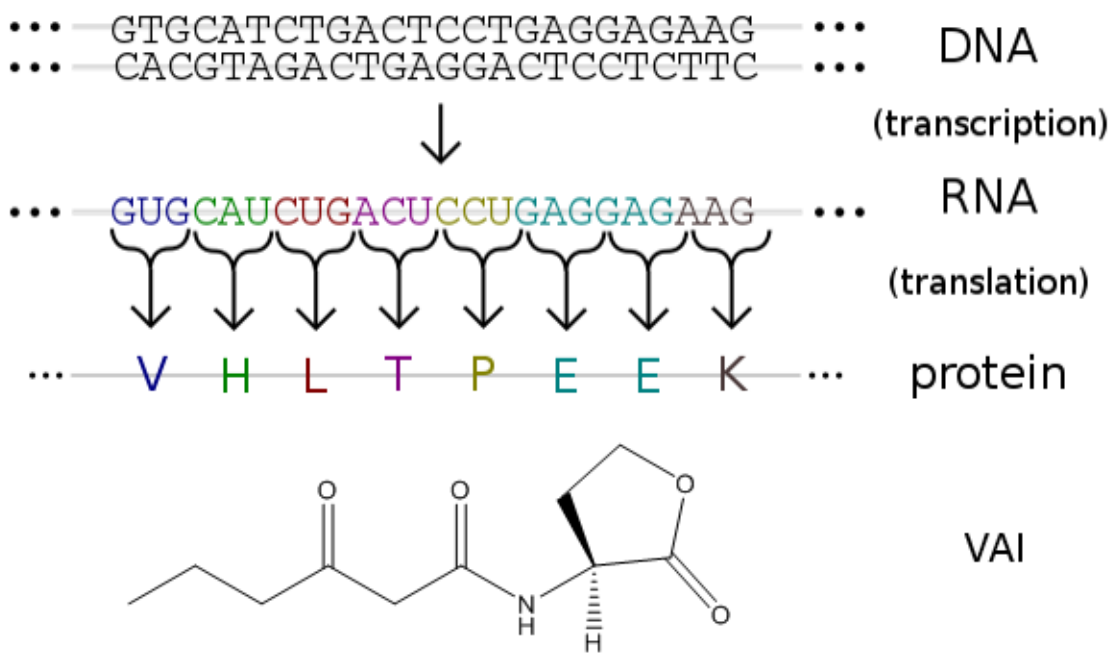

Figure 1.10: A cartoon representation of the process of gene expression from information storage in DNA, to the translation of information through RNA, and finally to the production of proteins through the ribosome. The molecule below the cartoon is the chemical structure of the autoinducer for the V. fascheri bacteria (VAI). Cartoon courtesy of Wikimedia Commons contributor Madprime, released under the creative commons license.

The gram stain test differentiates between gram-positive and gram-negative bacteria, which can quickly differentiate between two broad categories of bacteria based on the structure of their cell wall [76]. The compounds for intercellular autoinduction systems in gram-positive bacteria are autoinducing peptides, which induces a two-stage regulated gene transcription [77].

1.4.3.3 Routes to proto-communication through simple stimuli

Proto-communication has been attempted within protocell communities using simple signalling molecules such as hydrogen peroxide produced *via* a glucose oxidase (GOx) mediated signalling pathway [78]. The protocells developed by Mann *et al.* used clay and silica to stabilise different

populations of Pickering emulsions, water in oil emulsions that are stabilised with respect to coalescence by amphiphilic material bound at the interface between the two phases by hydrophobic and hydrophilic forces and interfacial tension energy minimisation [79]. These protocells could then be loaded with cargo that could perform catalysed reactions on substrates that could diffuse across their membranes, or could catalyse the production of a temperature surface polymer gate on their membrane allowing for 'gating', in effect the shielding of interstitial spaces between stabilising particles at the protocell boundary with a collapsed polymer, of the reactants and thus could control the rates of reactions being performed by the communities in response to their environments. See Figure 1.11 for a scheme illustrating the communication and subsequent properties of the protocell community produced.

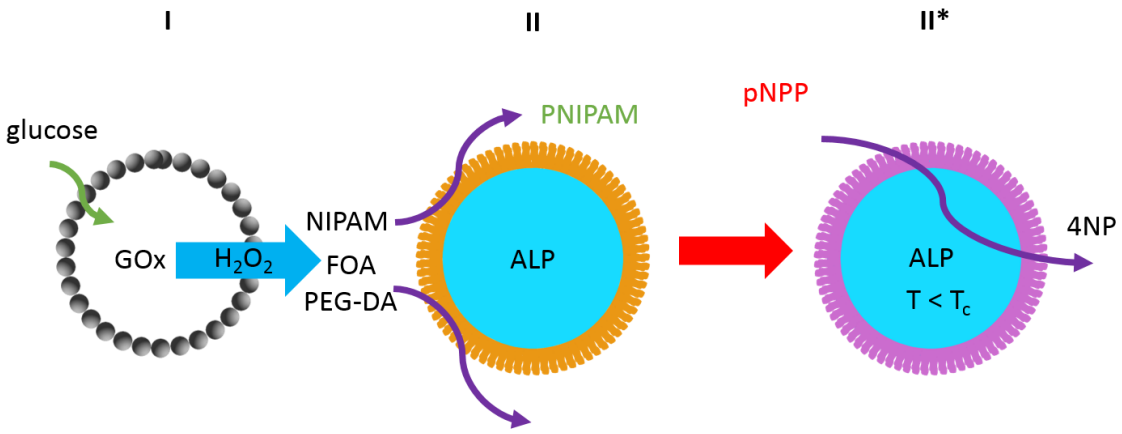

Figure 1.11: Scheme showing chemical communication between protocell populations within the community. Step I illustrates the addition of glucose to glucose oxidase containing colloidosomes, amphiphillic silica stabilised Pickering emulsion microdroplets; Step II shows the hydrogen peroxide produced in step I diffusing to an alkaline phosphatase (ALP) containing Fe(III)-enriched montmorillonite (FeM)-clay colloidosomes which then polymerise N-isopropylacrylamide (NIPAM) in the presence of fluorescein o-acrylate (FOA) and poly(ethylene glycol)-diacrylate (PEG-DA) to produce a green fluorescent PNIPAM shell; in step II 4-nitrophenyl phosphate (pNPP) can diffuse across the membrane to be dephosphorylated by the ALP to 4-nitrophenolate (4NP), this process can be controlled by lowering the temperature of the system to below the lower critical solution temperature (LCST) of the PNIPAM and thus gating the diffusion of the pNPP. Scheme adapted from [78].*

In work conducted by Williams *et al.* an inorganic compound was used to trigger the restructuration of a coacervate protocell model [80]. Polyoxometalate (POM) creates a surface templated membrane generating a three-tier hierarchical structure, firstly the semi-permeable POM outer membrane, the coacervate inner membrane which is condensed as a result of the charged outer membrane, and finally the inner aqueous lumen. By sequestering proteins and enzymes into the coacervates before the inorganic stimuli triggered spatial reconfiguration of the droplets, different protocells possessing different functional capabilities, dependant on the incarcerated payload. These functionally different protocells can then be linked to form tow-enzyme cascade reactions dispersed in aqueous media indicating that communication of substrates between different populations of compartments had been achieved.

Both of the above outlined systems rely on the diffusion of small molecules through aqueous environments within which discrete populations of synthesised protocells co-exist. However, modern cells are embedded within the extracellular matrix (ECM) [81] which can mediate cell to cell communication and provides biochemical support to the cells, supplying them oxygen, glucose etc. and removing waste products [82]. The ECM is formed in a process known as exocytosis, where cells produce proteins that assemble into the ECM and transport them from their interiors to their exteriors, this is heavily mediated via the utilisation of vesicles as containers for membrane materiel transduction [83]. The structure of the ECM and its interaction with the cell can be seen in Figure 1.12 [84]. The main chemical compounds that comprise this multifaceted environment are proteoglycans, composed of carbohydrate polymers attached to proteins, heparin, chondroitin, and keratan sulfates [85], linear polysaccharides, hyaluronic acid a potent water absorbing hydro-gelator [86], elastin, a protein to confer elasticity to the ECM [87], extracellular vesicles containing the aforementioned intercellular cargoes [88], and finally collagen, which constitutes over 90% of the ECM and provides structural support to cells [89].

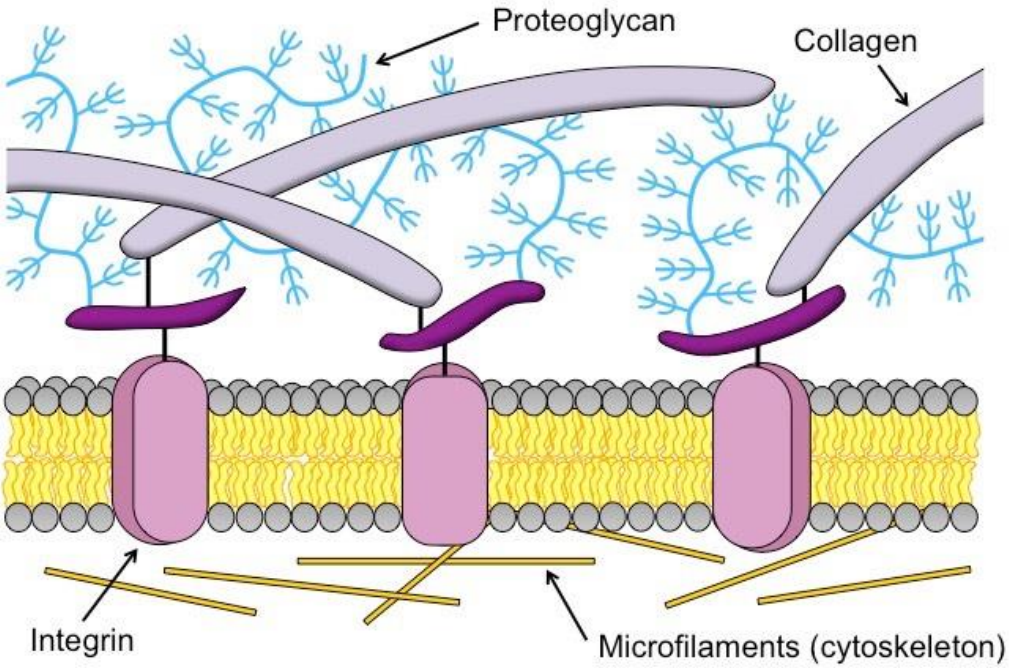

Figure 1.12: A cartoon illustrating the rich complexity of the extracellular matrix (ECM). An arc of the cell membrane can be seen, one side in contact with microfilaments providing internal structure and physical characteristics to the cell, the membrane itself embedded with membrane proteins that anchor the cell into the collagen network that comprises the ECM with fibronectin, a highly branched polysaccharide that permits the cell to move through the ECM. Cartoon released to the public domain courtesy of Carl Fredrik.

The ECM is central to intercellular communication and differentiation [90] and so when considering the problem of how cellular communication arose it is worth considering any candidate systems within the context of a proto-extracellular matrix.

This broad overview of approaches to understanding life through a chemical lens will be referred to throughout this thesis. The arguments presented in the experimental chapters that follow attempt to draw on the ideas and themes presented here to discuss the novel chemistry explored, and how their exciting properties could be of use to chemists who continue to be puzzled by the question – how did Life, come to be?

1.5 References

[1] M. W. Eysenck and M. T. Keane, Cognitive Psychology: A Student's Handbook (4th ed.), New York: Taylor & Francis, 2014.

[2] D. p. McAdams, The Stories we Live By, New York: The Guildford Press, 1993.

[3] N. Noffke, D. Christian, D. Wacey and R. M. Hazen, "Microbially Induced Sedimentary Structures Recording an Ancient Ecosystem in the ca. 3.48 Billion-Year-Old Dresser Formation, Pilbara, Western Australia," *Astrobiology,* vol. 13, no. 12, pp. 1103-1124, 2013.

[4] G. Wächtershäuser, "From pre-cells to Eukarya--a tale of two lipids," *Mol. Microbiol.,* vol. 47, no. 1, p. 13–22, 2003.

[5] N. R. Pace, "The universal nature of biochemistry," *Nat. Life Class. Contemp. Perspect. from Philos. Sci.,* vol. 9780521517751, no. 3, p. 157–163, 2010.

[6] M. Neveu, H.-J. Kim and S. A. Benner, "The "Strong" RNA World Hypothesis: Fifty Years Old," *Astrobiology,* vol. 13, no. 4, pp. 391-403, 2013.

[7] T. R. Cech, "The RNA Worlds in Context," *Cold Spring Hard Perspect Biol,* vol. 4, no. 7, 2012.

[8] A. K. Rana and S. Ankri, "Reviving the RNA world: An insight into the appearance of RNA methyltransferases," *Front. Genet.,* vol. 7, no. Jun, p. 1–9, 2016.

[9] L. S. Ji and H. F., "Small cofactors may assist protein emergence from RNA world: Clues from RNA-protein complexes," *PLoS One,* vol. 6, no. 7, p. 6–10, 2011.

[10] S. L. Miller and H. C. L. Urey, "Organic Compound Synthes on the Primitive Eart," *Science,* vol. 130, no. 3370, pp. 245-251, 1959.

[11] S. A., "On a new substance arising from acetaldehyde–ammonia [i.e., 1-aminoethanol] and hydrocyanic acid," *Annalen de Chemie und Pharmacie,* vol. 3, no. 91, pp. 349-351, 1854.

[12] J. Oró and A. P. Kimball, "Synthesis of purines under possible primitive earth conditions. I. Adenine from hydrogen cyanide," *Arch. Biochem. Biophys,* vol. 94, no. 2, pp. 217-227, 1961.

[13] L. E. Sanchez, F. Robert A. and O. James P., "Studies in Prebiotic Synthesis II," *J. Mol. Biol.,* vol. 30, no. 2, pp. 223-253, 1967.

[14] J. Cronin, S. Pizzarello and D. Cruikshank, Meteorites and the Early Solar System, Arizona Press, 1988.

[15] J. F. Kasting, "Earth's Early Atmosphere," *Science,* vol. 259, no. 5097, pp. 920-926, 1993.

[16] R. Nagarajan and E. Ruckenstein, "Theory of surfactant self-assembly: a predictive molecular thermodynamic approach," *Langmuir,* vol. 7, no. 12, pp. 2934-2969, 1991.

[17] J. L. Cape, P.-A. Monnard and B. J. M., "Prebiotically relevant mixed fatty acid vesicles support anionic solute encapsulation and photochemically catalyzed trans-membrane charge transport," *Chem. Sci.,* vol. 2, no. 4, p. 661, 2011.

[18] K. Morigaki, P. Walde, H. Misran and B. H. Robinson, "Thermodynamic and kinetic stability. Properties of micelles and vesicles formed by the decanoic acid/decanoate system," *Colloids Surf.,* vol. 213, pp. 37-44, 2003.

[19] D. Cistola, J. Hamilton, D. Jackson and D. Small, "Ionization and phase behaviour of fatty acids in water: application of the Gibbs phase rule," *Biochemistry,* vol. 44, p. 1881–1888, 1988.

[20] J. R. K. Shah, "Effect of Degree, Type, and Position of Unsaturation on the pKa of Long-Chain Fatty Acids," *J. Colloid Interface Sci.,* vol. 256, no. 1, p. 201–207, 2002.

[21] T. Namani and D. W. Deamer, "Stability of model membranes in extreme environments.," *Origins of life and evolution of the biosphere,* vol. 38, no. 4, pp. 329-41, 2008.

[22] T. C, S. A. M, C. R. F, U. R. V and S. A, "Fmoc-Diphenylalanine Self-Assembly Mechanism Induces Apprent pKa Shifts," *Langmuir,* vol. 25, no. 16, pp. 9447-9453, 2009.

[23] J. P. Schrum, T. F. Zhu and a. J. W. Szostak, "The Origins of Cellular Life," *Cold Spring Harb. Perspect. Biol.,* vol. 2, no. 9, p. a002212–a002212, 2010..

[24] J. W. Szostak, "Controlled Growth of Filamentous Fatty Acid Vesicles under Flow," *Langmuir,* vol. 30, p. 14916–14925, 2014.

[25] M. S. Almén, K. J. V. Nordström, R. Fredriksson and H. B. Schiöth, "Mapping the human membrane proteome: a majority of the human membrane proteins can be classified according to function and evolutionary origin," *BMC Biol.,* vol. 7, p. 50, 2009.

[26] D. W. Deamer and J. P. Dworkin, "Chemistry and Physics of Primitive Membranes," *Curr. Chem,* vol. 259, pp. 1-27, 2005.

[27] P. L. Luisi, F. Ferri and P. Stano, "Approaches to semi-synthetic minimal cells: A review," *Nat. Life Class. Contemp. Perspect. from Philos. Sci.,* p. 272–288, 2010.

[28] A. I. Oparin and K. L. Gladilin, "Evolution of self-assembly of probionts," *BioSystems,* vol. 12, pp. 133-145, 1980.

[29] F. Tiebackx, "Gleichzeitige Ausflockung zweier Kolloide," *Chem. Ind. Kolloide,* vol. 8, pp. 198-201, 1911.

[30] P. L. Madan, "Microencapsulation I. Phase separation or coacervation," vol. 4, no. 1, 1978.

[31] J. H. G. d. Bungenberg and R. K. H, "Coacervation (partial miscibility in colloid systems)," *Colloid Sci.,* vol. 1, pp. 232-255, 1949.

[32] S. Kogo, D. S. Williams, A. W. Perriman and S. Mann, "Peptide-nucleotide microdroplets as a step towards a membrane-free protocell model.," *Nature Chemsitry,* vol. 3, no. 9, pp. 720-724, 2011.

[33] D. Williams, A. J. Patil and S. Mann, "Spontaneous structuration in coacervate-based protocells by polyoxometalate-mediated membrane assembly," *Small,* vol. 10, no. 9, p. 1830–40, 2014.

[34] B. Mohanty and H. Bohidar, "Systematic of alcohol-induced simple coacervation in aqeuous gelatin solution," *Biomacromolecules,* vol. 4, no. 4, pp. 1080-6, 2003.

[35] A. Gupta and H. Bohidar, “Kinetics of phase separation in systems exhibiting simple coacervation,” vol. 72, no. 1, 2005.

[36] E. Kizilay, a. B. Kayitmazer and a. P. L. Dubin, “Complexation and coacervation of polyelectrolytes with oppositely charged colloids,” *Adv. Colloid Interface Sci.*, vol. 167, no. 1–2, p. 24–37, 2011.

[37] T.-Y. D. Tang, C. R. C. Hak, A. J. Thompson, M. K. Kuimova, D. S. Williams, A. W. Perriman and S. Mann, “Fatty acid membrane assembly on coacervate microdroplets as a step towards a hybrid protocell model.,” *Nat. Chem.*, vol. 6, no. 6, p. 527, 2014.

[38] D. S. Williams, S. Koga, C. R. C. Hak, A. Majrekar, A. J. Patil, A. W. Perriman and S. Mann, “Polymer/nucleotide droplets as bio-inspired functional micro-compartments,” *Soft Matter*, vol. 8, no. 22, p. 6004, 2012.

[39] B. Mohanty, V. Aswal, P. Goyal and H. Bohidar, “Small-angle neutron and dynamic light scattering study of gelatin coacervates,” *Pramana*, vol. 63, no. 2, pp. 271-276, 2004.

[40] D. M. Pickup, R. J. Newport, E. R. BArney, J.-Y. Kim, S. P. Valappil and J. C. Knowles, “Characterisation of phosphate coacervates for potential biomedical applications,” *Journal of biomaterials applications*, vol. 28, no. 8, pp. 1226-1234, 2014.

[41] C. Chai, J. Lee and Q. Huang, “The effect of ionic strength on the rheology of pH-induced bovine serum albumin/κ-carrageenan coacervates,” *Elsevier*, vol. 59, no. 1, pp. 356-360, 2014.

[42] S. Mann, “Systems of Creation: The Emergence of Life form Nonliving Matter,” *Accounts of Chemical Research*, vol. 45, no. 12, pp. 2131-2141, 2012.

[43] K. Ruiz-Mirazo, C. Briones and A. d. l. Escosura, “Prebiotic systems chemistry: new perspectives for the origins of life,” vol. 114, no. 1, p. 285–366, 2014.

[44] J. Crosby, T. Treadwell, M. Hammerton, K. Wasilakis, M. P. Crump, D. S. Williams and S. Mann, “Stabiliazation and enhanced reactivity of actinorhodin polyketide synthase minimal complex in polymer-nucleotide coacervate droplets,” vol. 48, no. 97, 2012.

[45] D. S. Williams, A. J. Patil and S. Mann, "Spontaneous structuration in coacervate-based protocells by polyoxometalate-mediated membrane assembly.," vol. 10, no. 9, 2014.

[46] T.-Y. D. Tang, C. C. Hak, A. J. Thompson, M. K. Kuimova, D. S.Williams, A. W. Perriman and S. Mann, "Fatty acid membrane assembly on coacervate microdroplets as a step towards a hybrid protocell model.," vol. 6, no. 6, 2014.

[47] D. A. Fletcher and R. D. Mullins, "Cell mechanics and the cytoskeleton," *Nature*, vol. 463, no. 7280, pp. 485-492, 2010.

[48] B. Wickstead and K. Gull, "The evolution of the cytoskeleton," *Journal of Cell Biology*, vol. 194, no. 4, pp. 513-525, 2011.

[49] M. Pilhofer, M. S. Ladinsky, A. W. McDowall, G. Petroni and G. J. Jensen, "Microtubules in Bacteria: Ancient tubulins build a five-protofilament homolog of the eukaryotic cytoskeleton," *PLoS Biology*, vol. 9, no. 12, 2011.

[50] M. Aridor and L. M. Traub, "Cargo selection in vesicular transport: the making and breaking of a coat," *Traffic*, vol. 3, no. 8, pp. 537-546, 2002.

[51] B. Alberts, A. Johnson and J. Lewis, Molecular Biology of the Cell. 4th edition., New York: Garland Science, 2002.

[52] B. Amsden, "Solute Diffusion within Hydrogels. Mechanisms and Models," *Macromolecules*, vol. 31, no. 23, pp. 8382-8395, 1998.

[53] S. Bai, X. Zhang, Q. Lu, W. Sheng, L. Liu, B. Dong and D. L. Kaplan, "Reversible Hydrogel − Solution System of Silk with High Beta-Sheet Content," *Biomacromolecules*, no. 15, pp. 3044-3051, 2014.

[54] M. Hamidi, A. Azadi and P. Rafiei, "Hydrogel nanoparticles in drug delivery," *Advanced Drug Delivery Reviews*, vol. 60, no. 15, pp. 1638-1649, 2008.

[55] K. Almdal, J. Dyre, S. Hvidt and S. Kramer, *Polym. Gels Networks*, vol. 1, p. 5, 1993.

[56] S. R. Raghavan and J. F. Douglas, *Soft Matter*, vol. 8, p. 8539, 2012.

[57] S. R. Raghavan and B. H. Cipiriano, Gel Formation: Phase Diagrams using Tabletop Rheology and Calorimetry, in Molecular Gels, Dordrecht: Springer, 2005.

[58] O. Wichterle and D. Lím, "Hydrophilic Gels for Biological Use," *Nature*, vol. 185, no. 4706, pp. 117-118, 1960.

[59] A. M. Mathur, S. K. Moorjani and A. B. Scranton, "Methods for Synthesis of Hydrogel Networks: A Review," *Journal of Macromolecular Science, Part C: Polymer Reviews,* vol. 36, no. 2, pp. 405-430, 1996.

[60] T. R. Hoare and D. S. Kohane, "Hydrogels in drug delivery: Progress and challenges," *Polymer,* vol. 49, no. 8, pp. 1993-2007, 2008.

[61] A. C. Jen, M. C. Wake and A. G. Mikos, "Review: Hydrogels for cell immobilization," *Biotechnology and Bioengineering,* vol. 50, no. 4, pp. 357-364, 1996.

[62] R. Krishna Kumar, X. Yu, A. J. Patil, M. Li and S. Mann, "Cytoskeletal-like Supramolecular Assembly and Nanoparticle-Based Motors in a Model Protocell," *Angewandte Chemie,* vol. 123, no. 40, pp. 9515-9519, 2011.

[63] R. K. Kumar, M. Li, S. N. Olof, A. J. Patil and S. Mann, "Artificial cytoskeletal structures within enzymatically active bio-inorganic protocells," *Small,* vol. 9, no. 3, p. 357–362, 2013.

[64] J. Dash, A. Patil, R. N. Das, F. L. Dowdall and S. Mann, "Supramolecular hydrogels derived from silver ion-mediated self-assembly of 5′-guanosine monophosphate," *Soft Matter,* vol. 7, no. 18, p. 8120, 2011.

[65] Y. Yin, L. Niu, X. Zhu, M. Zhao, Z. Zhang, S. Mann and D. Liang, "Non-equilibrium behaviour in coacervate-based protocells under electric-field-induced excitation," *Nature Communications,* vol. 7, p. 10658, 2016.

[66] J. F. Berret, "Local viscoelasticity of living cells measured by rotational magnetic spectroscopy," *Nat. Commun.,* vol. 7, p. 1–9, 2016.

[67] L. Cronin, N. Krasnogor, B. G. Davis, C. Alexander, N. Robertson, J. H. G. Steinke, S. L. M. Schroeder, A. N. Khlobystov, G. Cooper, P. M. Gardner, P. Siepmann, B. J. Whitaker and a. D. Marsh, "The imitation game - A computational chemical approach to recognising life," *Nature Biotechnology,* vol. 24, no. 10, pp. 1203-1206, 2006.

[68] R. Lentini, N. Y. Martín, M. Forlin, L. Belmonte, J. Fontana, M. Cornella, L. Martini, S. Tamburini, W. E. Bentley, O. Jousson and S. S. Mansy, "Two-Way Chemical Communication between Artificial and Natural Cells," *ACS Cent. Sci.,* vol. 3, no. 2, pp. 117-123, 2017.

[69] S. Elmore, "Apoptosis: A Review of Programmed Cell Death," *Toxicol. Pathol,* vol. 35, no. 4, p. 495–516, 2007.

[70] A. H. Wyllie, A. A. R. Currie and J. F. R. Kerr, "Apoptosis: a Basic Biological Phenomenon With Wide- Ranging Implications in Tissue Kinetics," *J. Intern. Med.,* vol. 258, no. 6, p. 479–517, 1972.

[71] G. Ichim and S. W. G. Tait, "A fate worse than death: Apoptosis as an oncogenic process," *Nat. Rev. Cancer,* vol. 16, no. 8, p. 539–548, 2016.

[72] D. K. a. R. Losick, "How and why bacteria talk to each other," *Cell,* vol. 73, no. 5, p. 873–885, 1993.

[73] F. J. Slonczewski JL, Microbiologu: an Evolving Science, New York: WW Norton, 2013.

[74] W. C. Fuqua, S. C. Winans and E. P. Greenberg, "Quorum sensing in bacteria: The LuxR-LuxI family of cell density- responsive transcriptional regulators," *J. Bacteriol.,* vol. 176, no. 2, p. 269–275, 1994.

[75] S. T. Rutherford, B. L. Bassler, C. S. Hayes, S. Koskiniemi, C. Ruhe, H. Ben-tekaya and J. Gorvel, "Bacterial Quorum Sensing : Its Role in Virulence and Possibilities for Its Control," *Cold Spring Harbour: Perspectives in Medicine,* vol. 2, no. 11, pp. 1-26, 2012.

[76] M. M. T and M. J. M, Brock Biology of Microrganisms 11th Ed., Pearson Prentice Hall, 2006.

[77] S. T. Rutherford, B. L. Bassler, C. S. Hayes, S. Koskiniemi, C. Ruhe, H. Ben-tekaya and J. Gorvel, "Bacterial Quorum Sensing : Its Role in Virulence and Possibilities for Its Control," *Cold Spring Harbour Perspectives in Medicine,* vol. 11, no. 2, pp. 1-26, 2012.

[78] S. Sun, M. Li, F. Dong, S. Wang, L. Tian and S. Mann, "Chemical Signaling and Functional Activation in Colloidosome-Based Protocells," *Small,* vol. 12, no. 14, p. 1920–1927, 2016.

[79] C. D. Keating, "Gated access to microreactors," *Nat. Publ. Gr.,* vol. 5, no. 6, p. 449–451, 2013..

[80] D. S. Williams, A. J. Patil and S. Mann, "Spontaneous structuration in coacervate-based protocells by polyoxometalate-mediated membrane assembly," *Small,* vol. 10, no. 9, p. 1830–1840, 2014.

[81] B. Alberts, Molcular Biology of the Cell (4th Ed.), New York: Garland, 2002.

[82] G. Michel, T. Tonon, D. Scornet, J. M. Cock and a. B. Kloareg, "The cell wall polysaccharide metabolism of the brown alga Ectocarpus siliculosus. Insights into the evolution of extracellular matrix polysaccharides in Eukaryotes," *New Phytol.,* vol. 188, no. 1, pp. 82-97, 2010.

[83] Y. R. RC, "Electron microscope studies of surface pili and vesicles of Salmonella 3,10:r:- organisms.," *Indian Journal of Animal Sciences,* vol. 63, no. 1, pp. 99-102, 1993.

[84] G. Michel, T. Tonon, D. Scornet, J. M. Cock and B. Kloareg, "The cell wall polysaccharide metabolism of the brown alga Ectocarpus siliculosus. Insights into the evolution of extracellular matrix polysaccharides in Eukaryotes," *New Phytologist,* vol. 188, no. 1, pp. 82-97, 2010.

[85] J. Gllagher and M. Lyon, "Molecular structure of Heparan Sulfate and interactions with growth factors and morphogens," in *Proteoglycans: structure, biology and molecular interactions,* New York, Marcel Dekker Inc., 2000, pp. 27-59.

[86] H. Lodish, A. Berk, P. Matsudaira, C. Kaiser, M. Krieger, M. Scott, S. Zipursky and J. Darnell, "Integrating Cells into Tissues," in *Molecular Cell Biology*, New York, WH Freeman and Company, 2003, pp. 197-234.

[87] P. G, "The extracellular matrix and cell adhesion," in *Cells*, Sudbury MA, Jones and Bartlett, 2007.

[88] L. Huleihel, G. S. Hussey, J. D. Naranjo, L. Zhang, J. L. Dziki, N. J. Turner, D. B. Stolz and S. F. Badylak, "Matrix-bound nanovesicles within ECM bioscaffolds," *Science Advances* , vol. 2, no. 6, 2016.

[89] B. Kern, J. Shen, M. Starbuck and G. Karsenty, "Cbfa1 contributes to the osteoblast-specific expression of type I collagen genes," *Journal of Biological Chemistry*, vol. 276, no. 10, pp. 7101-7107, 2001.

[90] A. Engler, S. Sen, H. Sweeney and D. Discher, "Matrix elasticity directs stem cell lineage specification," *Cell*, vol. 126, no. 4, pp. 677-689, 2006.

Chapter 2 : Experimental Materials and Methods

Abstract

Herein described are the materials and methods used to undertake the experiments described in chapters 3, 4, and 5. This includes brief overviews of the experimental techniques and how they function.

2. Experimental Materials and Methods

2.1 Materials

2.1.1 Poly(diallyldimethylammonium chloride) decanoic acid coacervate system

8.5 kDa poly(diallyldimethylammonium chloride) (PDDA, Polysciences, Inc.), decanoic acid (DA, Sigma-Aldrich), glucono-δ-lactone (GDL, Sigma-Aldrich), sodium chloride (NaCl, Sigma-Aldrich), sodium hydroxide (NaOH, Sigma-Aldrich), hydrogen chloride (HCl, Sigma-Aldrich), diallyldimethylammonium chloride(DADMAC, Sigma-Aldrich), diallylamine (DAA, Sigma-Aldrich), 1-pyrenecarboxaldehyde (PYCA, Fluka Analytical), 2,2' azobis(2 methylproionamidine)dihydrochloride (Sigma-Aldrich), fluorescein isothiocyanate (FITC, Sigma-Aldrich), 4,4-difluoro-5-(2-thienyl)-4-bora-3a,4a-diaza-s-indacene-3-dodecanoic acid (BODIPY C12, Life technologies), sulforhodamine 101 acid chloride (Texas Red, Life technologies), hydroxypyrene trisulfonic acid (HPTS, Sigma-Aldrich), poly(etheyleneglycol) (PEG; Sigma-Aldrich); Acridine Orange (Sigma-Aldrich); green fluorescent protein (GFP, expressed in house, using BL21 competent Escherichia coli, transformed with the plasmid vector pET45b(+) (Novagen, Germany). The bacteria were cultured in LB medium with carbenicillin (Apollo Scienti・c, UK) and expression was induced using isopropylthiogalactosidase (Apollo Scienti・c, Japan). A Polytron PT2500 homogenizer (Kinematica, Germany) was used to lyse the bacteria in a pH 8 lysis buffer containing 50 mM NaH2PO4, 300 mM NaCl, 10 mM imidazole and 200 mM phenylmethanesulphonyl ・uoride. The lysate was puri・ed using nickel nitriloacetic acid (Qiagen,UK) then dialysed into deionized water using 12–14 kDa molecular weight cut-off dialysis tubing (Medicell International, UK)); enhanced green fluorescent protein (eGFP, expressed in house); dextran 40 kDa (Sigma-Aldrich, tagged with fluorescein isothiocyanate in house); single stranded deoxyribosenucleic acid 7.6 kDa tagged with cyanine 5 (ssDNA-cy5, 5/-Cy5-ACCACTGAGATCCGGCTGCTAA-3/, Eurofins Genomics); 9-diethylamino-5-benzo[α]phenoxazinone (Nile Red, Sigma-Aldrich), sp3 hybridised carbon

nanodots (synthesised in house from cellulose *via* microwave by Noha Abu El Magd), were purchased and used without further purification.

2.1.2 Poly(allylamine hydrochloride) guanosine monophosphate coacervate system

Guanosine Monophosphate (GMP, Life Technoliges) ; 15 kDa Poly(allylamine hydrochloride) (PAH, Sigma-Aldrich) ; hydrogen chloride (HCl, Sigma-Aldrich); sodium hydroxide (NaOH, Sigma-Aldrich); silver nitrate ($AgNO_3$, Sigma-Aldrich); sodium chloride (NaCl, Sigma-Aldrich); hexamethyldisilizane (HMDS, Sigma-Aldrich); poly(etheyleneglycol) (PEG; Sigma-Aldrich); Acridine Orange (Sigma-Aldrich); and Hoechst 33258 (Sigma-Aldrich) were purchased and used without further purification.

2.2 Methods

2.2.1 Coacervate synthesis

2.2.1.1 Synthesis of PDDA/DA Coacervates

Equal volumes, 100 µL, of a 10 mM (monomeric concentration) 8.5 kDa PDDA solution at pH 9, adjusted with 100 mM hydrochloric acid sodium hydroxide solutions, and a 160 mM DA solution at pH 9, were mixed in a 1.5 mL Eppendorf tube at 25 °C to form a turbid suspension of coacervate droplets. The sample was then centrifuged at 13,200 rpm for 5 minutes to facilitate the separation of supernatant and bulk phases as can be seen in Figure 2.1. Samples were then redispersed by hand using a micropipette to generate microdroplets in a suspension of the low-polymer supernatant phase. All solutions were made with Milli-Q Pure deionised water (18.2 MΩ) dispensed from a Milli Q helix integral 3 filtration system.

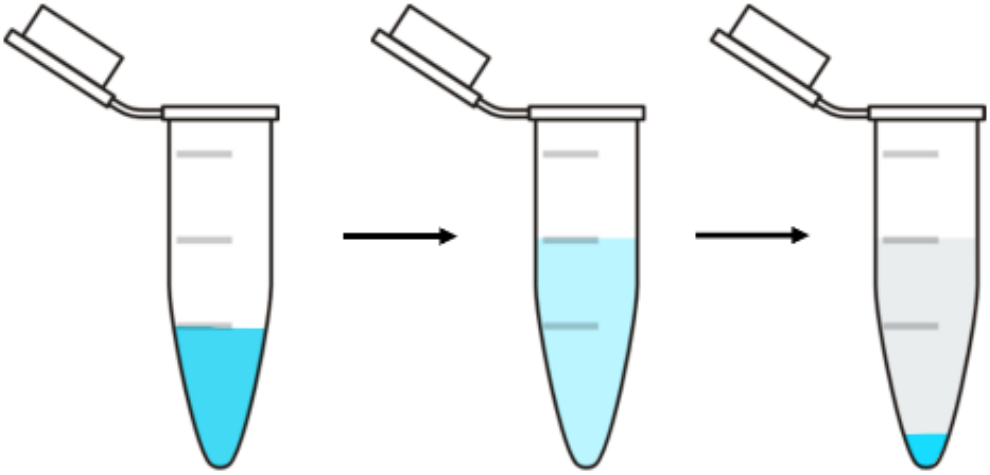

Figure 2.1: A cartoon of the coacervate synthesis beginning on the left with a transparent polymer solution. The second component is added yielding a turbid system which is then centrifuged to separate the coacervate, condensed polymer phase, seen as the blue pellet in the bottom of the rightmost Eppendorf with the transparent continuous phase above.

2.2.1.2 Synthesis of PAH/GMP Coacervates

A 100 µL aliquot of a 10 mM 15 kDa PAH at pH 0.5 solution was mixed with a 100 µL aliquot of a 16 mM GMP at pH 0.5 solution in a 1.5 mL Eppendorf centrifuge tube at 25 °C to form a turbid suspension of coacervate droplets. The sample was then centrifuged at 13,200 rpm for 5 minutes to facilitate the formation of a bulk polymer rich phase at the bottom of the Eppendorf tube. Samples were then redispersed by hand using a micropipette to generate microdroplets in a suspension of the low-polymer supernatant phase.

A 200 mM PAH solution was prepared at pH 7 and a 14 mM GMP solution was prepared at the same concentration. 1:1 Charge matched coacervates were formed via mixing equal volume aliquots of these two solutions together. All solutions were made with Milli-Q Pure deionised water.

2.2.1.3 Synthesis of coacervates under acoustic pressure

The synthesis of coacervates was undertaken in an acoustic trap to investigate the ability of the system to spatially organised and to determine the effects of the acoustic pressure upon the interplay between polymer interactions and osmotic pressure in vesicle growth in response to pH adjustment with GDL.

Acoustic trapping functions on the principle that sound, when passing from a medium of one density to another medium of sufficiently different density the wave front will scatter and impart momentum to the medium which it is scattering against. This was first modelled by King and later formalised by Gor'kov [1] [2]. The expression that describes the potential within the acoustic field is given by Equation 2.1.

$$U = 2\pi R^3 [\left(\frac{\overline{p_{in}^2}}{3\rho c^2}\right) f_1 - \left(\frac{\overline{v_{in}^2}}{2}\right) f_2]$$

Equation 2.1: The Gor'kov potential. Where $\overline{p_{in}^2}$ and $\overline{v_{in}^2}$ are the mean-square fluctuations of the pressure and velocity experienced by the particle within the field, R is the radius of the trapped particle ρ is the density of the fluid, and c is the speed of sound in the trapping medium e.g. air or water and the factors f_1 and f_2 are given by $f_1 = 1 - \rho c^2/\rho_s c_s^2$ and $f_2 = 2(\rho_s - \rho)/(2\rho_s + \rho)$ where ρ_s is the density of the particle and $c_s$is the speed of sound in the particle being trapped [3].

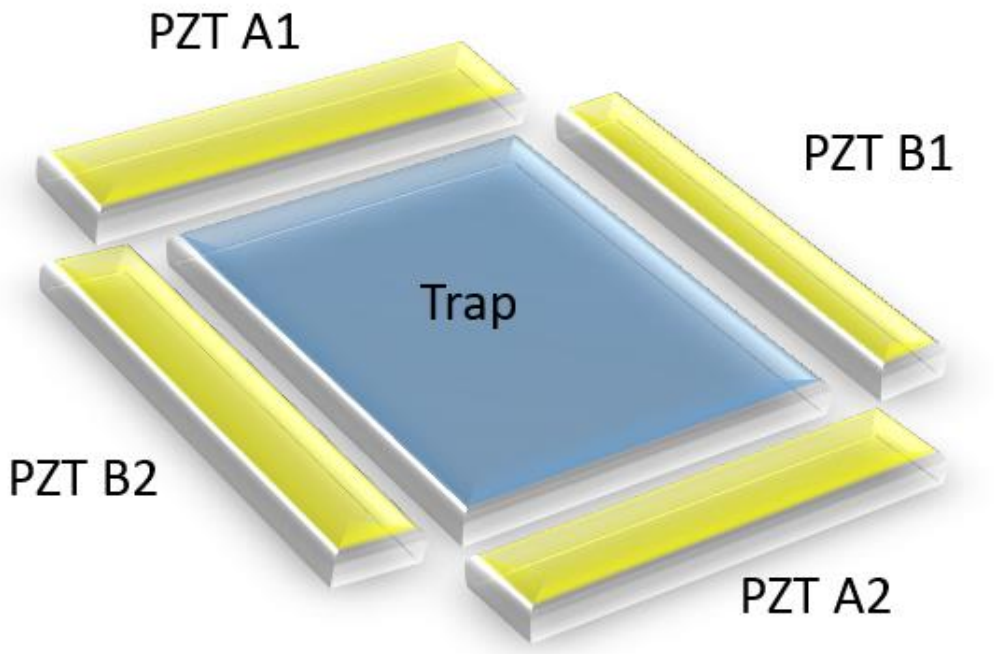

Figure 2.2: A cartoon of the paired sets of piezoelectric to make the acoustic trap with rectilinear spatial patterning. PZT A1 and A2 are paired and B1 and B2 are paired.

The acoustic trap was manufactured in-lab by Ms. Madeleine Nichols and the acoustic field was driven by a pair of signal generators, Agilent 33220a-001. The resonant frequency was 6.7 MHz and the peak voltage was set to 10 V. The pair were driven at, and just below, their resonant frequencies to generate a temporally uncorrelated field that produced a square field with 100 × 100 μm spacing. The configuration used can be seen in Figure 2.2.

2.2.2 Polymer synthesis

The synthesis of PDDA-co-DAA was undertaken to generate a fluorescent analogue of PDDA to be used in fluorescent microscopy experiments. The diallyldimethylammonium chloride monomer, the basic unit of the PDDA polymer chain, can be co-polymerised with diallylamine (DAA) to produce a similar polymer to PDDA which possesses amine groups. This can be achieved without affecting the structure of the PDDA chain greatly if synthesised at a low ratio

of DAA to DADMAC molecules. These amine groups can then be attacked, by nucleophilic addition, by amine-reactive dyes such as fluorescein isothiocyanate to produce a fluorescently tagged polymer that can be tracked using fluorescent microscopy.

Figure 2.3 shows the synthesis route for generating the new copolymer. The ratio of m : n, in effect diallyldimethylamonium monomer units to diallylamine monomer units, was set to 100 : 1 by molar ratio. This ratio was chosen to preserve the majority of the PDDA functionality within the coacervation process, in effect to minimise any interference to the system caused by the presence of a covalently bonded chromophore.

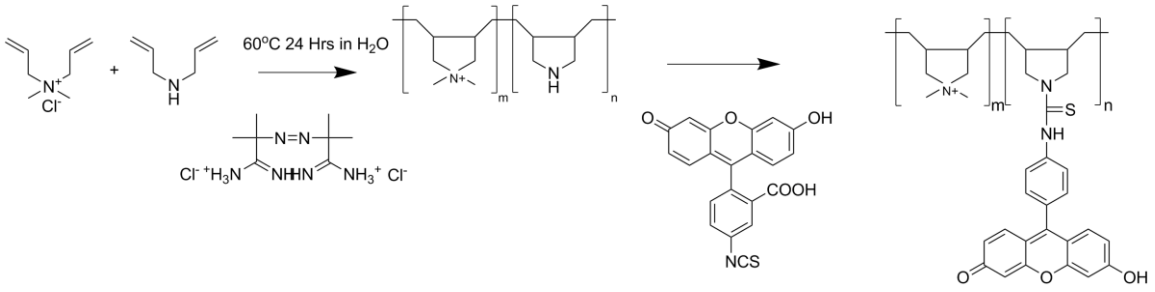

*Figure **2.3**: The synthetic route towards a functionalisable PDDA chain: PDDA-co-DAA. The polymer synthesis proceeds via a free radical polymerisation. The initiator, 2,2'-azobis(2-methylproionamidine)dihydrochloride, decomposes to form two radical initiators. These radicals then attack the double bonds on the DADMAC and DAA monomers to form further radical sites which propagates the chain growth. Termination occurs when two chains combine, or radical disproportionation occurs, abstracting a proton from one chain to another. Synthesis adapted from [4].*

Diallyldimethylammonium chloride (DADMAC) was prepared at 70 %wt in an aqueous solution. Diallylamine was then added to a final concentration of 26 mmol, the pH of the solution was then adjusted to pH 3 using 1 M HCl. 30 mg of 2,2'-azobis(2-methylproionamidine)dihydrochloride was then added to the solution and sealed within a round-bottom flask. N_2 was then bubbled through the solution for half an hour, to remove any oxygen from solution and atmosphere, and then sealed under positive pressure. The reaction then proceeded under N_2 at 60 °C for 24 hours.

700 µL of the solution was lyophilised: placed in a 15 mL centrifuge tube, placed in liquid nitrogen for 10 minutes and then held under vacuum and allowed to return to room temperature for 24 hours. The solution was rehydrated using deuterated water, D_2O, and then inspected using NMR. A Varian 400 machine was used, ^1H spectroscopy, with 256 cycles and 2 second relaxation period, was then conducted to determine whether the polymerisation was successful.

The solution was then transferred to an Amicon 2 mL centrifuge molecular weight filter. 100, 50 and 10 kDa weight filters were used to obtain PDDA-co-DAA within the 10-50 kDa range. The system was functionalised with fluorescein isothiocyanate by dissolving 12 mg of fluorescein isothiocyanate in 1.3 mL of ethanol and 1 mL of this solution was then added to the PDDA-co-DAA solution. The pH was then adjusted to 9 using a sodium borate buffer solution, comprising boric acid and NaOH, and left for 24 hours at room temperature in the dark. The resulting solution was dialysed against deionised water and then lyophilised and re-dispersed in deionised water.

2.2.3 Characterisation

2.2.3.1 Circular Dichroism

Circular dichroism (CD) makes use of the difference in absorption of left-handed and right handed circularly polarised light [5] by compounds that possess a chiral centre or form larger structures, as in the case of proteins and secondary and tertiary structures such as alpha helices, which have a helicity and absorb the corresponding handedness of light. This can be defined by the following correspondence:

$$Circular\ Dichroism = \ \Delta A(\lambda) = A(\lambda)_{LCPL} - A(\lambda)_{RCPL}$$

*Equation **2.2:** Circular dichroism: Where $\Delta A(\lambda)$ is the difference between the absorption on lefthanded circularly polarised light $(A(\lambda)_{LCPL})$ and righthanded circularly polarised light $(A(\lambda)_{RCPL})$*

In more detail; the origin of circularly polarised light arises from a phase difference between two linearly polarised light beams. Light can be linearly polarised by allowing its passage through a filter that removes all orientations of the electromagnetic field that oscillate outside of the given plane, for instance either horizontally or vertically [6]. To generate circularly polarised light from this, two sources of linearly polarised light are produced such that their electromagnetic oscillations interfere. If the phase of the maxima and minima of these oscillations are out by $\frac{\pi}{4}$, in effect, the geometric difference between the peak of one waves cycle and the peak of the next is out by 90° then the lights pointing vector, the dot product of its electric and magnetic fields will rotate either clockwise or anti-clockwise, also known as the handedness of the now circularly polarised light, as seen in Figure 2.4. This phase adjustment is accomplished using a quarter plate which is comprised of a birefringent material and so slows down one of linearly polarised light waves.

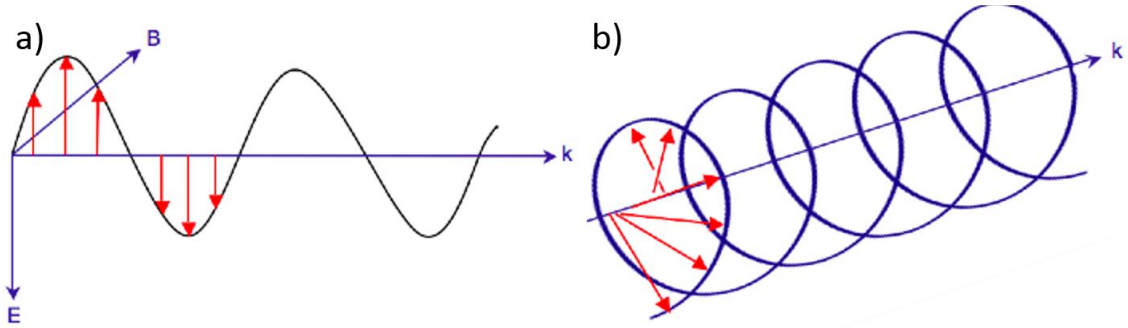

*Figure **2.4:** a) linearly polarised light with perpendicular electric (E) and magnetic (B) fields, b) circularly polarised light rotating in a left-handed fashion. Cartoons courtesy of Wikimedia commons user RASnyder released to the public domain.*

Circular birefringence, the chemical property that allows matter to interact with circularly polarised light in this fashion, occurs because of an anisotropy of the electronic configuration of the compound such that when it interacts with the electronic component of the light field it produces an anisotropic effect, in effect it possesses a different refractive index depending on the polarization that is passing through it. This is commonly observed using a polarimeter which measures the optical rotation.

Circular dichroism experiments were undertaken to measure the helicity of hydrogel fibrils formed upon addition of silver nitrate to the PAH/GMP coacervate suspensions. CD spectra were recorded at room temperature using a JASCO J-810 spectrometer through two quartz plates. Samples were prepared by spreading hydrogels (ca. 10 µL) between two quartz plates to produce a homogeneous film and to reduce scattering of light by the hydrogel sample. 5 scans at 50 $nmmin^{-1}$ were performed on each sample.

2.2.3.2 Differential Scanning Calorimetry

Differential scanning calorimetry (DSC), is a technique that measures the amount of heat required to keep the temperature difference between a sample and a reference negligible as the temperature is changed over various scans [7]. This is done to determine the presence of any phase changes in the sample, which will require either more, or less heat, to change the temperature of the sample than that of the reference. Endothermic phase changes will thus result in more heat being supplied to the sample whereas exothermic phase changes will require less. As a result, transition temperatures and heat capacities of materials can be measured to a high degree of accuracy using this technique.

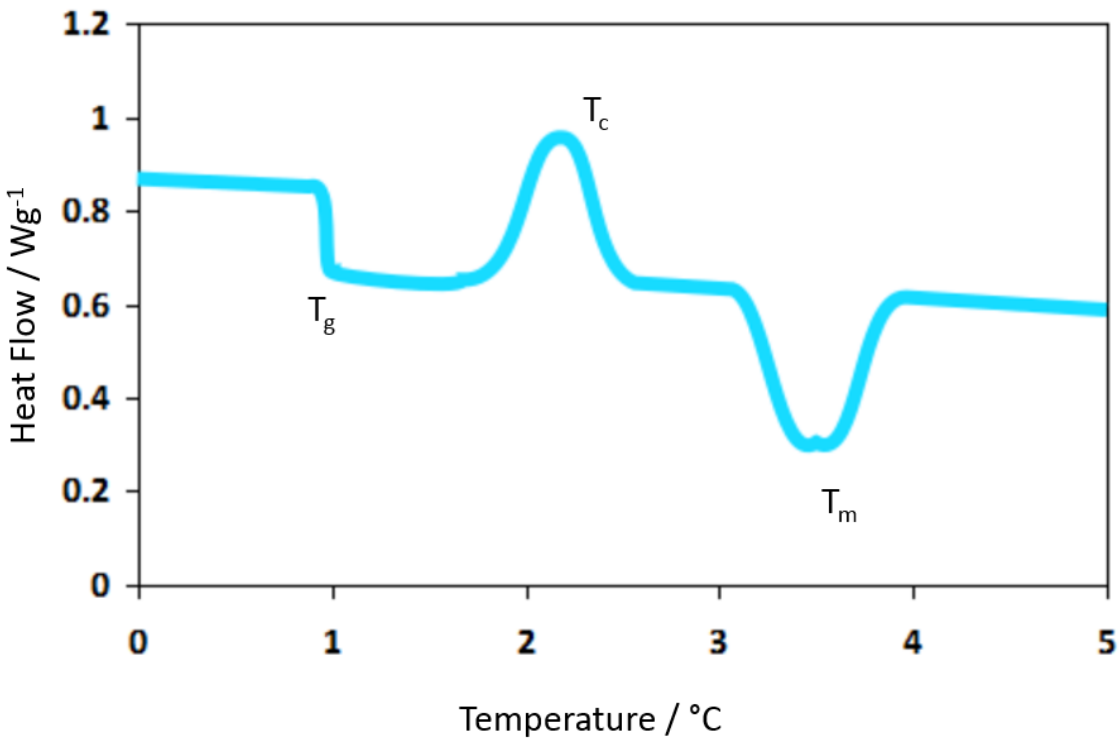

*Figure **2.5:** An exemplar DSC output graph illustrating endothermic and exothermic phase transitions. T_g and T_m, the glass transition and melting transition points respectively, are both exothermic and so heat flow required to change the temperature of the sample uniformly with respect to the sample pan decreases. The T_c, the crystallisation phase transition, is endothermic, and thus more energy is required to uniformly change the temperature of the sample with respect to the reference. Thus, various phase transitions can easily be determined using this technique.*

DSC was used to determine whether a gel phase had been formed upon addition of the silver nitrate to the coacervate suspension. Measurements were conducted on a Thermal Instruments DSC Q100 using aluminium hermetic pans. Samples were loaded at ca. 10 mg and measured against an air reference sample. Samples were then cycled from 20 – 90 °C six times and the curve of heat flux versus temperature recorded.

2.2.3.3 Transmission Electron Microscopy

Transmission electron microscopy (TEM) is a technique used to observe micro- to nano-structures with very fine resolution using the ability of electrons to be transmitted through samples. This

electron path can be seen in Figure 2.6. This is done as the limit with conventional light microscopy is defined by:

$$d = \frac{\lambda}{2n \sin \alpha}$$

*Equation **2.3:** Braggs' Law. Where d is equal to the feature scattering the light of wavelength λ, at the maximum half-angle at which the light enters the lens α.*

With electrons, which behave like waves, this size limit is much smaller and so smaller objects will scatter the electrons but would not have scattered the light.

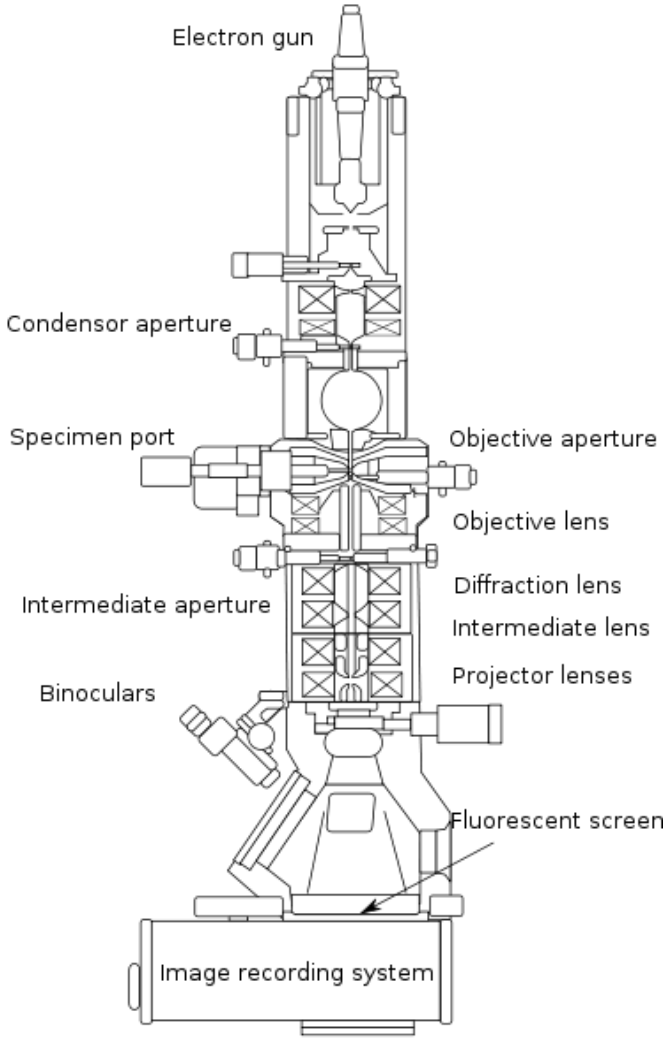

*Figure **2.6:** A cartoon illustrating the internal workings of a transmission electron microscope. An electron gun is used to generate a focused beam of energetic electrons which are focused, much in the same way that light is, by the condenser and aperture system that comprises the bulk of the apparatus. The electrons are then transmitted through the sample and areas that absorb the electrons are observed as dark patches. This cartoon is courtesy of Wikimedia commons user Gringer, released under the creative commons license.*

TEM was conducted on PAH/GMP samples after the addition of silver nitrate to observe the presence of any silver nanoparticles after UV photoreduction. Samples were dropcast onto carbon coated copper grids, manufactured in house, after a glow discharge procedure, also conducted in house, to prevent the samples from wetting out on the very hydrophilic surface. Samples were

dried overnight and loaded into a JEOL 1400 TEM instrument and the resulting micrographs were recorded.

2.2.3.4 Atomic Force Microscopy

Atomic force microscopy (AFM) is a technique that utilises an atomically fine probe to map the topography of a surface [9]. The atomically fine tip, usually composed of a conductive metal, is made via chemical etching and uses capillary forces to generate a one atom wide tip. This tip is then held in a cantilever which is rastered back and forth across the surface which is being investigated. This surface is usually atomically flat, Mica, a form of phyllosilicate, is usually sheared using adhesive tape and the chosen material that is being investigated is deposited on the surface and solvent is removed via drying. The sample then consists of the topographically interesting sample on a very flat surface of Mica. This is then loaded into the AFM at which point the atomically thin probe is lowered onto the surface, the vertical translation of the tip, in response to changes in surface height of the sample, is measured via laser light reflected from the back of the probe onto a four-point diode detector as can be seen in Figure 2.7. In this manner a picture of the heights differences can be built up over many scans of the surface.

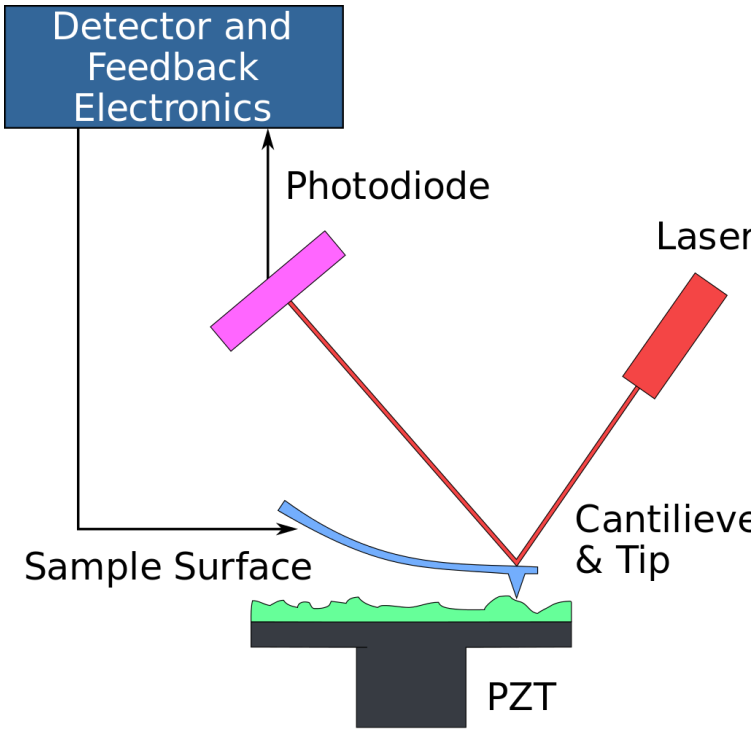

*Figure **2.7:** A cartoon illustrating the interaction of the AFM probe with the surface that is being investigated. The cantilever tip, responds to surface height and the laser's deflection is measured by the photodiode and the information is processed by software on the instrument PC. The PZT is a piezoelectric motor which is a common material used to actuate the very small translations required for high resolution inspection of sample surfaces. Image courtesy of Wikipedia user Nobelium, released under the creative commons licence.*

A conducting material is used as other data can also be collected using this technique, such as local conductivity, surface charge, elemental composition, surface adhesion and mechanical stress and strain properties. AFM can also be used in conjunction with thiol chemistry to bond biological polymers to the needle tip to determine elastic constants and deformation hysteresis loops.

PeakForce atomic force microscopy (AFM) was conducted by Dr R Harniman in the Chemical Imaging Facility, University of Bristol, with equipment funded by EPSRC under Grant "Atoms to Applications" Grant ref. "(EP/K035746/1) using a Bruker PeakForce multimode 8 AFM instrument with Nanoscope V controller and Picoforce extender. PDDA/DA samples were

prepared and deposited onto freshly cleaved mica then allowed to settle for one hour before being dried with nitrogen. For samples that had had their pH adjusted, GDL was added to the drop cast coacervate suspension and allowed to mix for five minutes before being dried with compressed nitrogen. Using Bruker Nanoscope Analysis v1.8 the topology of the systems was determined.

For PAH/GMP Ag samples, PAH/GMP suspensions were again deposited onto freshly cleaved mica. This was followed by the addition of 1 μL of 1M $AgNO_3$ and the mixture was agitated by pipette to mix. The system was then left to settle in the dark for one hour and then blown dried with nitrogen. Samples were stored in the dark until measurement. Using Bruker Nanoscope Analysis v1.8 the average Young's Modulus, *E*, could be determined for a given area within the sample. A 500 × 500 nm selection was made, and the roughness tool used to find the average *E* of that selection. An area selection average was used to compensate for a systematic error in the measurements which gave highly domed artefacts a stiffer side than the other, this is seen by the appearance of an apparent shadow on the droplets.

2.2.3.5 Small Angle X-Ray Scattering

SAXS experiments require an x-ray source; usually an x-ray tube which utilises the phenomena of *bremsstrahlung*, or breaking radiation. *Bremsstrahlung* produces a spectrum of x-rays from the rapid deceleration of electrons fired and accelerated from an electron source, usually a hot metallic element. As the electrons are deflected from their paths by the presence of heavy nuclei the excess kinetic energy is emitted as electromagnetic (EM) radiation, the frequency of which lies within the region of the EM spectrum so as to be called X-rays. The heavy nuclei are present in the form of a metal plate at which the electrons are fired at. The type of metal which is used in the tube dictates the characteristic peaks observed in an x-ray tubes emission spectrum. Not all electrons fired at the plate will be deflected by the electrostatic repulsion of the other electrons present in the atom. Some will collide with these electrons giving them enough energy to escape their orbits.

Higher energy electrons will then drop down to replace the missing electrons and their excess energy will be emitted again as an x-ray. This generates a peak in emissions as this process is discrete, the same jump will always produce a photon of the same energy, across all atoms in the material. As such these peaks dwarf the intensity of the *bremsstrahlung*.

An alternative x-ray source is a synchrotron. Electrons are accelerated using an electric field and then passed through a magnetic field. The magnetic field causes a deflection in the path of the electron in a circular fashion, which is equivalent to acceleration. This produces x-rays normal to the direction of acceleration.

The x-rays produced by the tube are directed and collimated, a process whereby the direction of travel of photons is made parallel to one another, towards the sample being investigated. When the x-rays are incident upon the sample, the presence of electrons will once again produce scattering effects, Figure 2.8. This scattering then produces interference effects between the x-rays that are travelling past the sample towards the detector and it is the changes in intensity in space that are measured and used to determine the size and form of the particles responsible for the scattering.

Intensity is defined as a function of q which is related to the angle of scattering by simple geometry:

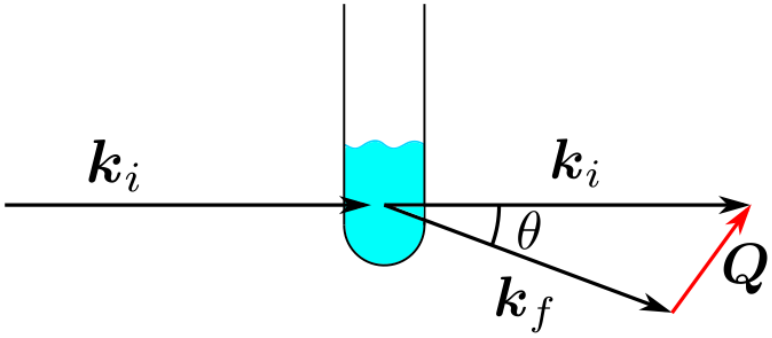

*Figure **2.8:** The diagram illustrates the vectors that describe the paths of the incident light, $\boldsymbol{k_i}$, the scattered light, $\boldsymbol{k_f}$, and the scattering vector **Q**.*

$$q = |\boldsymbol{k_i} - \boldsymbol{k_f}| = \frac{4\,\pi \sin\theta}{\lambda}$$

*Equation 2.4**:** The scattering Vector. Where q is the scalar value of the scattering vector, $\boldsymbol{k_i}$ is the incident photon vector, $\boldsymbol{k_f}$ is the scattered photon vector, λ is the wavelength of the photon being scattered and Θ is the angle at which the photon is scattered.*

This is then related to the intensity of scattering by:

$$I(q) = n_p \Delta\rho^2 V_p^2 P(q) S(q)$$

*Equation **2.5:** Intensity of Scattering. Where I(q) is the intensity of scattering as a function of q, n_p is the number density of particles per unit volume in the sample, Δρ is the scattering length density difference, V_p is the particle volume, P(q) is the intra-particle structure shape and S(q) is the inter-particle structure.*

Plots of *I(q)* vs *q* yield information as to the structure of the particles scattering the x-rays, and to the structure that they form together i.e. through aggregation or crystallisation.

2.2.3.5.1 PDDA/DA System

Coacervate suspension samples were prepared by mixing 100 µl of 160 mM DA and 100 µl 10 mM PDDA together. 80 mM DA control solutions were adjusted to pH 9, 7.5, and 5. Samples

were sealed within 1.5 mm quartz cuvettes supplied by Capillary Tube Supplies Ltd. using UV-curable glue, procured from Thor Labs, under 365 nm UV light.

Samples were loaded onto a rack and loaded into a SAXLAB GANESHA 300XL instrument in the School of Physics. Extremely small angle x-ray scattering (ESAXS, q range: 0.003 – 0.21 $Å^{-1}$) and medium angle x-ray scattering (MAXS, q range: 0.003 – 0.73 $Å^{-1}$) experiments were conducted upon the samples. Data was collected for three hours for ESAXS samples and for half an hour for MAXS samples.

The data was then processed using SAXSGUI software implemented in MatLab version 7.17 available online for free.

2.2.3.5.2 PAH/GMP System

Coacervate suspension samples were prepared by mixing 100 µL of 200 mM 15 kDA and 100 µL of 14 mM GMP, the pH was adjusted to 7 and they were sealed within 1.5 mm quartz cuvettes supplied by Capillary Tube Supplies Ltd. using UV-curable glue, procured from Thor Labs, under 365 nm UV light.

Samples were loaded onto a rack and loaded into a SAXLAB GANESHA 300XL instrument in the School of Physics. Extremely small angle x-ray scattering (ESAXS, q range: 0.003 – 0.21 $Å^{-1}$) and medium angle x-ray scattering (MAXS, q range: 0.003 – 0.73 $Å^{-1}$) experiments were conducted upon the samples. Data was collected for three hours for ESAXS samples and for half an hour for MAXS samples.

The data was then processed using SAXSGUI software implemented in MatLab version 7.17 available online for free.

2.2.3.6 Optical Microscopy

Optical microscopy relies upon the optical properties of lenses to enhance the apparent size of samples. The lens bends light due to the change in refractive index between the glass and the air at the interface between the lens and the air in the lab as can be seen in Figure 2.9. An optical microscope can also be equipped with a UV lamp which will allow for the light emitted by excited samples to be used to image the sample. Such microscopy is known as fluorescent microscopy and allows for the determination of location of fluorescent compounds within a sample. The resolution achievable from the micrographs captured via optical microscopy is dependent on the wavelength of light being used to illuminate the sample and pass through the lens.

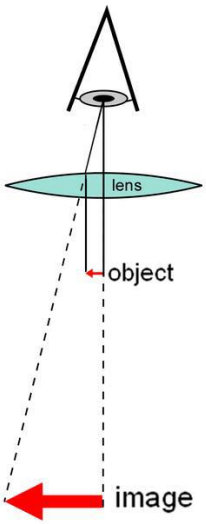

Figure 2.9 : A schematic of the apparent size of the object when viewed through the lens, or objective, of the microscope. Image courtesy of Wikipedia User: Fountains of Bryn Mawr, released under the creative commons licence.

Cross-polar microscopy was utilised by mounting a fixed horizontally polarised filter to the light source and placing another linearly polarised light between the sample and the camera aperture. The second filter could then be freely rotated to block all horizontally polarised light from passing

through. The presence of isotropic materials will not interact with the polarised light and so these samples will appear dark under cross-polar inspection. If there are birefringent materials present in the sample being inspected, then they will interact with the polarised light causing a rotation of the horizontally polarised light to become vertically polarised light and thus light will be observed.

Capillary slides were prepared using functionalised cover slips to prevent coacervate wetting on the glass surface. Functionalisation was undertaken via chemical etching with the use of Piranha solution, 1:4 parts H_2O_2:H_2SO_4, to enable the addition of 200 µL poly(ethyleneglycol) (PEG) (in 10 mL of toluene) to a pot containing the slides, which were left for 24 hours and then washes with deionised water and dried with compressed nitrogen. In the case of hexmethyldisilizane (HDMS) functionalisation, Piranha solution was again used to clean the glass slips which were then placed in a desiccator in 200 µL of HDMS overnight. In the case of varying MW PDDA functionalised slips, slips were washed thoroughly in deionised H_2O and ethanol and then left in baths of the PDDA solutions, these were left to electrostatically attach for 2 hours and then washed with deionised H_2O and dried with compressed nitrogen.

Channel slips were then made by attaching functionalised slips on top of two non-functionalised slips with UV glue on top of a microscope slide to generate a 10 mm channel. Approximately 65 µL of the coacervate suspensions were then placed inside the channel and then observed using a Leica DMI3000B inverted optical microscope with variable wavelength ultra-violet (UV) lamp attached. Brightfield, phase-contrast and fluorescence images were captured. Fluorescence microscopy filters wheel fitted are described in Table 2-1.

Table 2-1: the excitation and emission cut off wavelengths used in fluorescence microscopy.

Position	*Values*	*Fluorescence*	*Excitation*	*Emission Cut off*
1	I3	Blue	450-490	510
2	N2.1	Green	515-560	580
3	D	Violet	355-425	455
4	A	UV	340-380	400

Confocal microscopes were also used to image the coacervate droplets (Leica SP5 confocal; woolfson Bio-imaging Facility), to capture fine fluorescence intensity decay data to confirm gelation kinetics. All microscopy was undertaken under standard conditions: 1 atm and 25 °C.

Size data of the coacervate was extracted by applying a shape filter to the images captured using ImageJ (Available for free online). The drawings produced, as can be seen in Figure 2.10, could then be measured using a built-in macro for detecting circles.

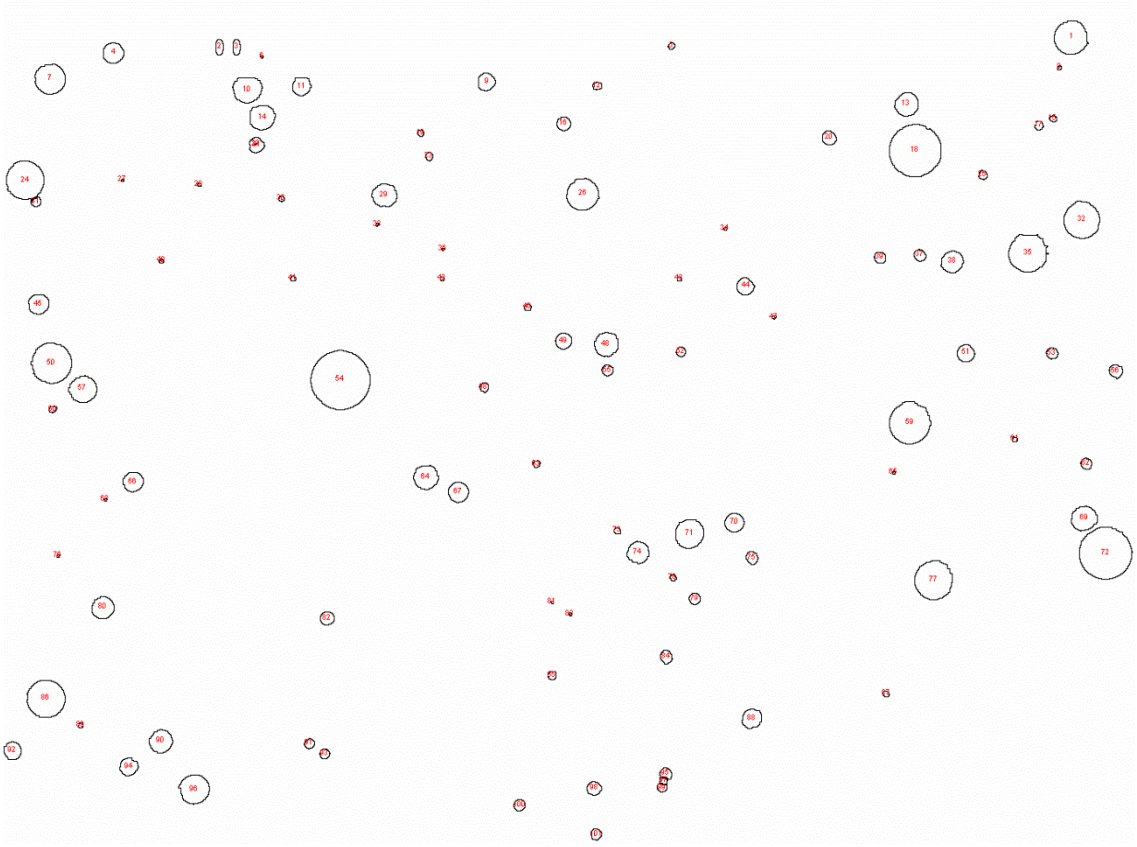

Figure 2.10: An example drawing of the optical micrograph after being processed in ImageJ with a circular filter, objects are identified as being circular and their perimeter is identified. The circles can then be measured, and the data analysed to determine the average diameters.

2.2.3.7 Ultra Violet -Visible Light Spectroscopy

UV-vis absorption spectroscopy is a method used to relate the absorbance of a given wavelength with the concentration of a chemical compound present in solution. Conversely the presence of a chemical compound in a solution, its production or consumption during a reaction, can also be determined using this method. The absorption of light is related to the concentration of the compound by the beer-lambert law as follows:

$$A = log_{10}\left(\frac{I}{I_0}\right) = \varepsilon C l$$

Equation 2.6: Beer-Lambert Law. Where A is absorption, I_0 is the intensity of transmitted light, I is the intensity of incident light, ε is the molar absorptivity of the compound, C is the concentration of the compound, and l is the path length of the sample.

Light is absorbed by the compound if the energy of the light ($E = hf$ where E is the energy of the photon, h is Planck's constant and f is the frequency of the photon) is commensurate with the energy gap between the highest occupied molecular orbital (HOMO) and lowest unoccupied molecular orbital (LUMO).

Solutions of PDDA/DA were made by adding 500 µL of 80, 40, 20 and 5 mM PDDA to the cuvette and then an appropriate amount of water and 160 mM DA to form solutions of the ratios given in Table 2-2 to a final volume of 1 ml. Disposable 1.5 mL polymethylmethacrylate cuvettes and a Perkin Elmer Lambda 25 spectrophotometer were used to determine the turbidity of the samples.

Table 2-2: The various concentrations used to determine the critical coacervation concentration.

[PDDA] / mM	**[DA] / mM**
5	5 - 80
20	5 - 80
40	5 - 80
80	5 - 80

DA concentration was increased by 1 mM per measurement by mixing fresh solutions of PDDA and DA. An absorbance scan monitoring the 500 nm transmission peak was recorded. This was repeated three times for each ratio of PDDA : DA.

To determine the point at which coacervation occurred, in effect the minimal amount of DA required for coacervate microdroplets to be formed, turbidimetric measurements were conducted. Ultra-violet visible light spectroscopy (UV-VIS) was used to determine the concentration at which coacervation occurs for various PDDA concentrations. Turbidimetry was then used to determine the point of coacervation utilising the following formula:

$$\textit{Turbidimetry} = 100 - \%T$$

Equation 2.7: Turbidimetry. Where %T is the transmitted radiation through the sample.

As the concentration of decanoic acid (DA) is increased within the sample it was expected that the turbidity of the sample would increase rapidly at the point of coacervation. No light absorbing aggregates should form before this point as the samples were prepared at pH 9 and therefore only micelles should exist, these are too small to scatter visible light, and the polymer solution is transparent at this point.

A NaCl solution was prepared at 1 M concentration and 1µL aliquots were added to the coacervate sample until the sample became transparent and an opaque white sediment was observed at the bottom of the cuvette. The turbidity of the system was monitored by measuring the absorbance at 500 nm.

2.2.3.8 Energy dispersive X-Ray Spectroscopy

Energy dispersive X-Ray spectroscopy (EDX) is an analytical technique used to determine the elemental composition of a sample via characteristic X-rays emitted from atomic elements when

electrons fill vacant K-orbitals with a lower energy, which have been made vacant by stimulation with high energy X-ray beams [11]. As an electron drops into the lower K shell, it will lose a discrete quantum of energy, this energy corresponds to the total potential and kinetic energy difference between the two orbitals. This energy is then emitted from the sample in the form of an X-ray and the emission spectrum recorded by the instrument will be possess very characteristic peaks corresponding to the energy of the x-rays produced by the element. These peaks are unique and as such this is a powerful technique for elemental analysis.

The PAH/GMP samples that were prepared for TEM were also subjected to EDX analysis. The Jeol 1400 TEM is equipped with an EDX x-ray source Oxford Instruments ISIS 300 system with a silicon detector.

2.2.3.9 Nuclear Magnetic Resonance Spectroscopy

This technique makes use of a strong magnetic field and its ability to change the spin of atoms [12]. This effect can only be exploited that possess nuclear spin (S) = $\frac{1}{2}$. As the atoms nucleus spins, which is charged, it produces a magnetic field that possesses a magnetic moment. When this magnetic moment is exposed to an external field the population of spins will evolve into two populations, either aligned or anti-aligned. These two populations possess different energies and this energy difference can be described as follows:

$$\Delta E = \gamma \hbar \beta_0$$

*Equation **2.8:** Transition Energy. Where ΔE is the difference in energy, γ is the gyromagnetic ratio (a characteristic property of the nucleus), ħ is the reduced Planck's constant ($\hbar = \frac{h}{2\pi}$), and β_0 is the applied magnetic field.*

Absorption occurs if the frequency of the applied radio electromagnetic radiation is commensurate with the energy gap between the two, spin aligned, or anti-aligned, populations. Furthermore, this resonant frequency can be modified by the interaction of electrons orbiting the nuclei, which also produce a magnetic field, and this can yield information about the arrangement of these nuclei in space. This absorbance is compared with a standard reference sample and the shift in field strength is described by the chemical shift (δ) in parts per million (ppm):

$$\delta = \frac{\nu - \nu_{TMS}}{\nu_0}$$

*Equation **2.9**: Chemical Shift. Where ν is the resonance frequency of the nucleus, ν_{TMS} is the resonant frequency of the reference sample (commonly tetramethyl silane), and ν_0 is the operating frequency of the NMR instrument.*

All proton NMR measurements were conducted in D_2O on a Varian 400 MHz instrument, with a 64 scan, 30 second relaxation period and at standard temperature and pressure, in effect 25 °C and 1 ATM.

All phosphorous NMR measurements were conducted in D_2O on a Varian 500 MHz instrument for one scan with a 30 second relaxation period and at standard temperature and pressure, in effect 25 °C and 1 ATM.

2.2.3.9.1 PDDA/DA Coacervate System

Solutions of 10 mM PDDA and 160 mM DA were prepared using deuterated water (D_2O). 500 µL of each solution were then mixed to form the coacervate system. Malic acid was then added to this at a final concentration of 10 mM to act as a standard known concentration within the sample. The sample was then centrifuged and 700 µL of the supernatant was placed within a Veol

NMR tube, to determine the concentration of DA within the supernatant. Control samples of 80 mM DA at pH 9, 7.5 and 5 were also prepared and placed within VEOL NMR tubes for analysis.

NMR experiments were conducted on a Varian 400 machine. 256 cycles per sample with 2 second relaxation periods, were used, and spectra obtained were analysed using MestreNova software (proprietary software available online).

2.2.3.9.2 PAH/GMP Coacervate System

For PAH/GMP samples, solutions of 7mM GMP, 100 mM PAH, PAH/GMP coacervates, PAH/GMP Ag gelled coacervates were all made using D_2O and 700 µL of volume of each was placed within VEOL NMR tubes. ^{1}H – spectra were recorded on a Varian 400 NMR machine using 256 cycles with 2 second relaxation periods. For gelled samples a 30 second relaxation period was used. For ^{31}P-spectra the samples were loaded into a Varian 500 NMR machine and scanned once for 30 seconds with a 30 second relaxation period. Spectra were then analysed using the standard package MestreNova.

2.2.3.9.3 PDDA-co-DAA Synthesis

To determine whether synthesis of the polymer had been successful solutions of DDA, DAA, PDDA, and PDDA-co-DAA were made in D_2O and ca. 700 µL of each was sealed within VEOL NMR tubes. The ^{1}H - spectra were recorded on a Varian 400 NMR machine using 256 cycles with 2 second relaxation periods. Spectra were then analysed using the software package MestreNova.

2.2.3.10 Fluorimetry

Fluorescence spectroscopy, fluorimetry, measures the photons emitted from a sample after being stimulated by higher energy photons. This is a consequence of photons being absorbed, moving an electron from the HOMO to the LUMO, by the compound and being re-emitted at a lower

wavelength. This difference in wavelengths results from non-radiative transitions within vibrational states between each electronic state. These energetic processes are outlined in Figure 2.11 in the form of a Jablonski Diagram [13]. Using this technique, it is possible to monitor the changes in $\pi \rightarrow \pi^*$, $n \rightarrow \pi$, and $n \rightarrow \pi^*$ transitions as π stacking produces changes in electronic transitions upon formation of nanofibrils.

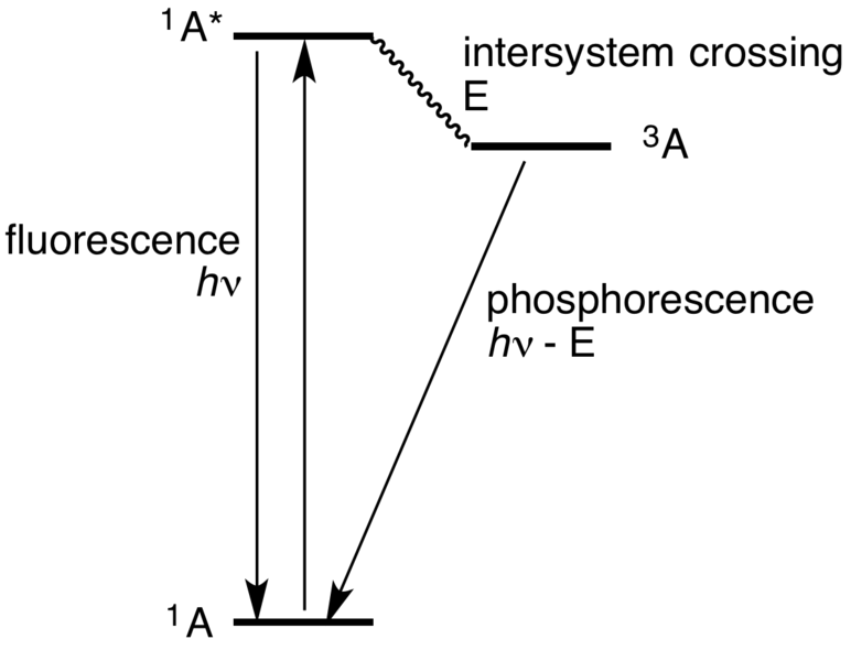

*Figure **2.11:** A simplified Jablonski diagram illustrating the excitation of molecule A to its singlet excited state($^1A^*$). At this point inter-system crossing (ICS) can occur, a low probability transition where by the triplet state is accessed (^3A) and which can then relax back to the singlet state and emit a photon, this emission is known as phosphorene. The wavelength of the phosphorescence is equivalent to the energy of the fluorescence minus the energy difference between the triplet and the excited triplet state. It is possible for there to be non-radiative relaxation, known as vibrational relaxation (VR) via internal conversion (IC).*

2.2.3.10.1 PDDA/DA System

1-Pyrenecarboxaldehyde (PYCA) was obtained from Fluka Analytical. PYCA was then added to water until a saturated solution of concentration 10^{-6} M was formed. Using this PYCA saturated H_2O solution, solutions of 160 mM DA, and 10 mM PDDA, were produced and from these

PDDA/DA coacervate suspensions were made. 3D fluorescence spectra were then obtained using a Horiba Fluoromax 4. Samples were stimulated with 250 - 450 nm wavelength light and emission readings were recorded from 350 - 600 nm. Emission and excitation radiation was increased in increments of 2 nm and the excitation slit was kept at 1 nm and the emission slit at 2 nm. Rayleigh scattering for 1st and second mode was engaged with 3 nm total slit width.

2.2.3.11 Dynamic light scattering and Zeta Potential

DLS measures the intensity of scattered light from a laser that is incident with particles in solution. Polarised light will become out of phase if scattered from different depths, this leads to constructive or destructive interference and therefore the intensity of scattered light will vary dependant on the size and speed of suspended particles. Therefore, if one can detect the rate at which scattering varies then one can determine the speed at which the particles are moving in suspension and thus determine an estimate for the sizes of the particles. This data is of course an average of the particles in solution and so takes the form of a size distribution where the centre of the distribution is the mean size of the particles.

Zeta potential measurements are conducted the same instrument as DLS measurements as the experiment makes use of the same scattering data to determine the motion of the particles under the influence of an external potential difference applied in a uniform manner. The motion of such particle is influenced by their size and surface charge as can be seen in

Figure 2.12. The surface charge of the object being measured will attract ions of an opposite charge in solution to the particle being measured, this will form an ion layer around the object and this will change the hydrodynamic radius of the object. This will affect its motion in the field and fluid. The results obtained from zeta measurements are thus related to the charge at the surface of the sample but are in fact a measure of the charge at the zeta-plane, or the layer at which ions attracted to the charged ions associated with the surface of the sample can be moved via thermal energy, also known as the diffuse layer or the slipping plane as can be seen in

Figure 2.12**.**

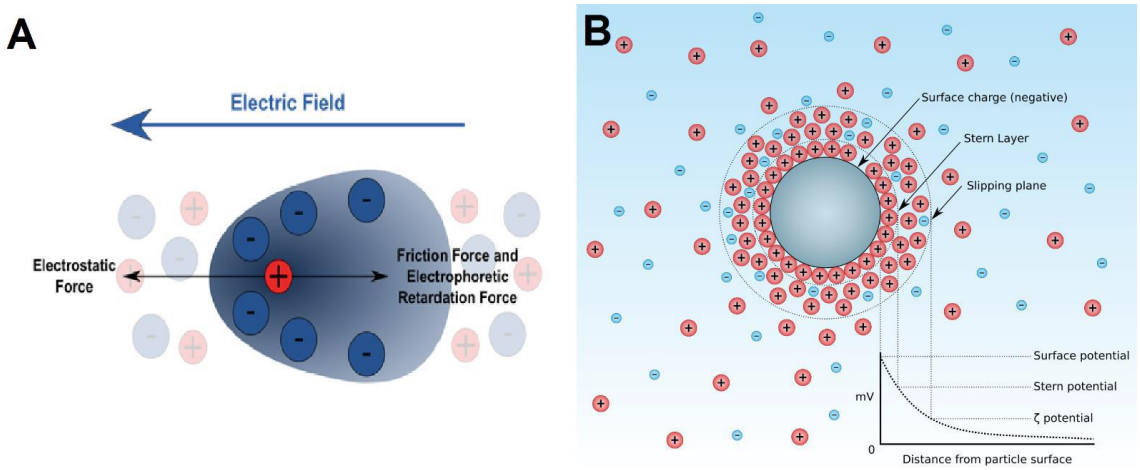

Figure 2.12: (A) A cartoon illustrating the motion of a charged particle in a uniform electric field. The speed and direction in which the particle moves will be dictated by its charge, the strength of the field applied. The viscosity of the solution and the size of the particle. (B) A cartoon illustrating the charge associated with each layer surrounding the sample being measured. The highest potential is the surface potential, the potential associated with the first layer of oppositely charged ions is known as the Stern potential and the potential measured at the diffuse layer or the slipping plane is known as the zeta-potential. Images courtesy Wikipedia users Aushulz and Larryisgood, released under the creative commons licence.

1 mL of the 80 : 5, DA : PDDA coacervate suspension was prepared in a poly(methyl methacrylate) (PMMA) disposable cuvette at 25 °C and Dynamic light scattering (DLS) measurements were conducted upon them on a Malvern Zetasizer Nano ZS. The machine has a size limit of Stability measurements were conducted on the same instrument, by leaving 1 mL of coacervate system overnight with size measurements being conducted every 110 s. Typically measurements were taken 30 seconds after combining the PDDA and DA at a distance of 1.06 mm and with 0.6 attenuation setting at 25 °C.

Coacervate samples were prepared by adding 350 µL of the 10 mM PDDA solution into the disposable Malvern zeta potential cuvette. To this 350 µL of 160 mM decanoic acid solution,

prepared at pH 9, was added and the vial was sealed, ensuring no air was trapped within and the solution covered the internal electrodes. The cuvette was then inverted until the solution was well mixed. The cuvette was placed within the DLS, noting the correct placement of the cuvette within the machine as the potential applied across the sample is directional. All ζ-potential measurements were conducted at 25 °C.

750 µL suspensions of GMP PAH coacervates were formulated and loaded into a Malvern Mastersizer Nano ZS at 25 °C where Dynamic Light Scattering (DLS) measurements were conducted. Automatic attenuation settings were used and samples were scanned 10 times each.

ζ-potential measurements were conducted in the same machine suing disposable Malvern electropotential cuvettes at 25 °C. Automatic attenuation and voltage settings were used and all samples were averaged over ten runs.

2.2.3.12 Fluorescence Lifetime Imaging

Fluorescence lifetime imaging microscopy relies on molecular dyes that possess a moiety that is free to rotate within the solution [14]. As the system is energised using the correct excitation wavelength the energy of the molecule can be dissipated via a number of routes. The initial route involves production of a photon as the excited electron drops from the S1 level to the S0 ground level, this photon will possess a lower wavelength than the excitation photon as energy will have been lost to vibrational modes. Another route is via rotational modes and this the key component in FLIM measurements. As the viscosity of the environment increases this prohibits free rotation of the molecular dye. This prevents energy loss via this route and so more energy must be dissipated via the fluorescence pathway, as a result the molecules fluorescence lifetime, the period of time after excitation that photons are emitted from the molecule, increases. The Förster-Hoffman equation [15]:

$$\log \tau_F = \log\left(\frac{z}{k_r}\right) + \alpha \log \eta$$

Equation 2.10: The Förster-Hoffman Equation. where τ_F is the fluorescence lifetime, k_r is the radiative decay, η is the viscosity, and z and α are constants.

Plotting $\log \eta$ vs. $\log \tau_F$ as a straight line will yield the slope and intercept being equal to α and $\log(\frac{z}{k_r})$ respectively, thus allowing for the calculation of viscosities from measured lifetimes.

To determine the constant α a calibration curve was produced. Solutions of Kiton red in methanol and varying amounts of glycerol were produced, varying from 100% methanol to 100% glycerol. Kiton red was dissolved in these solutions to a final concentration of 2 mM. This technique was used previously to determine the viscosity of other microenvironments by Kuimova et al. [14]. Rheometry was performed using a Malvern Kinexus fitted with a parallel plate geometry (gap width of 200 μm) at room temperature. Samples were added to the rheometer using a spatula to minimize shear. The samples were then taken to the Woolfson bioimaging facility where with the assistance of Dr Dominic Alibhai, the fluorescence lifetime of Kiton Red in each viscous solution was measured using the Leica SP8 AOBS confocal laser scanning microscope attached to a Leica DMi8 inverted epifluorescence microscope. Two gated 'hybrid' SMD GaAsP detectors with photon counting modes and time gating to maximise signal to noise ratios were employed to measure the lifetimes. Coacervate samples were then loaded with Kiton Red and the fluorescence lifetimes in the coacervate microdroplet environment were then measured to determine the local viscosity of the condensed polymeric phase.

2.3 References

[1] L. v. King, "On the acoustic radiation on spheres," *Proceedings of the Royal Society of London,* vol. 147, no. 3, pp. 212-240, 1934.

[2] L. P. Gor'kov, "On the forces acting on a small particle in an acoustical field in an ideal fluid," *Soviet Physiks Doklady,* vol. 6, p. 773, 1962.

[3] M. Barmatz and P. Collas, "Acoustic radiation potential on a sphere in plane, cylindrical, and spherical standing wave fields," *The Journal of the Acoustical Society of America,* vol. 77, no. 3, pp. 928-945, 1985.

[4] N. Becker, D. Bennet, B. Bolto, D. Dixon, R. Eldridge, N. Le and C. Rye, "Research Report No 14: Measurement of Flocculant Residuals by Fluorescent Tagging," vol. 14, 2002.

[5] P. Atkins and J. d. Paula, Elements of Physical Chemistry, Oxford Univeristy Press, 2005.

[6] J. Shipman, J. D. Wilson and C. A. Higgins, An introduction to Physical Science 14th Ed., Cengage Learning, 2015.

[7] E. Pungor, A practical guide to Instrumental Analysis, Florida: Boca Raton, 1995.

[8] K. Vernon-Parry, "Scanning electron microscopy: an introduction," *III-Vs Review,* vol. 13, no. 4, pp. 40-44, 2000.

[9] S. B. Kaemmar, "Introduction to Bruker's ScanAsyst and PeakForce Tapping AFM Technology," *Application note,* vol. 133, no. Rev A0, pp. 1-13, 2011.

[10] P. Griffiths and J. A. de Hasseth, Fourier Transform Infrared Spectroscopy 2nd Ed., Wiley-Blackwell, 2007.

[11] J. Goldstein, Scanning Electron Microscopy and X-ray Microanalysis, Springer, 2003.

[12] K. C. Wong, "Review of NMR Spectroscopy: Basic Principles, Concepts and Applications in Chemistry," *Journal of Chemical Education,* vol. 91, pp. 1103-1104, 2014.

[13] A. Jablonski, "Efficiency of Anti-Stokes Fluorescence in Dyes," *Nature*, vol. 131, no. 3319, p. 839–840, 1933.

[14] J. W. Borst, "Fluorescence lifetime imaging microscopy in life sciences," *Meas. Sci. Technol.*, vol. 21, pp. 102002/1-102002/21, 2010.

[15] T.-Y. D. Tang, C. R. C. Hak, A. J. Thompson, M. K. Kuimova, D. S. Williams, A. W. Perriman and S. Mann, "Fatty acid membrane assembly on coacervate microdroplets as a step towards a hybrid protocell model.," *Nat. Chem.*, vol. 6, no. 6, p. 527, 2014.

Chapter 3 : Stimuli triggered coacervate to vesicle polymer mediated transformation

Abstract

In this chapter a coacervate system comprising a hydrophilic polymer, poly(diallyldimethylammonium chloride) (PDDA), and a fatty acid, decanoic acid (DA), undergoes a morphological, and phase change, in response to a lowering of pH. This response is mediated by the molecular weight of the polymer used to form the coacervates. In the case of low polymer weights, <10 kDa, unilamellar vesicles grow from the droplets. These second-generation vesicles possess, possessing very high aspect ratios and can retain guest compounds that were sequestered within the coacervates, grow from the droplets. In the case of intermediate polymer weights, ~ 40 kDa, multi-lamellar vesicle buds appear and grow at the surface of the droplets. At high polymer weights, ~275 kDa, a multi-lamellar shell of fatty acid bilayers is formed at the surface of the coacervate. In this fashion, pre-loaded dye molecules, fluorescently tagged oligomers, fluorescent proteins, and fluorescently tagged single stranded DNA can be transferred to uni-lamellar fatty acid vesicles 'second generation' proto-cells from the 'first generation' coacervate protocell model. The characteristics of the resulting microdroplets were investigated using: optical and fluorescent microscopy in conjunction with a fluorescently tagged co-polymer poly(diallyldimethylammonium chloride)-co-diallylamine (PDDA-co-DAA); ultra-violet/visible light spectroscopy (UV/VIS); dynamic light scattering (DLS); zeta potential (ζ-potential); fluorimetry in conjunction with a dielectric sensitive dye 1-pyrenecarboxaldehyde (PYCA); small angle x-ray scattering (SAXS), atomic force microscopy (AFM), kymographic analysis, and fluorescence lifetime imaging (FLIM).

3. Introduction

The protocell, as discussed in chapter one as a potential precursor to the modern Darwinian cell, could have arisen first as a membrane free coacervate microdroplet, and it was Oparin who thought that colloidal coacervate systems were important precursors to cellularity [1] [2] [3]. Coacervates, a form of chemical compartment, in the case of complex coacervation comprising a polyelectrolyte and oppositely charged partner species, possess no membrane. They can partition dyes favourably within their interior, dependent on hydrophilicity and charge of the guest species [4]. Coacervates as protocells provide reaction compartments for biologically relevant processes as shown by Crosby *et al* [5]. This system allowed for compartmentalisation of the minimal complex of actinorhodin polyketide synthase which produced elevated yields of the products under various ionic strength conditions. This indicated that the coacervate microdroplet presented a preferential pathway for systems that utilised this reaction by molecularly crowding the process, thus reducing kinetic inhibition of the pathway.

Additionally, coacervates have been utilised to encapsulate other compounds, in a facile manner, before being restructured, via the addition of further biologically relevant molecules, to form more complex protocell models: inorganic components, phosphotungstate polyanionic clusters, were introduced to the PDDA ATP coacervate to generate a novel three-tiered structure comprising a phosphotungstate/PDDA shell, a PDDA ATP sub-membrane and an aqueous filled lumen that responded to osmotic pressure changes, as demonstrated by Williams *et al.* [6]. Organic prebiotically relevant molecules have also been added to coacervate systems to generate new structures: PDDA ATP and oligolysine/ATP coacervates were formed and oleic acid micelles were added to form thin multilamellar vesicles at the surface of the coacervate microdroplets as shown by Tang *et al.* [7]. These systems make use of the polymers PDDA and oligolysine, along with various counter-charged species such as adenosine triphosphate (ATP) and carboxymethyl-dextran (CM-dextran), to generate coacervate microdroplets as models for protocells. The

molecular weights (MW) of the polymers used are generally quite high, i.e. greater than one hundred kDa, as the length of the polymer has an influence on the size of the microdroplets formed, and encapsulation of other guest molecules were key to the investigations being conducted [8].

Fatty acids are well known for their ability to self-assemble into a variety of structures dependent on their protonation, including micelles, tubular micelles, vesicles, and oil droplets [9] [10] [11]. Vesicles, formed when the pH of the fatty acid solution is such that fifty percent of the carboxylic groups are protonated, in effect at its pK_a, the pKa for a 26 mM DA solution is 7.6 but as discussed in Chapter 1 this varies with concentration, are prevalent in modern cell biology and used in chemistry as containers of large molecules, and as such are useful in protocell research. Herein, we exploit the charge present on a fatty acid molecule, decanoic acid (DA), at high pH to undergo coacervation with an oppositely charged polyelectrolyte, PDDA (various MWs), to form a novel coacervate microdroplet suspension that would then respond to the change in pH of solution upon addition of an acid, glucono-δ-lactone (GDL), a slowly hydrolising acid [12] [13]. The system could lend itself to the encapsulation of often difficult to incarcerate compounds within vesicles by forming the coacervates with the target molecule in solution, thereby sequestering targets easily in the membrane-less coacervate compartments and then forming fatty acid vesicles upon addition of the acid. As the fatty acid is a component within the coacervate droplets, the guest molecule should then be encapsulated within the newly formed vesicle, which could aid in cellular transfection *in vivo*.

3.1 Additional Materials and Methods

Materials: All reagents were purchased and used as delivered: poly(diallyldimethylammonium chloride) 8.5 kDa, 40 kDa, and 200 – 300 kDa (PDDA (8.5 kDa) PolySciences GMBH, (40 and 200 – 300 kDa) Sigma-Aldrich) ; decanoic acid (DA, Sigma-Aldrich) ; hydrogen chloride (HCl, Sigma-Aldrich); sodium hydroxide (NaOH, Sigma-Aldrich); glucono-δ-lactone (GDL, Sigma-Aldrich); sodium chloride (NaCl, Sigma-Aldrich); hexamethyldisilizane (HMDS, Sigma-Aldrich); poly(etheyleneglycol) (PEG; Sigma-Aldrich); Acridine Orange (Sigma-Aldrich); green fluorescent protein (GFP, expressed by Dr James Armstrong in the Adam Perriman Research Group to a final concentration of 5 mg/mL); enhanced green fluorescent protein (eGFP, expressed by James Armstrong in the Biomedical Sciences School to a final concentration of 5 mg/mL); dextran 40 kDa (Sigma-Aldrich, tagged with fluorescein isothiocyanate in house); single stranded deoxyribosenucleic acid 7.6 kDa tagged with cyanine 5 (ssDNA-cy5, Eurofins); 4,4-Difluoro-5,7-Dimethyl-4-Bora-3a,4a-Diaza-s-Indacene-3-Dodecanoic Acid (BODIPY FL C12, ThermoFisher Scientific); 9-diethylamino-5-benzo[α]phenoxazinone (Nile Red, Sigma-Aldrich); poly-L-lysine (PLL, Sigma Aldrich); (3Z,3'Z)-3,3'-[(3,3'-dimethylbiphenyl-4,4'-diyl)di(1Z)hydrazin-2-yl-1-ylidene]bis(5-amino-4-oxo-3,4-dihydronaphthalene-2,7-disulfonic acid) (Trypan Blue, Sigma-Aldrich);

Coacervate formulation: Equal volumes, 100 µL, of a 10 mM (monomeric concentration) 8.5 kDa PDDA solution at pH 9 and a 160 mM DA solution at pH 9, were mixed in a 1.5 mL Eppendorf tube at 25 °C to form a turbid suspension of coacervate droplets. The sample was then centrifuged at 13,200 rpm for 5 minutes to facilitate the separation of supernatant and bulk phases. Samples were then redispersed by hand using a micropipette to generate microdroplets in a suspension of the low-polymer supernatant phase. All solutions were made with Milli-Q Pure deionised water (18.2 MΩ) dispensed from a Milli Q helix integral 3 filtration system.

Transformation of the system was triggered by the addition of 1 μL of 2M GDL to 100 μL of coacervate suspension. A non-mineral, slowly hydrolising acid, was chosen to extend the period of time over which the pH transition could be observed [14].

UV-Vis spectroscopy: Suspensions of PDDA/DA coacervates were produced via the mixing method previously detailed but with 500 μL of each component to generate final volumes of 1 mL. These were pipetted into 1.5 mL polymethylmethacrylate (PMMA, purchased from Thermo-Fischer and cleaned with compressed air) cuvettes and loaded into a Perkin Elmer Lambda 35 UV-Vis spectrophotometer. Wavescans from 400 – 600 nm were conducted to determine the turbidity change of the solution with varying DA concentration.

Dynamic light scattering: 750 μL suspensions of PDDA/DA coacervates were formulated and loaded into a Malvern Mastersizer Nano ZS at 25 °C where Dynamic Light Scattering (DLS) measurements were conducted. Automatic attenuation settings were used, and samples were scanned 10 times each and then averaged.

Zeta potential measurements: ζ-potential measurements were conducted with the Malvern Mastersizer Nano ZS using disposable Malvern electropotential cuvettes at 25 °C. Automatic attenuation and voltage settings were used and all samples were averaged over 10 runs.

Nuclear magnetic resonance: All proton NMR measurements were conducted in D_2O on a Varian 400 MHz instrument, with a 64 scan, 30 second relaxation period and at standard temperature and pressure (25 °C and 1 atm). Acetone was used as an internal standard against which to calibrate the quantitative analysis of protons generating the observed signals. This, and the following equation, allowed for the quantification of DA in the bulk phase of the coacervate suspension:

$$C = CCF \times \frac{AI}{NN}$$

Equation 3.1: Chemical Conversion Factor. Where C is equal to the concentration of substance generating the chemical shift peak; CCF is the chemical conversion factor, a calculated proportionality constant; AI is the absolute integral value; and NN is the number of nuclides, in this case the number of protons associated with the environment producing the chemical shift.

Performing a scan of the supernatant of the PDDA/DA coacervate suspension after centrifugation showed no signals corresponding to the presence of PDDA and we can therefore assume that all the PDDA had partitioned within the bulk phase. If we assume the bulk phase volume to be ca. 1 µL after centrifugation we can calculate the concentration of GMP in this phase to be ca. 2 M. The amount of DA observed in the supernatant phase by this method however was found to be 63 mM, indicating that not all the fatty acid partitioned within the coacervate phase. Assuming the volume of the bulk phase to be 1 µL again the concentration of the DA within the coacervate droplets can be calculated and was found to be 3.4M.

Atomic force microscopy: PeakForce atomic force microscopy (AFM) was conducted by Dr R Harniman in the Chemical Imaging Facility, University of Bristol, with equipment funded by EPSRC under Grant "Atoms to Applications" Grant ref. "(EP/K035746/1) using a PeakForce multimode 8 AFM instrument. PDDA/DA samples were prepared and deposited onto freshly cleaved mica then allowed to settle for one hour before being dried with compressed nitrogen. For samples that had had their pH adjusted, GDL was added to the drop cast coacervate suspension and allowed to mix for five minutes before being dried with compressed nitrogen. Using Bruker Nanoscope Analysis v1.8 the heights of the coacervate and

surrounding material, thought to be crystalline decanoic acid, surrounding and emanating from the droplets, were analysed.

Optical microscopy: Capillary slides were prepared using functionalised cover slips to prevent coacervate wetting on the glass surface. Functionalisation was undertaken via chemical etching with the use of Piranha solution, 1:4 parts H_2O_2:H_2SO_4, to enable the addition of 200 µL poly(ethyleneglycol) (PEG) (in 10 mL of toluene). In the case of hexmethyldisilizane (HDMS) functionalisation, Piranha solution was again used to clean the glass slips which were then placed in a desiccator in 200 µL of HDMS overnight. In the case of varying MW PDDA functionalised slips, the slips were washed thoroughly in deionised H_2O and ethanol and then left in baths of the PDDA solutions. These were subsequently left to electrostatically attach for 2 hours and then washed with deionised H_2O and dried with compressed nitrogen.

Capillary slides were then made by attaching functionalised slips on top of two non-functionalised slips with UV-curing glue, on top of a microscope slide to generate a 10 mm channel, seen in Figure 3.1. Dishes were made by taking small petri dishes and boring a hole through the bottom, functionalised slips were then attached with UV curable glue to their underside and fixed under a 365 nm UV lamp. Approximately 65 µL of the coacervate suspensions was then placed inside the channel and observed using a Leica DMI 3000 inverted optical microscope with variable wavelength ultra-violet (UV) lamp attached. Brightfield, phase-contrast, and fluorescence images were captured.

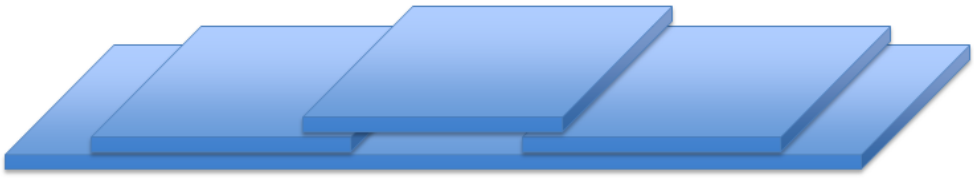

Figure 3.1: A cartoon of the capillary slide manufactured. A microscope slide has two cover slips glued to its surface with a small channel between them. Two strips of glue are then applied

to the cover slips to allow a third slip to be fixed over the channel forming a small capillary space between the microscope slide and the third cover slip. The third coverslip can be functionalised. When used on the microscope the slide is inverted so the solution rests on the slip.

Confocal microscopes were also used to image the coacervate droplets (Leica SP5-AOBS confocal laser scanning microscope attached to a Leica DM I6000 inverted epifluorescence microscope, equipped with Equipped with 100 mW Ar laser (458, 476, 488, 496, 514 nm lines), 10 mW solid state yellow laser (561 nm), 2mW Orange HeNe (594 nm), 10 mW Red He/Ne (633 nm) and 50 mW 405 nm diode laser.; Wolfson Bio-imaging Facility), to capture fine fluorescence intensity decay data to confirm gelation kinetics. All microscopy was undertaken under standard conditions (1 atm and 25 °C).

Acoustic manipulation: Acoustic manipulation of coacervates was undertaken using twin sets of piezoelectric manipulators. The acoustic trap was manufactured in-lab by Ms. Madeleine Nichols and the acoustic field was driven by a pair of signal generators, Agilent 33220a-001. The resonant frequency was 6.7 MHz and the peak voltage was set to 10 V. The pair were driven at, and just below, their resonant frequencies to generate a temporally uncorrelated field that produced a square field with 100 × 100 μm spacing.

3.2 Results and Discussion

3.2.1 Coacervate synthesis and characterisation

The method previously explained was used to generate PDDA/DA coacervates and the solution immediately became turbid, indicating that coacervation had occurred and aggregates which could scatter light were present, as seen in Figure 3.2.

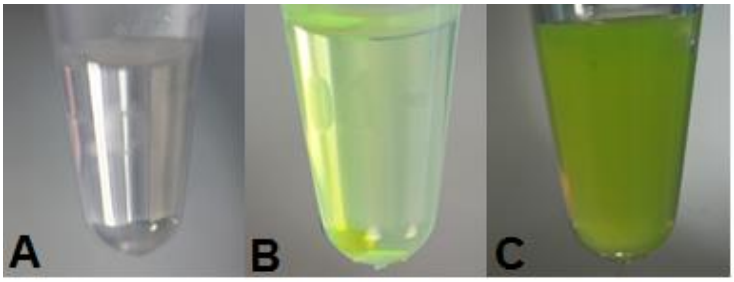

Figure 3.2: a) PDDA solution (transparent colourless), b) PDDA solution and BODIPY C12 dye (transparent and green), c) The PDDA/DA/BODIPY C12 loaded solution (turbid and green).

Optical microscopy imaging of the suspension produced by the method of centrifuging and then re-dispersing a PDDA/DA coacervate phase within its own supernatant revealed the presence of polydisperse spherical droplets. that exhibited high optical contrast (Figure 3.3). The droplets could readily uptake hydrophobic dyes, as observed by epifluorescence microscopy (Figure 3.3)

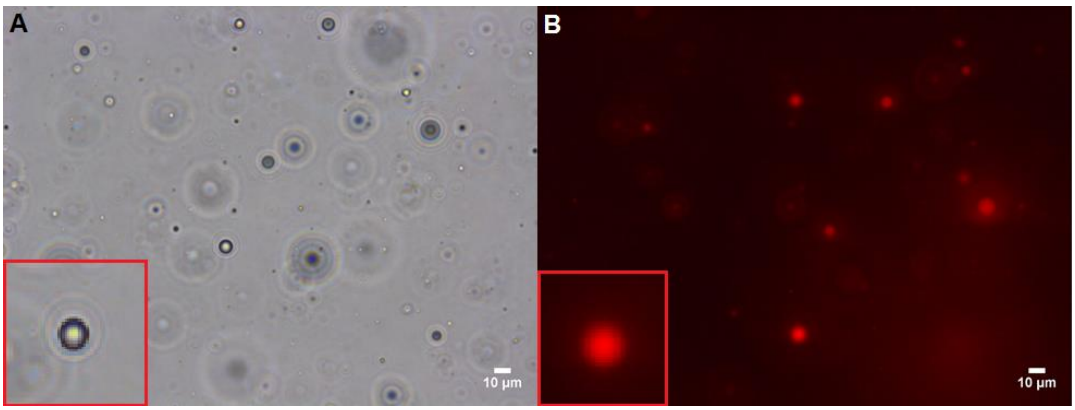

Figure 3.3: a) An optical micrograph of the PDDA/DA coacervate microdroplets, highlight shows the spherical nature of the coacervate microdroplets formed. b) A fluorescent micrograph

of the PDDA/DA coacervate microdroplets, loaded with Texas Red dye, highlight inset image illustrates the localisation of the dye to the coacervate microdroplet. Scale bars = 10 µm.

Size data of the coacervate was extracted by applying a shape filter to the images captured using ImageJ as discussed in Chapter 2. This yielded the data that gives the average size of the droplets as 11 µm however the deviation from this average is very large, 17 µm, indicating that the sample was highly polydisperse. This high polydispersity is most likely a result of low stability with respect to coalescence. As the coacervates form their lack of membrane and low interfacial tension will enable them to coalesce readily and the polydispersity of the system will as a result change with time.

Droplet size and polydispersity was further characterised using DLS. Figure 3.4 illustrates the various average sizes presented by coacervate droplets within the PDDA/DA concentration solutions, the concentrations of which are as described in Table 3-1. As can be seen in Figure 3.4, coacervates formed with 5 mM PDDA concentration produced the most consistently sized coacervate droplets, 1.5 ± 0.1 µm, which gave an indication as to their stability and polydispersity.

However, at this concentration, 80 mM DA and 5 mM PDDA, the coacervate system would appear to be unstable easily coalescing to form large particles of a diameter greater than 6 µm within 1.5 hours. Captured using DLS, Figure 3.5 illustrates how the diameter of the coacervate droplets change with time. Figure 3.5 shows the entire course of the experiment, with a DLS measurement being recorded every ten seconds for sixteen hours. The ability of the Malvern Zetasizer machine to measure particles is only accurate for samples smaller than 6000 nm (6 µm). This shows that the average size of the coacervate microdroplets rapidly increases in the first 15 minutes and gradually coalesce to a size larger than is reliably measured within the next 2 hours, which is likely when gravity driven sedimentation of the denser coacervate microdroplet phase begins to take effect.

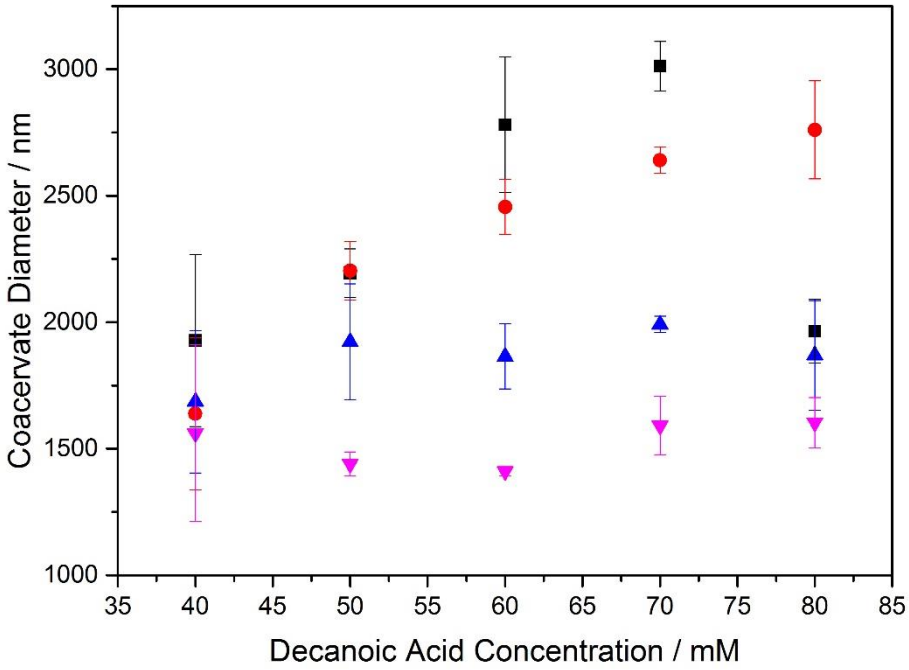

Figure 3.4: The coacervate diameter as measured by DLS with respect to increasing DA concentration. The following symbols correspond to the varying final concentrations of PDDA used during the experiment: ■ 80mM, ● 40 mM, ▲ 20mM, ▼ 5 mM. Measurements performed in triplicate.

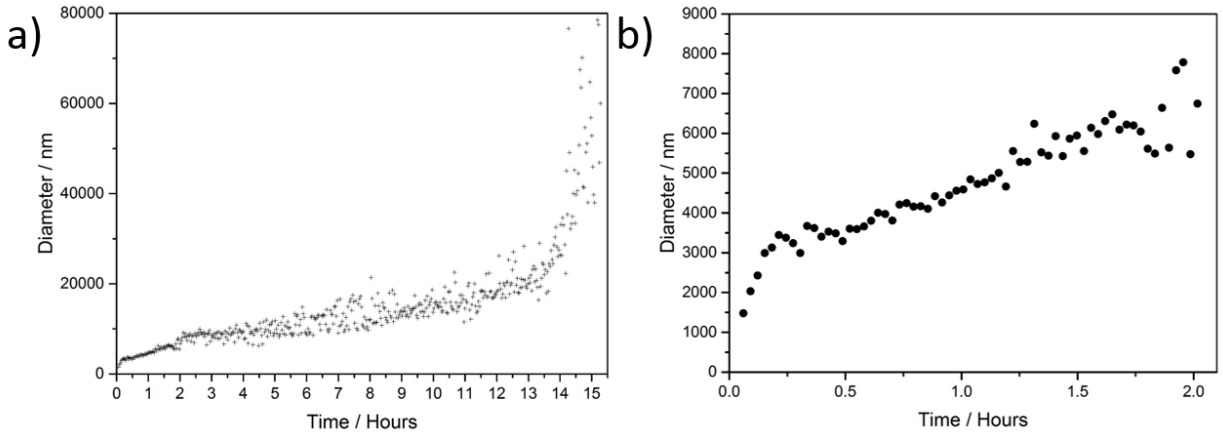

Figure 3.5: a) The graph shows the average size of particles measured via DLS at 80 mM DA 5 mM PDDA concentrations. Size increase with time is attributed to settling and coalescence. b) An enhancement of a) focusing on the first two hours of the experiment. Measurements performed in triplicate.

The data collected by DLS measurements indicated that the sizes of the aggregates formed varied quite substantially with DA concentration. As such, turbidimetry experiments were performed to determine the point at which coacervation occurred. Figure 3.6 shows the turbidimetry data acquired for the various PDDA/DA solutions generated. From this graph the critical coacervation concentration (CCC) was calculated using the linear slope extrapolated from the linear section on the turbidity data, which is displayed in Table 3-1.

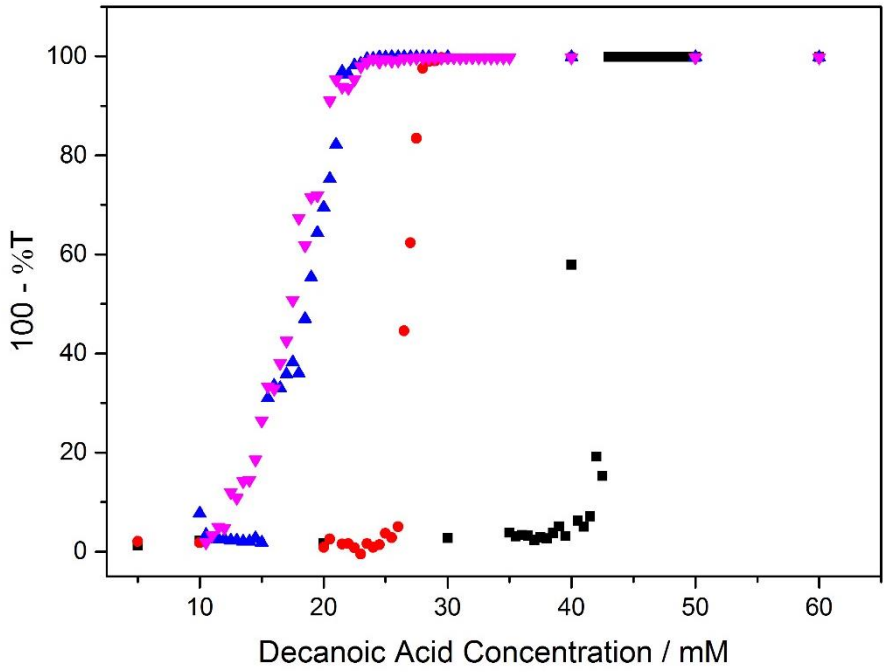

Figure 3.6: Turbidity measurements for various coacervate compositions, measured at 500 nm. The following symbols correspond to the varying final concentrations of PDDA used during the experiment: ■ 80mM, ● 40 mM, ▲ 20mM, ▼ 5 mM. Measurements performed in triplicate.

Table 3-1: The critical coacervation concentrations found for various PDDA concentrations using the linear fit and finding the intercept with the x axis.

PDDA / mM	DA / mM
80	40.5 ± 0.5
40	26.5 ± 0.5
20	15.0 ± 0.5
5	12.5 ± 0.5

All experiments conducted to determine sizes of aggregates formed, at the concentrations used in the DLS experiments, were above the concentrations at which aggregates large enough to scatter visible light can be found by turbidimetry experiments. The concentration at which coacervation occurs for the 5mM system is at 12.5 mM. At this minimal concentration of DA the charge ratio is as follows in Table 3-2.

Table 3-2: The table describes the ratio of charges in the 'minimal' coacervate system.

	DA	PDDA
Conc. / mM	12.5	5
Ratio	2.5	1
Total Charges	- 2.5	+1

At the molar ratios found by UV/VIS spectroscopy required for coacervation the coacervate microdroplets are expected to present a net negative charge. To verify this, zeta potential measurements were conducted on a 12.5 mM DA/ 5mM PDDA sample and the zeta-potential was found to be 25 ± 2 mV. This positive value indicates that the coacervate microdroplets at this molar ratio should be stable with respect to coalescence and that the charge at their surface is positive. This was unexpected and so NMR was conducted to determine the location of the components within the coacervate bulk phase and the continuous, or supernatant, phase.

NMR spectra were collected for pH 5, 7.5, and 12, 80 mM DA solutions, 5 mM PDDA, 80 mM DA/ 5mM PDDA coacervate supernatant and the supernatant of an 80 mM DA/5 mM PDDA redispersed in deionised water and then centrifuged again to produce bulk and supernatant phases. The first set of peaks (orange), reading from right to left in Figure 3.7 are a result of the terminal methyl group of the alkane chain in DA, the next peak (green) is a result of the six carbon atom environments in the chain, the third (blue) peak as a result of the eighth carbon atom environment and the final (red) peak is resultant from the carbon environment closest to the carboxylic group.

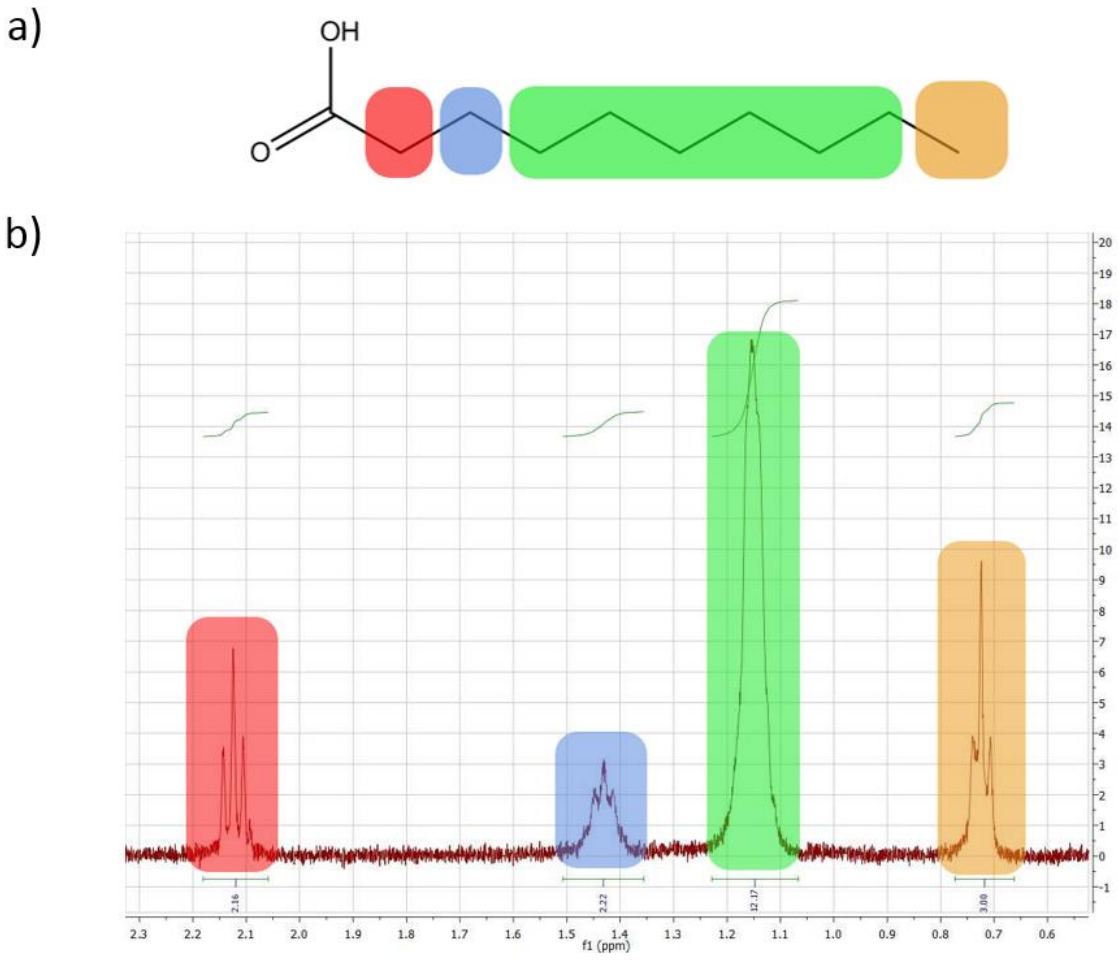

Figure 3.7: a) The chemical structure of decanoic acid with highlighted proton environments that correspond to the ^{1}H – spectra. b) The ^{1}H spectra obtained from a control pH 5 DA in D_2O solution. The relative peak integrals from right to left are: 3.00, 12.17, 2.22 and 2.16. The chemical shift maxima of the peaks are centred at, from right to left: 0.72, 1.15, 1.43, and 2.12 ppm.

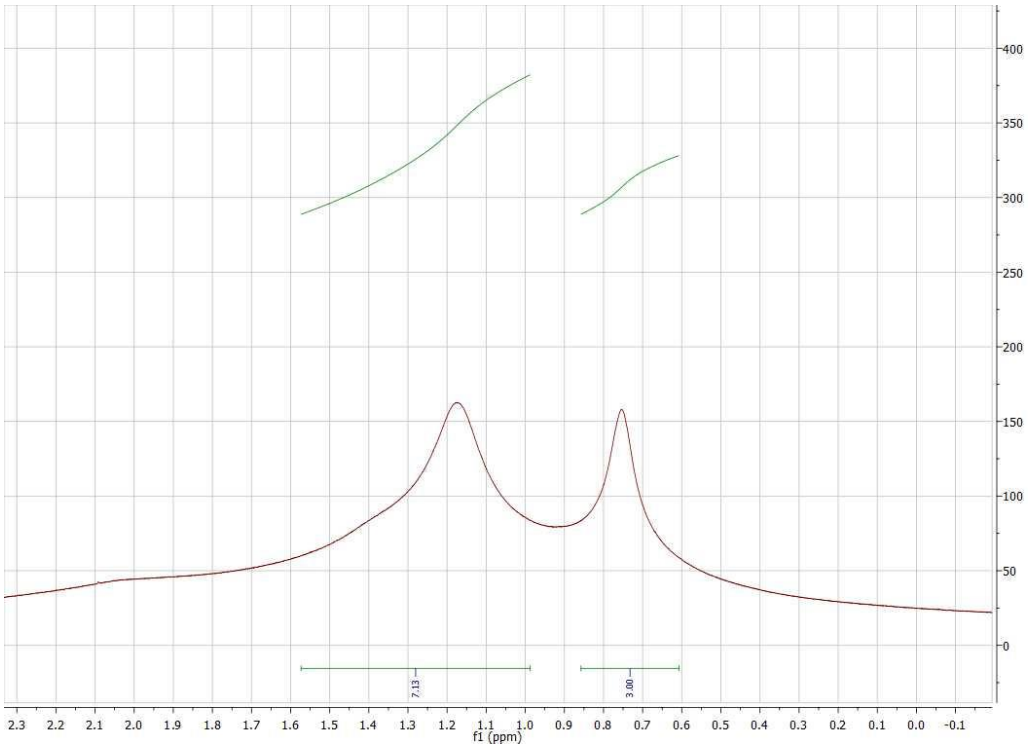

Figure 3.8: A spectra obtained of a control pH 7.5 DA in D_2O solution. The chemical shift maxima of the peaks are centred at from right to left at: 0.75 and 1.17 ppm.

Decanoic acid forms vesicles at pH 7.5, with Figure 3.8 illustrating the broadening of peaks as a result of the rapid relaxation of the protons at the surface of the vesicle membrane. If their precession is near that of the Larmor frequency of the applied field, they will be able to relax very rapidly once the applied field is removed. As the time of relaxation is then known to a high degree of precision, the chemical shift, which is representative of the energy of the excited state as a result of the applied magnetic field, cannot be known to a high degree of precision due to Heisenberg's uncertainty principle – this results in the broadening of peaks for hydrogen environments in chemical shift. The two spectra show that NMR can resolve the difference between a sample that contains DA in its de-protonated state and in a mixed composition at this intermediate pH, which are important controls for understanding the form that the DA takes within the coacervate microdroplets and in the supernatant.

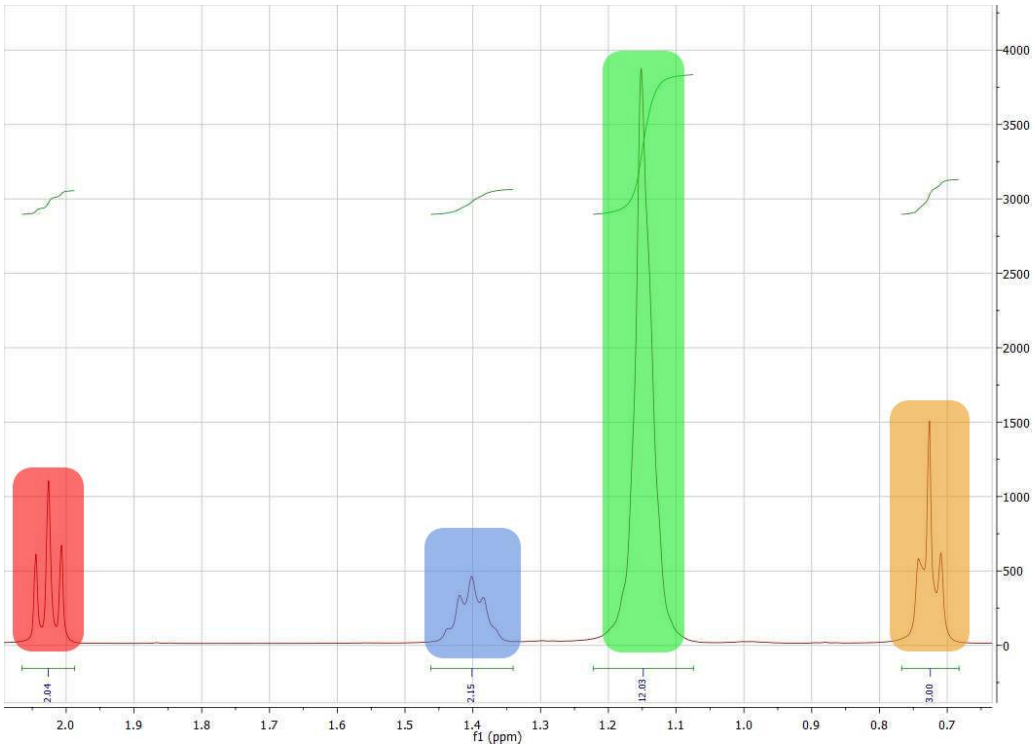

Figure 3.9: A spectra obtained of a control pH 12 DA in D_2O solution. The relative peak integrals from right to left are: 3.00, 12.03, 2.15 and 2.04. The chemical shift maxima of the peaks are centred at, from right to left: 0.72, 1.15, 1.40, and 2.03 ppm.

At pH 12 the DA is completely deprotonated and forms micelles, the spectra from Figure 3.9 is not too dissimilar to that of Figure 3.7 for DA in pH 5 solution. However, the relative peak intensity is much greater for the DA in the pH 12 solution. This implies a greater number of protons involved in the chemical shift, however, both experiments were conducted at the same concentration of 80 mM, indicating that not all DA molecules participate in the formation of micelles at high pH.

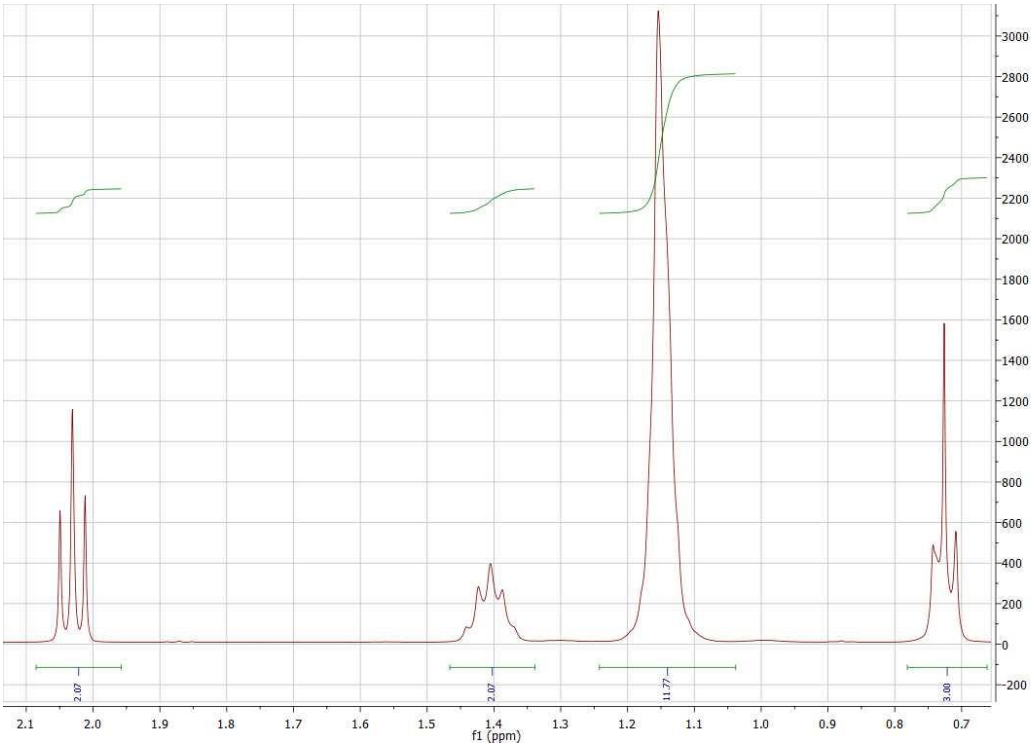

Figure 3.10: A spectrum obtained from the supernatant of a coacervate sample in D_2O. The chemical shift maxima of the peaks are centred at, from right to left: 0.72, 1.15, 1.40, and 2.03 ppm.

In Figure 3.10 a coacervate sample prepared in a D_2O was centrifuged for 5 minutes at 13,200 rpm and ^1H spectroscopy was performed upon it. The same peaks, and relative strengths, are observed as in the pH 12 DA Figure 3.9. This is indicative of the presence of DA in the supernatant. Taking the absolute integrals of the peaks centred on 1.15 ppm chemical shift, one can calculate the concentration of DA in the Supernatant sample:

$$[\boldsymbol{Supernatant}] = \frac{\boldsymbol{Peak}^{\boldsymbol{Absolute}}_{\boldsymbol{Supernatnt}}}{\boldsymbol{Peak}^{\boldsymbol{Absolute}}_{\boldsymbol{pH\ 12\ DA}}} \times [\boldsymbol{pH\ 12\ DA}]$$

Equation 3.2: Concentration in NMR. Where $[Supernatant]$ is the concentration of micellar DA in the supernatant phase, $Peak^{Absolute}_{Supernatnt}$ is the absolute integral value of the Supernatant peak centred at 1.15 ppm, $Peak^{Absolute}_{pH\ 12\ DA}$ is the absolute integral value of the DA pH 12 peak centred at 1.15, and $[pH\ 12\ DA]$ is the concentration of the DA in the pH 12 DA control sample.

In this case [pH 12 DA] = 80 mM, and the ratio of the two integrals for the alkane section of the DA yields a value of 0.7875. This gives [$Supernatant$] = 63 mM. The coacervates are formulated at 5 : 80 mM ratio of PDDA : DA. This would appear to show that 78 % of the DA remains unassociated with the PDDA. The concentration of decanoic acid within the coacervate microdroplet then becomes a matter of estimating the volume occupied by the microdroplets, as the amount of DA within them is now known by mass. Measuring the volume occupied by the microdroplets is difficult, however, if we estimate the volume to be 1 µL we then find that the concentration of DA in the microdroplets is approximately 3.4 M.

An experiment was conducted with the supernatant of the PDDA/DA coacervate system to more accurately determine the DA concentration that remains unassociated with the PDDA polymer chain by utilising an internal standard, Malic Acid (Figure 3.11). This eliminates any calibration errors between NMR cycles.

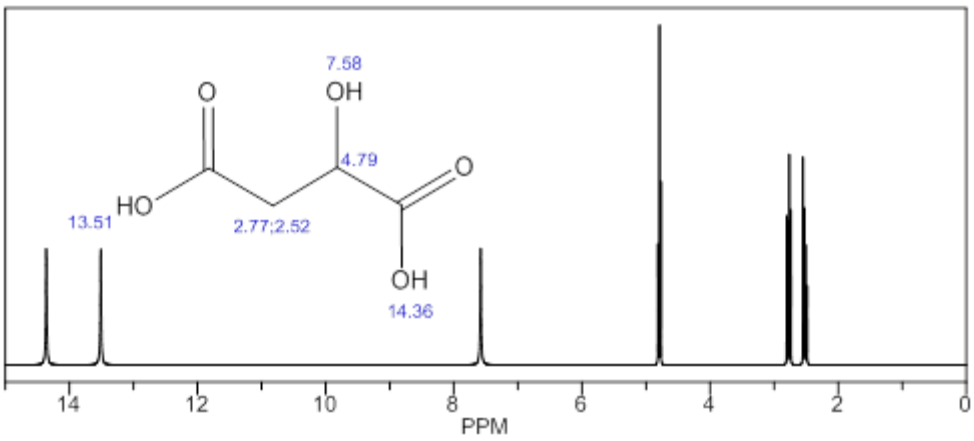

Figure 3.11: The calculated chemical shifts and chemical structure of Malic Acid. Drawn and computed in ChemBioDraw software package.

As can be seen in Figure 3.12 the spectra for decanoic acid and malic acid can both be clearly resolved. Taking the absolute values for the integrals of the Malic acid peaks one can calculate

the ratio of intensity to concentration and thus calculate the concentration of decanoic acid in the supernatant phase.

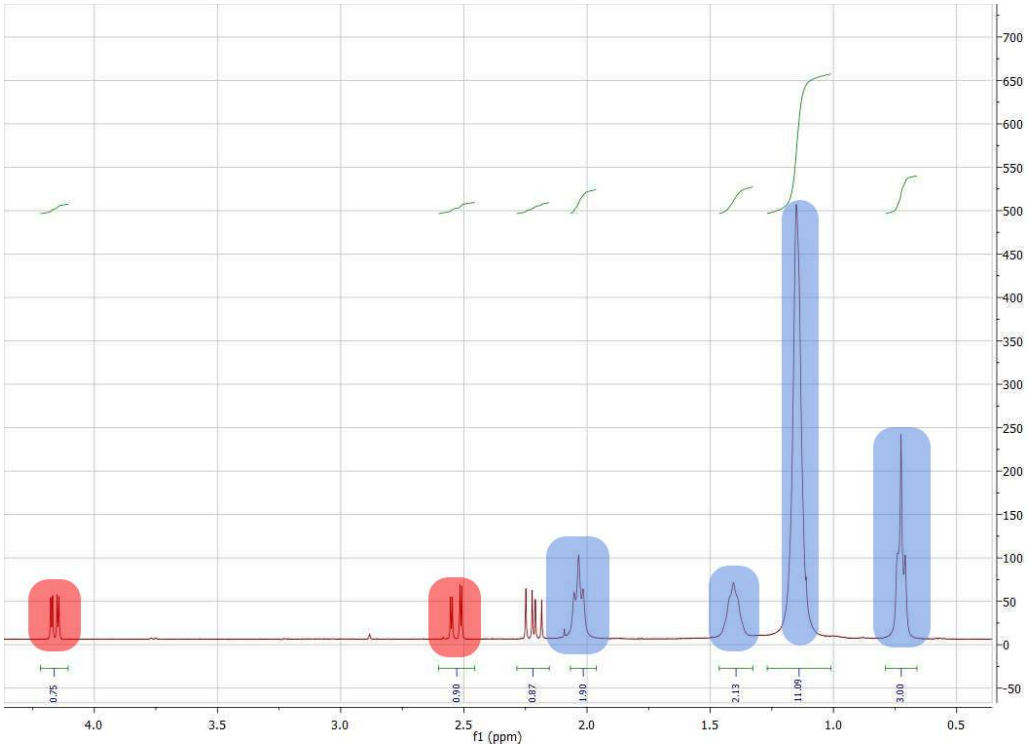

Figure 3.12: A spectra obtained of the coacervate supernatant with internal Malic acid (10 mM) standard. The peaks highlighted in red are indicative of the presence of Malic acid. The blue highlighted peaks are indicative of the presence of decanoic acid. The relative peak integrals are from right to left: 3.00, 11.09, 2.13, 1.90, 0.87, 0.90 and 0.75. The centres of the highlighted chemical shift peaks are, from right to left: blue; 0.72, 1.15, 1.41, and 2.03, red; 2.53 and 4.16 ppm.

Taking the peaks from Figure 3.12 we can calculate the *CFF*, using the method outlined in the additional materials and methods section, from the first of the red highlighted peaks, at position 2.53 ppm. The concentration of malic acid is known, 10 mM, and the number of nuclides associated with this environment is 2. Therefore, this yields a *CFF* of 0.00326. Using this with the *AI* from the first blue highlighted peaks, at position 0.72 ppm, the calculated concentration for DA in the supernatant phase is approximately 22 mM.

The two methods of calculating concentration of DA in the supernatant phase of the coacervate system yield quite different values: 63 mM from the control sample and 22 mM from the internal standard.

Evidently there is a large amount of free DA in solution. At the ratio of 5 : 80 mM , PDDA : DA, the total charges are expected as follows in Table 3-3.

Table 3-3: The table of calculated charges within the PDDA/DA coacervate system.

	DA	**PDDA**
Conc. / mM	80	5
Ratio	16	1
Total Charges	-16	+1

This shows that the excess DA found in the supernatant phase of the coacervate suspension, could be due to excess negative charge being associated with the colloidal polymer dense microdroplets. Zeta potential measurements of these microdroplets returned poor data due to poor scattering from the solutions. This could be due to the high polydispersity of the coacervates formed at this molar ratio.

The amount of salt required to shield the interactions of the PDDA chain and the DA was quantified using UV/VIS spectroscopy and NaCl solution. The turbid 80 : 5 mM DA/PDDA suspensions immediately became less turbid upon the addition of salt and the system appeared to reach a plateau in absorbed light at 800 mM NaCl as can be seen in Figure 3.13, indicating that all of the structures in the system that could have scattered light had been disassembled by having their electrostatic attractions screened by the additional salt present in solution.

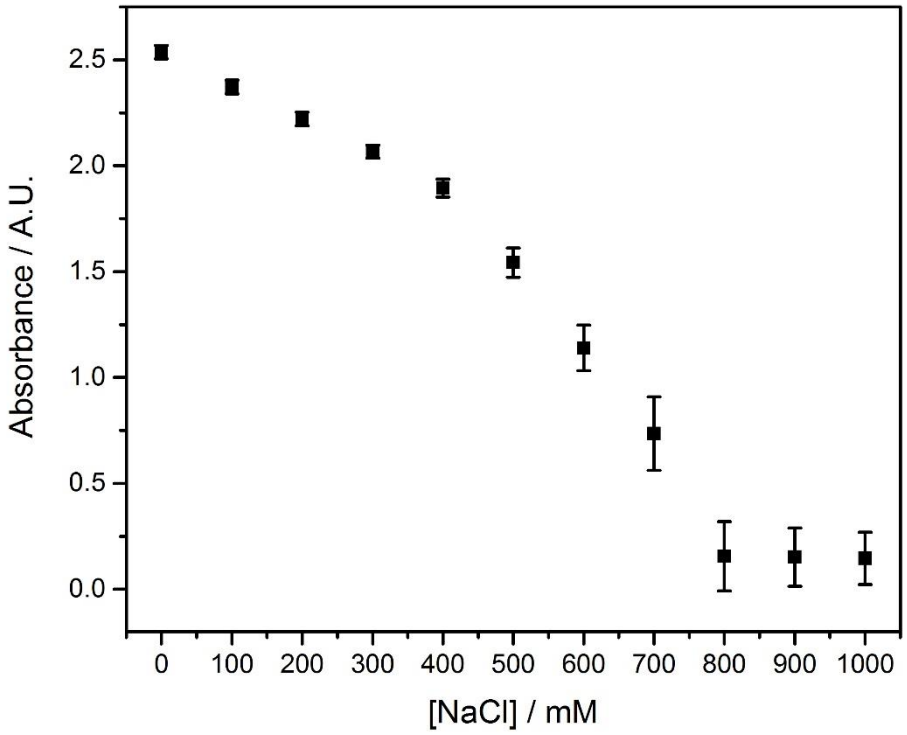

Figure 3.13: The graph illustrates how absorbance at 500 nm decreases with increasing salt concentration in solution. This indicates a decrease in turbidity which indicates that the aggregates scattering and absorbing light, are being disassembled by the presence of the salt ions in solution. Measurements performed in triplicate.

To summarise this section: a novel complex coacervate system comprising poly(diallyldimethylammonium chloride) (PDDA) and decanoic acid (DA), has been synthesised and characterised. The characteristics of the resulting coacervate microdroplets were analysed using: optical and fluorescent microscopy, to determine the presence of polymer-rich coacervate microdroplets in solution; ultra-violet/visible light spectroscopy (UV/VIS) to determine the critical coacervation concentration of 12.5 ± 0.5 mM DA; dynamic light scattering (DLS) to determine the size distribution and polydispersity of the microdroplets at 80 : 5 DA : PDDA ratios to be 1.5 ± 0.1 μm in the first minute after formation; zeta potential (ζ-potential) measurements for a minimal version of the system showed a positive charge of 25 ± 2 mV which was unexpected

and led to NMR experimentation that concluded a large amount of DA was left in the continuous phase around the polymer rich microdroplets. It was found that all the microdroplets could be disassembled in solution by the addition of salt up to a concentration of 0.8 M.

3.2.2 Response to pH Change

As mentioned in the introduction the structures formed by DA are dependent on the protonation of the carboxylic group. Therefore, a study was undertaken to understand the effect of pH upon the system. The slowly hydrolising acid Glucono-δ-lactone was chosen as opposed to the addition of mineral acids as the process was to be studied via optical microscopy. The GDL undergoes a base catalysed ring opening hydration to form gluconic acid and this ensures that the pH adjustment can be made reproducible across experiments starting at a given pH and proceeding over a given time [12]. Work using fatty acids and pH adjustments has previously been conducted by Garenne et al. [15] where coacervates formed from cylindrical fatty acid micelles can be transformed into vesicles.

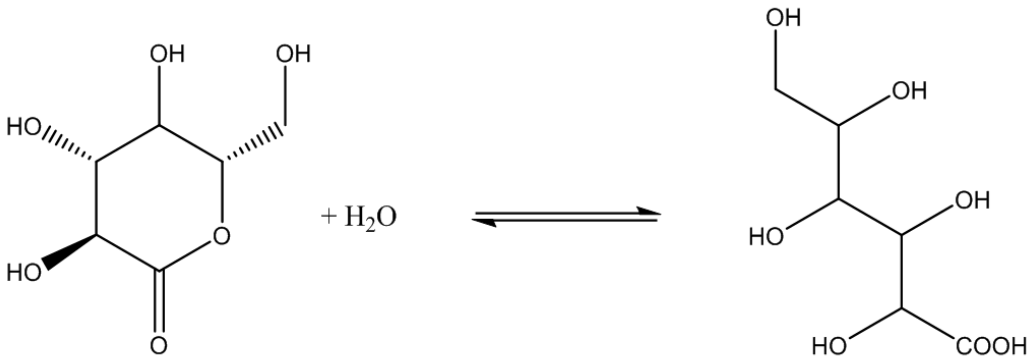

Figure 3.14: The reaction between GDL and water that yields D-gluconic acid. Adapted from [12].

The pH response of the system was found to vary depending on the molecular weight of the polymer used in the coacervate formulation and these are discussed in subsequent subsections but are summarised here: low polymer weight formulations produced high aspect ratio vesicles growing from the coacervate surface that were unilamellar; medium polymer weight formulations

produced multi-lamellar spherical bud-like vesicles at the surface; and high molecular weight polymer formulations produced multi-lamellar shells across the surface of the coacervate microdroplets. However, before delving further into the responses of each of these systems, an effort was made to understand the composition of the starting coacervate microdroplet from which these structures emanated upon pH adjustment.

As the local environment of the PDDA/DA coacervate droplet changes, so does the protonation of the DA, and hence the composition of the microdroplets. The droplets were prepared at pH 9 and above the CMC of DA, 60 mM [11], to ensure that when mixed with PDDA the DA is in micellar form. If this is the case, one might expect the droplets to be homogenous DA micelles entangled in PDDA chains. However, various other structures could exist, each of which would imply different mechanisms to produce the observed vesicles upon pH adjustment. If the protonation of the DA changes before electrostatically binding to the PDDA chains within the microdroplet, one could expect monomeric association of DA with the PDDA chain. Alternatively, there could be an aggregation of micelles and the PDDA chains could wrap around this micellar core, generating a permeable polymeric shell. Again, if the internal microdroplet local pH is different to that of the bulk, this core could be vesicular in nature. The fluorescence of 1-pyrenecarboxaldehyde (PYCA) in each of these scenarios should be different and thus provide a measure of the DA protonation state [15].

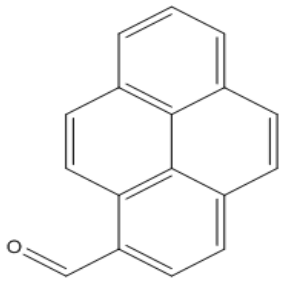

Figure 3.15: Chemical composition of 1-Pyrenecarboxaldehyde (PYCA).

Figure 3.15 shows the chemical structure of PYCA. The carboxaldehyde group allows for the non-polar pyrene conjugated system to become solvated at boundaries between polar and non-polar regions. Vesicles, micelles, and monomers all introduce different polarities in the solution. The fluorescence spectrum of PYCA varies according to the environment within which it is sequestered. Therefore, by preparing a series of control solutions it should be possible to determine the 'form', in effect the protonation state, of the DA within the coacervate systems.

The shift in λ_{MAX}, the wavelength with the highest measured intensity, of the PYCA fluorescence can be related to the Dielectric constant of the environment around the polar/non-polar boundary, by the following equation [16]:

$$\boldsymbol{\lambda_{MAX} = 0.52D + 431.5}$$

Equation 3.3: Dielectric Constant from PYCA. Where D is the dielectric constant and λ_{MAX} is the wavelength of the most intense fluorescent emission.

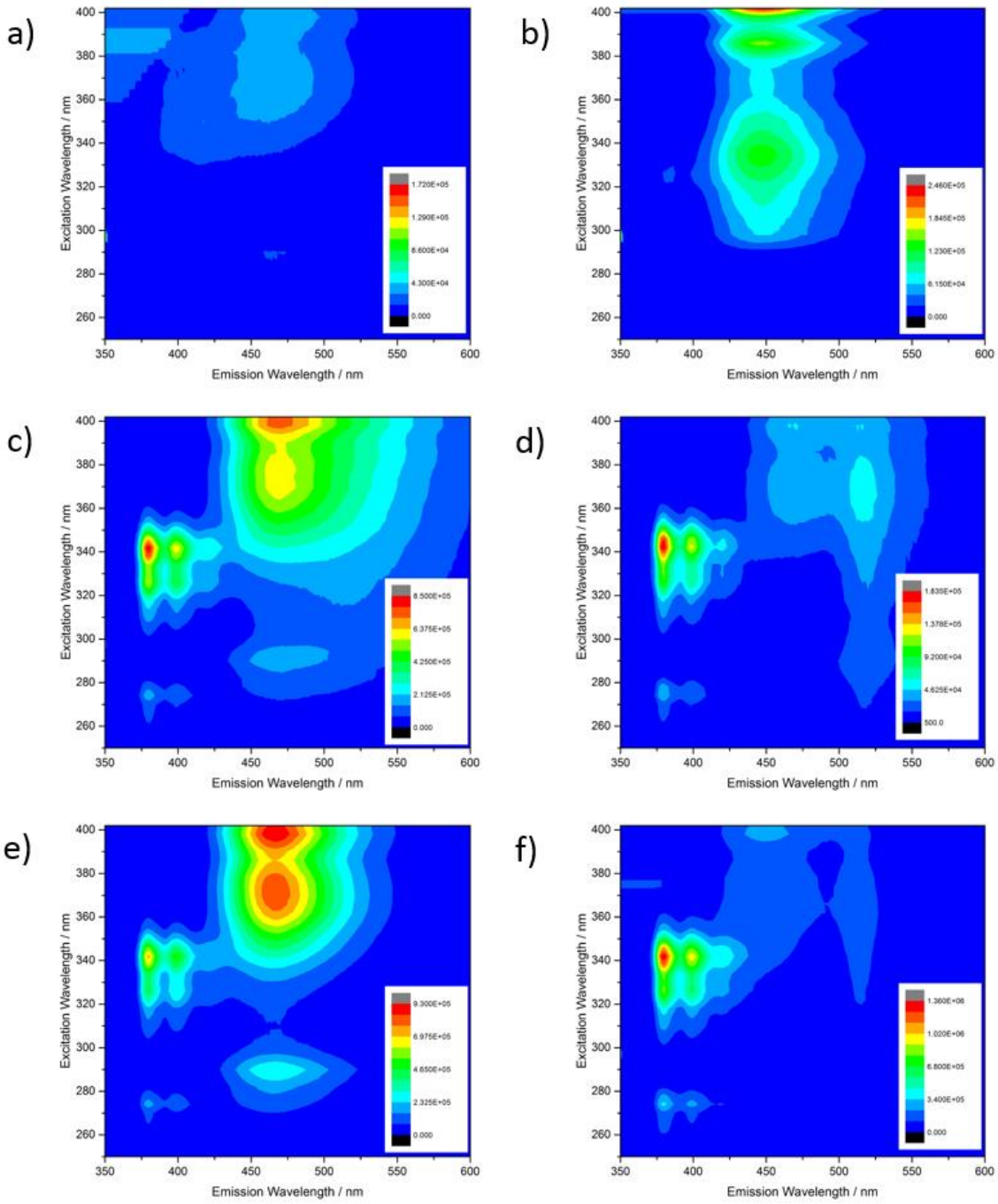

Figure 3.16: The 2D fluorescence spectra of 10 × 10^{-6} M PYCA in a) 80 mM DA at pH 5, b) 80 mM DA at pH 7, c) 80 mM DA at pH 9, d) 5 mM 8.5 kDa PDDA at pH 9, e) coacervates 5 mM PDDA and 80 mM DA at pH 9, and f) coacervates after the addition and equilibration of 2mM GDL.

pH 9, 7.5, and 1, 80 mM DA, 5 mM PDDA and aqueous 10^{-6} M PYCA control solutions were investigated. Selected emission data for these samples is shown in Figure 3.16. Solutions of DA at these pH values respectively give dielectric constant values for PYCA solvated at micellar,

vesicular, or oil water interfaces and thus indicate the protonation state of the DA. The results of the fluorescent maxima are described in Table 3-4.

Table 3-4: The various emission wavelengths and calculated dielectric constants of the coacervate system and its controlled components.

Sample	**λ_{MAX} (nm)**	**Dielectric Constant**
DA pH 9	465	64 ± 8
DA pH 7	446	27 ± 5
DA pH 5	456	47 ± 21
Coacervate	467	68 ± 2
Coacervate and GDL	448	31 ± 10
Coacervate Supernatant	469	72 ± 3
Coacervate Supernatant and GDL	467	68 ± 3
Re-dispersed Coacervate	454	43 ± 1
Re-dispersed Coacervate GDL	451	37 ± 3
Re-dispersed Coacervate Supernatant	455	45 ± 3
Re-dispersed Coacervate Supernatant and GDL	453	41 ± 8
PDDA	493	118 ± 57
$PYCA_{(aq)}$	453	41 ± 35

PYCA was sequestered within PDDA/DA microdroplets, PDDA/DA polymer-poor supernatant, 80 mM DA solutions at pH 5, 7, and 9, 5 mM PDDA, and PDDA/DA microdroplets after the addition and incubation of GDL and the same for the supernatant phase, to determine how the form that the DA takes within each of these instances, to understand how the system responds to pH adjustment. PYCA has one peak when stimulated with 360 nm wavelength light which shifts depending on the polarity of the solution that the molecule resides in. However, when this system

forms Schiff bases, when the aldehyde group of the PYCA reacts with primary or secondary amines, which are then subsequently reduced to substituted amines of the form $R'CH_2NHR$, PYCA exhibits a trio of peaks. Work done by Kalyanasundaram *et al*. showed that this occurred when the molecule was associated with micelles formed from dodecyltrimethylammonium chloride in the presence of $LiAlH_4$. Interestingly, while there are no primary or secondary amines present in this system, when micellar or vesicular structures are expected, in the case of the DA control solutions at basic and neutral pHs respectively, this trio of peaks was observed. Whilst this result was unexpected it did allow for the determination of the form of DA in the control solutions, in effect, micellar vesicular and oil-water phase separated. It could be that an interaction between the hydrophobic pyrene body of the PYCA and the tails of the DA leads to an interaction between the carboxylic group at the 'head' of the DA molecules and the aldehyde moiety on the intercalated PYCA molecule, which might modify the electronic structure of the chromophore such that its fluorescence spectra resembles that of pure pyrene. As can be seen in Figure 3.16 the superposition of the spectra of the micellar formulation of DA and PDDA can be directly contrasted with the spectrum of the PDDA/DA coacervate microdroplets. This shows that in the coacervate microdroplets the DA is highly likely to be in the micellar form, as expected as the microdroplets are formulated a pH 8.5. After the addition and incubation of GDL to reduce the pH of the system to the pK_a of DA, when vesicles should begin to self-assemble, we can see a reduction in the traditional PYCA emission at ca. 460 nm indicating a reduction in the micellar environments capable of sequestering PYCA.

The 5 : 80 mM PDDA/DA coacervates made using PYCA and redispersed in their own supernatant were studied under optical microscopy and fluorescence from the PYCA could be observed at the edges of the coacervates, indicating that the majority of the PYCA was sequestered at that point, as shown in Figure 3.17. This could indicate some structuration within the coacervate microdroplets, such as a hydrophobic/hydrophilic boundary within the polymer dense phase. The results from the fluorimetry investigation and optical microscopy experiment

using PYCA as a fluorophore were indicative of a distinction between DA protonation state within the PDDA/DA coacervate microdroplets.

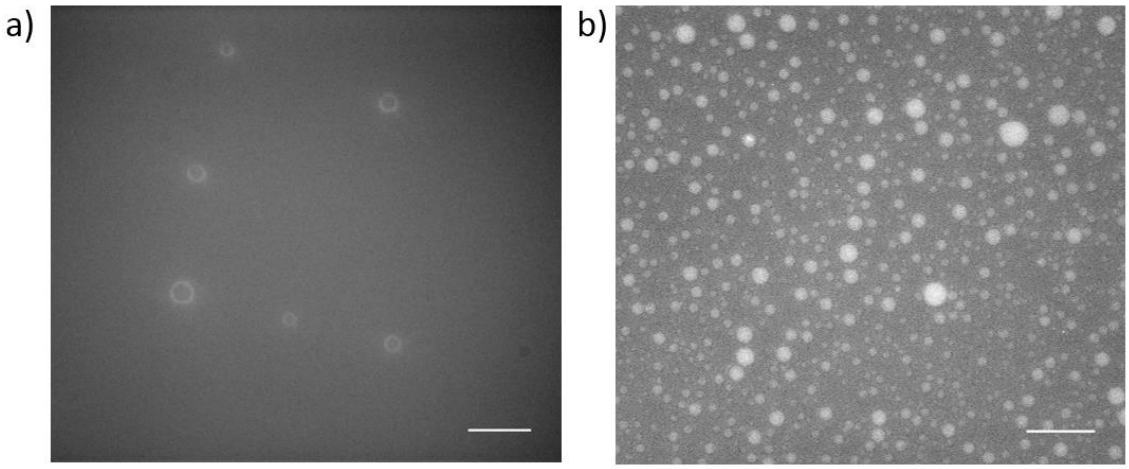

Figure 3.17: a) The micrograph shows the PYCA fluorescence within re-dispersed coacervates, fluorescence is observed at the edges of the polymer-rich microdroplet, b) the micrograph shows the PYCA fluorescence within carboxymethyl-dextran PDDA coacervates, another commonly made coacervate within the group [8], fluorescence is evenly distributed across the coacervate droplets.

Another method of understanding the structure and determining the localisation of the PDDA post transformation was performed by synthesising a fluorescent PDDA analogue. PDDA-co-DAA was thought to have a similar enough structure to PDDA to not interfere with coacervation and yet allow for the addition of a fluorescent moiety on the chain. The synthesis was performed as described above and characterised using ^{1}H-NMR spectroscopy, Varian 400 instrument with D_2O solvent. Below, in Figure 3.18, is the spectra for the synthesised PDDA-co-DAA. Peak A integrates for 20 H and is a pentamer, this indicates that the polymerisation of the DAA and DDA into the penta-cycles that form the backbone of the polymer chain have been successfully synthesised. Peak B integrates for 6H and is a singlet indicating that the quaternary ammonium salt has been preserved during the synthesis. This indicates that the synthesis has been successful.

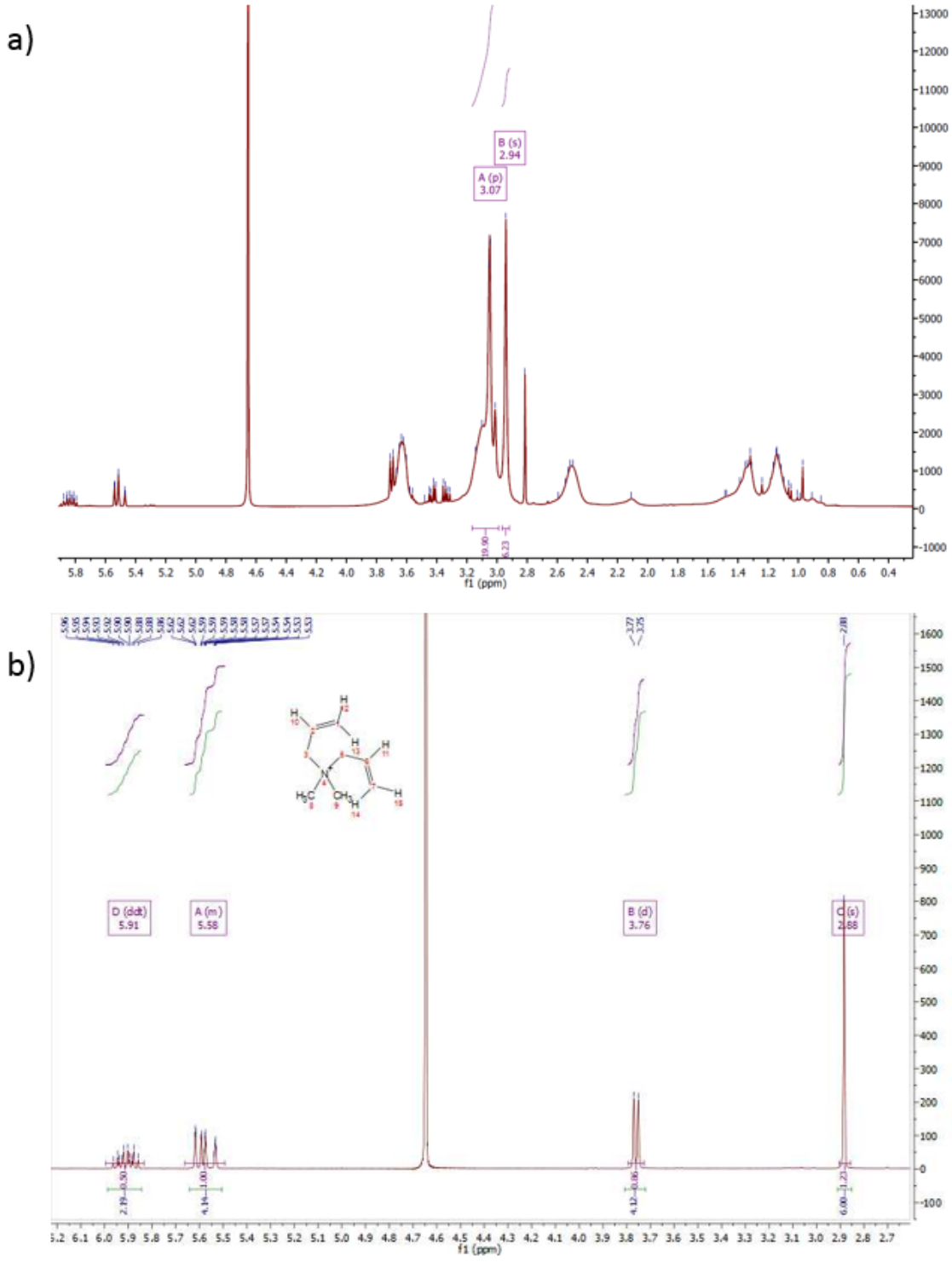

Figure 3.18: The [1]H Spectra for a) the PDDA-co-DAA synthesis product. Peaks 1, 3 and 5 correspond to hydrogen environments that do not exist in the precursor monomeric solution and are indicative of the desired structure being present, b) the DAA precursor monomer which does not exhibit the same pentamer signal.

As can be seen in Figure 3.19 the process of coacervation appears undisturbed when the tagged PDDA-co-DAA is combined with DA. Turbidity rapidly increases upon addition of DA indicating the presence of microdroplets.

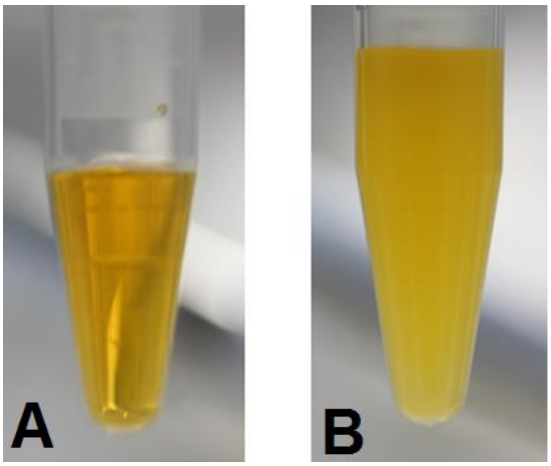

Figure 3.19: Photographs of a coacervate system formed from the FITC tagged PDDA-co-DAA. a) shows the transparent solution of FITC tagged PDDA-co-DAA. b) shows the solution after addition of 100 µL of 160 mM DA to form the coacervate microdroplets. As a result of the formation of the microdroplets, the solution becomes opaque.

To verify the presence of microdroplets, optical micrographs of the system were captured, and in Figure 3.20 coacervate microdroplets can clearly be seen. The coacervates can be seen buckle and begin to extrude vesicles after the addition of GDL. Fluorescence from the evolved vesicles can be seen, indicating that PDDA is transported from the microdroplets to the interior of the vesicles. The birefringence observed under crossed polarisers indicates that the vesicles evolved are multi-lamellar, Figure 3.20. This evolution and multi-lamellarity are similar in nature to optical micrographs captured of coacervate microdroplets produced using higher molecular weight polymer chains and higher polymer concentrations, which will be explored later in this chapter. This indicates that the synthesised PDDA-co-DAA is likely to be of a higher molecular weight than the desired 8.5 kDa used previously.

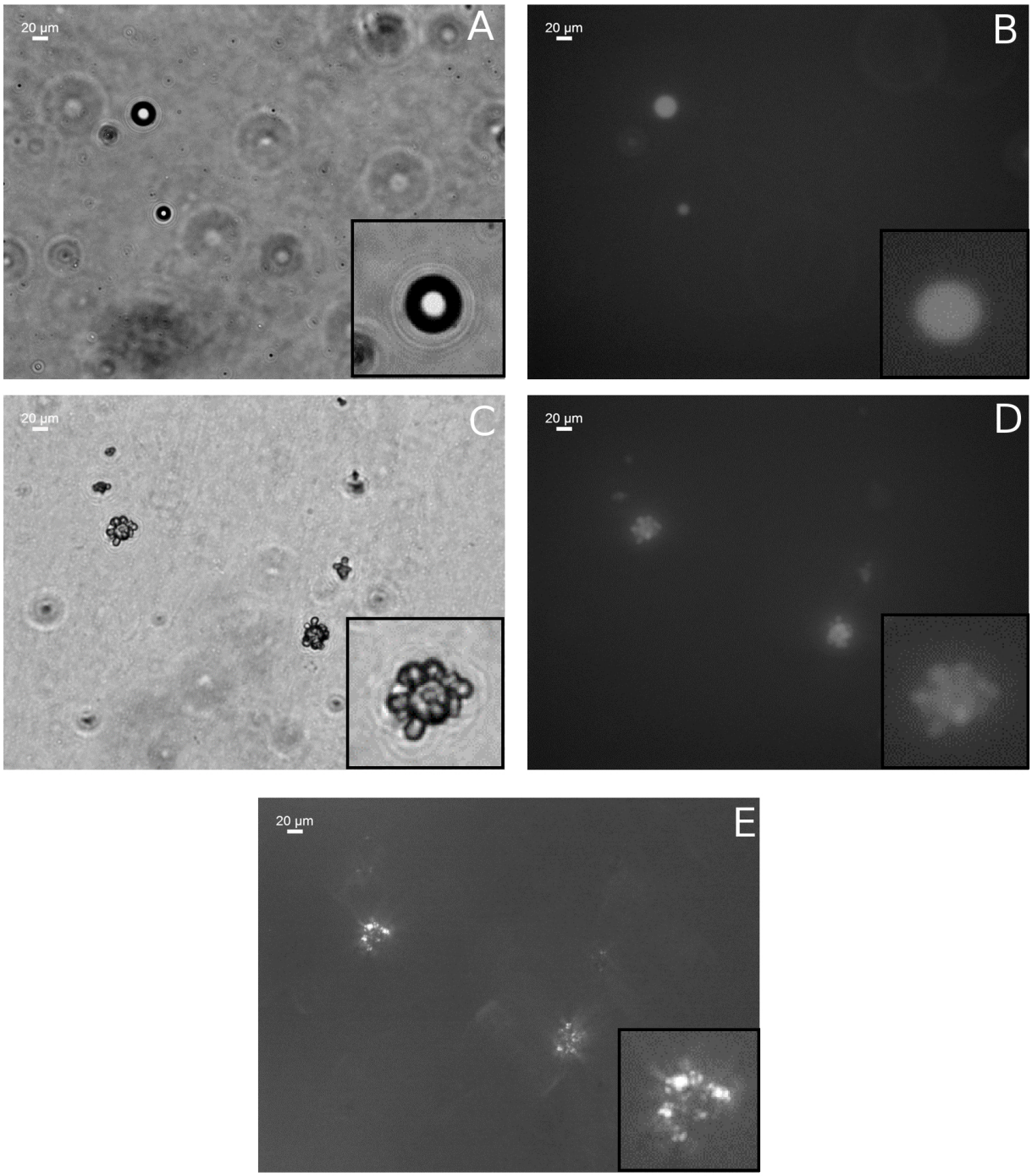

Figure 3.20: A set of optical micrographs which illustrate: a) the coacervates formed by the addition of DA to the FITC tagged PDDA-co-DAA solution, b) the localised fluorescence as a result of the tagged polymer that has undergone coacervation, c) the budding as a result of the addition of GDL, d) the localised fluorescence in the buds as a result of the fluorescent polymer, e) the Maltese crosses observed under crossed polarisers, indicating the multi-lamellar nature of the evolved buds and hence the high molecular weight of the synthesised polymer.

To preserve the character of the system during pH adjustment, a sample of 8.5 kDa PDDA was doped with PDDA-co-DAA synthesised and tagged with rhodamine isothiocyanate (RITC), at a doping percentage of 1%. The resulting transformation preserved the morphologies seen for low molecular weight formulations of the polymer in the coacervates as can be seen in Figure 3.21, where PDDA localisation is in red, BODIPY C12 illustrates the localisation of the DA and the presence of long vesicles that fluoresce in both red and green channels shows that PDDA is retained within the evolving vesicles structures that are attached to the coacervate microdroplets.

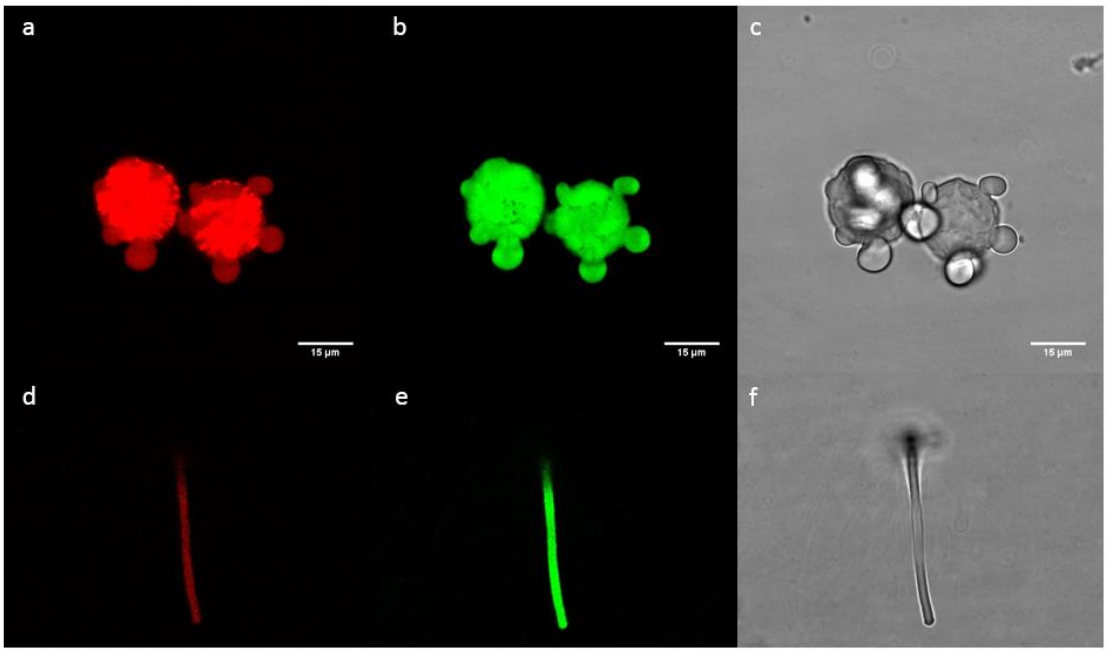

Figure 3.21: Fluorescent confocal micrographs of a) RhITC tagged Polydiallyldimethylammonium chloride – co – diallyldimethylamine localised within a budding coacervate, b) BODIPY doped DA localised within in a budding coacervate, c) brightfield image of the sample, d) the localisation of the tagged polymer after the evolution of the budding vesicle has extended into a characteristic elongated finger-like shaped vesicle, e) similarly for the BODIPY within the vesicle, f) and finally the brightfield, exhibiting no birefringence.

Having developed a methodology for investigating the PDDA location throughout the transformation process the next step was to develop one for the counter-species: DA. Determining the concentration of DA within the coacervate bulk phase and that of the supernatant phase is an

important step as this could be critical in understanding the transformation phenomena, it raises such questions as; do the vesicles draw DA monomer units from within the microdroplets or from the polymer poor phase? To do this the technique of nuclear magnetic resonance (NMR) was utilised.

The DA content of the re-dispersed coacervate system supernatant, shown in Figure 3.22, was also investigated in an attempt to understand the difference in polydispersity observed in the optical micrographs of the re-dispersed coacervate microdroplets, and the lack of vesicles evolved upon the adjustment of pH.

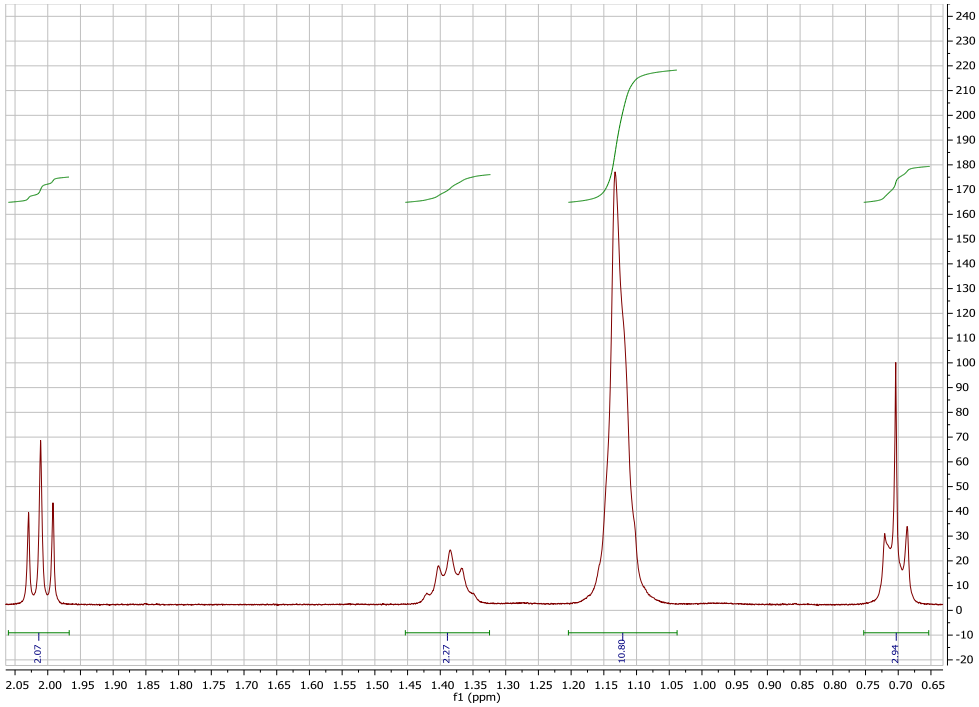

Figure 3.22: The ^{1}H-spectra for DA in the supernatant phase of re-dispersed PDDA/DA coacervates. The relative integral values for the chemical shift peaks are as follows from right to left: 2.94, 10.80, 2.27 and 2.07. The centres of the chemical shift maxima are, from right to left: 0.70, 1.13, 1.38 and 2.01.

Comparing the absolute integral value of the first peak in the spectra with that of the equivalent peak in the pH 12 DA 80 mM control, the calculated DA concentration is found to be

approximately 4 mM. This is significantly less than that for the non-redispersed coacervate suspensions found by the same methodology. Excess DA may be involved in the growth of the vesicles and the reduction in polydispersity may indicate an internal reconfiguration of the conformation of the PDDA/DA interactions that prevents evolution of vesicles.

3.2.3 Polymer Mediation

The system was found to exhibit various morphological responses to pH adjustment induced by addition of GDL, and subsequent incubation, when the weight of the polymer was varied. At low molecular weights (MWs), 8.5 kDa, long tendril-like unilamellar vesicles grew from the surface of the coacervate droplets, at medium MW, ca. 40 kDa, the system exhibited multiple, multi-lamellar structures at the surface of the coacervate, and at high MW, ca. 275 kDa, the droplets formed multi-lamellar shells templating around the entire droplet. Each of these instances is shown in Figure 3.23. The following sections illustrate these cases further.

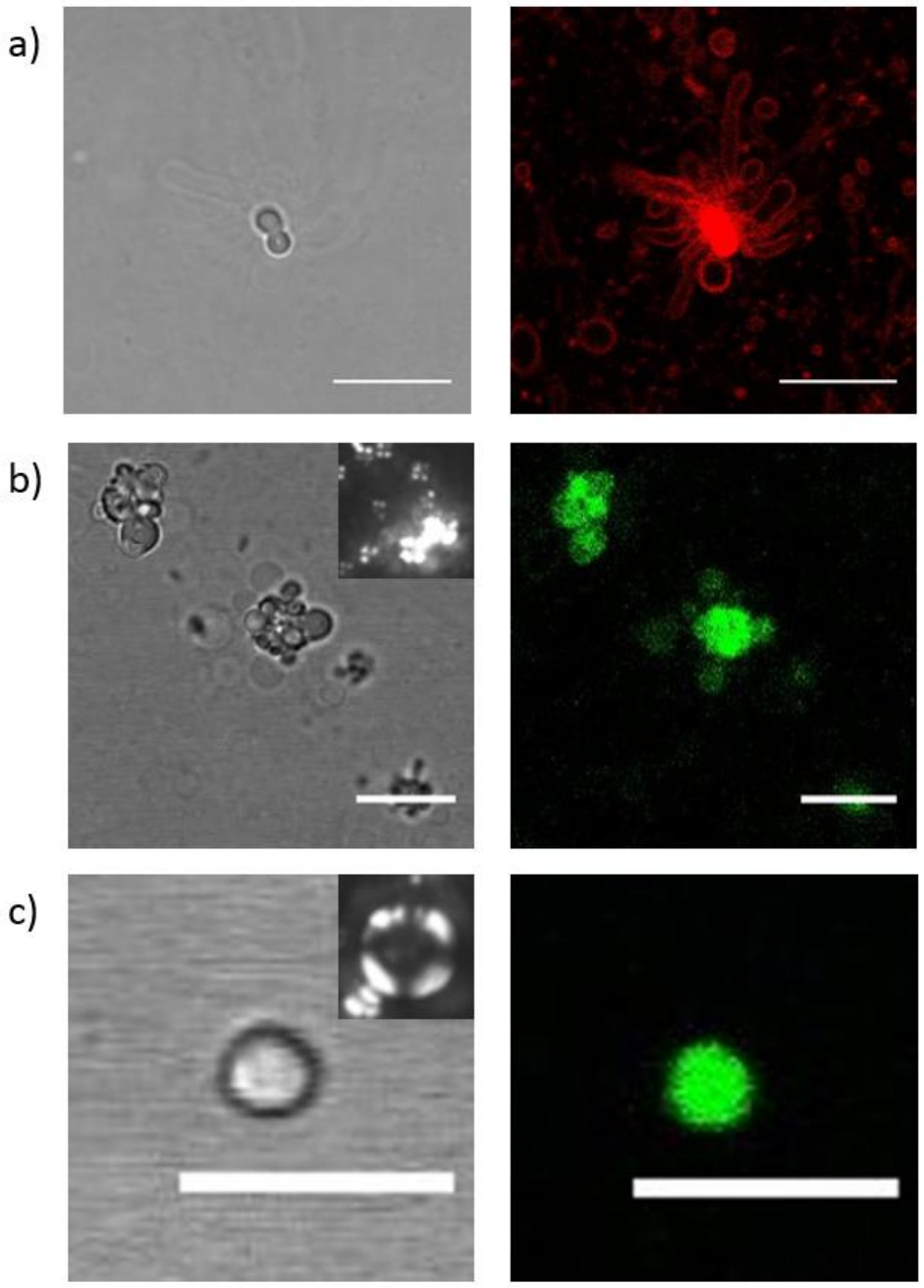

Figure 3.23: Brightfield and fluorescence micrographs of a) 8.5 kDa PDDA/DA coacervates stained with Nile Red, b) ca. 40 kDa PDDA/DA coacervates stained with acridine orange, inset illustrates Maltese crosses of each of the evolving vesicles from the microdroplets c) ca. 275 kDa PDDA/DA coacervates stained with acridine orange inset illustrates Maltese cross across the entire microdroplet indicating multi-lamellar structure forming over the microdroplet surface. Scale bars = 10 µm.

3.2.3.1 Low polymer weight

The system was formulated using PDDA with a MW of 8.5 kDa and the results of the effect upon morphological change are summarised in Figure 3.24. As GDL hydrolyses to form gluconic acid slowly lowering the pH of the system, production of high aspect ratio vesicles in response to the protonation of the fatty acid in the coacervate microdroplet was observed.

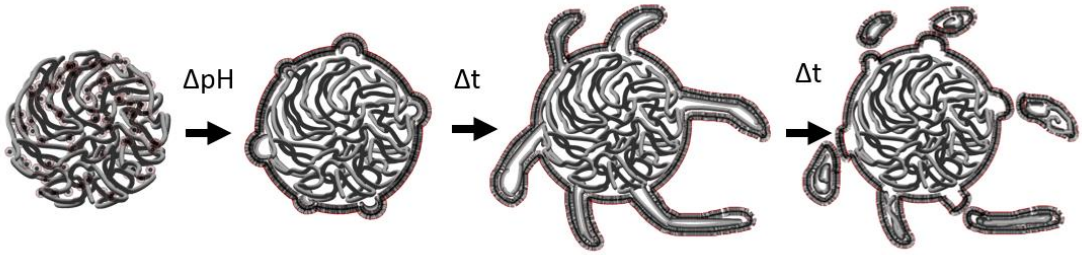

Figure 3.24: A scheme illustrating the response of PDDA/DA coacervate droplets when formulated with low molecular weight polymer upon exposure to GDL. Long, thin, high aspect ratio vesicles bud from the surface and grow with time, and eventually, through the process of vesicle fission, detach from the coacervate droplet.

From optical microscopy, multiple micrographs were captured and the average size distribution of the coacervates prior to and after pH adjustment with GDL was measured. In Figure 3.25 it can be seen that the coacervate polydispersity narrows after pH adjustment indicating that coacervates are disassembled during this process, their components either being drawn into the interior of the vesicles, as illustrated by the localisation of the polymer explored via fluorescence microscopy earlier, as they or formed or returning to a new equilibrium with the continuous phase.

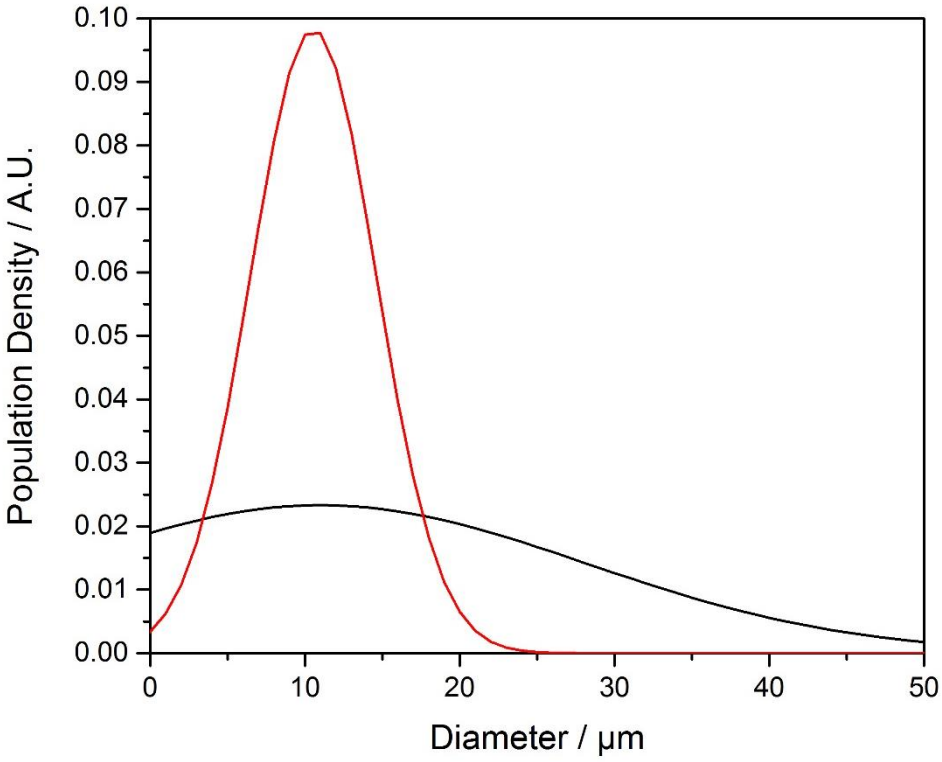

Figure 3.25: The size distributions modelled as Gaussian probability functions after obtaining the average size from optical microscopy measurements and calculating the standard deviation from that value. The black line represents the coacervate microdroplet diameter prior to GDL addition. The red line represents coacervate microdroplet diameter after the evolution of vesicles has begun.

This process was further investigated using atomic force microscopy (AFM), the results of which are summarised in Figure 3.26. The topology of the surface was revealed to be amorphous for the coacervates, which had been deposited onto the atomically flat mica substrate, whereas the structures seen surrounding the amorphous regions were seen to be uniform and crystalline in nature. This indicated that the vesicles emanating from the coacervates, in this low polymer weight scenario, were dehydrating under the drying process prior to the investigation, and this was forming the crystalline form of DA, as the pH of the system would have drastically increased as the water content decreased. The height analysis of these regions was compared to the theoretically expected height of a monolayer of DA and the heights were found to be

commensurate indicating that these structures were indeed comprised of fatty acid: it shows the crystalline structures possess a height of approximately 3.5 nm which is commensurate with the long axis from the crystallographic data which shows that the a-axis is ca. 2.2 nm, indicating that these could be bilayers of DA adhered to the surface of the mica with some intercalation of the alkyl chains.

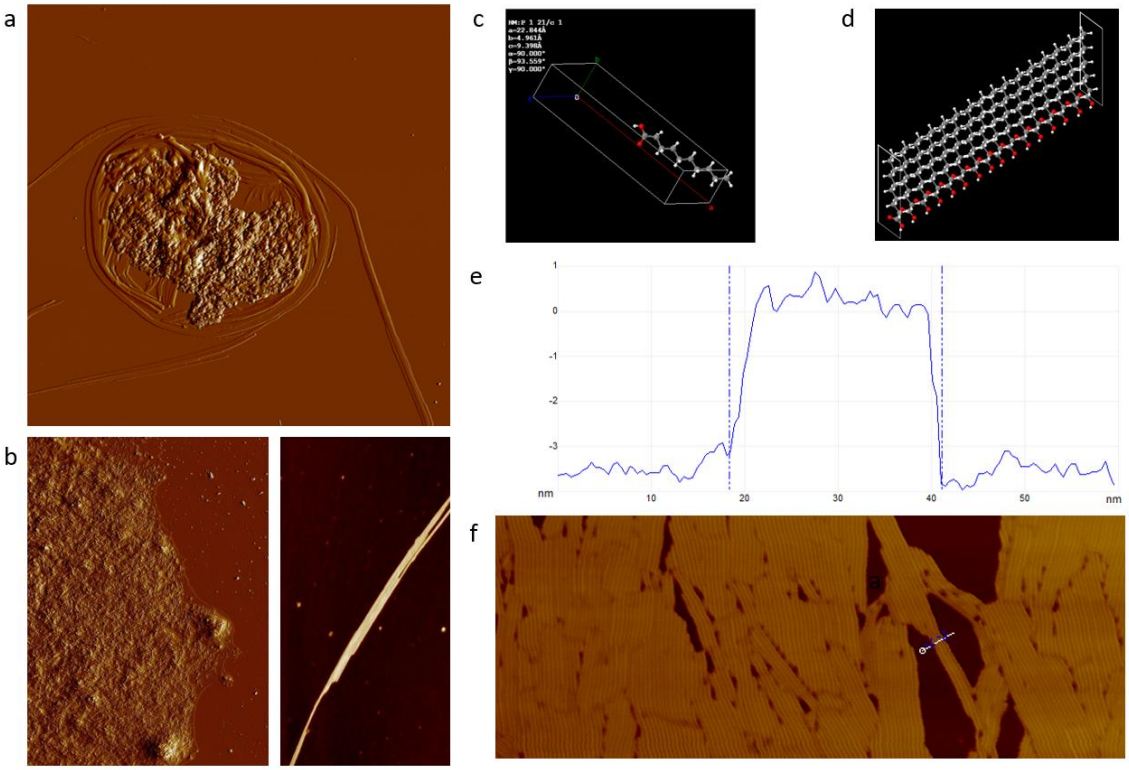

Figure 3.26: a) 10 µm scan of a PDDA/DA coacervate after addition of GDL. Sample illustrates amorphous coacervate interior and crystalline DA shell and tendrils leaving the droplet. DA will change protonation state as the sample was dried yielding an oil phase as opposed to vesicle phase, thus crystalline structures are indicative of the presence of where vesicles might have been in solution. b) 3 µm scan of PDDA/DA coacervate dried immediately after addition of GDL, various higher structures can be seen near the edge of the droplet indicating possible areas of vesicle evolution about to occur had the solvent remained. The right image is a 1.8 µm scan of a tendril from a) and shows the fine crystalline structure of the tendril. c) The crystallographic dimensions of decanoic acid, model from http://crystallography-online.com/structure/7050150. d) A model of the proposed structure for the DA tendrils observed from the crystallographic structure in (c). e) A line profile for the AFM segment illustrated in (f), it shows the crystalline structures possess a height of approximately 3.5 nm which is commensurate with the long axis from the crystallographic data in (c).

The mechanism by which this evolution occurs was further elucidated by using a kymographic analysis of the process as captured on video through confocal microscopy. A montage of this process is shown in Figure 3.27 which clearly illustrates the transformation from spherical deposited coacervate microdroplet to the distended multiple unilamellar vesicle extruding system.

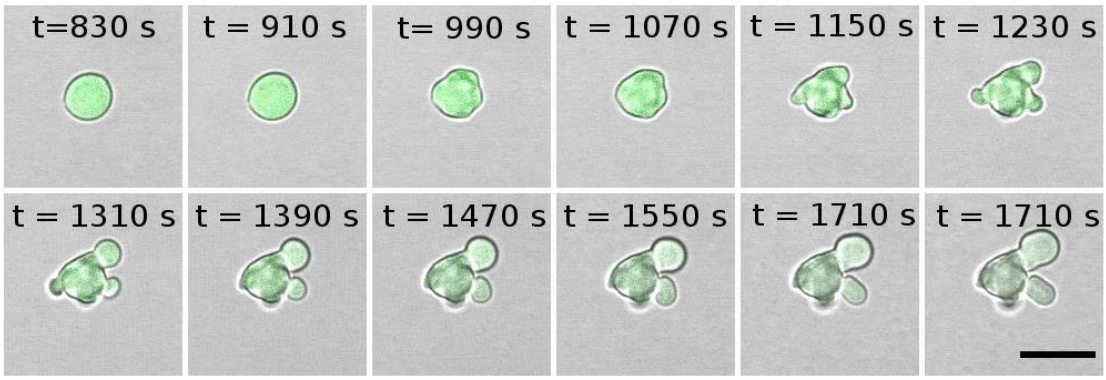

Figure 3.27: A montage of overlaid brightfield and fluorescent channels taken from a confocal video of the evolution of vesicles from Acridine orange containing coacervate microdroplet in response to addition of GDL. Scale bar = 10 µm.

Figure 3.28 is the analysis of this montage whereby a line segment was drawn across the boundary of a developing vesicle bleb and the change in greyscale value of the pixels being monitored was recorded with time.

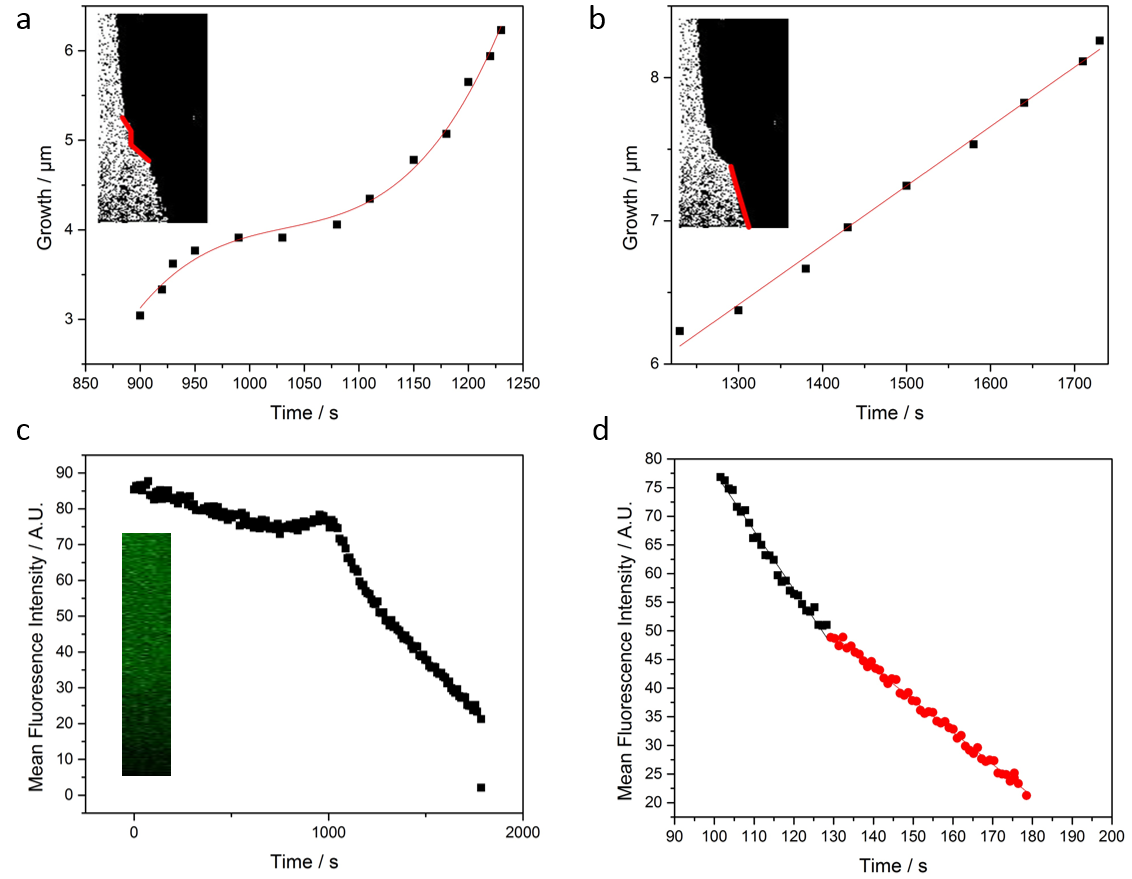

Figure 3.28: Kymographic data extracted from the montage of the vesicle evolution from Figure 3.27 a) A power series fit of the initial growth section of the vesicle bleb, the fit used followed the equation: $y = c + (B1 \times x) + (B2 \times x^2) + (B3 \times x^3)$; where the power coefficients were found to be $B1 = 7 \pm 1$, $B2 = -0.07 \pm 0.01$, and $B3 = 2.30 \times 10^{-4} \pm 3 \times 10^{-5}$; the adjusted R^2 for this fit was 0.96, indicating a good fit; inset shows the data from which the points were taken, this is a resliced of the vesicle growth front in the montage from Figure 3.27; b) A linear fit of the second growth region of the vesicle bleb as extracted from the Kymograph inset, the slope of this fit was found to be 0.04 ± 0.001 and the adjusted R^2 for this fit was 0.99, again indicating a good fit; c) a graph highlighting the mean fluorescence of the coacervate after vesicle growth which again illustrates the biphasic kinetics of the vesicle growth from the coacervate droplet, linear fits were used to describe the loss in intensity over the two regions and the slope for the first was found to be -0.102 ± 0.002 and for the second $-0.0560 \pm 6.3 \times 10^{-4}$, which is in agreement with the fits from (a) and (b) in indicating that the second growth regime of the vesicle is slower than that of the first.

The growth behaviour observed and analysed using the kymograph extracted from the recorded video of the vesicle extrusion, is biphasic. The first phase of the growth of the vesicle is faster than the second phase and this could be a result of the initial higher concentration of DA available to be incorporated into the vesicle membrane from the coacervate interior and the supernatant of the coacervate suspension. After this stock has been exhausted the only remaining avenue for further monomer incorporation is from the surrounding solution and this is limited by the surface area of the vesicle membrane, which yields a linear growth rate as observed. This behaviour of fatty acid vesicle growth has been observed and characterised by Szostak et al [17].

As a result of this bi-phasic growth behaviour, the following schematic of vesicle growth has been postulated, this is illustrated in Figure 3.29.

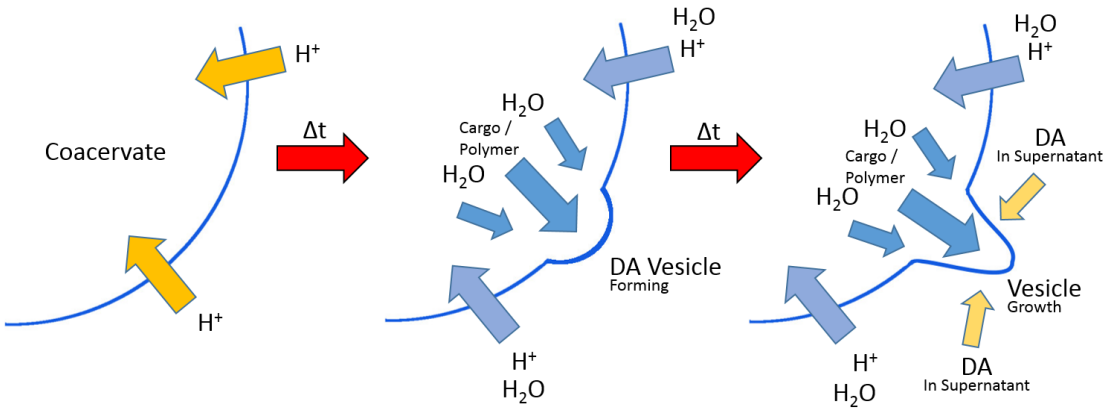

Figure 3.29: The system begins as a uniform coacervate droplet which experiences a change in pH as acid is added to the system. As time progresses the influx of protons to the interior of the coacervate microdroplet changes the protonation of the DA comprising the coacervate and begins to reach the pK_a of DA, at this point the decanoic acid will begin to form vesicle structures and DA within the coacervate and in the supernatant around the coacervate will contribute to the increase in vesicle volume. Once the DA localised in the region of the vesicle has been exhausted, the only source of DA molecules available for further increase in membrane surface area will be from the supernatant. Influx of water into the rapidly disassembling interior of the coacervate microdroplet is then drawn into the interior of the growing vesicle membrane. An imbalance between the influx of water and growth rate of the membrane creates an osmotic pressure which produces long tendril like vesicles which swell with time, when the membrane ceases to grow.

The two phases of vesicle growth can be related to the amount of free DA available to being incorporated into the vesicle membrane. In the first phase, the membrane can draw on DA within the coacervate and within the supernatant solution surrounding it. As the DA within the coacervate becomes exhausted the DA available for incorporation come solely from the surrounding solution, thus decreasing the rate at which the membrane can grow. This growth is limited by the surface area of the vesicle as incorporation of free DA into the membrane is driven via flip-flop of molecules until equilibrium is reached between the vesicle membrane and the monomeric surrounding solution.

To further investigate this membrane small angle x-ray scattering was utilised. The technique makes use of the ability of nucleons to scatter x-ray photons when arranged in a crystalline structure. This scattering is dictated by Bragg's law which determines the angle of the scattering vector of the x-rays as discussed in chapter 2 of this thesis. Three scattering peaks were observed in the spectra obtained performing SAXS as can be seen in Figure 3.30. These peaks could correspond with bilayer and monolayer DA leaflets, 4.7 and 6.5 nm respectively, but given the large amount of DA in solution it is feasible that DA adhered to the quartz container and that these signals are as a result of these structures, as opposed to vesicles in solution as a result of pH adjustment and evolution from coacervate microdroplets. Again, due to the amorphous directionality of the vesicles formed and their spatial anisotropy scattering data is likely only ever to be able to reveal this level of detail.

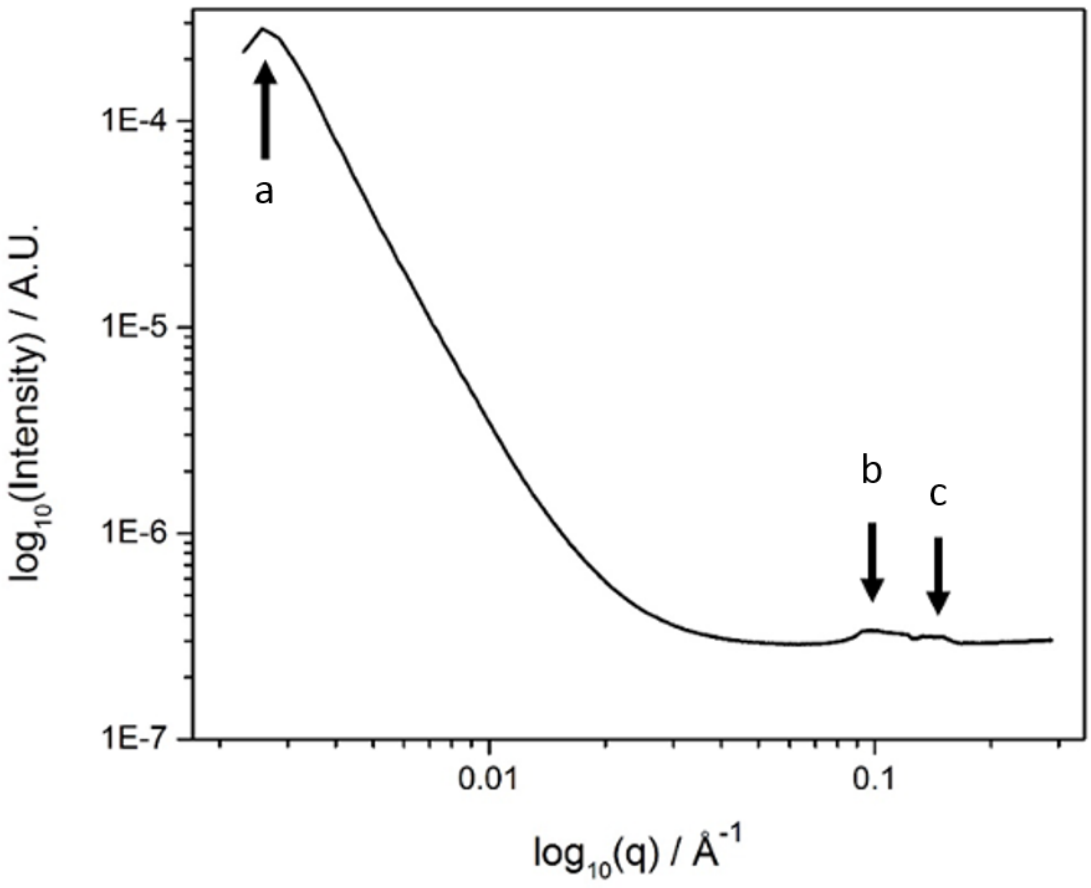

Figure 3.30: 1D averaged scattering data of PDDA/DA coacervates formulated with 8.5 kDa PDDA and activated with GDL, obtained via SAXS, illustrating three peaks, from left to right, which correspond to structures corresponding to spacing every 243.5, 6.5, and 4.7 nm (a, b and c) respectively.

It was hoped that the technique might be able to reveal information as to the structure of the microdroplets however a very broad peak centred on 243 nm indicates only that there is a large polydisperse population of structures at this size. As to whether these are nano-sized microdroplets or domains of polymer within the suspension, the technique was not able to resolve this. Potentially small angle neutron scattering (SANS), and deuterated polymers would be able to produce data of sufficient enough precision to further investigate this but the production of deuterated polymers was prohibitively expensive.

3.2.3.2 Medium polymer weight

When the PDDA/DA system was formulated using 40 kDa PDDA the morphological transformation can be seen summarised in Figure 3.31 and Figure 3.32. The microdroplets produce multi-lamellar buds at their surface. These buds fluoresced along with the coacervate interior indicating that there was a contiguous coacervate phase within the buds and the interior of the droplet that the dye could diffuse through, illustrating that these objects were connected without a boundary between them, Figure 3.32.

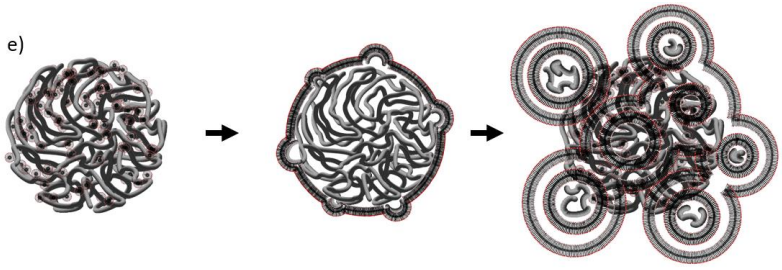

Figure 3.31: A scheme illustrating the response of PDDA/DA coacervate droplets when formulated with medium molecular weight polymer upon exposure to GDL. Small vesicles bud at the surface of the coacervate but exhibit birefringence under crossed-polarisers indicating a multi-lamellar surface has been formed around each of these protrusions.

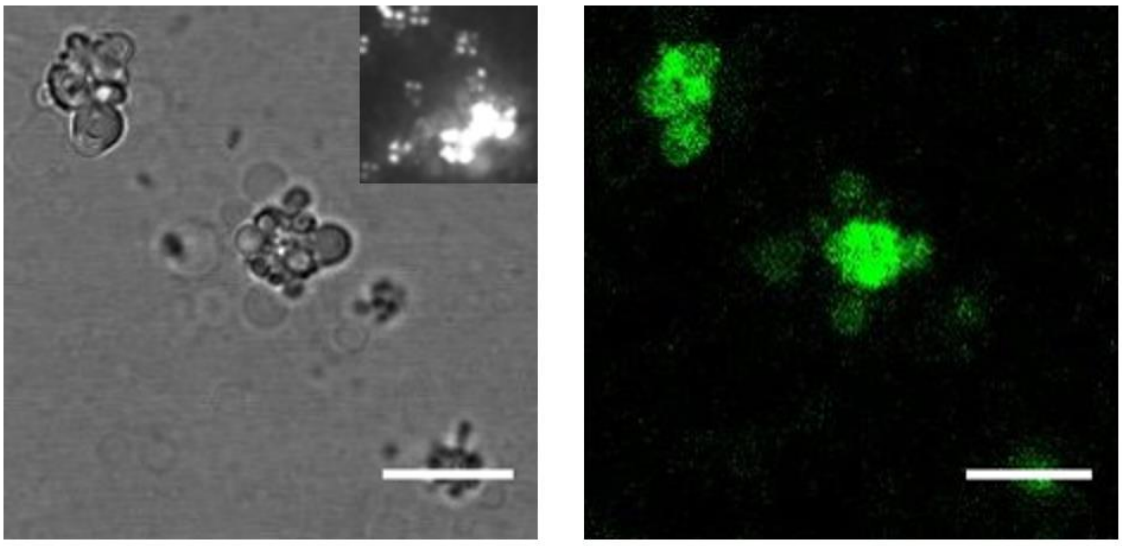

Figure 3.32: Brightfield and fluorescence micrographs of the ca. 40 kDa PDDA/DA coacervates after addition of GDL. The inset, a crossed-polarizers micrograph, illustrates the

multilamellar nature of the vesicles that evolve from the coacervate droplets, which also preserve molecular dyes which are sequestered within the coacervate droplets before the pH adjustment, as can be seen in the fluorescence channel, acridine orange sequestered within. Scale bars = 10 µm.

3.2.3.3 High polymer weight

The system was formulated using PDDA with a MW of 275 kDa and the results of the effect upon morphological change are summarised in Figure 3.33 and Figure 3.34. The morphological change in this instance appeared to be the formation of multi-lamellar fatty acids at the surface of the coacervate microdroplets.

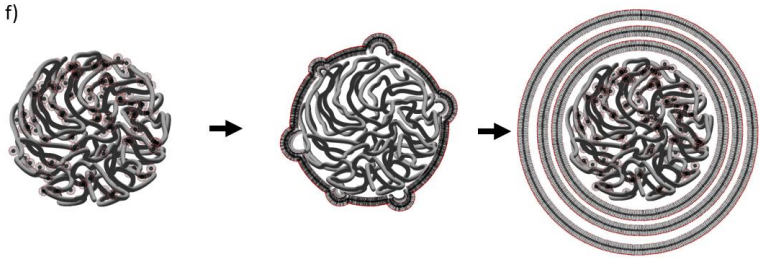

Figure 3.33: A scheme illustrating the response of PDDA/DA coacervate droplets when formulated with high molecular weight polymer upon exposure to GDL. The surface of the coacervate buckles and distorts but remains mostly spherical, the entire object begins to exhibit strong birefringence observed under crossed-polarisers indicating a multi-lamellar structure all over the microdroplet.

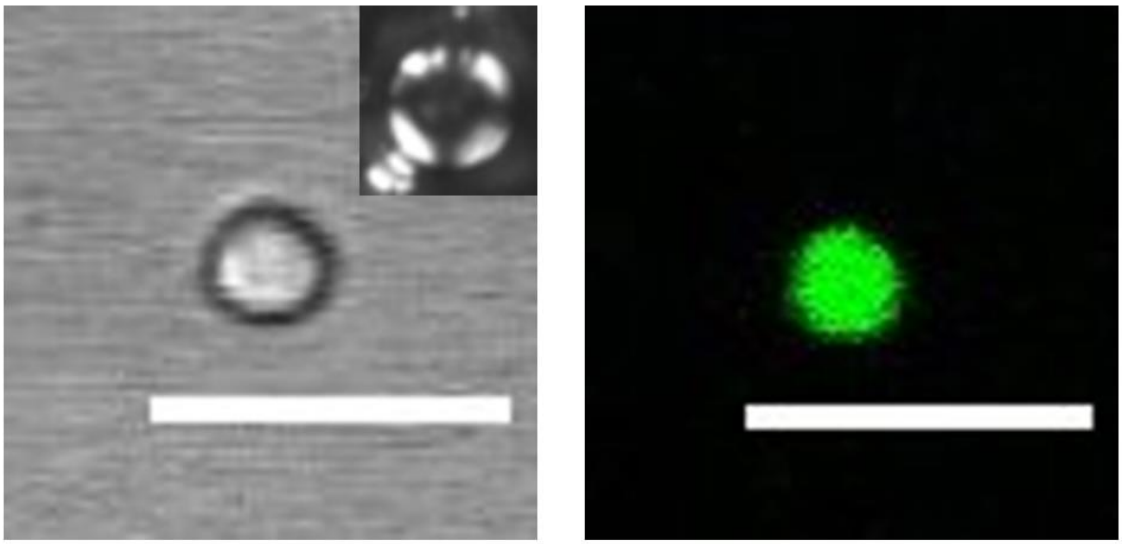

Figure 3.34: Brightfield and fluorescence micrographs of the ca. 275 kDa PDDA/DA coacervates after addition of GDL. The inset, a crossed-polarizers micrograph, illustrates the Maltese cross that is seen over the surface of the coacervate droplet after the pH adjustment, indicating that DA forms multi-lamellar bilayers over the surface of the microdroplet, with acridine orange sequestered within. Scale bars = 10 µm.

3.2.3.4 Polymer weight mediation hypothesis

To understand how the polymer weight was affecting the morphological response of the DA vesicle formation in response to the pH adjustment of the coacervate environment being lowered by the addition of GDL, it was thought that there might be a difference in composition of the coacervates, that there might be domains of polymer of varying sizes, due to chain connectivity increasing with polymer weight. To investigate this, and the effect it might have on local viscosity in the coacervate microdroplets (as this would affect the diffusion of compounds through the system and hence affect the formation of the vesicles), fluorescence lifetime imaging (FLIM) was utilised to determine the internal structure of the microdroplets.

This technique relies on the quenching of fluorescence of a molecular that possesses a moiety that is free to rotate within the molecule. The rotating group functions as an energy dissipater for the

molecule, which when excited with a photon can either; re-emit the photon to dissipate the energy that it received when it emitted, in effect via fluorescence; or the rate of rotation of the freely moving moiety can change and thus increase its rotational kinetic energy to be commensurate with the energy absorbed, and subsequently transmitted to its environment via collisions with the rotating group. The experimental method described in Chapter 2 was used to determine the following data with regards to the composition of the PDDA/DA coacervate systems.

Figure 3.35 shows the data collected to determine the fluorescence lifetimes of sulforhodamine B, which was sequestered within the coacervates, the polymer solution, and the fatty acid solutions. The heatmap shown maps the pixel by pixel fluorescence lifetime which can be correlated to a viscosity and illustrates that the coacervates were homogenous throughout, illustrating no regions of significantly higher or lower viscosity which would indicate regions of concentrated polymer or fatty acid. This was consistent across all coacervates measured and did not vary with polymer weight indicating that the molecular crowding of the coacervate microdroplet interior was not responsible for the variation in morphological responses observed when adjusting pH with GDL.

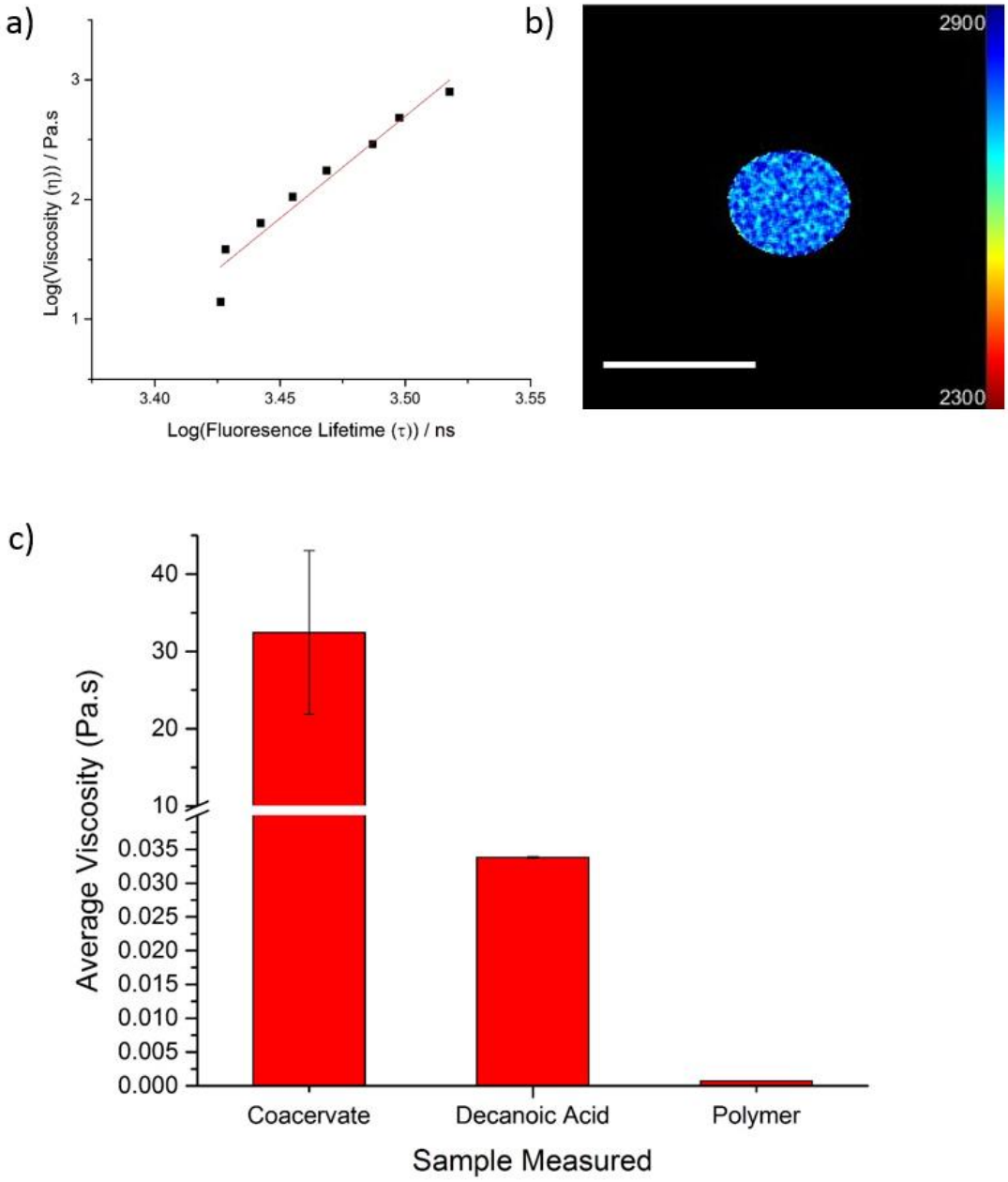

Figure 3.35: a) the fluorescence lifetime decay of the sulforhodamine B molecular rotor in varying viscosities produced by varying mixtures of glycerol and methanol, b) a fluorescence lifetime heatmap of a coacervate droplet as imaged on the confocal instrument equipped with the FLIM instrumentation, and c) the collected data for the average viscosities recorded for the coacervate droplets, the free micellar fatty acid solution, and the polymer solution. Scale bar = 10 µm.

Dervaux *et al.* [18] studied the effect of vesicle growth via fatty acid insertion into preformed vesicles, and varied the osmotic pressure on the vesicles, their size, and whether they contained a polymer (poly(etheyleneglycol)). They observed and determined a phase diagram for stable and unstable growth of the vesicles. From this they produced a simple physical growth model that can be described thus:

$$\frac{\partial A}{\partial t} = \frac{Na^2cDA_0^3\phi^2}{8\sqrt{\pi}lv_s}\frac{1}{A^{\frac{3}{2}}}$$

Equation 3.4: Rate of Growth. Where A is the surface area of the vesicle, N is the Avogadro constant, a is the area per fatty acid molecule, D is the fatty acid diffusion constant, A_0 is the initial area of the vesicle, ϕ is the initial volume fraction of the polymer, l is the diffusive boundary layer of the vesicle, v_s is the volume of the solvent molecule, and c is the external fatty acid concentration.

To solve this non-linear differential equation, the authors posit the following solution:

$$A = (A_0^{\frac{5}{2}} + \frac{5}{2}\alpha t)^{\frac{2}{5}}$$

Equation 3.5: Differential Solution. Where A is the surface area of the vesicle and t is time.

and:

$$\alpha = \frac{Na^2cDA_0^3\phi^2}{8\sqrt{\pi}lv_s}$$

Equation 3.6: Differential constant. Where N is the Avogadro constant, a is the area per fatty acid molecule, D is the fatty acid diffusion constant, A_0 is the initial area of the vesicle, ϕ is the initial volume fraction of the polymer, l is the diffusive boundary layer of the vesicle, v_s is the volume of the solvent molecule.

This model agreed well with their experimental data and illustrates that the volume fraction of the polymer within the vesicle as it grows with respect to fatty acid incorporation into the bilayer

from the external well has a stabilising or destabilising effect upon the growth regime of the vesicles. With respect to the PDDA/DA system investigated in this chapter, one could link the polymer weight to the volume fraction present within the vesicle, due to increased connectivity of the monomer units with increasing chain length, as individual polymer chains are sequestered within the growing membranes. Thus, this will influence the stability of the vesicle growth as outlined by Deveraux *et al.*, as fatty acid becomes incorporated into the bilayer that is formed as the pH of the system begins to fall upon hydrolysis of the GDL, the membrane will also interact with the polymer from the coacervate microdroplet.

When using this model to explore the stability of vesicles formed in the systems explored in this chapter, one can consider the volume fraction of the PDDA chain which varies with the molecular weight of the polymer. Constant monomeric concentrations were used to preserve the charge stoichiometry of the coacervate droplets, however, the connectedness of these monomers changes with molecular weight, as chain length increases with the polymer weight increasing. This places a constraint on the number of molecules that can charge match along the alkyl backbone through electrostatic interactions due to steric hinderance.

To investigate this link between polymer weight, chain connectivity, length, and interaction with fatty acid membranes forming from a pool of excess fatty acid, the following experiment was undertaken. Glass slides were functionalised electrostatically with various weights of PDDA, as described in the Section 3.1. These slides were then used to image solutions of monomeric basic DA with a molecular dye, hydroxypyrenetrisulfonic acid (HPTS) a common bilayer dye. The system fluoresced homogenously prior to the addition of GDL as there were no bilayers present and the dye was distributed homogenously throughout the solution. As GDL was added to the solution, the formation of vesicles was monitored at the surface of the slides and in the bulk solution above. The vesicles in the bulk of the solution formed a variety of polydisperse

morphologies, ranging from high aspect ratio tubes to low aspect ratio spheres and multi-component forms in between, ranging from oblate spheroids to biconcave discs, although all possessed some form of symmetry axis. However, at the surface of the glass slides, where polymer was bound and free to interact with the forming vesicle surfaces, a more homogenous morphology was formed. This can be observed in Figure 3.36.

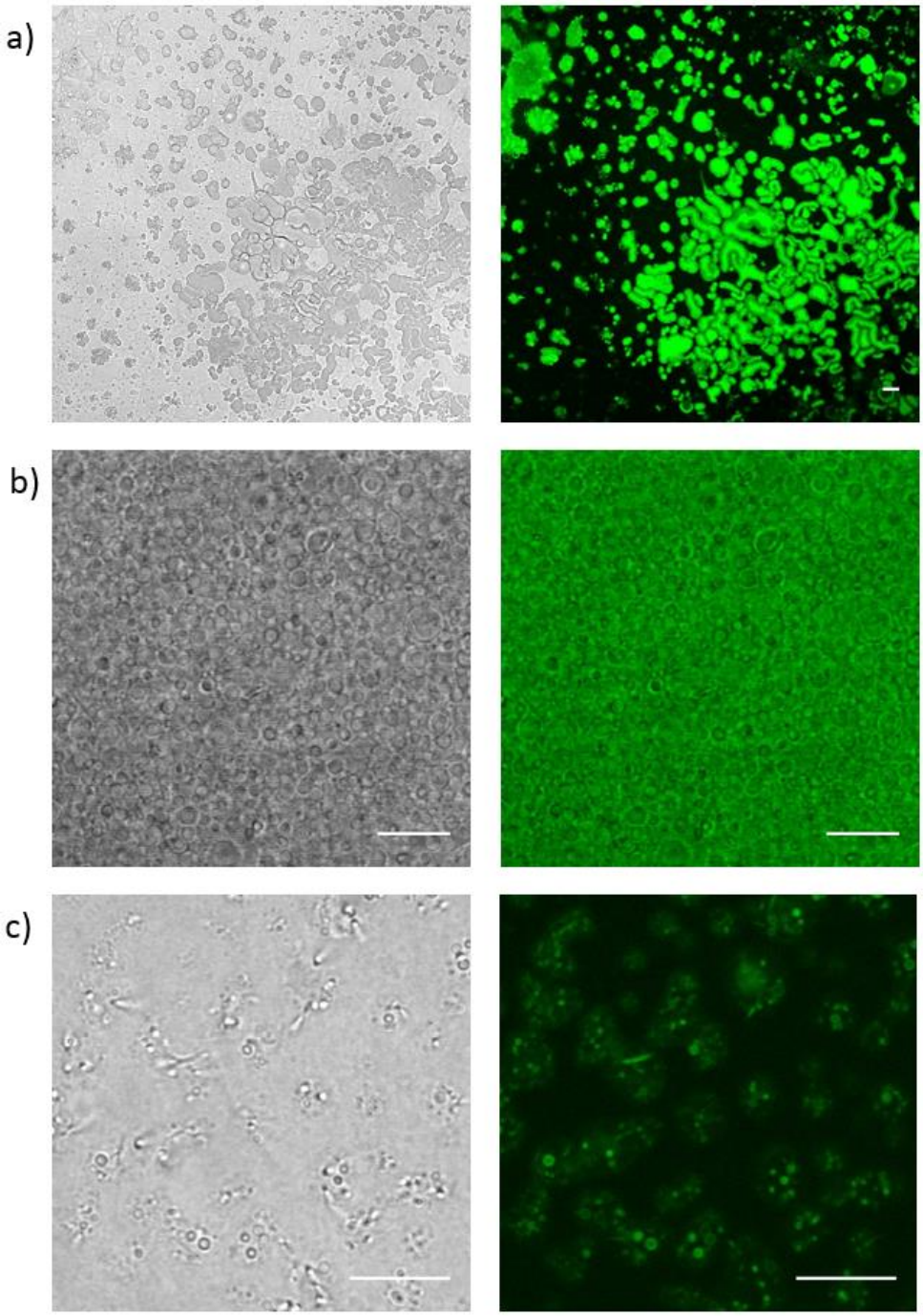

Figure 3.36: Micrographs of micellar DA transformed into vesicles via controlled pH adjustment through the addition of GDL in the presence of electrostatically functionalised glass cover slips coated with varying molecular weights of PDDA; the images portrayed are of brightfield and fluorescent micrographs for a), 8.5 kDa, b), 40 kDa, and c) 275 kDa MW PDDA stained with HPTS. Scale bars = 10 µm.

The micrographs illustrate the vesicle morphologies for a), 8.5 kDa, b), 40 kDa, and c) 275 kDa MW PDDA. For the low polymer slides, elongated high aspect ratio vesicular tubes are readily observed all over the functionalised surface. For intermediate polymer weights, low aspect ratio multi-lamellar vesicles were found all over the slide. At high polymer weights, the vesicles seemed to form dense highly spatially localised low aspect ratio objects, grouped within a larger amorphous geometry, which presumably reflected the inhomogeneity of the polymer binding to the glass.

To determine whether the only factor affecting the formation of various morphologies of fatty acid vesicles was polymer length, another experiment, utilising acoustic tweezers was undertaken – a powerful method for arranging arrays of soft matter objects into arrays in solution, that relies on density differences between the objects that are desired to be manipulated and the medium in which they reside [19]. PDDA/DA coacervates with low polymer weight were formulated by pipetting the polymer solution into the acoustic cavity and applying a continuous acoustic force from the driving oscilloscopes. The driving frequencies were set such that a standing wave pattern was formed, and the fatty acid solution was then added to this. As the size of the forming coacervate microdroplets, increased via coalescence, as the fatty acid solution diffused through the polymer solution, the droplets began to feel the acoustic force as they came up to the critical size and move to the minima of the applied force field. This process terminates with coacervate droplets of larger than normal size distribution, 23 ± 11 μm, patterned into a square grid, as can be seen in Figure 3.37. Any dyes added to this system that favourably partition within the bulk phase do so and the resulting localisation of fluorescence can be also observed in Figure 3.37.

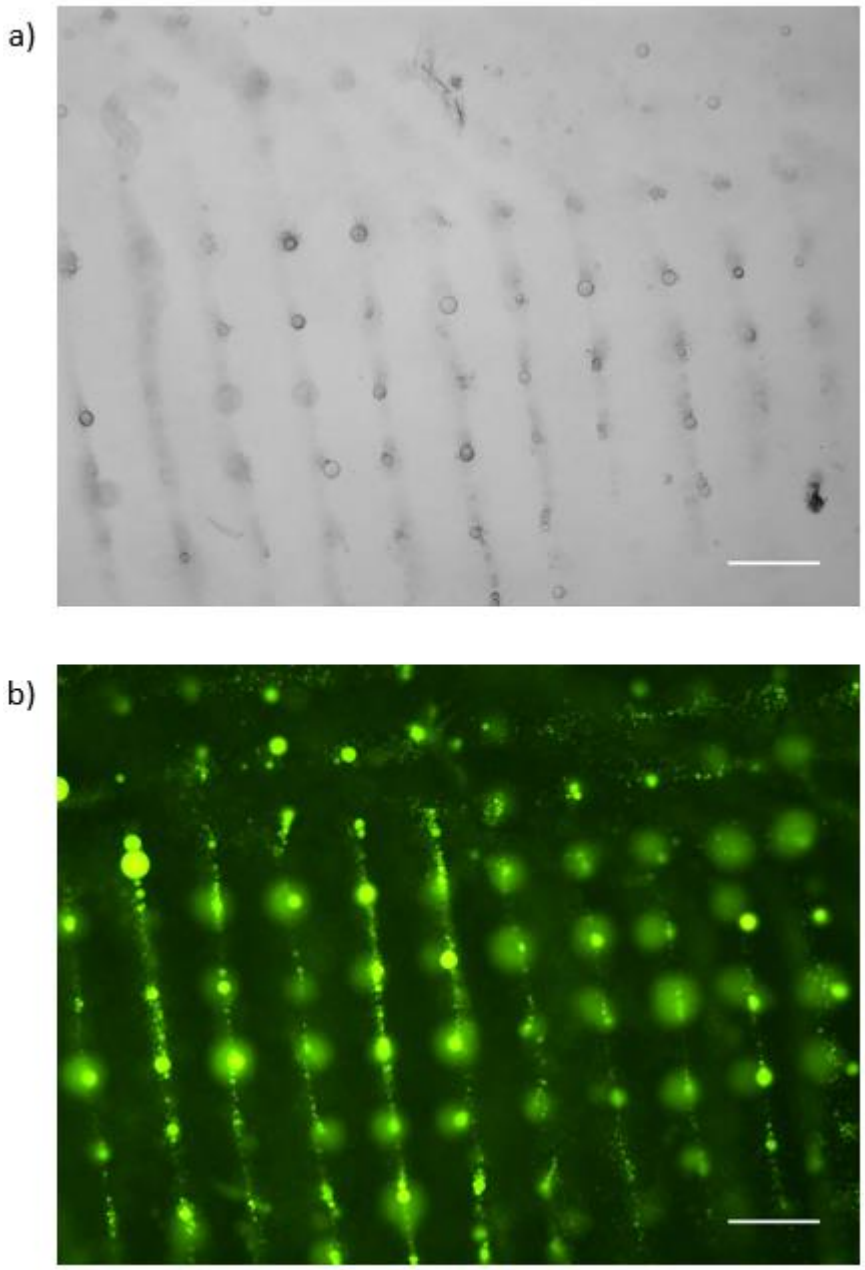

Figure 3.37: a) brightfield and, b) fluorescent micrographs of PDDA/DA coacervates with Acridine Orange sequestered within, formed under acoustic pressure in an acoustic trap patterned to form a grid-like array of droplets. Scale bars = 100 µm

It was suspected that the unstable growth of the fatty acid bilayer was driven by a difference in the growth rate of the membrane and the rate at which the volume of the vesicle changed as water filled its interior via osmosis. The growth of the membrane would be mediated by the polymer

weight as explored previously in the various coacervate formulations and via the functionalisation of the glass plates. The osmotic pressure pushing the membrane outwards would compete with the acoustic pressure acting on the coacervates exteriors to push them towards the nodes of the acoustic field, producing the organised pattern of the microdroplets.

As can be seen in Figure 3.38 the effect of GDL added to the patterned coacervates with and without the acoustic field being applied is marked. In a) the acoustic field remains applied and the overall spatial localisation of the droplets remains as the acoustic force overcomes Brownian motion which would disrupt the organisation of the droplets. The acoustic force providing this organisation also appears to have competed with vesicles being formed, which in this low polymer weight formulation would have been expected to be of a high aspect ratio emanating from the surfaces of the droplets. However, the vesicles formed appear to have been internalised within the coacervate droplets, forming spherical water filled vesicles of a low aspect ratio presumably due to the isotropic force felt around the coacervate from the acoustic field. In b) the field was turned off with the addition of the GDL. As the GDL hydrolyses lowering the pH of the system there is time for the microdroplets to randomly ‘walk’ around their grid positions, Brownian motion here disrupts the spatial organisation driven by the initial application of the acoustic field. Here, microdroplets have a series of vesicle ‘bumps’ emanating from their surfaces. However, due to the increased size of the microdroplets, because of the forced aggregation of many coacervate microdroplets into a smaller area and subsequent coalescence (due to lack of membrane and low interfacial surface tension) into larger ‘mesodroplets’, these vesicles do not possess the same characteristic high aspect ratio unilamellar composition observed in the normal coacervate system.

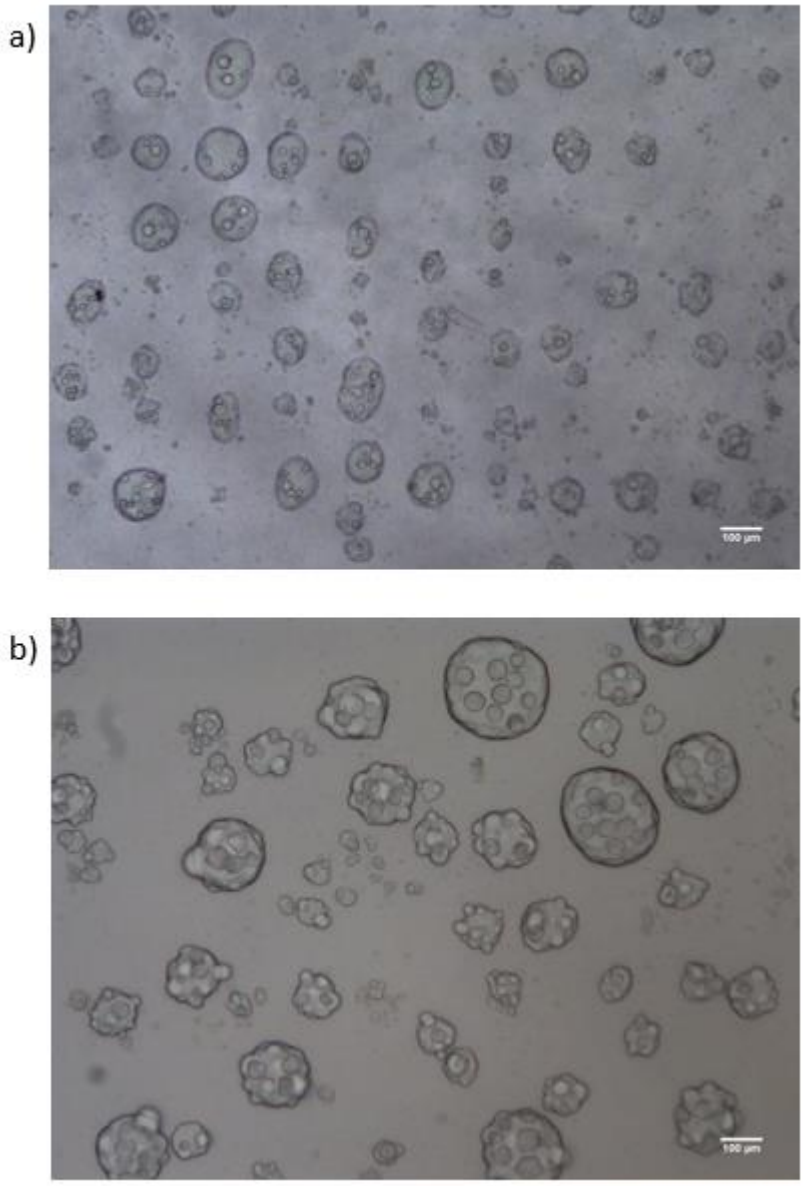

Figure 3.38: Brightfield micrographs of a) PDDA/DA coacervates transformed with GDL in the presence of an acoustic field from a rectilinear acoustic patterned trap, and b) PDDA/DA coacervates transformed with GDL after being acoustically patterned but the acoustic field removed after the addition of GDL.

Nonetheless, this experiment illustrates, along with the varying polymer weight functionalised glass slide micellar to vesicular experiment, that the unusual geometries observed when the coacervate protocell model experiences a pH change, is a result of a fine interplay of physical forces that governs the resulting vesicles. This balance of osmotic, acoustic, electrostatic, and

surface interactions can be used to produce a protocell model for forming spontaneous selective compartments that can respond to the chemistry of their surroundings.

3.2.4 Cargo Transport

It was observed that the system, in the low polymer weight formulations that produced distinct vesicles after exposure to GDL, that the fluorescently tagged compounds sequestered within the coacervate microdroplets, were transferred to the newly formed vesicles. In the case of the low polymer weight, vesicle fission was directly observed and unilamellar vesicles containing the guest compounds were produced. The loading of guest compounds into coacervate microdroplets and subsequent preservation of their spatial localisation within the evolving high aspect ratio vesicles can be clearly seen in Figure 3.39.

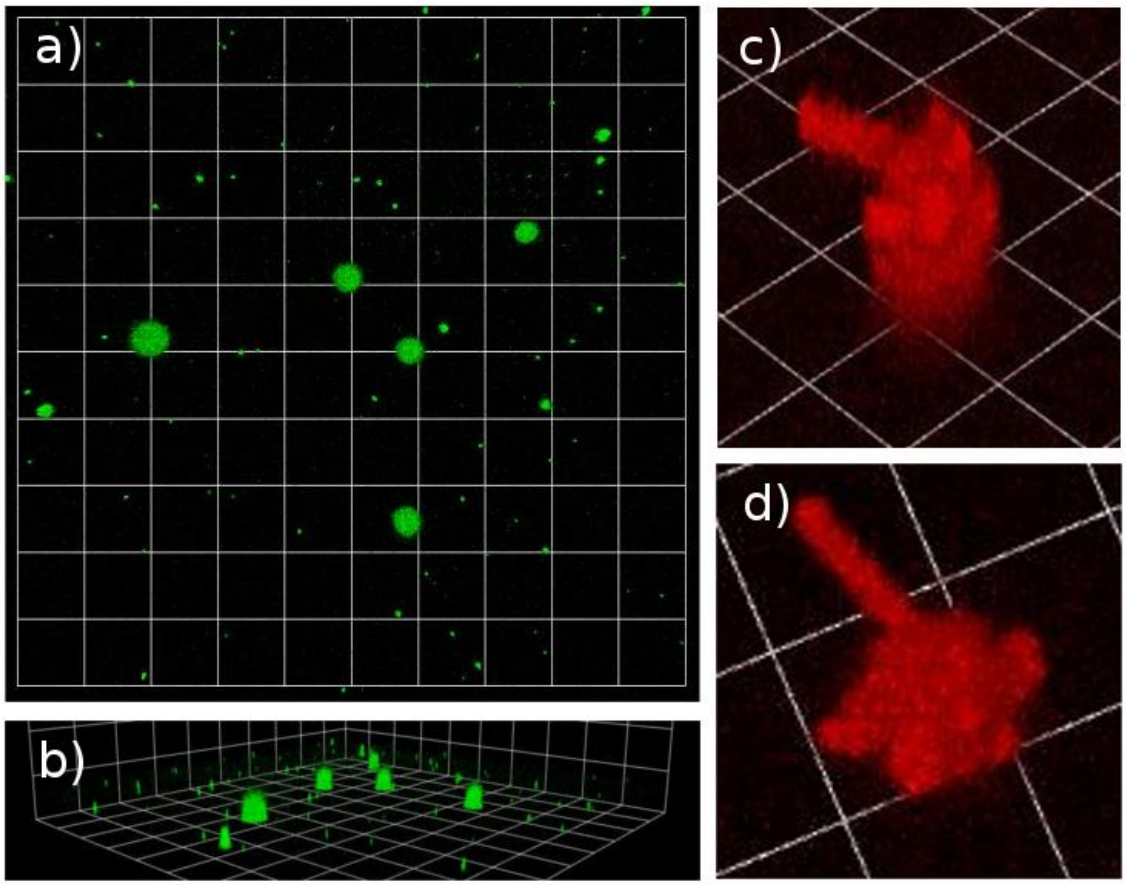

Figure 3.39: a) Confocal x-y view of a 3D reconstruction of PDDA/DA coacervates with BODIPY sequestered. Background Scale Grid = 24.75 µm. b) x-y-z view of BODIPY stained

PDDA/DA coacervates illustrating spherical structure and localisation of dye. Scale grid = 24.75 μm. c) An x-y-z view of a Nile Red stained coacervate droplet after the addition of GDL, the localisation of the dye illustrates the ability of the system to recover cargo within the evolved vesicles, which bleb from the surface of the coacervate droplets in response to the addition of the acid and shows that other Vesicles in solution do not fluoresce. Scale grid = 12.43 μm. d) An x-y view of the coacervate stained with Nile Red post transformation. Background Scale Grid = 12.43 μm.

A subsequent thorough investigation into the ability of this system to transport a variety of chemically and physically diverse compounds and structures from the coacervate droplet, 'first generation protocell', to the evolved vesicles, the 'second generation protocells', was conducted. The system showed the capacity to transfer a variety of molecular dyes, cationic and anionic, organic nanostructures, such as carbon nanodots (CNDs), to single-stranded DNA tagged with cy5 molecular dye These examples are shown in Figure 3.40. Furthermore, the selective nature of this sequestration and transport can be used to illustrate that these vesicles originate from the coacervates and are not a result of material being released into solution and subsequent uptake into the evolved vesicles. This is a contiguous process, whereby the spatial localisation of guest molecules is constantly preserved, and selective uptake and transfer of guest molecules can be shown. The process is chemoselective as the coacervates do not sequester GFP or dextran as can be seen in Figure 3.40. This selectivity seems to be molecular weight sensitive as anionic (hydroxypyrenetrisulfonic acid), cationic (BODIPY FL), lipophilic and hydrophobic (nile red) dyes were sequestered within the droplets, whereas GFP and Dextran were not taken up by the droplets, and have significantly higher molecular weights than any of the dyes, nanodots, or DNA that was sequestered, indicating that this selective uptake is indeed size exclusionary in nature.

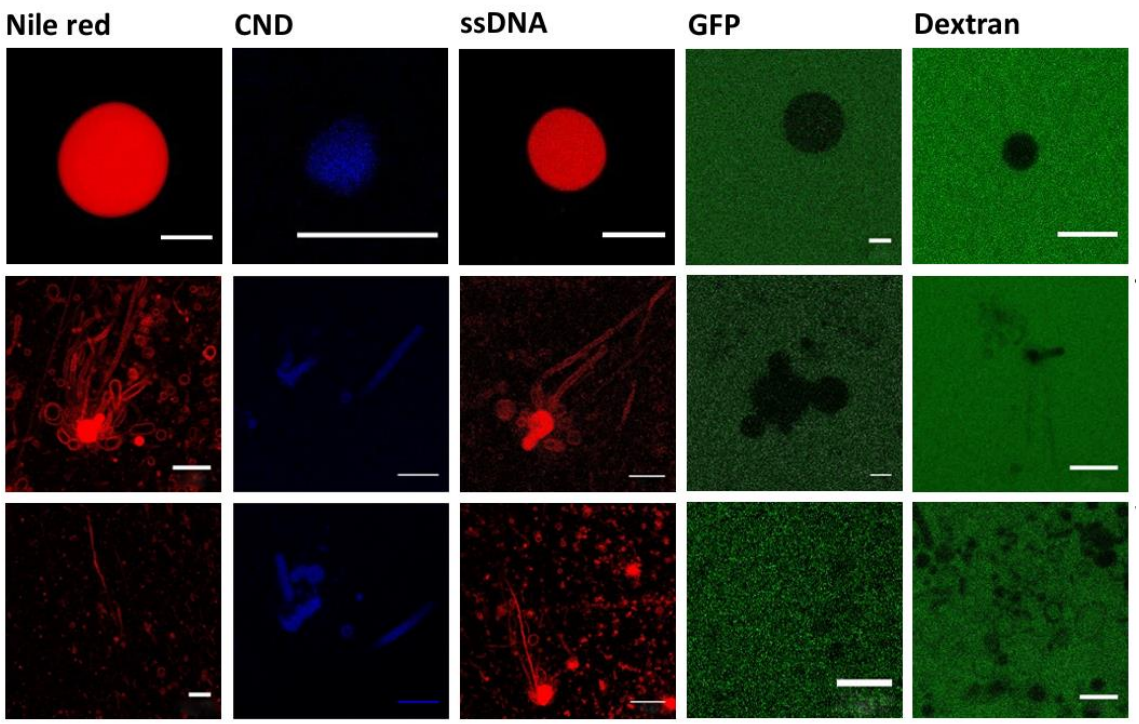

Figure 3.40: A series of confocal fluorescent optical micrographs illustrating the coacervate systems ability to sequester various payloads and undergo transformation when the pH of the system is adjusted through the introduction of GDL. As can be seen from the rows, the system sequesters fluorescent cargo and then transports it to the interior of the evolved vesicles. All scale bars = 10 µm.

3.3 Conclusions

A novel complex coacervate system comprising poly(diallyldimethylammonium chloride) (PDDA) and decanoic acid (DA), has been synthesised and characterised. The characteristics of the resulting coacervate microdroplets were analysed using: optical and fluorescent microscopy, to determine the presence of polymer-rich coacervate microdroplets in solution; ultra-violet/visible light spectroscopy (UV/VIS) to determine the critical coacervation concentration of 12.5 ± 0.5 mM DA; dynamic light scattering (DLS) to determine the size distribution and polydispersity of the microdroplets at 80 : 5 DA : PDDA ratios to be 1.5 ± 0.1 μm in the first minute after formation; zeta potential (ζ-potential) measurements to assess the surface charge of the microdroplets and hence their stability, measured for a minimal version of the system returning a surprising positive charge but this can be explained via the presence of excess DA in equilibrium with the microdroplets in the polymer-poor phase; small angle x-ray scattering (SAXS) to investigate the hetero- or homogeneity of the internal structure of the microdroplets; and nuclear magnetic resonance (NMR) was used to further investigate the composition of the microdroplet phase and the polymer-poor continuous, or supernatant, phase.

The system was found to possess a morphological response to a pH change of the solution. Coacervate microdroplets extrude long tendril-like unilamellar vesicles in response to the addition of acid and subsequent lowering of solution pH to below 7.8. At intermediate MW the system evolves vesicle buds that exhibit a multi-lamellar structure and were also able to retain the polymer from the coacervate microdroplet and guest molecules that were sequestered prior to addition of GDL. High MW polymer formulations exhibited multi-lamellar structures across the entire surface of the microdroplets after addition of GDL. Optical and fluorescent microscopy were used to determine the ability of the system to transport cargo from the coacervate microdroplet to the newly formed vesicles. A fluorescent analogue of PDDA, poly(diallyldimethylammonium chloride)-co-diallylamine (PDDA-co-DAA) a copolymer with

amine functionality that was reacted with fluorescein isothiocyanate (FITC), was synthesised and used to investigate the destination of the polymer during this morphological transformation. Pyrenecarboxaldehyde (PYCA) was added to the various pH formulations of DA and its fluorescence measured and compared to the fluorescence observed within the coacervate to determine the protonation state of the DA within the coacervate microdroplets, which indicated that the DA is in a mixed state within the coacervate droplet of micellar and vesicular configurations.

Vesicles containing transferred cargo undergo fission events producing fluorescing vesicles that are distinct from the coacervate microdroplets that they evolved from. These vesicles contain the payload from the first generation coacervate protocell and now contain the polymer from the original microdroplet and can be considered second generation membrane bound protocell models. This is an exciting result as it not only illustrates the facile transformation of a molecularly crowded chemoslective protocell model into one that is membrane bound, but that this transformation preserves information between generations and could point towards rudimentary replication mechanisms.

PDDA is a synthetic flocculant developed for use in waste water treatment, due to its highly charged cationic properties. However, in the context of origins of life studies it may be considered a compound that might stretch the definition of chemistry that was available in the prebiotic setting. A commonly used polymer that could have plausibly existed in such a setting is poly-L-lysine, a polymer composed of the amino acid lysine. Lysine, as discussed in Chapter 1, could have plausibly existed at the time of proto-life emerging from the synthetic cauldron of the prebiotic Earth.

The preparation of PLL requires dialysis and subsequent concentration determination via the use of Trypan Blue (TB) [20]. This method can be used to track the concentration and complexation of PLL within the system, this can be seen in Figure 3.41 from which the concentration of PLL can be determined within the coacervate droplets.

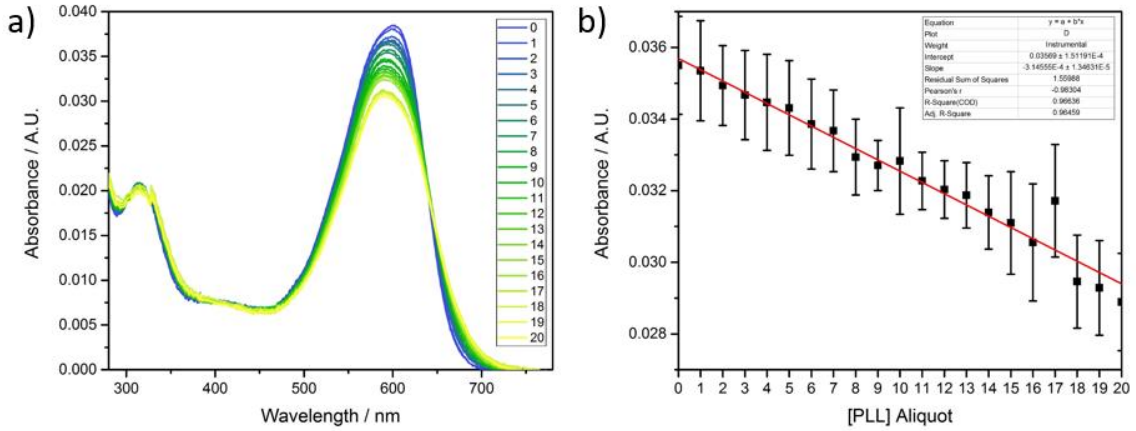

Figure 3.41: a) the absorbance of Trypan blue with respect to the addition of aliquots of PLL b) the absorbance of Trypan Blue at 580 nm with respect to the addition of PLL aliquots.

From this a coacervate droplet could be formulated which complexes DA as part of its composition. Furthermore, the use of glucose oxidase (GOx) could be sequestered within the microdroplets which could then take up glucose from its environment which would then be oxidised to form D-Glucono-δ-lactone [21] which would then hydrolyse to from gluconic acid, which would then trigger the morphological transformation, transferring the pH adjusting enzyme 'machinery' to the membrane bound vesicle second generation. This system would then be more closely related to the chemical composition of an autonomous potential ancestor to LUCA and thus give us another exciting perspective to investigate the origins of life.

3.4 References

[1] A. I. Oparin and K. L. Gladilin, "Evolution of self-assembly of probionts," *BioSystems,* vol. 12, pp. 133-145, 1980.

[2] H. B. Bungenberg de Jong and H. R. Kruyt, "Coacervation (Partial Miscibility in Colloid Systems)," *Proc. Sect. Sci, Koninkijke Nederlandse Akademie van Wetenschappen,* vol. 32, no. 1927, pp. 849-856, 1929.

[3] J. T. Overbeek and M. J. Voorn, "Phase separation in polyelectrolyte solutions; theory of complex coacervation.," *Journal of cellular physiology. Supplement,* vol. 49, no. Suppl 1, pp. 7-22, 1957.

[4] F. Tiebackx, "Gleichzeitige Ausflockung zweier Kolloide," *Chem. Ind. Kolloide,* vol. 8, pp. 198-201, 1911.

[5] J. Crosby, T. Treadwell, M. Hammerton, K. Wasilakis, M. P. Crump, D. S. Williams and S. Mann, "Stabiliazation and enhanced reactivity of actinorhodin polyketide synthase minimal complex in polymer-nucleotide coacervate droplets," vol. 48, no. 97, 2012.

[6] D. S. Williams, A. J. Patil and S. Mann, "Spontaneous structuration in coacervate-based protocells by polyoxometalate-mediated membrane assembly.," vol. 10, no. 9, 2014.

[7] T.-Y. D. Tang, C. C. Hak, A. J. Thompson, M. K. Kuimova, D. S.Williams, A. W. Perriman and S. Mann, "Fatty acid membrane assembly on coacervate microdroplets as a step towards a hybrid protocell model.," vol. 6, no. 6, 2014.

[8] D. S. Williams, S. Koga, C. R. C. Hak, A. Majrekar, A. J. Patil, A. W. Perriman and S. Mann, "Polymer/nucleotide droplets as bio-inspired functional micro-compartments," *Soft Matter,* vol. 8, no. 22, p. 6004, 2012.

[9] R. Nagarajan and E. Ruckenstein, "Theory of surfactant self-assembly: a predictive molecular thermodynamic approach," *Langmuir,* vol. 7, no. 12, pp. 2934-2969, 1991.

[10] E. Blöchliger and M. Blocher, "Matrix effect in the size distribution of fatty acid vesicles," *The journal of physical chemistry B,* vol. 102, pp. 10383-10390, 1998.

[11] K. Morigaki, P. Walde, H. Misran and B. H. Robinson, "Thermodynamic and kinetic stability. Properties of micelles and vesicles formed by the decanoic acid/decanoate system," *Colloids Surf.,* vol. 213, pp. 37-44, 2003.

[12] Y. Pocker and E. Green, "Hydrolysis of D-glucono-δ-lactone. I. General acid-base catalysis, solvent deuterium isotope effects, and transition state characterization," *J. Amer. Chem. Soc.*, vol. 95, pp. 113-119, 2012.

[13] C. G. D. Kruif, "Skim milk acidification," *J. Colloid Interface Sci.,* vol. 185, no. 1, p. 19–25, 1997.

[14] Y. P. a. E. Green, "Hydrolysis of D-glucono-δ-lactone. I. General acid-base catalysis, solvent deuterium isotope effects, and transition state characterization," *J. Amer. Chem. Soc.*, vol. 95, pp. 113-119, 1973.

[15] K. Kalyanasundaram and J. K. Thomas, "Solvent-Dependent Fluorescence of Pyrene-3-carboxaldehyde and Its Applications in the Estimation of Polarity at Micelle-Water Interfaces," *J. Phys. Chem.*, vol. 81, no. 23, p. 2176–2180, 1977.

[16] K. P. Ananthapadmanabhan, E. D. Goddard, N. J. Turro and P. L. Kuo, "Fluorescence probes for critical micelle concentration," *Langmuir,* vol. 1, no. 3, pp. 352-355, 1985.

[17] I. a. Chen and J. W. Szostak, "A kinetic study of the growth of fatty acid vesicles.," *Biophysical journal,* vol. 87, no. 2, pp. 988-98, 2004.

[18] J. Dervaux, V. Noireaux and A. Libchaber, "Growth and instability of a phospholipid vesicle in a bath of fatty acids," *The European Physical Journal Plus,* vol. 132, no. 284, pp. 1-5, 2017.

[19] L. Tian, N. Martin, P. G. Bassindale, A. J. Patil, M. Li, A. Barnes, B. W. Drinkwater and S. Mann, "Spontaneous assembly of chemically encoded two-dimensional coacervate droplet

arrays by acoustic wave patterning," *Nature Communications,* vol. 7, no. May, pp. 1-10, 2016.

[20] A. Grotzky, Y. Manaka, S. Fornera, M. Willeke and P. Walde, "Quantification of α-polylysine: a comparison of four UV/Vis spectrophotometric methods," *Analytical methods,* vol. 2, no. 10, p. 1448, 2010.

[21] W. CM, W. KH and C. XD, "Glucose oxidase: natural occurrence, function, properties and industrial applications," *Applied Microbiology and Biotechnology,* vol. 78, no. 6, 2008.

[22] A. Gupta and H. Bohidar, "Kinetics of phase separation in systems exhibiting simple coacervation," vol. 72, no. 1, 2005.

Chapter 4 : Generating localised supramolecular hydrogels in coacervates with an inorganic stimulus

Abstract

A microdroplet suspension, formed *via* complex coacervation, of a polycation, poly(allylamine hydrochloride) (PAH), and a nucleotide, guanosine monophosphate (GMP); undergo hydrogelation upon addition of an inorganic stimulus. First, PAH and GMP condense to form spherical droplets of polymer-rich solution within a polymer-poor solution *via* entropic and electrostatic interactions [1]. Subsequent addition of silver ions added to the surrounding polymer-poor phase can abstract protons from the amine groups of the GMP forming a silver stabilised GMP complex. Self-association of the complexes within the microdroplets leads to the formation of 1D nano-filaments which are stabilised by interactions with water as a result of hydrophilic outer moieties, to form a hydrogel network [2]. The GMP, being localised within the coacervate microdroplets, forms spherical micro-hydrogel compartments. Initial results of the hydrogelation of the novel system are presented here utilising NMR and fluorescence lifetime imaging microscopy (FLIM) to illustrate the formation of the hydrogel, and Quantitative Nanomechanical Property Mapping AFM (QNM-AFM) and TEM to elucidate the structure in the coacervate microdroplets. The system could then be exploited as a functional nanostructure template, as the silver present in the system can be reduced upon exposure to UV light to form anti-microbial nano-particles [2], and as such, the system presents itself as an interesting avenue for further anti-microbial and non-membrane bound drug delivery platform technology research.

4. Introduction

Cells have structure, strength, and motility [3]. These aspects of their character are derived from the structure known as the cytoskeleton, comprised a series of proteins which allow cells to be rigid, to undergo division and replication, and to translate themselves within in an environment to hunt for food or to hunt down invasive foreign bodies [4]. One example of the structures found within the cytoskeleton is the very high aspect ratio microtubule, which maintains cellular structure by working in conjunction with a variety of other filaments in the cytoskeleton [5]. A current model for cytoskeletons in protocellular research, to understand the origin of physio-mechanical properties of cellularity, are hydrogels.

Gels are a solid-like material of two, or more, components; one, which is a liquid, present in substantial quantity, and second, a three-dimensional self-supporting network of filaments [6]. This viscoelastic property can be classified using rheological measurements. Measuring frequency sweeps of the storage modulus (G') and the loss modulus (G'') as a function of angular frequency (ω) one can illustrate the gels moduli independence for several decades with $G' > G''$ (G': $G'' > 10$), which is required for the material to be classed as a gel) over the range of frequencies scanned [7]. The storage modulus, G' also known as elastic modulus, plateaus at low frequencies of shear allowing for the deformation in the gel to persist for a time on the scale of a few seconds [6]. This behaviour denotes the presence of a 'network' capable of storing energy imparted to the gel during deformation. A facile test for the formation of a gel is the 'vial-inversion' test, if the material supports its own weight upon turning the container it is in upside down, it can be considered a gel [8].

In the case of hydrogels, the solvent is water. The supramolecular nature of many cross-linked chains, or fibres, allows the system to be resilient to dissolution. In addition to this, the hydrophilic

functionality of the chains allows the hydrogel network to sequester and incorporate the additional water into the fibrous network that forms the gel. There are two commonly widely used routes for generation of hydrogels [9]: functionalisation of pre-existing polymers; and polymerisation of monomeric units with pre-requisite functionality. In the former case, Michael additions have been extensively used to cross-link polymers in situ. In the latter case, the hydrogels formed, consist of a series of biomonomeric units with hydrophilic functionality [10]. These units are then polymerised, non-covalently, to form a fibrous network which sequesters water to generate a gel phase. The gel phase is an interesting one in that it allows for the immobilisation of large molecules within it [11]. It can adhere to surfaces and possesses a higher viscosity than the solutions of its individual components and its high water-content and amphiphilic network allow for high loading of guest molecules, such as dyes, into the gel. Hydrogels are responsive to a variety of stimuli, such as heat, pH, etc. and respond with a variety of dynamic responses, shrinking, expanding, stiffening, becoming more elastic, etc.

A common structure in the formation of hydrogels form low-weight molecular gelators (LWMGs) such as nucleosides and oligonucleotides, is the G-Quartet [12]. This cation-templated macrocycle is produced by hydrogen binging and was first identified in 1962 in the case of 5'-guanosie monophosphate (5'-GMP, or GMP) aggregation [13]. After the formation of the quartet G-quadruplexes are formed via the stacking of these new assemblages [14]. These structures, when probed with light scattering techniques, such as small angle x-ray scattering (SAXS) have been shown to possess a 3.3 Å spacing [15]. This directional stacking is a result of the strong molecular dipole present in the G-quartet and leads to face-to-face interactions that build the G-quadruplex filaments that then entangle to become the self-supporting hydrogel network [16]. It is possible to form G-Quadruplexes without cavity complexation at low pH however to form these structures at neutral pH this cavity complexation, process of cation-templating at the centre of the G-quartet and hence through the core of the G-quadruplex filaments formed, is necessary [17].

There are two examples of hydrogel systems that have been explored by the Mann group previously as models for cytoskeletons. Work conducted by Kumar et al. centred on a hydrogel system that consisted of an Alkaline Phosphatase (ALP)-mediated dephosphorylation of N-fluorenylmethyloxycarbonyl tyrosine-(O)-phosphate (FMOC-Tyr-P) first discussed by Bing Xu [18] [19]. Dephosphorylation leads to a change in amphiphilicity of the molecule, as a result the products spontaneously self-assemble via π-stacking to form a one-dimensional structure; a nano-fibre. These highly entangled nano-fibres then gel water. The second system utilised the same methodology of hydrogelation of monomeric units to generate the hydrogel network. Guanosine monophosphate (GMP), which has been used previously to form stable G-quartets, arrangements of four guanine residues in a planar cyclic hydrogen bonding motif stabilised by small metal ions in the centre (of the stacks), seen in Figure 4.1, which can then self-assemble into fibrils [20]; and $AgNO_3$ were combined to generate a hydrogel [21].

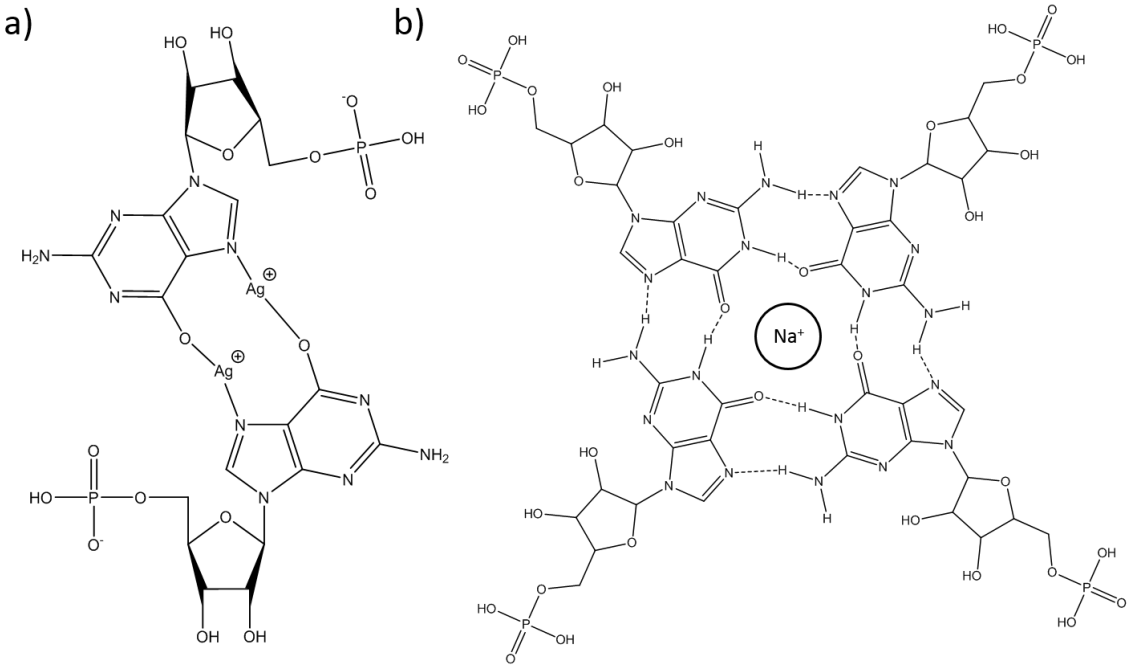

Figure 4.1: a) the chemical structure of the silver stabilised enolate tautomer of GMP, b) the sodium ion stabilised G-quartet of the GMP exhibiting Hoogsteen bonding along their edges to from a cyclic planar complex.

Modified hydrogen bonding, because of ion-mediation, abstracts a proton from the N1 site and stabilises the enolate tautomer, which is in constant flux with the keto structure in solution. This

then ensures silver binding at the O6 and N7 sites which then form the GMP-Ag dimer via the modified hydrogen bonding, seen in Figure 4.1. Through π-stacking these dimers then form the fibrils which exhibit the pre-requisite hydrophilic structures which are stabilised by the presence of water and generate fibril entanglement and water encapsulation, necessary for the generation of the gel phase. Both examples of self-assembling hydrogel networks can be thought of within the framework of origins of life research as models for cytoskeletal networks as their rheological properties were analogous to the properties observed in modern cells and further molecular crowding and spatial confinement of bio-relevant reactions is favourable and can produce non-equilibrium behaviour [22].

Protocells are compartments that have been designed to mimic systems that could have evolved into modern cells [23]. They ought to be self-assembling in ambient conditions and possess characteristics such as proto-metabolism, proto-informatics machinery, or be compartmentalised. These protocells can then be used as models for how complexity arose in cellular systems and can be applied today as engineered microcompartments or as microbioreactors. Coacervates, one such protocell model [24], the formation of which was first described by Tiebackx et al. [25] allow for the facile self-assembly of localised liquid droplets dispersed within another liquid phase. Their ability to partition molecules selectively based on their chemical character can be used to generate molecularly crowded environments. Work in the Mann group has shown that it is possible to generate coacervate microcompartments using the nucleotide adenosine triphosphate (ATP) [26]. Is it then possible to formulate a coacervate phase using the nucleotide GMP and exploit its ability to form hydrogels after interaction with small metal ions - this route towards creating chemical complexity within a spatially localised microdroplet is another interesting route to forming microgels.

Herein is described, the use of an inorganic stimulus to form a highly locally ordered, and unexpected, G quartet hydrogel system templated by spherical droplets formed via the electrostatically mediated entropically driven condensation of a polymer rich phase within a polymer poor phase, also known as coacervation.

4.1 Additional Materials and Methods

Materials: All reagents were purchased and used as delivered: guanosine monophosphate (GMP, Life Technologies); 15 kDa poly(allylamine hydrochloride) (PAH, Sigma-Aldrich) ; hydrogen chloride (HCl, Sigma-Aldrich); sodium hydroxide (NaOH, Sigma-Aldrich); silver nitrate ($AgNO_3$, Sigma-Aldrich); sodium chloride (NaCl, Sigma-Aldrich); hexamethyldisilane (HMDS, Sigma-Aldrich); poly(ethylene glycol) (PEG; Sigma-Aldrich); Acridine Orange (Sigma-Aldrich); and Hoechst 33258 (Sigma-Aldrich).

Coacervate formulation: Equal volumes, 100 µL, of a 200 mM (monomeric concentration) 15 kDa PAH solution at pH 7 and a 14 mM GMP solution at pH 7, were mixed in a 1.5 mL Eppendorf tube at room temperature to form a turbid suspension of coacervate droplets. The sample was then centrifuged at 13,200 rpm for 5 minutes to facilitate the separation of the supernatant and bulk phases. Samples were then redispersed by hand using a micropipette to generate microdroplets in a suspension of the low-polymer supernatant phase. All solutions were made with Milli-Q Pure deionised water (18.2 MΩ•cm) dispensed from a Milli-Q helix integral 3 filtration system.

Stimuli incorporation: Gelation of the coacervate microdroplets was triggered by the addition of an aliquot of 1M $AgNO_3$ to a final concentration of 5 mM in the dark. Samples were agitated using a pipette during this time to ensure rapid mixing of the silver salt.

UV-Vis spectroscopy: Suspensions of PAH/GMP coacervates were produced via the mixing method previously detailed but with 500 µL of each component to generate final volumes of 1 mL. These were pipetted into 1.5 mL polymethylmethacrylate (PMMA) cuvettes and loaded into a Perkin Elmer Lambda 35 UV-Vis spectrophotometer. Wavescans at 500 nm were

conducted to determine the turbidity change of the solution with varying GMP concentration.

Dynamic light scattering: 750 μL suspensions of PAH/GMP coacervates were formulated and loaded into a Malvern Mastersizer Nano ZS at 25 °C where Dynamic Light Scattering (DLS) measurements were conducted. Automatic attenuation settings were used, and samples were scanned 10 times each.

Zeta potential: ζ-potential measurements were conducted with the Malvern Mastersizer Nano ZS using disposable Malvern electropotential cuvettes at 25 °C. Automatic attenuation and voltage settings were used and all samples were averaged over 10 runs.

Nuclear magnetic resonance: All proton NMR measurements were conducted in D_2O on a Varian 400 MHz instrument, with a 64 scan, 30 second relaxation period and at standard temperature and pressure (25 °C and 1 atm). Acetone was used as an internal standard against which to calibrate the quantitative analysis of protons generating the observed signals. This and the following equation allowed for the quantification of GMP in the bulk phase of the coacervate suspension:

$$C = CCF \times \frac{AI}{NN}$$

Where *C* is equal to the concentration of substance generating the chemical shift peak; *CCF* is the chemical conversion factor, a calculated proportionality constant; *AI* is the absolute integral value; and *NN* is the number of nuclides, in this case the number of protons associated with the environment producing the chemical shift.

Performing a ^{1}H scan of the supernatant of the PAH/GMP coacervate suspension after centrifugation showed no signals corresponding to the presence of GMP and we can, therefore, assume that all the GMP had partitioned within the bulk phase. If we approximate the bulk phase volume to be ca. 1 µL, which appeared to be comparable upon visual inspection with a 1 µL aliquot, after centrifugation we can calculate the concentration of GMP in this phase to be ca. 1.4 M. The solubility of GMP disodium salt is 369 mg/mL in water, which is equivalent to ca. 0.9 M.

Energy dispersive x-ray spectroscopy: PAH/GMP suspensions (5 µL), were centrifuged and resuspended in the supernatant, were dried onto carbon-coated SEM stubs, and a JEOL JSM 6330F (SEM) was used to determine the morphology of the coacervates prior to and post addition of $AgNO_3$ for gelation. Samples were coated with 5 nm of silver, except for EDX measurements.

Atomic force microscopy: PeakForce atomic force microscopy (AFM) was conducted by Dr R Harniman in the Chemical Imaging Facility, University of Bristol, with equipment funded by EPSRC under Grant "Atoms to Applications" Grant ref. "(EP/K035746/1) using a PeakForce multimode 8 AFM instrument. PAH/GMP samples were prepared and deposited onto freshly cleaved mica then allowed to settle for one hour before being dried with nitrogen. For PAH/GMP Ag samples, PAH/GMP suspensions were again deposited onto freshly cleaved mica. This was followed by the addition of 1 µL of 1M $AgNO_3$ and the mixture was agitated by pipette to mix. The system was then left to settle in the dark for one hour and then blown dried with nitrogen. Samples were stored in the dark until measurement. Using Bruker Nanoscope Analysis v1.8 the average Young's Modulus, *E*, could be determined for a given area within the sample. A 500 × 500 nm selection was made, and the roughness tool used to find the average *E* of that selection. An area selection average was used to compensate for a systematic error in the measurements

which gave highly domed artefacts a stiffer side than the other, this is seen by the appearance of an apparent shadow on the droplets.

Optical microscopy: A Leica SP8 AOBS confocal laser scanning microscope, attached to a Leica DMi8 inverted epifluorescence microscope with 'Adaptive Focus Control' (to correct focus drift during time-courses), was used to collect fluorescence lifetime (FLIM) data for a series of glycerol/methanol solutions dyed with 2 μM kiton red. From this a viscosity calibration curve was determined. 100 μL aliquots of PAH/GMP coacervate suspensions, and PAH/GMP Ag suspensions, were loaded onto microscopy dishes and imaged using the same instrument and their local viscosity data was back calculated from the measured fluorescence lifetime data gathered.

Transmission electron microscopy: TEM measurements were conducted on a Jeol 1400 transmission electron microscope operating at 120 keV. Samples were prepared by depositing coacervate suspensions onto carbon-coated copper grids and left to air dry. No staining was used to enhance the contrast of the samples.

Confocal microscopy: Capillary slides were prepared using functionalised cover slips to prevent coacervate wetting on the glass surface. Functionalisation was undertaken via chemical etching with the use of Piranha solution to enable the addition of 200 μL poly(ethylene glycol) (PEG) (in 10 mL of toluene). Capillary slides were then made by attaching functionalised slips on top of two non-functionalised slips with UV-curing glue, on top of a microscope slide to generate a 10 mm channel. Approximately 65 μL of the coacervate suspensions were then placed inside the channel and observed using a Leica DMI 3000 inverted optical microscope with variable wavelength ultra-violet (UV) lamp attached. Brightfield, phase-contrast, and fluorescence images were captured. Confocal microscopes were also used to image the coacervate droplets (Leica SP5 confocal; Wolfson Bio-imaging Facility), to capture fine fluorescence

intensity decay data to confirm gelation kinetics. All microscopy was undertaken under standard conditions (1 atm and 25 °C).

Differential scanning calorimetry: Differential scanning calorimetry (DSC) experiments were undertaken to determine the presence of hydrogels in the system after the addition of the silver. The experiments were conducted on a Mettler Toledo DSC1 system. Samples of ca. 20 mg were loaded into aluminium hermetic dishes and sealed using the crimper supplied with the machine. Reference pans were prepared using either water of the same mass as the sample being investigated or of air. The samples were cycled through a heating and cooling cycle from room temperature to 90 °C six times and the difference in heat flow in Wg^{-1} between the sample and reference pans recorded.

4.2 Results and Discussion

4.2.1 Coacervate formation and characterisation

After attempting to formulate coacervates using PDDA and GMP, the polymer poly(allylamine hydrochloride) was used to generate novel GMP charge balanced coacervates. PAH/GMP coacervates were formed *via* the mixing of polymer and nucleotide solutions to form a turbid suspension, Figure *4.2*, and subsequent centrifugation facilitated the separation of supernatant and bulk phases. Coacervates were then agitated by pipette to produce a spherically polydisperse population of bulk phase within the supernatant phase. The coacervates were observed via bright-field and phase contrast microscopy, Figure *4.3*, confirming the presence of polydisperse dense polymer rich droplets was confirmed, they were also found to be able to sequester the dye Hoechst 33258, Figure 4.3. The critical coacervation concentration was found to be 2 mM GMP with a fixed polymer concentration of 5 mM via UV-vis spectroscopy, at pH 7 15% of the PAH will be protonated yielding a charge ratio of 0.75:2 [27]. This charge ratio indicates that we should observe a negative overall charge of the coacervate droplets. The zeta-potential was 42 ± 4 mV and the average hydrodynamic radius 1 minute after formation was 800 ± 160 nm, Figure 4.3. This unexpected positive surface charge could indicate a localisation of positively charged PAH at the surface of the coacervates.

Figure 4.2: A photograph illustrating increasing turbidity of the polymer solution as GMP is added to the polymer suspension producing a stable turbid coacervate suspension. The point at

which turbidity is detected is known as the critical coacervation concentration and is indicative of the presence of light scattering microdroplets forming the solution.

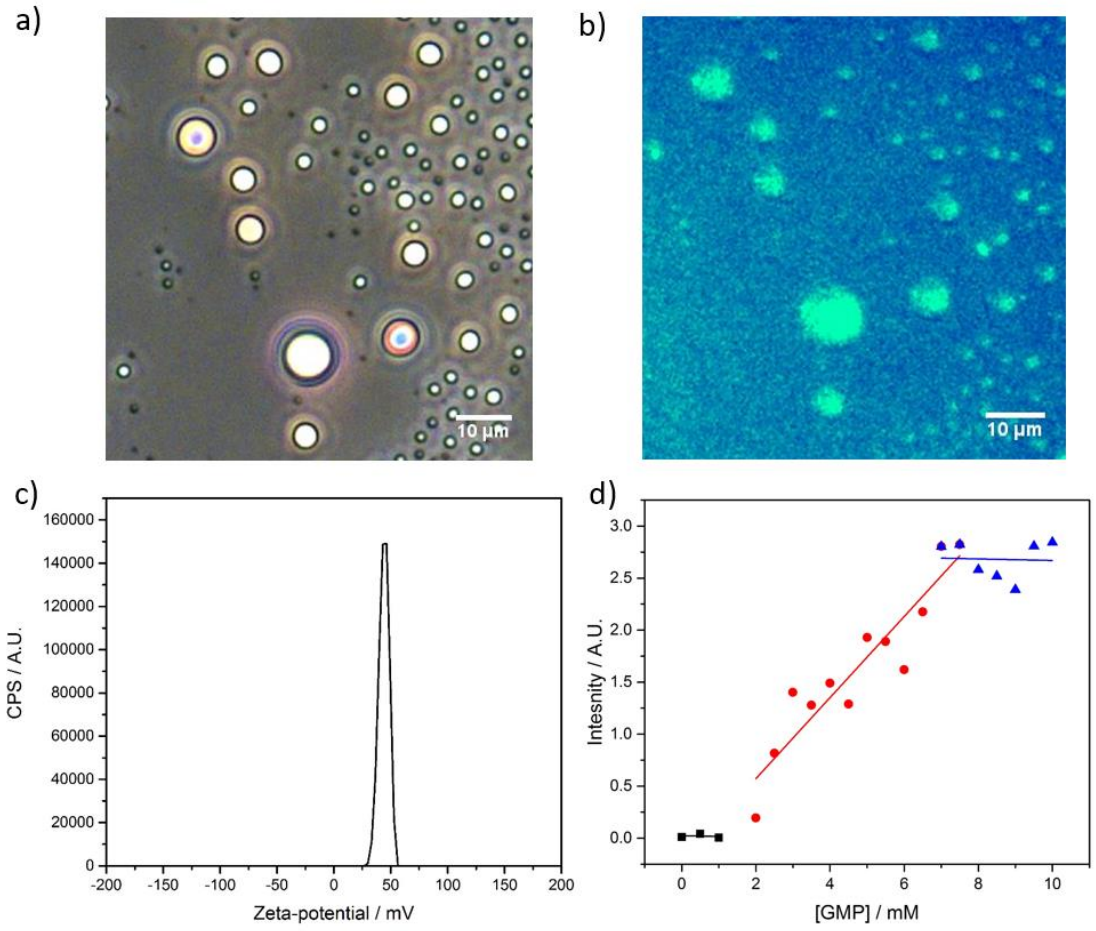

Figure 4.3: a) and b) optical and fluorescent micrographs of PAH/GMP coacervates and Hoechst, c) representative zeta profile for the PAH/GMP coacervate microdroplets, average surface charge was measured at 42 ± 4 mV, d) the UV-Vis data used to extract the critical coacervation concentration for the PAH/GMP coacervate system.

Having formulated a stable coacervate microdroplet suspension the next step was to introduce the inorganic stimulus to trigger any structural reorganisation of the internalised components.

4.2.2 Response to silver

Having characterised the coacervate system, we next studied the effect of adding the silver salt, $AgNO_3$, to the suspension. work by Dash *et* al. indicated that the GMP, within the coacervates, should undergo dimerization and subsequent π-stacking to form a highly entangled network of hydrophilic nanofilaments that would result in a hydrogel. Hoechst 33258 dye, a common helical fibril stain [28] undergoes fluorescent quenching when bound to silver-containing fibrils, was loaded into the coacervate droplets and its fluorescence was monitored with time after the addition of $AgNO_3$. Hoechst fluorescence decreased intensity indicating the formation of GMP Ag fibrils. This is illustrated in Figure 4.4. UV-Vis experiments were conducted taking a coacervate suspension and adding $AgNO_3$ via micropipette from a stock 100 mM solution to a final concentration in the coacervate suspension of 1 mM. The 250 nm absorbance band, resulting from the presence of GMP in the solution, decayed with time, indicating again the presence of fibrils, as π stacking of the GMP complexes will alter the photochemical properties of the GMP, leading to hypochromicity as can be seen in Figure 4.4.

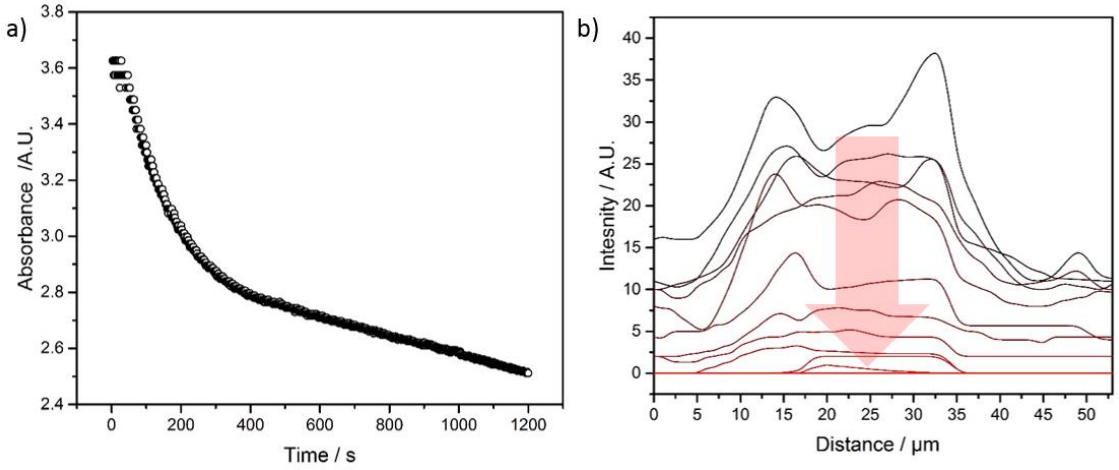

Figure 4.4: a) the evolution of absorbance of GMP at 250 nm in PAH/GMP coacervate suspension after the addition of $AgNO_3$ indicating the formation of silver containing complexes which are undergoing π-stacking, b) Fluorescent optical micrograph of Hoechst 33258 loaded PAH/GMP coacervate droplet inset, yellow line represents fluorescent intensity line-profile measured during the addition of AgNO3, in the time evolution of the line-profile, measured using the ImageJ package, indicating quenching of the Hoechst fluorescence as silver diffuses into the coacervate droplets.

The coacervates before (Figure 4.5 (spectra 2)), and after (Figure 4.5 (spectra 4)), the addition of $AgNO_3$ were inspected using ^{1}H-NMR spectroscopy Figure 4.5. The peak observed at chemical shift 3.8 ppm, in spectra three of Figure 4.5, indicates that there is an interaction between the GMP and PAH before addition of the $AgNO_3$, as the signal transforms from a triplet in (1) to a pair of doublets in (2). The clear reduction in signal from the GMP in spectrum 4 is indicative of the increase in local viscosity preventing relaxation of the protons being probed, preventing a signal from being distinguished from the background of the spectrum.

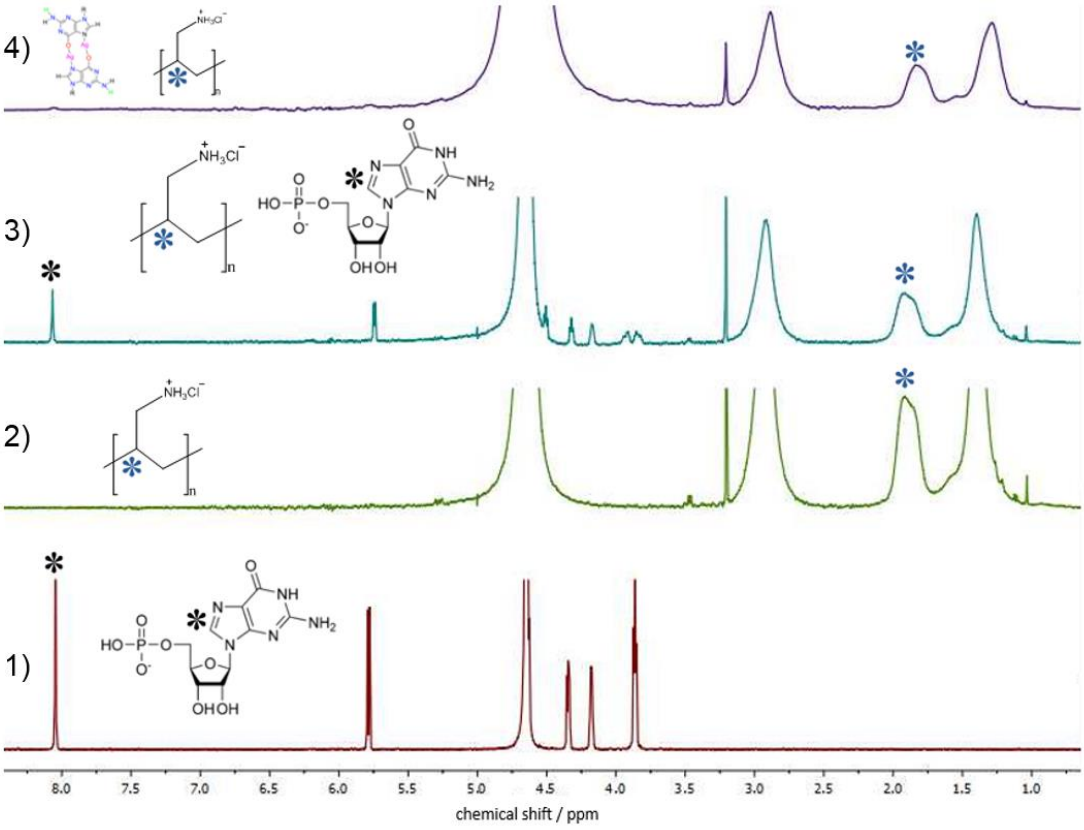

Figure 4.5: ^{1}H-NMR spectra for: 1) PAH, 2) GMP, 3) PAH and GMP coacervate droplets, and 4) PAH/GMP coacervate droplets after addition of $AgNO_3$ to trigger gelation of the droplets. The absence of GMP peaks in spectrum 4 indicates the interaction of silver (I) ions with the GMP. ^{1}H NMR spectra recorded in D_2O and referenced against residual water.

Data from the NMR experiments allowed for the quantification of the concentrations of GMP and PAH within the coacervate droplets formed. Extrapolating from this data showed that due to the concentrating effects of the microdroplet formation and subsequent partitioning of GMP and PAH between the bulk and continuous phases, a bulk hydrogel could not be formed as the GMP concentration in the droplets, 1.4 M (see experimental methods for calculations), is above the solubility limit of GMP in water.

Having explored the effect of silver ions on the system initial results indicated that the internal structure of the microdroplets was indeed being affected by the silver ions. This response is summarised in the scheme illustrated in Figure 4.6. To investigate this further a range of new techniques were employed to determine the nature of this transformation.

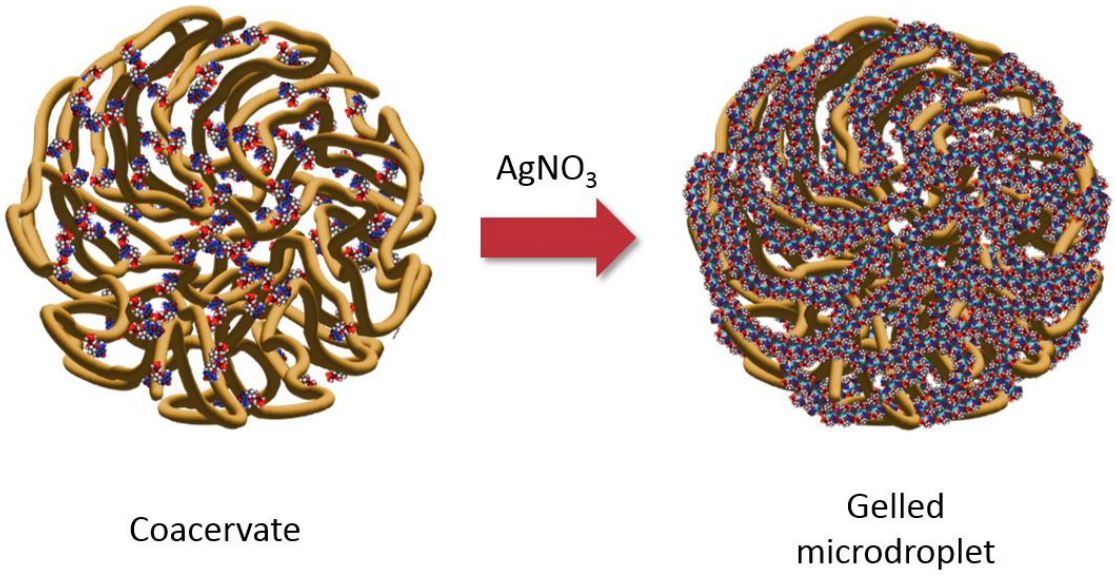

Figure 4.6: A scheme illustrating the response to the addition of silver nitrate to the PAH/GMP coacervate microdroplet.

4.2.3 Characterisation of local structure

Circular dichroism experiments were undertaken to determine the local organisation of the GMP within the coacervate, Figure 4.7. As can be seen from comparing control spectra of the bulk

hydrogel stabilised with Ag^+ ions to form dimers, and the hydrogel formed when experimental variables are set to ensure the presence of G-quartets stabilised with Na^+ ions, the helicity of both of which are opposite, we can clearly observe in the spectrum of the coacervate after addition of silver the same handedness of absorption as the G-quartets. It was expected that the silver would produce the same local organisation as in the bulk system after addition of silver, however, the presence of the polymer yields the G-quartet configuration instead. This is most likely a result of electrostatic interactions between the amine moieties on the PAH restricting the motions of the associated GMP phosphate groups and hence preventing them from forming dimers. Interestingly, for the control experiment, where complexation of the GMP within the coacervate droplet was initiated with NaCl as opposed to $AgNO_3$ no change in helicity was measured, indicating that no helical complexes were formed. The charge density of the ion used to stabilise GMP complexes within a coacervate could have a crucial role to play here in overcoming any GMP-polymer charge interactions and sodium evidently is not strong enough to overcome this, whereas silver appears to be.

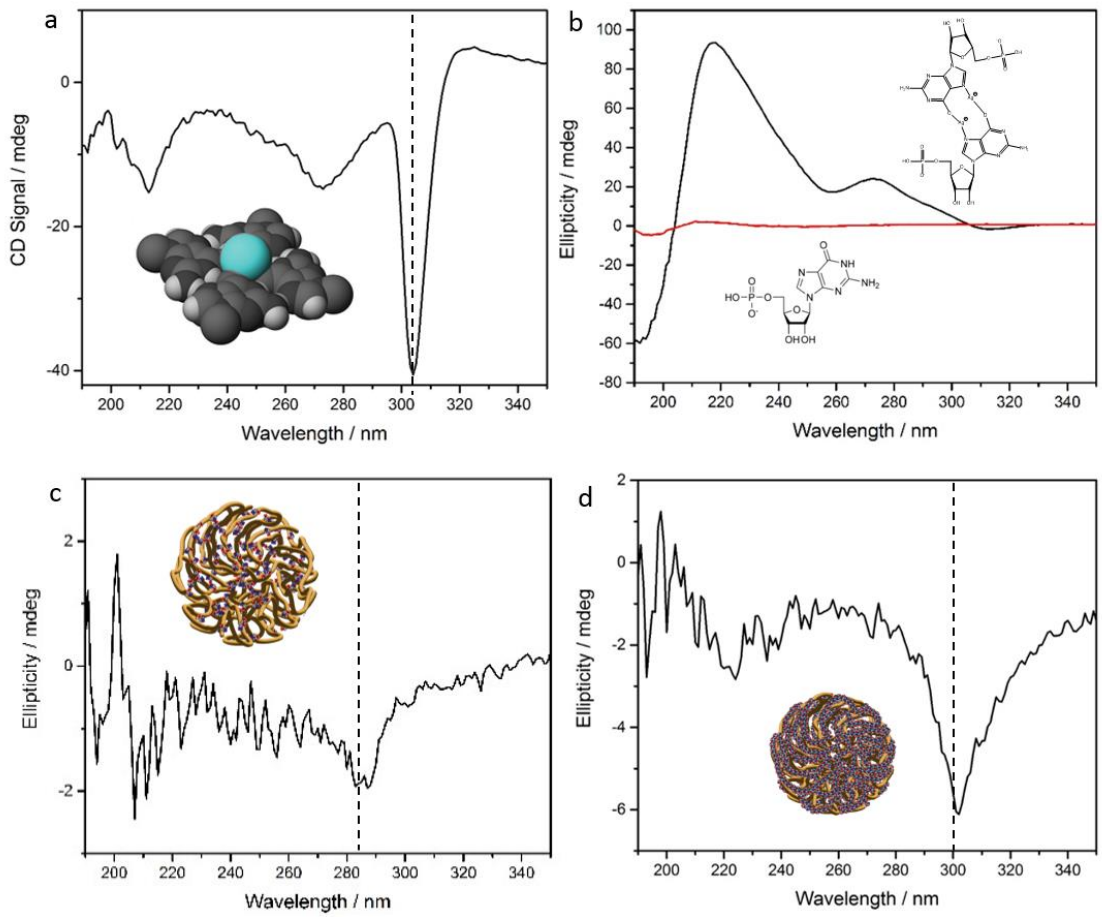

Figure 4.7: a) CD spectrum of a gelled GMP 40 mg mL^{-1} in 200 mM NaCl solution displaying a strong absorbance at 303 nm indicating the presence G-quartet structures, inset cartoon is a space filling model of a GMP G-quartet stabilised by a sodium ion, b) CD spectra of GMP monomers, in red, and GMP Ag dimers in a hydrogel sample following protocol of by Dash et al. (black), chemical structures are of GMP and silver stabilised Ag-GMP dimer, c) CD spectrum of PAH/GMP coacervates prior to addition of Ag, weak G-quartet absorption measured at 280 nm the signal is markedly weaker as a result of the colloidal nature of the suspension and scattering of the signal, and presumably low concentration of structures that possess the chirality necessary for absorption, inset cartoon is of a PAH/GMP coacervate microdroplet d) CD spectrum of PAH/GMP coacervate after the addition of Ag showing an increase in signal strength and shift towards 303 nm absorption indicative of G-quartet structures being formed in the coacervate phase, inset is of a PAH/GMP coacervate microdroplet with GMP G-quartet π-stacking fibrils throughout the interior of the microdroplet.

Having determined an unusual complexation of GMP within the coacervates, in effect, G-quartet-like structures, over the expected dimerization previously found in the case of GMP Ag ion mixing, the properties of this system were further investigated.

4.2.4 Characterisation of hydrogelated coacervates

DSC experiments were conducted on the coacervate system before and after $AgNO_3$ addition to determine the presence of any gel-sol transitions that would be indicative of the presence of a supramolecular hydrogel, Figure 4.8, as it was expected that any complexes of GMP stabilised by the silver ions would be forming elongated structures which possessed a chiral nature and hence produced the signals observed in the CD spectroscopy experiments above. A gel-sol transition for the system was observed and was centred around 64 °C with a maximum endothermic heat flow at 70 °C of -56 W g^{-1}, compared to the transition temperature in the bulk (52°C) which is lower, however this could be as a result of the increased concentration of GMP involved in the gelation due to the molecular crowding from the coacervate and thus could result in a denser hydrogel matrix which requires greater thermal energy to disrupt. To confirm the local gelation of GMP within the coacervate droplets TEM and AFM experiments were also conducted, in the hope that these nanoscale topographical techniques would illustrate the presence of localised entangled fibril networks. This was indeed confirmed by TEM as can be seen in Figure 4.8. TEM micrographs in conjunction with EDX revealed a high concentration of photo-reduced silver nanoparticles and after serial dilution of the coacervate suspension yielded localised fibril network, Figure 4.9. The localisation of Ag and P elements within the deposited coacervate microdroplets illustrate the interaction between the silver and the GMP and the localisation of the elements P, O, Na, Cl, and Ag, show how the network is localised within the imaged deposited droplet.

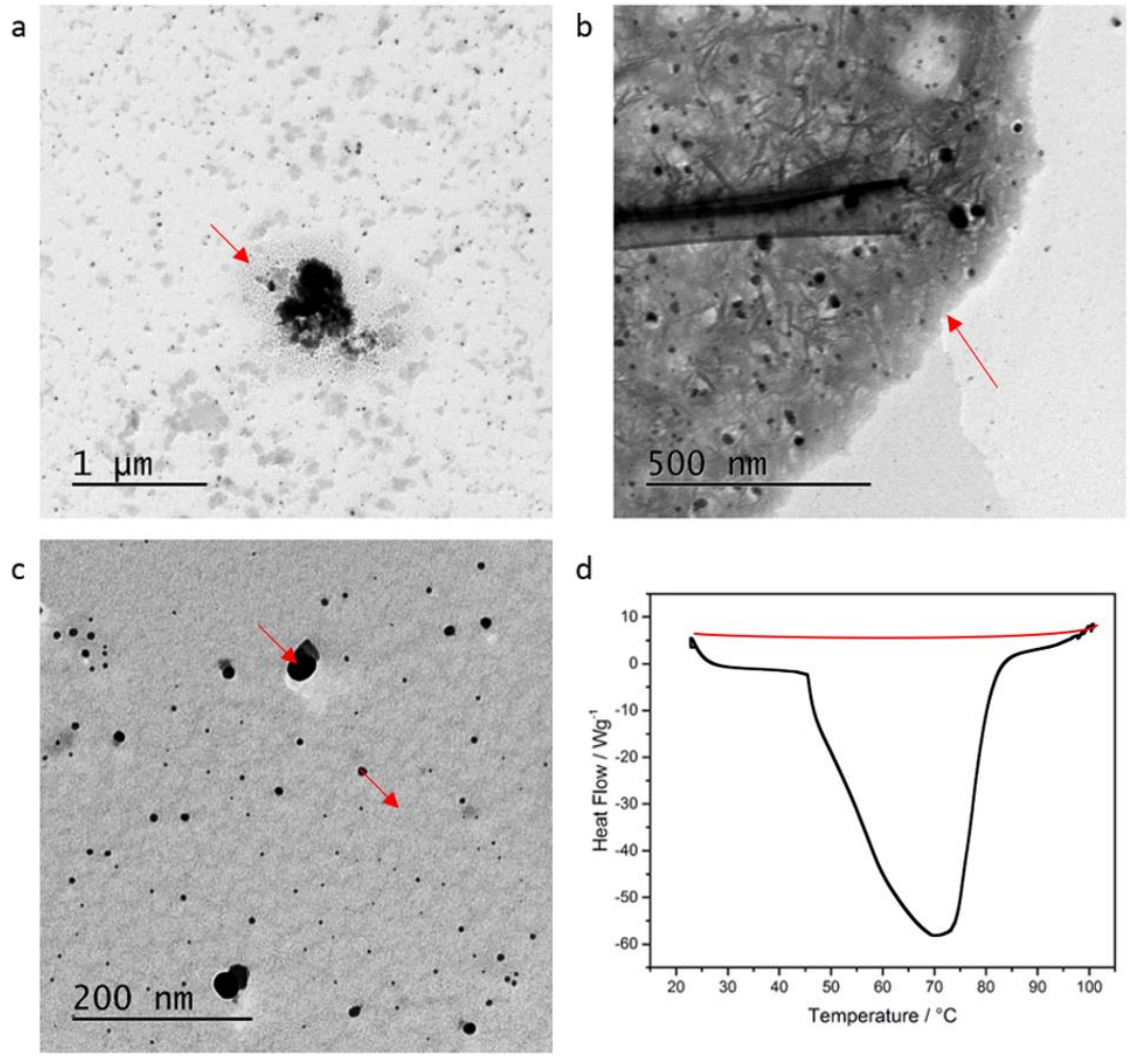

Figure 4.8: a), b) and c) are unstained TEM micrographs of deposited PAH/GMP coacervates at various magnifications, arrows in a) and b) refer to the coacervate microdroplets which have been deposited on the surface, in c) the arrow points to the darker areas which are silver NPs and the lighter grey areas which are the networks of GMP Ag nanofibrils which are decorated with the silver NPs, d)the black line is a DSC thermograph of PAH/GMP Ag coacervate microdroplet suspensions in a cyclic 25 – 100 °C experiment illustrating the gel-sol transition for the gelled microdroplets centred at 64 °C, the red line is a DSC thermograph of the control un-gelled coacervate microdroplet suspension.

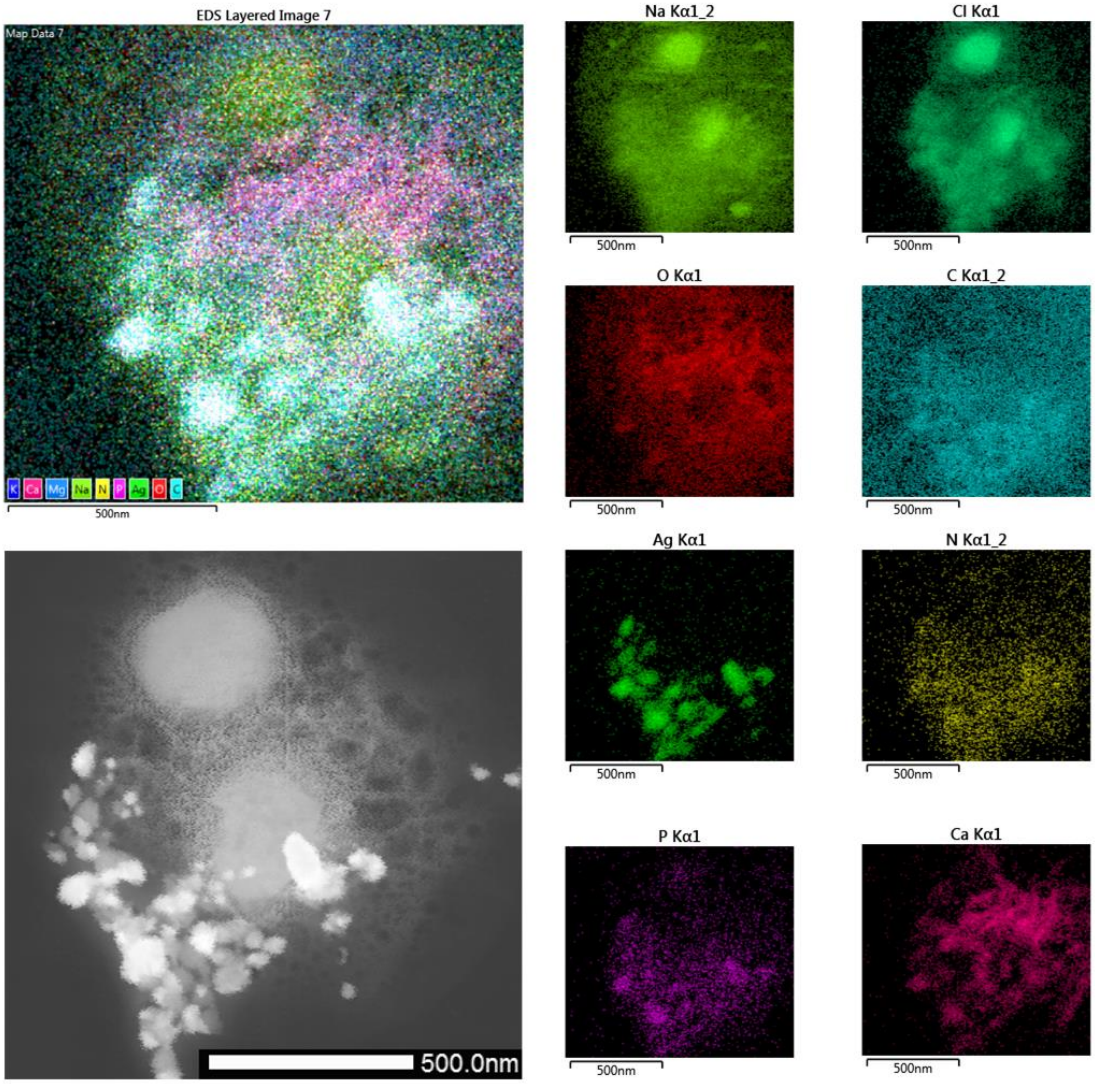

Figure 4.9: TEM EDX micrographs illustrating the localisation of Na, Cl, O, C, Ag, N, P, and Ca, in the microdroplet. The Na, Cl, O, C, P, and N elements are present throughout the entirety of the deposited coacervate structure whereas the Ag is strongly localised in the bright, hence electronically denser regions of the deposited coacervate microdroplet, confirming that these structures are indeed Ag nanoparticles. The Ca signal is a contaminant and is shown to illustrate the ability of the droplets to uptake divalent ions.

Size data for the bright smaller particles were collected from the SEM micrographs, and the average size of the particles was found to be 175 ± 22 nm. Dash *et al* reported to be 2 - 4 nm in sized silver nanoparticles but the nanoparticles formed in the PAH/GMP Ag system are most likely to have different nucleation and growth conditions conferred by the presence of the polymer

to form the coacervate microdroplets. Work by Li *et al.* showed that through the use of producing deoxy-guanosine monophosphate (dGMP) G-quartets stabilised by silver ions and then non-covalently bonded to cationic surfactants that ordered thermotropic liquid crystal phases could be produced and the silver in these phases could then be reduced to form well defined silver nanoparticles as well [29]. These G-quartet structures formed from dGMP again hint at the forces involved in producing these cyclic quartemers. The dGMP is missing a hydroxyl group from the 2' position on the ribose and as such will possess a lower hydrophilicity. These additional hydrophobic forces would provide an additional factor in allowing the formation of the G-quartet structure, as the assembly would provide a favourable environment for these moieties in aqueous solutions.

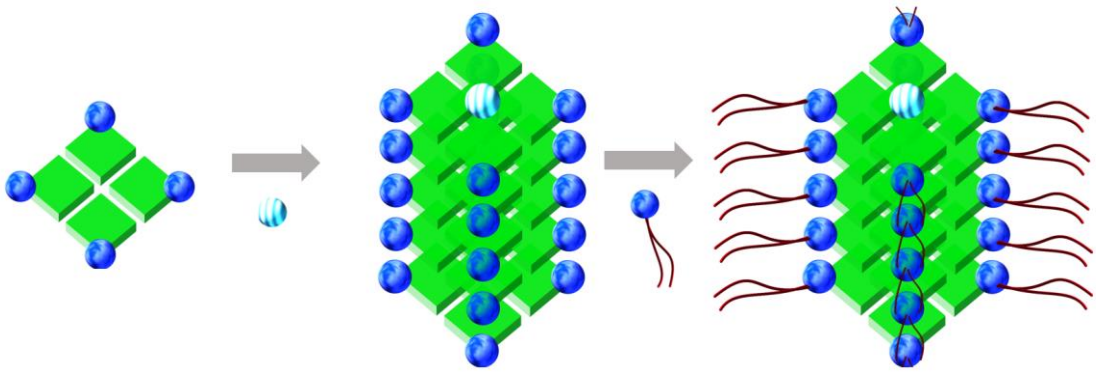

Figure 4.10: A schematic illustrating the complex functional nanomaterials produced by Li et al. using silver and deoxy-guanosine monophosphate (dGMP) in conjunction with cationic surfactants to form well-ordered thermotropic liquid crystals. Schematic adapted from [29].

To elucidate the viscoelastic properties of the localised micro-hydrogel phase, a viscosity sensitive dye, Kiton Red, was partitioned within the coacervate droplets and the fluorescence lifetime was measured before and after gelation. The calibration data for this experiment can be found in Chapter 2. The viscosities measured were 95 ± 0.7 Pa.s for the PAH/GMP supernatant, 190 ± 7 Pa.s for the PAH/GMP microdroplets, 97 ± 0.3 Pa.s for the PAH/GMP supernatant after the addition of $AgNO_3$, and 187 ± 17 Pa.s PAH/GMP microdroplets after the addition of $AgNO_3$. The difference in local viscosities of the coacervates and the gelled droplets is not appreciable

and could illustrate how FLIM may not be able to detect the macroscopic viscoelastic properties of the newly formed hydrogel network, however as traditional macroscopic methods, such as rheometry, for measuring the systems viscosity would have yielded fluid like viscosities much lower than these so the technique has yielded some pertinent information.

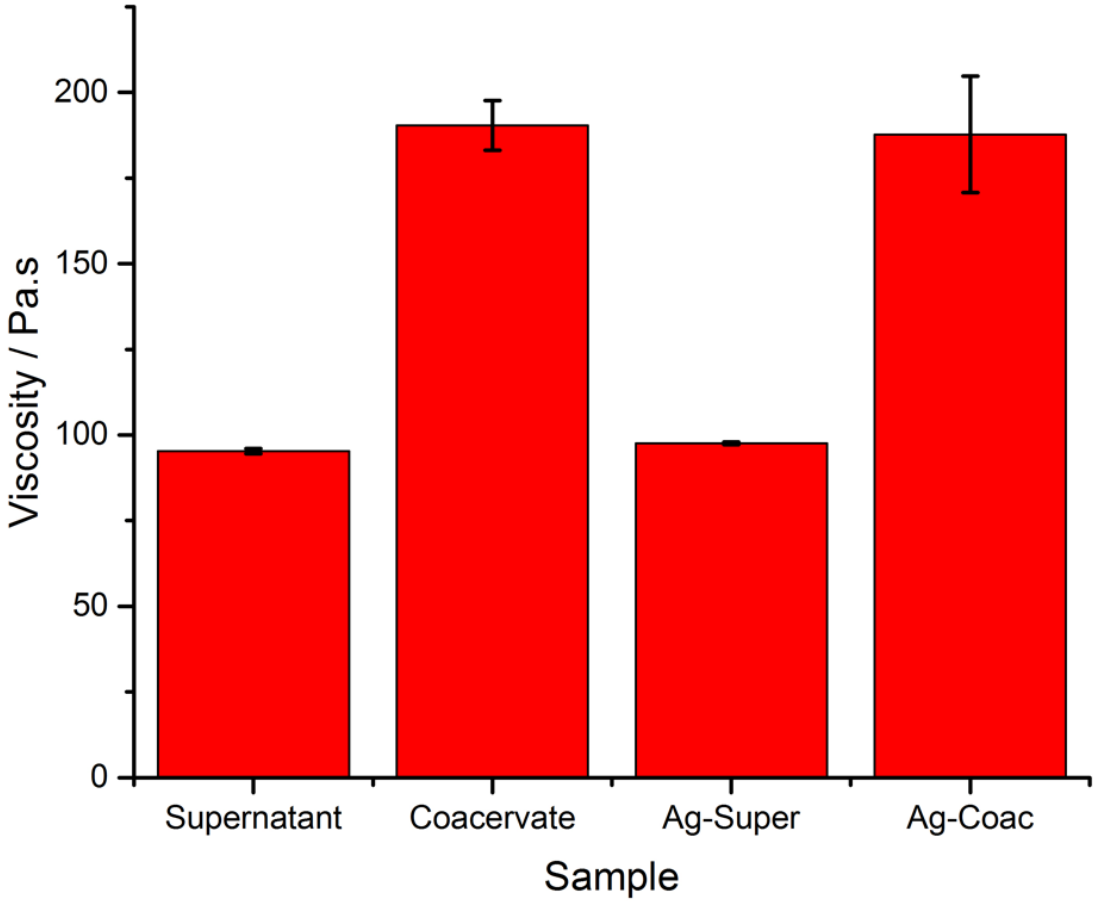

Figure 4.11: FLIM determined viscosity data for PAH/GMP coacervates before and after the addition of Ag.

The viscoelastic properties of the coacervate were measured using AFM experiments. The Young's modulus before and after mixing with $AgNO_3$ was found to be 673 kPa and 803 kPa ± 50 kPa respectively, Figure *4.12*, indicating a change in stiffness and hence an indication of localised gelation having occurred.

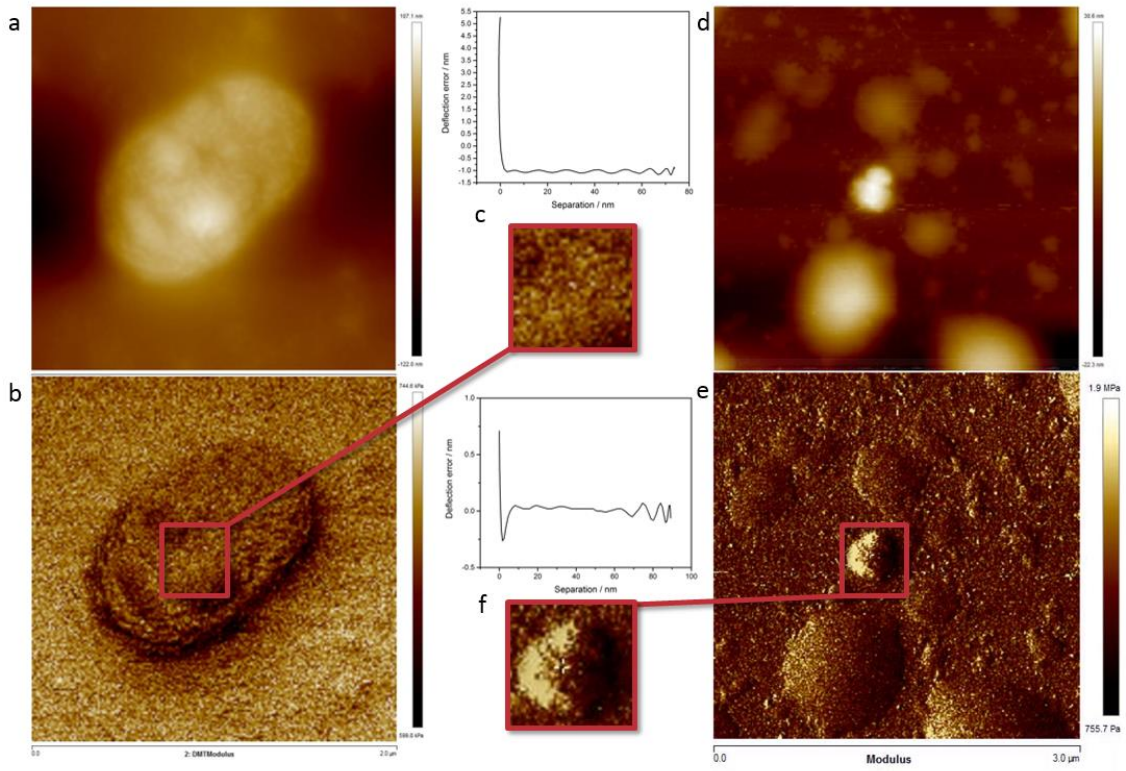

Figure 4.12: a), b) Height and modulus maps from AFM scans of a PAH/GMP microdroplet, c) inset of modulus and corresponding representative force curves extracted from quantitative nanoscale mechanical characterisation, force curve is indicative of thin polymer layer coating surface of mica, as expected from the wetting of the coacervate droplet d), e) height and modulus maps from AFM scans of PAH/GMP microdroplets after the addition of $AgNO_3$, f) inset of modulus and corresponding representative force curves extracted from quantitative nanoscale mechanical characterisation, here the force curve shows the deformation expected from a robust interlinked hydrogel network, Scale bars: a) 2 µm across, height heat map -122 nm – 107 nm, b) 2 µm across, stiffness heat map 599 kPa – 744 kPa, d) 3 µm across, height heat map -22 nm – 30 nm, e) 3 µm across, stiffness heat map 755 kPa – 1900 kPa.

The nature of the entangled network of GMP and PAH should confer different physical characteristics to the droplet. this has been confirmed by QNAFM but can be further investigated by the simple technique of UV-vis spectroscopy. The PAH/GMP coacervates and PAH/GMP Ag microdroplets were exposed to a lowered pH environment by the addition of the mineral acid HCl. As the pH decreases with increasing amounts of HCl, the absorbance of the system decreases in the case of the PAH/GMP coacervates, indicating disassembly of the microdroplets causing scattering, registered as absorbance. This, and the improved stability of the system with respect

to pH change after the addition of silver nitrate in the PAH/GMP Ag system can be seen in Figure 4.13, where the two sets of data are compared.

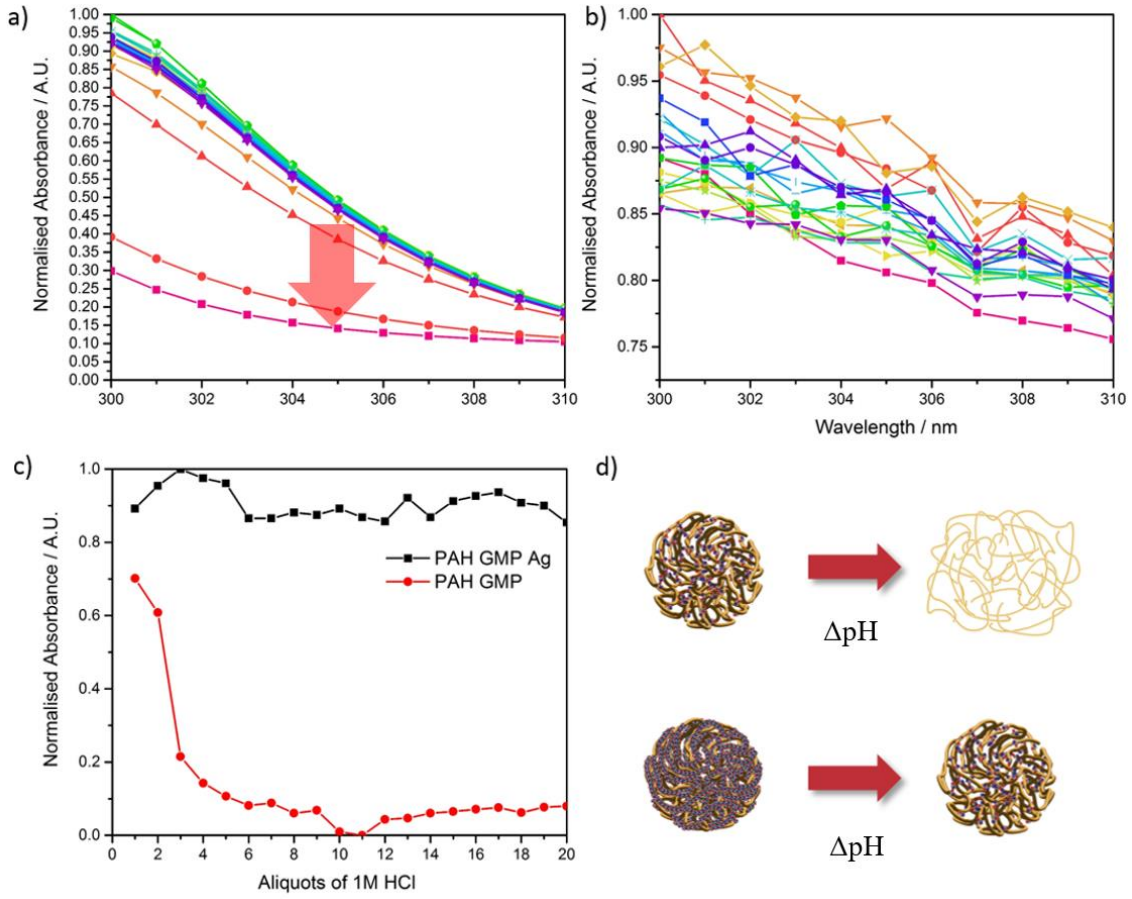

Figure 4.13: a) UV-vis spectrograph of PAH/GMP coacervates absorption with respect to addition of the mineral acid HCl, as colours go from cool to warm, in effect blue to red, the system increases in pH, b) the UV-vis spectrograph for PAH/GMP Ag structured microdroplets absorption with respect to the addition of HCl, c) a comparison of the absorbance of the two systems at 300 nm illustrating the robust nature of the gelled droplets with respect to increasing pH as a result of the hydrogel network, d) a scheme illustrating the disassembly of the PAH/GMP microdroplets to form a low concentration polymer and nucleotide solution with a decrease in pH; and the retention of the microdroplet architecture for the PAH/GMP Ag microdroplets as the pH is lowered but with the disassembly of the hydrogel network.

Having investigated the effects of silver salt on the system and having characterised the resulting gelated microdroplets comprising G-quartet GMP fibrils entangled with the poly(allylamine), which retained their structure and could flow in the macroscopic suspension, the ability of the gels to undergo a gel-sol transition to release any guest molecules was of great interest as

temperature could be used as a physical variable to control the state of these structured microdroplets.

4.2.5 Capture and release abilities

The ability of the system to undergo a sol-gel transition whilst having been preloaded with a cargo, in this case, a molecular dye, acridine orange, was conducted using a heat plate in conjunction with the fluorescence microscope. The system was ramped to 65 °C and held there. The localisation of the fluorophore was then monitored by taking line profiles of melting droplets as can be seen in Figure 4.14. The fluorescence in the droplets decreases with time indicating that droplets can be disrupted with temperature and the sequestered guest molecules released.

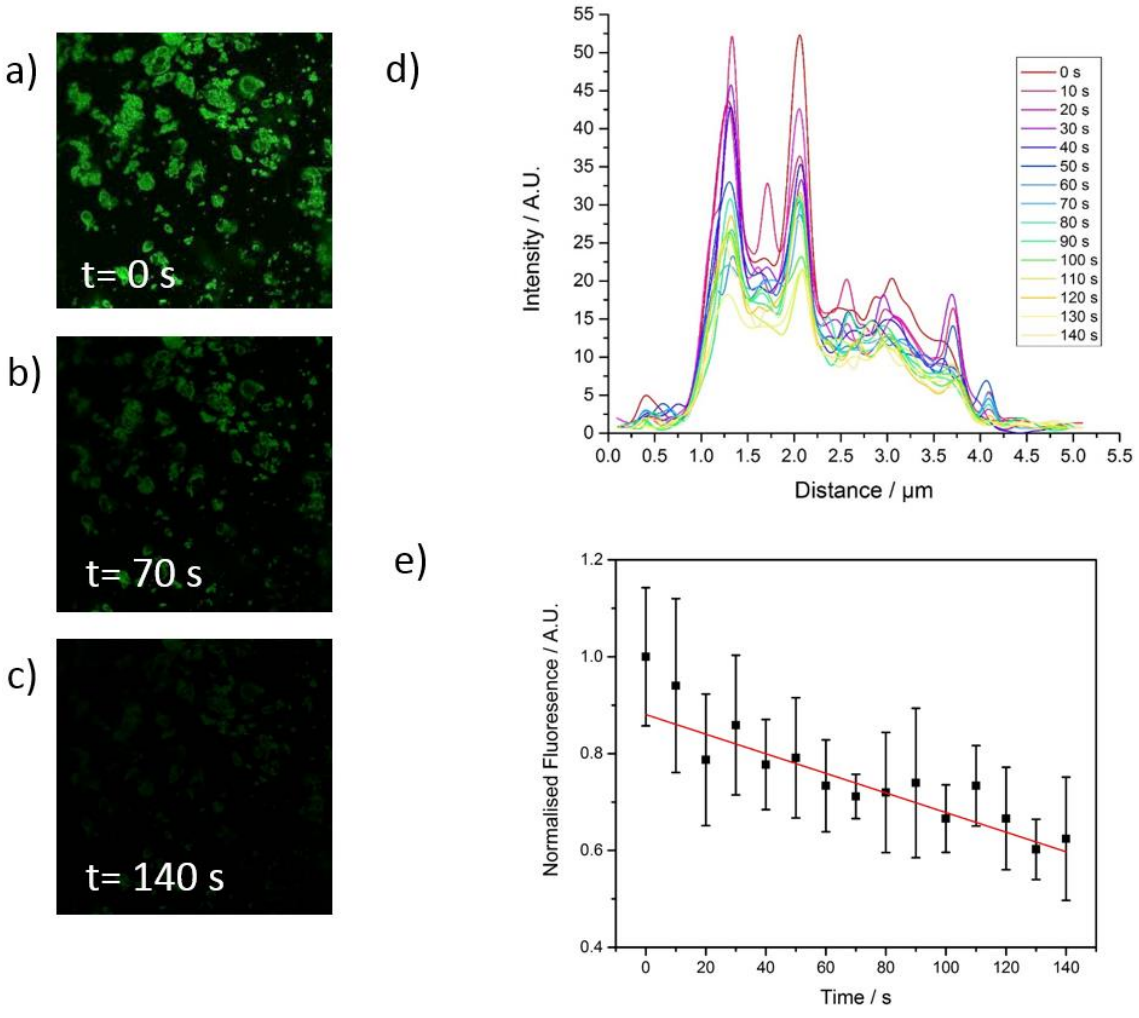

Figure 4.14: a), b), c) fluorescence micrographs illustrating the localisation of acridine orange fluorescence within gelled coacervates decreasing with increasing time as the system was held at 65 °C, d) is the fluorescence line profile, as monitored in ImageJ, over time and e) is the intensity over time for one point within the coacervate droplet as it melts and releases its fluorescent payload.

This property could be further exploited with the sequestration of gold nanorods which have been shown to produce local heating effects upon irradiation by light of wavelength commensurate with the surface plasmon frequency of the metal nanostructure [30]. This could be used to target individual gelled microdroplets and release their payloads at precise spatial and temporal locations.

4.3 Conclusions

A complex coacervate system that comprises a hydrogelating nucleotide as one of its components undergoes localised gelation when silver ions diffuse into the coacervate microdroplets and assembles into a hydrogel network of π-stacked silver stabilised GMP dimers. This resulting hydrogel microdroplet can template the formation of photo-reduced silver nanoparticles that are embedded within the hydrogel network which are known to exhibit anti-microbial properties. The anti-microbial nature of the system will need to be investigated to understand how the embedding of the silver nanoparticles within the hydrogel network affects the NP target interaction. The ability of the system to deliver hydrogel viscoelasticity, and the partitioning and release abilities, whilst retaining a liquid coacervate suspension bulk property, could be of great interest to those researching drug delivery systems and biomedical technology platforms.

In the context of origins of life research, these membrane free droplets present an exciting new way to reorganise nucleotides in a spatially confined microdroplet that spontaneously self-assembles and possess the ability to sequester, hold, and release guest compounds, such as molecular dyes.

4.4 References

[1] J. Crosby, *Chem Commun.*, vol. 48, pp. 11832-11834, 2012.

[2] J. Dash, *Soft Matter*, vol. 7, pp. 8120-8126, 2011.

[3] D. A. Fletcher and R. D. Mullins, "Cell mechanics and the cytoskeleton," *Nature*, vol. 463, no. 7280, pp. 485-492, 2010.

[4] B. Wickstead and K. Gull, "The evolution of the cytoskeleton," *Journal of Cell Biology*, vol. 194, no. 4, pp. 513-525, 2011.

[5] M. Pilhofer, M. S. Ladinsky, A. W. McDowall, G. Petroni and G. J. Jensen, "Microtubules in Bacteria: Ancient tubulins build a five-protofilament homolog of the eukaryotic cytoskeleton," *PLoS Biology*, vol. 9, no. 12, 2011.

[6] K. Almdal, J. Dyre, S. Hvidt and S. Kramer, *Polym. Gels Networks*, vol. 1, p. 5, 1993.

[7] S. R. Raghavan and J. F. Douglas, *Soft Matter*, vol. 8, p. 8539, 2012.

[8] S. R. Raghavan and B. H. Cipiriano, Gel Formation: Phase Diagrams using Tabletop Rheology and Calorimetry, in Molecular Gels, Dordrecht: Springer, 2005.

[9] A. M. Mathur, S. K. Moorjani and A. B. Scranton, "Methods for Synthesis of Hydrogel Networks: A Review," *Journal of Macromolecular Science, Part C: Polymer Reviews*, vol. 36, no. 2, pp. 405-430, 1996.

[10] T. R. Hoare and D. S. Kohane, "Hydrogels in drug delivery: Progress and challenges," *Polymer*, vol. 49, no. 8, pp. 1993-2007, 2008.

[11] A. C. Jen, M. C. Wake and A. G. Mikos, "Review: Hydrogels for cell immobilization," *Biotechnology and Bioengineering*, vol. 50, no. 4, pp. 357-364, 1996.

[12] J. T. Davis, "G-quartets 40 years later: from 5'-GMP to molecular biology and supramolecular chemistry.," *Angewandte Chemie (International ed. in English)*, vol. 43, no. 6, pp. 668-98, 2004.

[13] W. Guschlbauer, J. F. Chantot and D. Thiele, *Journal of Biomolecular Structural Dynamics*, vol. 8, pp. 491-511, 1990.

[14] S. L. Forman, J. C. Fettinger, S. Pieraccini, G. Gottarelli and J. T. Davis, *Journal of American Chemical Society*, vol. 144, p. 4060 – 4067, 2000.

[15] X. Shi, J. C. Fettinger and J. T. Davis, *Angewandte Chemie International Edition*, vol. 40, pp. 2827-2831, 2001.

[16] A. Calzolari, R. D. Felice, E. Molinari and A. Garbesi, *Phys. E*, vol. 13, pp. 1236-1239, 2002.

[17] T. J. Pinnavaia, C. L. Marshall, C. M. Mettler, C. L. Fisk, H. T. Miles and E. D. Becker, *Journal of the American Chemical Society*, vol. 100, p. 3625 – 3627, 1978.

[18] R. Krishna Kumar, X. Yu, A. J. Patil, M. Li and S. Mann, "Cytoskeletal-like Supramolecular Assembly and Nanoparticle-Based Motors in a Model Protocell," *Angewandte Chemie*, vol. 123, no. 40, pp. 9515-9519, 2011.

[19] Y. Zhang, H. Gu, Z. Yang and B. Xu, "Supramolecular hydrogels respond to ligand-receptor interaction," *J. Am. Chem. Soc.*, vol. 125, no. 45, p. 13680–1, 2003.

[20] B. Adhikari, A. Shah and H.-B. Kraatz, "Self-assembly of guanosine and deoxy-guanosine into hydrogels: monovalent cation guided modulation of gelation, morphology and self-healing properties," *J. Mater. Chem. B*, vol. 2, no. 30, p. 4802, 2014.

[21] J. Dash, A. Patil, R. N. Das, F. L. Dowdall and S. Mann, "Supramolecular hydrogels derived from silver ion-mediated self-assembly of 5′-guanosine monophosphate," *Soft Matter*, vol. 7, no. 18, p. 8120, 2011.

[22] Y. Yin, L. Niu, X. Zhu, M. Zhao, Z. Zhang, S. Mann and D. Liang, "Non-equilibrium behaviour in coacervate-based protocells under electric-field-induced excitation," *Nature Communications*, vol. 7, p. 10658, 2016.

[23] S. Mann, "Systems of Creation: The Emergence of Life form Nonliving Matter," *Accounts of Chemical Research*, vol. 45, no. 12, pp. 2131-2141, 2012.

[24] A. I. Oparin and K. L. Gladilin, "Evolution of self-assembly of probionts," *BioSystems,* vol. 12, pp. 133-145, 1980.

[25] F. Tiebackx, "Gleichzeitige Ausflockung zweier Kolloide," *Chem. Ind. Kolloide,* vol. 8, pp. 198-201, 1911.

[26] T.-Y. D. Tang, C. C. Hak, A. J. Thompson, M. K. Kuimova, D. S.Williams, A. W. Perriman and S. Mann, "Fatty acid membrane assembly on coacervate microdroplets as a step towards a hybrid protocell model.," vol. 6, no. 6, 2014.

[27] J. Suh, H. Paik and B. Hwang, "Ionnization of Poly(ethylenimine) and Poly(allylamine) at Various pH's," *Bioorganic Chemistry,* vol. 22, no. 3, pp. 318-327, 1994.

[28] A. Juergens, "Recent developments acid synthesis," *J. Histochem. Cytochem.,* vol. 23, no. 7, pp. 493-505, 1975.

[29] M. Li, R. J. Oakley, H. Bevan, B. M. Smarsly, S. Mann and C. F. J. Faul, "Nucleotide-based templates for nanoparticle production-Exploiting multiple noncovalent interactions," *Chemistry of Materials,* vol. 21, no. 14, pp. 3270-3274, 2009.

[30] J. Cao, T. Sun and K. T. V. Grattan, "Gold nanorod-based localized surface plasmon resonance biosensors: A review," *Sensors Actuators, B Chem.,* vol. 195, p. 332–351, 2014.

Chapter 5 : Sequential stimuli - inroads to protocell communication

Abstract

Herein, the process of combining the systems in chapters three and four is described, creating a hybrid system that retains the behaviour of both previous systems and a spatially localised system that exhibits a call and response like behaviour. When the hydrogelating coacervate system from chapter four undergoes gelation as the stimulus is added, the system undergoes a pH change, this pH change is communicated via a custom-made agarose hydrogel bridge to a neighbouring population of the fatty acid containing coacervate system described in chapter three. The fatty acid containing system then begins to produce vesicles containing any payload sequestered within the coacervate phase prior to the signal transduction by the nucleotide containing coacervate system.

5. Introduction

Communication in nature

Communication is an integral procedure for cells in nature. One key example of communication between bacteria is that of quorum sensing. Quorum sensing is a process whereby a population wide response is produced after a chemical threshold has been crossed [1]. This process can be thought of as cell-cell communication for sharing information about cell density [2]. Reactions of populations to meeting quoracy can vary from initiating sporulation, to biofilm formation [3]. As can be seen in Figure 5.1, the network containing environmental factors and the stimulated response they generate that mediates virulence, biofilm formation amongst other concerted responses from the bacterial colony are illustrated and is highly complex and interdependent.

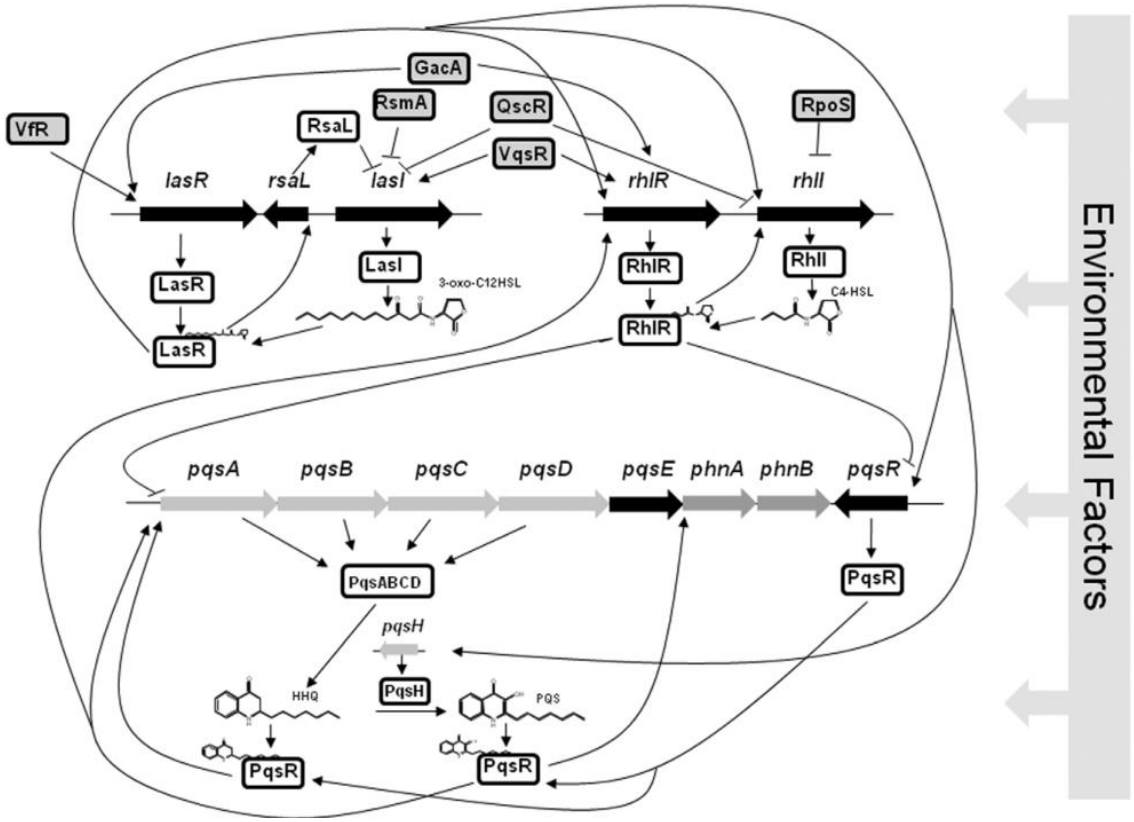

Figure 5.1: Schematic depicting quorum sensing network in P. aeruginosa. Each Schematic adapted from [3].

As such, when seeking the routes by which such systems came to exist, more simplistic models are required.

Synthetic communicating populations

Much focus on communication with synthetic systems has been focused on mimicking communication in nature. Moreover, work by Lentini *et al*. investigated communication between synthetic and natural cells [4]. Exploiting simple chemical messages that can be produced by the artificial cells and the resulting chemical signals produced by the natural cells conferring a change in the artificial populations, a feedback cycle can be established and investigated.

Work conducted by the Davis group inn Oxford made us of an incarcerated formose-based metabolic cycle to produce complex carbohydrates from simple chemical feedstocks to produce a molecule that induces bioluminescence as a result of quorum sensing processes [5].

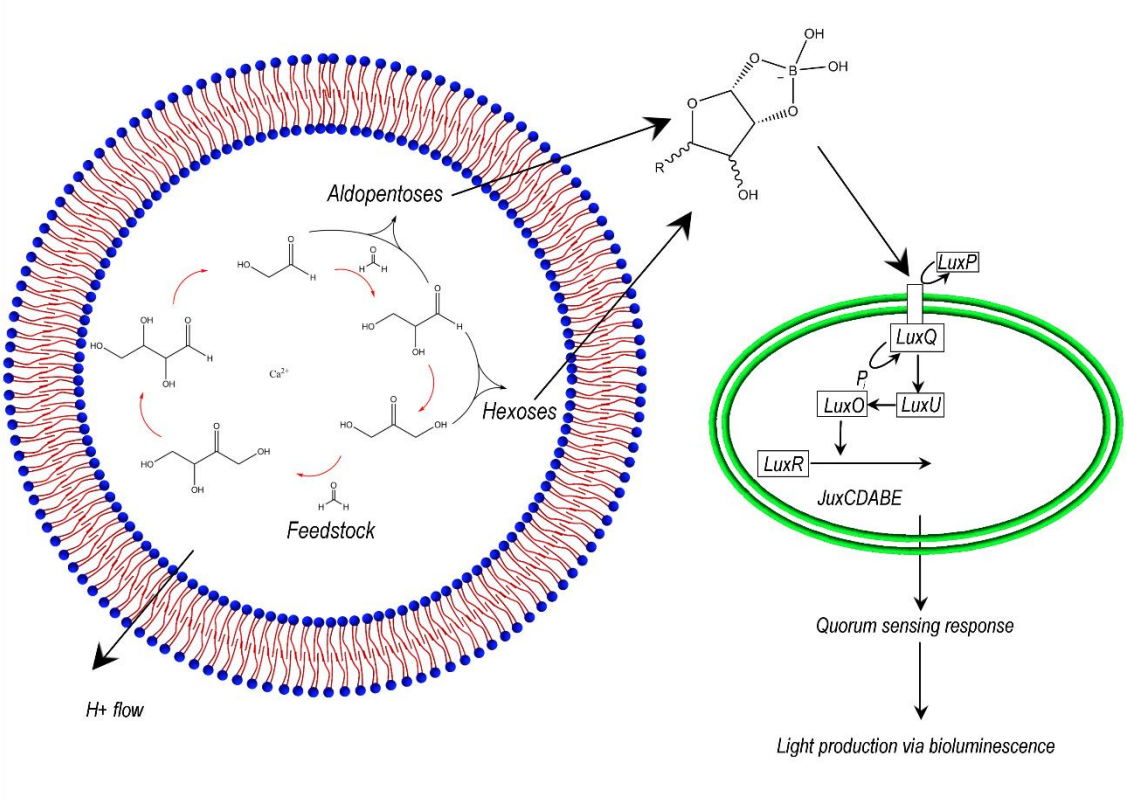

Figure 5.2: A schematic of an artificial cell produced by Gardener et al. that exploits a lipid container that holds a rudimentary metabolic cycle that produces a carbohydrate-borate complex that interacts with bacteria after diffusing out of the protocell. Scheme adapted from [5].

This ability to trigger the quorum response of the bacterial colony indicates that synthetic systems have the capacity to undertake the 'Turing Test' of passing for living systems – in as much as bacteria can assess and deem other systems to be alive. Whilst this might not be a concrete example of how synthetic systems contribute to the sphere of Origins of Life research they certainly point the way to making more nuanced systems for communication and the utilisation of chemicals as signalling molecules between synthetic and natural systems.

In this chapter, pH gradients are explored as a chemical communication pathway between synthetic populations of protocells. This is further explored in how these systems combine to

produce hybrid functional models and how there spatial interactions can be mediated by the presence of an extracellular matrix analogue which can transduce this stimulus.

pH responsive systems

Work conducted by Kumar *et al.* in the Mann group explored the potential of small-molecule dipeptide reconfiguration upon pH adjustment of a protocell system [6]. Novel coacervate microdroplets were formulated using *poly*(diallyldimethylammonium chloride) (PDDA) and *N*-(fluorenyl-9-methoxycarbonyl)-D-alanine-D-alanine (FMOC-AA) to produce 'discrete aster-like micro-architectures' upon the lowering of the solution of pH from 8.5 to 4.5. These micro-architectures consist of tangled inter-penetrating fibrous network of dipeptide hydrogel fibrils. This process can be seen in Figure 5.3.

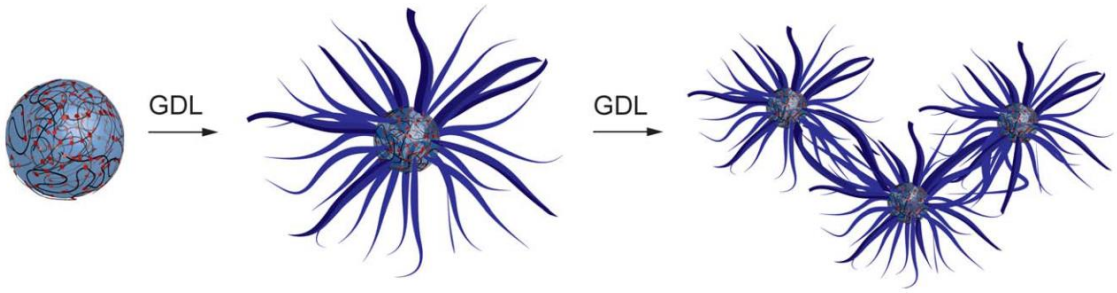

Figure 5.3: A cartoon illustrating the response of the PDDA FMOC-AA coacervates to GDL addition and subsequent gradual hydrolysis to form gluconic acid which lowers the pH of the system to produce FMOC-AA filaments which emanate from the coacervate microdroplets. Image adapted from [6].

Agarose gel, the structure of which can be seen in Figure 5.4, commonly used in gel electrophoresis experiments [7] as a stationary phase in separation and analysis of organic macromolecules such as DNA, RNA and Proteins [8], is comprised of alpha-helices of agarose which are bundled into supercoiled that aggregate to form the three-dimensional self-supporting network of hydrophilic fibrils, that through hydrogen bonding create a hydrogel, sequestering large volumes by weight of water compared to the volumes of water used to form the gels [9].

This hydrogel network is highly interconnected and as such impedes the diffusion of molecules through it, discriminating between compounds on the basis of size, as such, in the case of electrophoresis, where an applied electric field is used to agitate compounds produced in destructive testing of the contents of cells, in some cases searching for changes to DNA or RNA, single strand breaks (SSBs) etc. [10], the gel acts as a sieve and the progress of the various sized molecules can be selectively stained post-test [11]. The sizes of fragments liberated from cells which can be analysed using agarose gel electrophoresis can be controlled by varying the weight percentage of the agarose compound in the gels made, for high molecular weight compounds, in effect larger molecules, a lower weight percentage of agarose in the gel is required, approximately 0.7 %, to distinguish smaller molecules, higher weight percentage of agarose is required, approximately 3 % [12]. Therefore, for limiting diffusion of low molecular weight polymers such as PDDA and PAH a 2 % by weight agarose gel would suffice, whilst easily permitting diffusion of protons through the entangled hydrogel network.

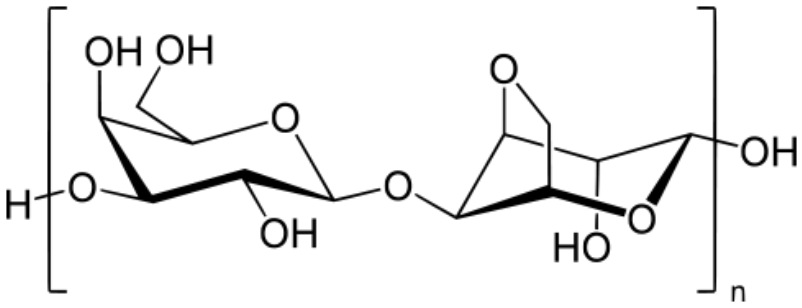

Figure 5.4: The chemical structure of agarose, a linear polymer consisting of alternating D-galatcose and 3,6-anhydro-L-galactopyranose. The compound can be hydroxyethylated to alter the physical characteristics of the gel formed by agarose [13].

As described in Chapter 1, modern cells are embedded within the extracellular matrix (ECM) [14] which can mediate cell to cell communication and provides biochemical support to the cells, supplying them oxygen, glucose etc. and removing waste products [15]. Herein, we exploit the

properties of agarose explored above in conjunction with functionalised microscope coverslips, the creation of which is described in Chapter 2. These functionalised wells would function as domains of the cells connected by the ECM analogue, agarose gel, made at a high enough weight percentage such that the diffusion of coacervate components is prohibited but messenger compounds, such as protons, can diffuse between the two populations. This experimental setup is described in Figure 5.5. Agarose gel was chosen as the neutral 3D self-supporting network has been used previously for tissue engineering work. It can be processed under mild conditions and presents an ECM analogue that is robust yet easily manipulated physically and can be readily degraded when the need for the scaffold is no longer required [16].

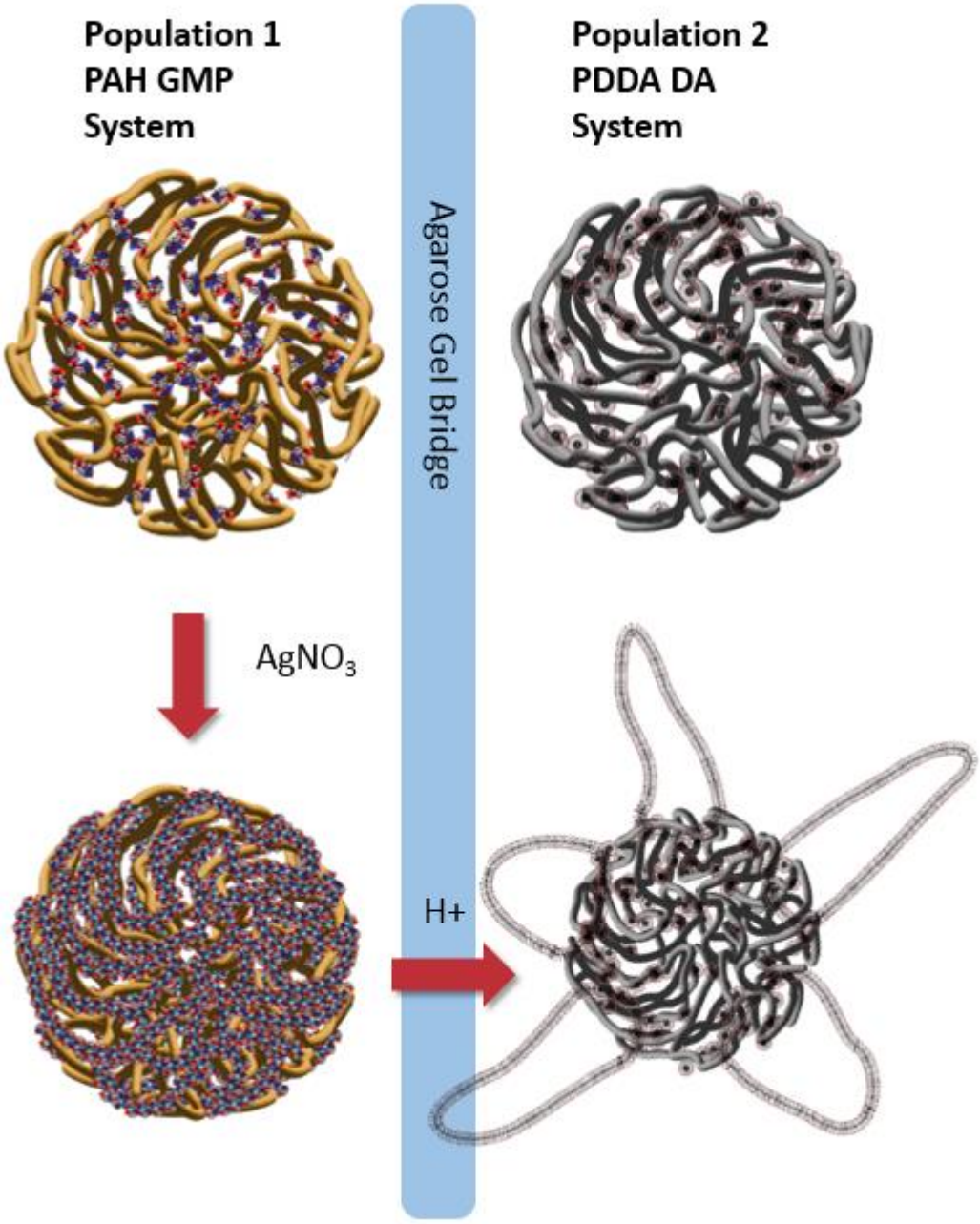

Figure 5.5: A cartoon illustrating the experimental hypothesis illustrating the preservation of discrete populations of transforming coacervate protocell populations via the use of an agarose gel bridge which will allow for the diffusion of molecules but not macroscopic molecular assemblies due to the highly entangle nature of the agarose polymer network making up the hydrogel. As the silver nitrate is added to the first population, the pH change that is induced will create a pH gradient that will stretch across the gel bridge to trigger the transformation of the second population which is sensitive to pH change.

5.1 Additional Materials and Methods

Materials: All reagents were purchased and used as delivered: poly(diallyldimethylammonium chloride) 8.5 kDa, 40 kDa, and 200 – 300 kDa (PDDA (8.5 kDa) PolySciences GMBH, (40 and 200 – 300 kDa) Sigma-Aldrich) ; decanoic acid (DA, Sigma-Aldrich) ; hydrogen chloride (HCl, Sigma-Aldrich); sodium hydroxide (NaOH, Sigma-Aldrich); glucono-δ-lactone (GDL, Sigma-Aldrich); sodium chloride (NaCl, Sigma-Aldrich); hexamethyldisilizane (HMDS, Sigma-Aldrich); poly(etheyleneglycol) (PEG; Sigma-Aldrich); Acridine Orange (Sigma-Aldrich); guanosine monophosphate (GMP, Life Technologies); 15 kDa poly(allylamine hydrochloride) (PAH, Sigma-Aldrich) ; hydrogen chloride (HCl, Sigma-Aldrich);); and Hoechst 33258 (Sigma-Aldrich).

Dialysis communication experiments were conducted using 5000 Da cut-off Amicon filtration tubing. Two dialysis tubes were prepared by micro-pipetting coacervate solutions, 500 µL of PDDA/DA and 500 µL of PAH/GMP, separately, into the tubes and were sealed with flexible plastic clamps. Both samples were then placed in a 1L beaker with 500 mL deionised water (Milli-Q Pure deionised water (18.2 MΩ) dispensed from a Milli Q helix integral 3 filtration system), with a magnetic stirrer bar. The reaction was left to proceed in the dark for one hour. Samples were then transferred to microscope dishes and imaged on a Leica DMI3000B inverted optical microscope with variable wavelength ultra-violet (UV) lamp attached.

Hydrogel formation: Agarose BioReagent was purchased from Sigma Aldrich. A 10 mL 2% wt. solution of agarose was made and then microwaved for 30 seconds on medium setting in a 1000W microwave. This produced a hot, transparent, liquid that could then be syringed into position.

Communication dish procedure: Microscope dishes were prepared for functionalisation and experimental setup using a Dremel drill to create two or three holes within the area of a 25 × 25 mm square. Once the holes were drilled a flat circular attachment was used to cut channels between the holes. These channels were always ca. 3 mm wide. A microscope slip which had been functionalised with PEG, functionalisation was undertaken via chemical etching with the use of Piranha solution, 1:4 parts H_2O_2:H_2SO_4, to enable the addition of 200 μL poly(ethyleneglycol) (PEG) (in 10 mL of toluene) to a pot containing the slides, which were left for 24 hours and then washes with dioinsed water and dried with compressed nitrogen, was then attached to the underside of the dish with ThorLabs UV-curable glue. This was then fixed using 365 nm UV light for 10 minutes. Hot agarose gel solution was then syringed into the channels between the holes and could cool and form a solid hydrogel. Excess gel was trimmed from the wells in the dish and confocal experiments were carried out within twenty minutes of the hydrogelating process. The resulting dish can be seen in Figure 5.6.

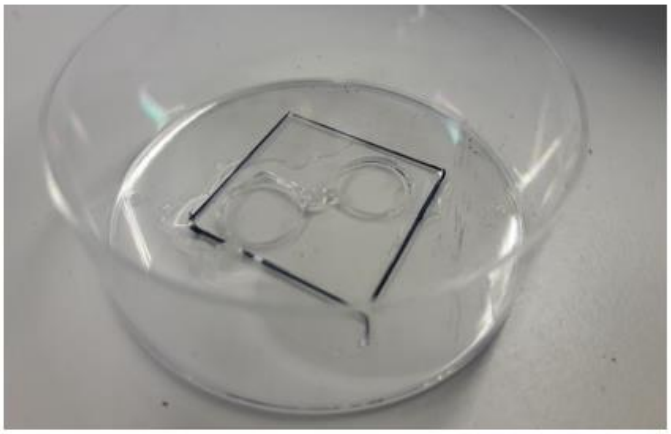

Figure 5.6: A photograph of the first simple diffusion experimental functionalised well set-up consisting of two wells separated by a 2% wt. agarose gel bridge, two distinct protocell populations can be kept spatially confined within each well, preventing coalescence and direct contact, but chemical communication can still be facilitated via the gel connection. Black line in image = 25 mm.

pH sensitive coacervate formulation: Equal volumes, 100 µL, of a 10 mM (monomeric concentration) 8.5 kDa PDDA solution at pH 9 and a 160 mM DA solution at pH 9, were mixed in a 1.5 mL Eppendorf tube at 25 °C to form a turbid suspension of coacervate droplets. The sample was then centrifuged at 13,200 rpm for 5 minutes to facilitate the separation of supernatant and bulk phases. Samples were then redispersed by hand using a micropipette to generate microdroplets in a suspension of the low-polymer supernatant phase. All solutions were made with Milli-Q Pure deionised water (18.2 MΩ) dispensed from a Milli Q helix integral 3 filtration system.

Inorganic stimulus sensitive coacervate formulation: Equal volumes, 100 µL, of a 200 mM (monomeric concentration) 15 kDa PAH solution at pH 7 and a 14 mM GMP solution at pH 7, were mixed in a 1.5 mL Eppendorf tube at 25 °C to form a turbid suspension of coacervate droplets. The sample was then centrifuged at 13,200 rpm for 5 minutes to facilitate the separation of supernatant and bulk phases. Samples were then redispersed by hand using a micropipette to generate microdroplets in a suspension of the low-polymer supernatant phase. All solutions were made with Milli-Q Pure deionised water (18.2 MΩ) dispensed from a Milli-Q helix integral 3 filtration system.

Separate communication procedure: Samples were transferred to the microscope dishes by micropipette and gelation of the PAH/GMP coacervate microdroplets was triggered by the addition of an aliquot of 1M $AgNO_3$ to a final concentration of 5 mM in the dark. Care was taken to ensure that during this addition there was no overflow of sample onto the top of the microscope dish, so the only contact different populations had was via diffusion of solvents and ions through the agarose gel connections. In Figure 5.7 three distinct populations can be contained and have interpopulation communication facilitated by the presence of the agarose gel bridges.

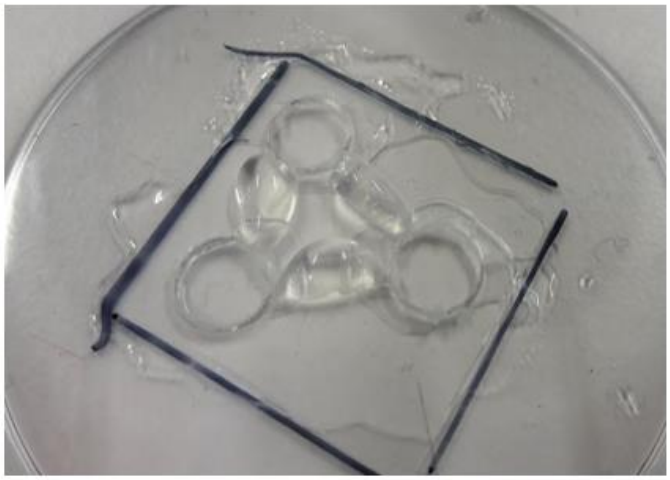

Figure 5.7: An example of a triple population communication chamber, fashioned from three wells which can keep three distinct protocell populations spatially separate whilst allowing for chemical diffusion through the agarose gel bridges. Black line in image = 25 mm.

5.2 Results and Discussion

5.2.1 pH adjustment via hydrogelation of PAH/GMP System

The pH of the PAH/GMP coacervate suspension, the system discussed in Chapter four, was monitored over time after the addition of silver nitrate, $AgNO_3$, the source of silver ions sued to generate the proto-cytoskeleton hydrogel. As can be seen in Figure 5.8 the pH of the system changes with time after the addition of the silver nitrate. The original work on the hydrogel system described how proton abstraction from the GMP stabilised dimeric enolate tautomers of GMP Ag complexes which π – stacking to form the hydrogel. In the GMP containing coacervate system, co-complexation of GMP with the polyelectrolyte PAH, yields an equilibrium whereby GMP is in both the continuous and discrete phases of the system, the polymer rich and polymer poor phases. The silver interacting with the GMP in the continuous polymer poor phase is free to abstract protons and form dimer complexes and it is this that produces the pH change in the system upon addition of silver nitrate.

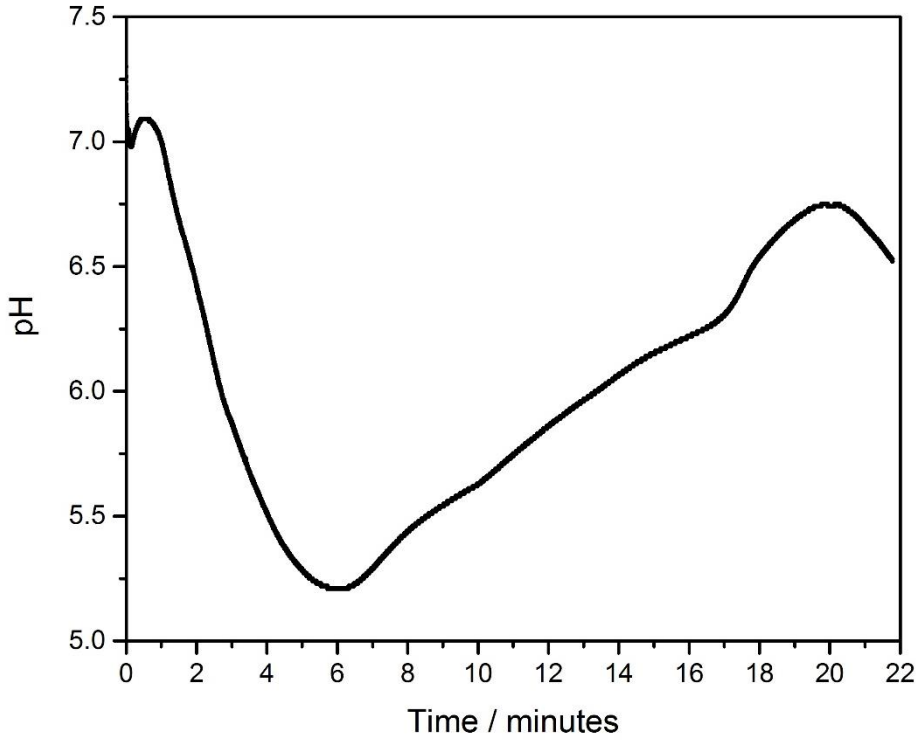

Figure 5.8: A graph showing the pH change of the PAH/GMP coacervate suspension after addition of $AgNO_3$ to a final concentration of 20 mM.

The ability to produce a pH change using the PAH/GMP system has thus been demonstrated. The initial pH of the system is pH 7.0 and at its lowest the pH of the system reaches 5.2, well into the region that should produce a morphological transition in the PDDA/DA system discussed in chapter 3.

To allow the two systems to 'communicate', in effect, produce a signal in response to a stimulus, the two systems must be able to exchange chemical information. However, due to the non-membrane bound nature of the coacervate droplets, initial experiments showed that it was difficult to retain discrete populations of the protocells. However, the product of these coacervate systems mixing was unexpected, as it produced a hybrid system that retained the responsive behaviour of both 'parent' systems.

As can be seen in Figure 5.9 PDDA/DA and PAH/GMP coacervates did not remain as discrete populations, easily mixing to form large coalesced multi-component coacervate structures. However, upon addition of silver nitrate these structures could be seen to exhibit behaviour similar to that of both systems prior to mixing; vesicles retaining fluorescent compounds sequestered in the initial PDDA/DA system were transferred, and filament structures were also stained on the interior of the new coalesced systems of fused coacervates.

An attempt was made to load GMP as a guest molecule into the interior of the PDDA/DA system and then add silver nitrate to generate the pH change locally within the coacervates. As can be seen in Figure 5.9 this yielded promising results for the ability of the system to respond to a pH change induced by GMP silver interactions. Both internal restructuration of the coacervate droplet and the formation of vesicles was observed.

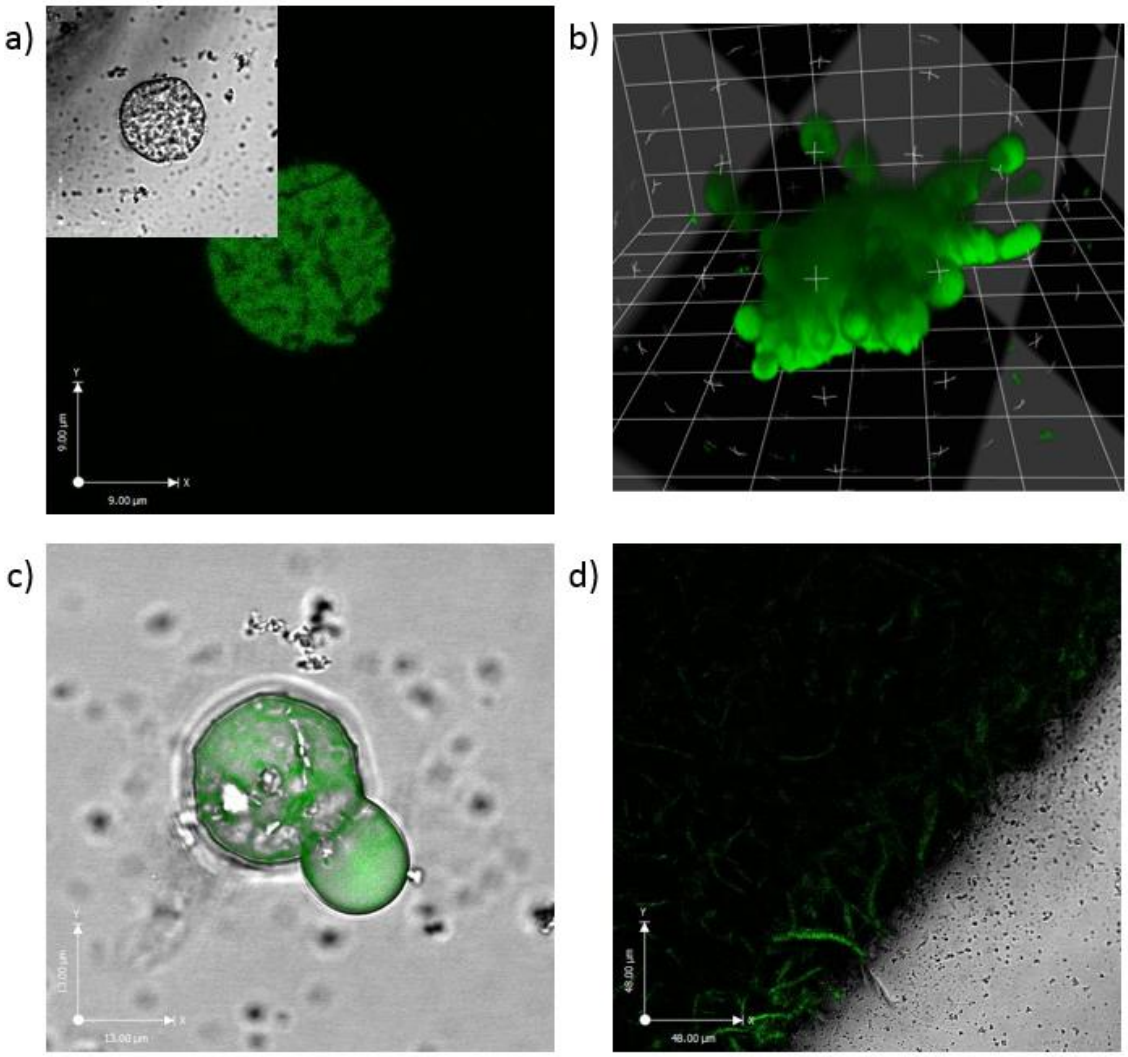

Figure 5.9: Four confocal micrographs of initial experiments where PAH/GMP PDDA/DA coacervate merged and the subsequent structures they formed post silver nitrate addition: a) PDDA/DA GMP droplet that exhibits internal structuration upon silver nitrate addition, inset is the brightfield channel, b) a 3D reconstruction of a PDDA/DA GMP system that has evolved some small vesicles, c) a cross section of PDDA/DA GMP coacervate droplet exhibiting both internal structure and ballooning vesicle, d) a matted structure yielded after combining PAH/GMP and PDDA/DA vesicles and adding silver nitrate, the acridine orange stain has highlighted large filamentous structures present in the system. Scale bars = 9, 24, 13, and 48 µm respectively.

As can be seen in Figure 5.10 this interplay of responses produces quite interesting overall behaviour. The presumed gelation of the interior, as silver diffuses within the interior of the

microdroplet, seems to have an effect of the morphology of vesicles evolved from the surface of the droplet.

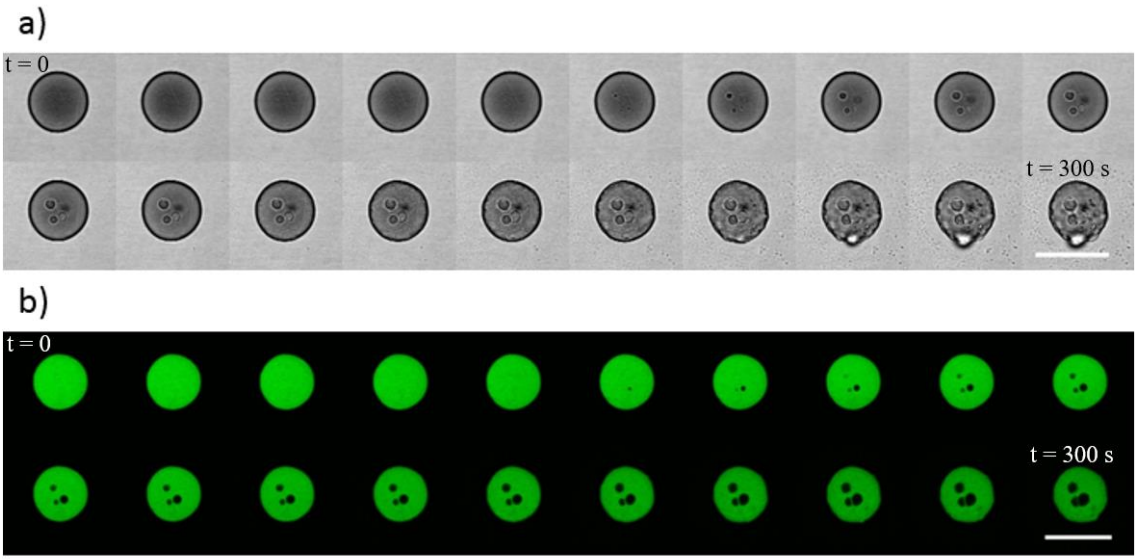

Figure 5.10: a) brightfield and, b) fluorescence channels of a PDDA/DA coacervate loaded with acridine orange and GMP after the addition of silver nitrate to a final concentration of 20 mM. Scale bars = 20 µm. Time of montage duration ca. 300 s.

This production of lower aspect ratio vesicles, smaller and more spherical than the ones observed produced by PDDA/DA coacervates formulated with low polymer weight polyelectrolyte, is complimentary to the hypothesis that the polymer content of the coacervate droplet has a constraining effect on the morphology of the vesicles evolved. As the GMP silver complexes begin to form the π-stacked fibrils necessary for the formation of the spatially localised hydrogel, that is analogous to a cytoskeleton as discussed previously in Chapter Four, it can be conceived of that these fibrils also interact with the charged surface of the fatty acid bilayer being formed, in a similar manner to the polyelectrolyte present in the microdroplets. Alternatively, the rate at which water moves across the fatty acid boundary due to the formation and hydration of the fibrils being formed could alter the balance between the internal volume change of the vesicles and the

rate at which new bilayer can be assembled from excess DA within the microdroplet and from the surrounding continuous phase. Both of these factors necessarily play a role in explaining the altered behaviour, but this behaviour is expected from the hypothesis presented in Chapter Three.

5.2.2 Retaining discrete populations

In an effort to prevent the mixing of the protocells, in order to retain discrete populations and study their communicative capabilities, the microscope dishes in section 5.1 were manufactured. These dishes were produced to be able to facilitate communication of small chemical compounds between two or more protocell populations. These neighbouring cells were connected by agarose gel bridges, comprising a 2% by weight agarose hydrogel cut to dimensions of 1 × 1 × 3 mm oblongs, the square faces of which were in contact with the materiel placed in the functionalised microscope well.

5.2.3 Polymer mediated vesicle extrusion in response to gelation of secondary protocell population in response to an inorganic stimulus in competition with aster-like FMOC-AA local restructuration

To test the limits of this ECM analogy and to observe the effects of competition within the system, a classic goal of synthetic communicative populations [16] [17], the agarose gel bridge system was modified to allow diffusion of protons from the PAH/GMP system to the PDDA/DA system and the FMOC-AA systems which had their spatial localisation preserved by separate microscopy wells. The experiment was initiated again with the addition of silver nitrate and the two systems were observed via confocal microscopy.

Both systems exhibited characteristic responses to a decrease in pH in their local environments, indicating that the PAH/GMP system was able to produce a large enough pH gradient such that it could transduce the inorganic silver nitrate signal to trigger the production of aster-like

dipeptide microarchitectures, in the case of the PDDA FMOC-AA system, and the evolution of payload carrying unilamellar decanoic acid vesicles, in the case of the PDDA/DA system. The growth of the hydrogel structures can be seen in Figure 5.11 and Figure 5.12 and the growth of the vesicles can be seen in Figure 5.13.

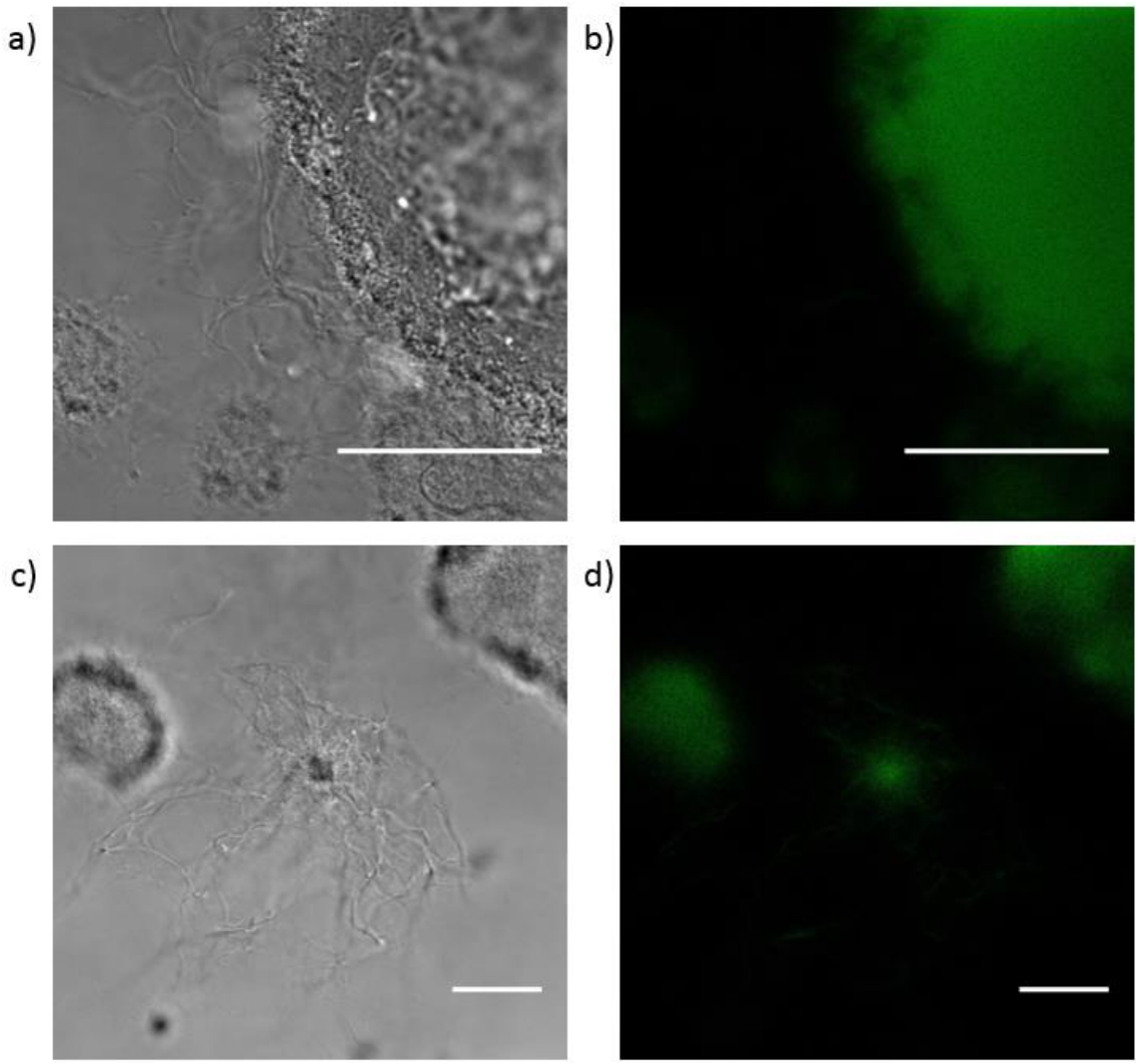

Figure 5.11: Confocal micrographs of aster-like FMOC-AA structures produced from PDDA FMOC-AA coacervates, a second pH-responsive system that could be used in the multi-well signal diffusion device made to investigate proto-communication. Scale bars = 10 µm.

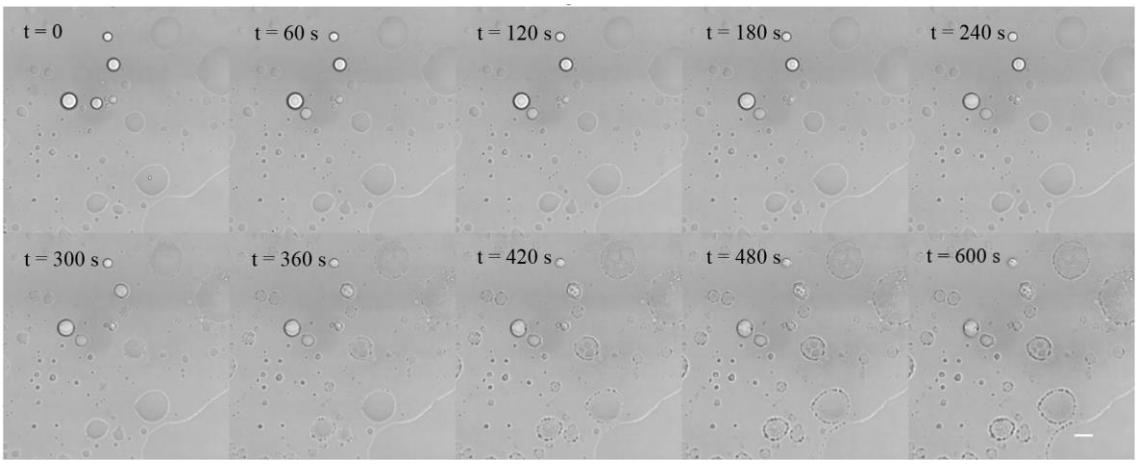

Figure 5.12: A montage of FMOC-AA PDDA coacervates responding to a pH change induced in a neighbouring cell by the addition of silver nitrate to PAH/GMP coacervates. Scale bar = 10 µm.

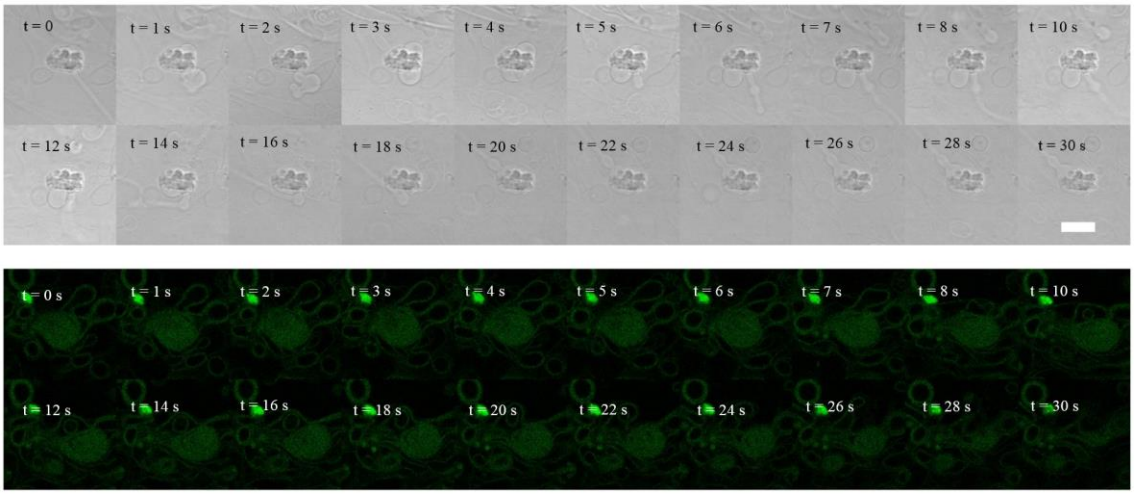

Figure 5.13: A montage of brightfield confocal micrographs capturing the morphological transformation of a PDDA/DA coacervate system in response to a pH change induced by the addition of silver nitrate to a PAH/GMP coacervate system in a neighbouring cell. Below it is a fluorescent channel of another example within the same system. Scale bar = 10 µm.

The kinetics of the system were highly dependent on the length of the agarose gel bridge but as this was kept fixed there was a lag period which, when passed, normal growth kinetics for the systems were observed.

5.3 Conclusions

Herein, the process of combining the systems in chapters three and four was illustrated, creating a hybrid system that preserves the functionality of its 'parent' systems, and a spatially localised system mediated by an ECM analogue that exhibits a call and response like behaviour. When the hydrogelating coacervate system from chapter four underwent gelation as the inorganic stimulus was added, the system underwent a pH change; this pH change is communicated via a custom-made agarose hydrogel bridge to a neighbouring population of the fatty acid containing coacervate system described in chapter three, as a model for extracellular matrix mediated communication. The fatty acid containing system, PDDA/DA coacervates, then began to produce vesicles containing any payload sequestered within the coacervate phase prior to the signal transduction by the nucleotide containing coacervate system, PAH/GMP coacervates.

5.4 References

[1] R. P. Novick and E. Geisinger, "Quorum Sensing in Staphylococci," *Annual Review of Genetics,* vol. 42, no. 1, pp. 541-564, 2008.

[2] S. T. Rutherford, B. L. Bassler, C. S. Hayes, S. Koskiniemi, C. Ruhe, H. Ben-tekaya and J. Gorvel, "Bacterial Quorum Sensing : Its Role in Virulence and Possibilities for Its Control," *Cold Spring Harbour Perspectives in Medicine,* pp. 1-26, 2012.

[3] P. Williams and M. Cámara, "Quorum sensing and environmental adaptation in Pseudomonas aeruginosa: a tale of regulatory networks and multifunctional signal molecules," *Current opionion in microbiology,* vol. 12, no. 2, pp. 182-191, 2009.

[4] R. Lentini, N. Y. Martín, M. Forlin, L. Belmonte, J. Fontana, M. Cornella, L. Martini, S. Tamburini, W. E. Bentley, O. Jousson and a. S. S. Mansy, "Two-Way Chemical Communication between Artificial and Natural Cells," *ACS Cent. Sci.,* vol. 3, no. 2, pp. 117-123, 2017.

[5] P. M. Gardner, K. Winzer and B. G. Davis, "Sugar synthesis in a protocellular model leads to a cell signalling response in bacteria," *Nature Chemistry,* vol. 1, no. 5, p. 377–383, 2009.

[6] R. K. Kumar, R. L. Harniman, A. J. Patil and a. S. Mann, "Self-transformation and structural reconfiguration in coacervate-based protocells," *Chem. Sci.,* pp. 5879-5887, 2016.

[7] V.J.McKelvey-Martin, M.H.L.Green, P.Schmezer, B.L.Pool-Zobel, M. Méo and A.Collins, "The single cell gel electrophoresis assay (comet assay): A European review," *Mutation Research/Fundamental and Molecular Mechanisms of Mutagenesis,* vol. 288, no. 1, pp. 47-63, 1993.

[8] D. S. Kryndushkin, I. M. Alexandrov, M. D. Ter-Avanesyan and V. V. Kushnirov, "Yeast [PSI+] Prion Aggregates Are Formed by Small Sup35 Polymers Fragmented by Hsp104," *Journal of biological chemistry,* vol. 278, pp. 49636-49643, 2003.

[9] J. Sambrook and D. Russel, Molecular Cloning - A Laboratory Manual, Cold SPring Harbour Labroartory Press, 2001.

[10] J. Berg, J. Tymoczko and L. Stryer, Biochemistry (5th Ed.), New York: WH Freeman, 2002.

[11] R. JF and W. BJ, Biochemical Techniques THeory and Practice, New York: Waveland Press, 1990.

[12] D. L. Smisek and D. A. Hoagland, "Agarose gel electrophoresis of high molecular weight, synthetic polyelectrolytes," *Macromolecules,* vol. 22, no. 5, pp. 2270-2277, 1989.

[13] S. Hill, D. A. Ledward and J.R. Mitchell, Functional Properties of Food Macromolecules, New York: Springer, 1998.

[14] B. Alberts, Molcular Biology of the Cell (4th Ed.), New York: Garland, 2002.

[15] G. Michel, T. Tonon, D. Scornet, J. M. Cock and a. B. Kloareg, "The cell wall polysaccharide metabolism of the brown alga Ectocarpus siliculosus. Insights into the evolution of extracellular matrix polysaccharides in Eukaryotes," *New Phytol.,* vol. 188, no. 1, pp. 82-97, 2010.

[16] S. Sun, M. Li, F. Dong, S. Wang, L. Tian and S. Mann, "Chemical Signaling and Functional Activation in Colloidosome-Based Protocells," *Small,* vol. 12, no. 14, pp. 1920-1927, 2016.

[17] P.-A. Monnard and P. Walde, "Current Ideas about Prebiological Compartmentalization," *Life,* vol. 5, no. 2, pp. 1239-1263, 2015.

Chapter 6 : Conclusions and Future Work

Abstract

Herein, conclusions from the previous three experimental chapters are drawn, the overall state of the work with reference to the field within which it is contextualised is discussed, and finally, the future directions and applications of this work are explored.

6. Conclusions and Future Work

6.1 Stimuli triggered coacervate to vesicle polymer mediated transformation

A novel complex coacervate system comprising poly(diallyldimethylammonium chloride) (PDDA) and decanoic acid (DA), has been synthesised and characterised. The characteristics of the resulting coacervate microdroplets were found using: optical and fluorescent microscopy, to determine the presence of polymer-rich coacervate microdroplets in solution; ultra-violet/visible light spectroscopy (UV/VIS) to determine the critical coacervation concentration of 12.5 ± 0.5 mM DA; dynamic light scattering (DLS) to determine the size distribution and polydispersity of the microdroplets at 80 : 5 DA : PDDA ratios to be 1.5 ± 0.1 μm in the first minute after formation; zeta potential (ζ-potential) measurements to assess the surface charge of the microdroplets and hence their stability, measured for a minimal version of the system returning a surprising positive charge but this can be explained via the presence of excess DA in equilibrium with the microdroplets in the polymer-poor phase; and small angle x-ray scattering (SAXS) to investigate the hetero- or homogeneity of the internal structure of the microdroplets. The system was found to possess a morphological response to a pH change of the solution. Coacervate microdroplets extrude long tendril-like unilamellar vesicles in response to the addition of acid and subsequent lowering of solution pH to below 7.8. Optical and fluorescent microscopy were used to determine the ability of the system to transport cargo from the coacervate microdroplet to the newly formed vesicles. A fluorescent analogue of PDDA, poly(diallyldimethylammonium chloride)-co-diallylamine (PDDA-co-DAA) a copolymer with amine functionality that was reacted with fluorescein isothiocyanate (FITC), was synthesised and used to investigate the destination of the polymer during this morphological transformation. Pyrenecarboxaldehyde (PYCA) was added to the various pH formulations of DA and its fluorescence measured and compared to the fluorescence observed within the coacervate to determine the protonation state of the DA within the coacervate microdroplets, which indicated that the DA is in a mixed state within the coacervate droplet of micellar and vesicular configurations. Furthermore, the polymer weight of

the PDDA used to formulate the coacervate microdroplets was found to mediate the morphology of the vesicles produced and the dependence was investigated outside the realm of self-assembled droplets by using electrostatically functionalised glass slips and monomeric DA solutions which verified the dependence of morphologies upon PDDA that was electrostatically interacting with negatively charged membranes that were being formed as the pH of the solutions was adjusted to the pKa of the carboxylic head group. Various cargos, molecular dyes, carbon nanodots, fluorescently tagged polymers, tagged proteins, and single stranded DNA, were transported, illustrating the ability of the system to retain guest molecules during the morphological transformation in response to the stimuli of pH adjustment.

Expanding upon the idea of guest molecules one could exploit the presence of recovered PDDA within the new vesicles after transformation. Numerous systems undergo transformation, all that is required is complementarily paired charged molecules in sufficient quantities. Introducing adenosine triphosphate (ATP, Figure 6.1 (a)), or 2',3'-O-(2,4,6-Trinitrophenyl)adenosine-5'-triphosphate (TNP-ATP, Figure 6.1 (b)) a fluorescent analogue, to the system immediately after the addition of GDL, would initiate the formation of a new coacervate microdroplet within the confines of the DA vesicle. ATP can be tagged with various fluorophores and so different populations of fluorescent microdroplet containing vesicles could be generated and their mixing and fusing studied.

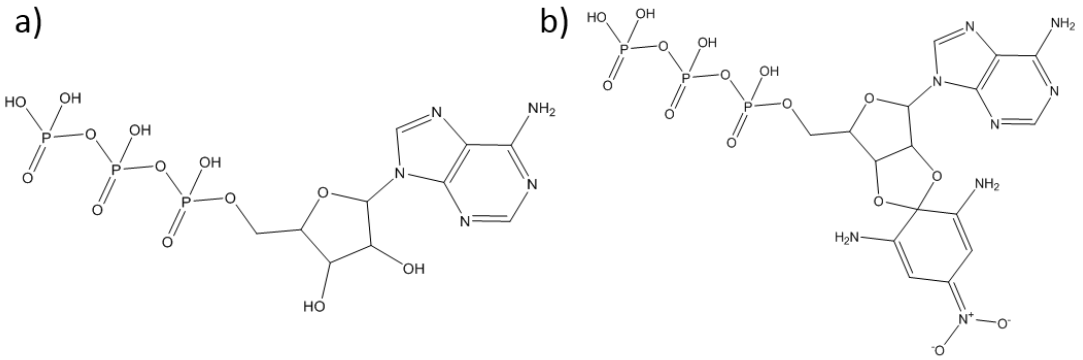

Figure 6.1: a) The chemical structure of adenosine triphosphate, b) The chemical structure of 2',3'-O-(2,4,6-Trinitrophenyl)adenosine-5'-triphosphate (TNP-ATP). An example of a fluorescently tagged ATP molecule. Created using ChemBioDraw software.

Preliminary experiments illustrate that the addition of ATP to the PDDA/DA system can produce new structures within the evolved coacervates, in the case of the low polymer weight coacervate formulation. As can be seen in Figure 6.2 optically dense regions are observed with the high aspect ratio vesicle emanating from the coacervate droplet.

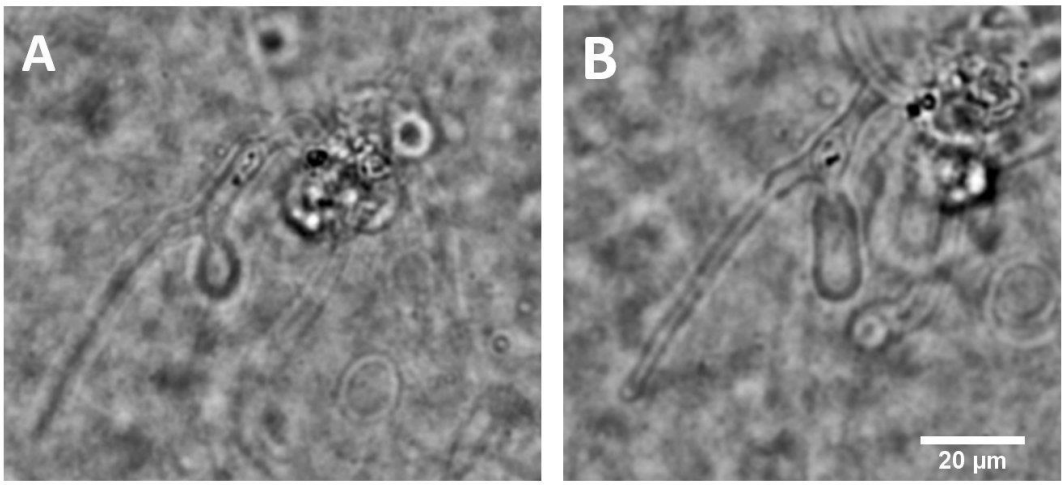

Figure 6.2: Optical micrographs A and B, taken at t = 0 and t ≈ 2.5 minutes respectively, illustrate the structures observed within vesicles which were evolved from the PDDA/DA coacervate system. These structures are thought to be PDDA/ATP coacervates as they formed after the introduction of ATP to the system.

To enable finer control over the composition of the surrounding environment of the coacervate microdroplet it is the hope of the author to be able to utilise the technique outline by Dr. Kishimura *et al.* on their work with polyionic complexes (PICs) [1], in microfluidic set-ups as shown in Figure 6.3.

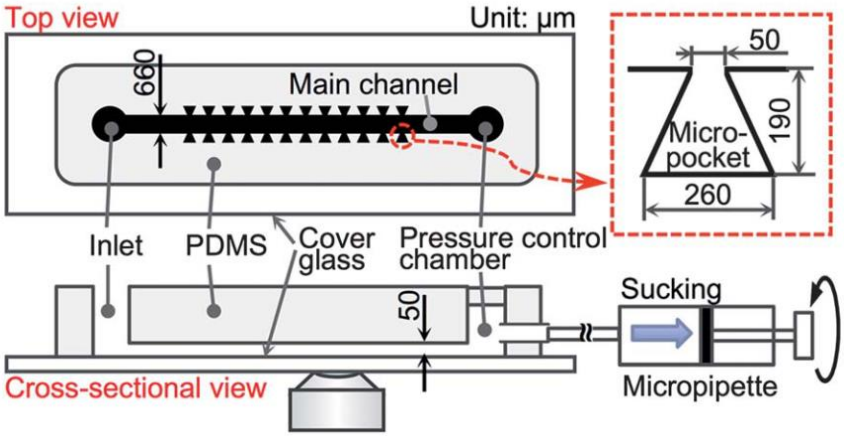

Figure 6.3: A schematic illustrating the microfluidic set-up used to observe the growth of giant unilamellar vesicles (GUVs), schematic reproduced from [1].

The system has the ability to capture PICs of a size comparable to the coacervate droplets formed in my research. The device design, in which a series of side pockets attach to a main channel, allows the surrounding solution to then be modified or replaced whilst retaining the complexes within the side pockets. A similar device could be used to capture PDDA/DA coacervates. The main channel could then be flooded with a low pH solution lowering the pH of the solution within the side pockets allowing for the transformation described in this report to occur. This ability to capture and control the environment of the coacervate microdroplets would greatly enhance the reproducibility of recorded responses from the system and might also be another way of trapping multiple protocell models in a facile manner so that communication studies can be undertaken on the meso-scale.

6.2 Generating localised supramolecular hydrogels in coacervates with an inorganic stimulus

A novel coacervate system comprising low molecular weight Poly(allylamine hydrochloride) (PAH) and Guanosine Monophosphate (GMP), was used as a template to produce spherical hydrogel droplets upon addition of silver nitrate as a chemical stimuli to enable π-stacking of GMP G-quartets to form the hydrophilic hydrogel network. The PAH/GMP coacervate system was prepared by simple mixing of the chemical components and then characterised using ultra-violet/visible light spectroscopy (UV/VIS); dynamic light scattering (DLS); nuclear magnetic resonance spectroscopy (NMR); and via visual inspection via confocal microscopy.

Kinetics of the gelation were investigated using Kiton Red, a molecular dye sensitive to local viscosity, in conjunction with the Woolfson Bio-imaging facilities Fluorescence Lifetime Imaging Microscope (FLIM), however it was found that the system did not yield a distinction between the gelated and non-gelated droplets and it was hypothesised that the molecular rotors remained in highly solvated regions within the coacervate droplet and within the hydrogel network.

Atomic force microscopy (AFM) was used to determine the adhesion and physical characteristics of the gelled coacervate droplets. Using the adhesion of the AFM probe, it is possible to gather data on the elastic moduli of the coacervate droplets, and the difference in Young's modulus before and after gelation was found to be commensurate with the young's modulus of the bulk hydrogel previously investigated in the group [2]. Further work using atomic force microscopy could involve using PeakForce TUNA mode, an electronic tunnelling mode where it might be possible to quantify the conductivity of the hydrogel network as the regular localisation of silver throughout the hydrogel network may yield conductive samples.

The system poses itself as a fascinating tool to investigate structured, or templated, hydrogel systems. Coacervates can be manipulated by optical and acoustic tweezers and can accommodate a wide variety of guest molecules. If a variety of populations of coacervates with various bio-relevant components to, say, a metabolic cascade reaction, were immobilised within the hydrogelated coacervates, these could then be arranged within a three-dimensional pattern or structure and then released upon dissolution of the hydrogel network, thus allowing for communication of protocellular models and fine control over mass transport, release and molecular control over chemical localisation. Moreover, this system, presents itself as a way of controlling communication between various populations of protocells via localised heating, inclusion of metallic rods and laser light to generate enough heat to force the system to undergo gel-sol transition [3], and so could easily investigate colonies of protocell's ability to communicate.

Their biological similarity to biological tissues also offers an interesting inroad to synthetic tissue engineering. The extracellular matrix (ECM) which surrounds cells is highly complex [4] and so attempts to imitate it using hydrogels have been difficult [5]. However, this system could be used in conjunction with acoustic tweezer systems allowing for facile arrangement of hydrogel droplet 'building blocks', allowing for construction of complex 3D scaffolds.

An issue that is apparent when considering this coacervate hydrogel system is that of bio-compatibility. Due to the presence of silver ions in the hydrogel fibrils, which can form nano-particles on exposure to UV light [2], it is conceivable that the system would be cytotoxic [6]. However, this could be exploited in the use of anti-microbial applications [7]. The system preserves its macroscopic fluid properties but the gelled microdroplets have gel-like viscoelastic properties which can be disrupted with temperature or pH. Therefore, one could imagine using

this suspension of microgel droplets embedded with silver NPs as a convenient and facile delivery method for sustained release of anti-microbials in the arena of wound dressing, for instance.

6.3 Sequential stimuli - inroads to protocell communication

Having combined the two synthetic protocells produced in Chapters Three and Four, it was shown that a hybrid protocell model, that preserved the responsive behaviour of the 'parent' protocells could be produced. The hybrid system was a hydrogelating coacervate that extruded vesicles in response to the inorganic stimulus of silver ions in its environment, and was comprised of PAH PDDA GMP and DA.

The ability to transduce signals between protocell populations has been illustrated utilising a 2% wt. agarose gel bridge as an analogous environment to the extra-cellular matrix. This was preceded by illustrating the capability of the PDDA/DA system to sequester the nucleotide guanosine monophosphate and to generate a localised pH change that could interact with the decanoic acid present and produce vesicles.

The hybrid system in the future could be used to further investigate the interaction that mediates membrane growth when the pH of the system changes such that self-assembly of the DA into vesicle bilayers begins. As this occurs the hydrogel network begins to form which will interact with the membrane being formed by the DA, potentially in a similar fashion to the polymer in the pure PDDA/DA system. In terms of applications, one could imagine the further engineering of populations of specialised protocells that might have precise trigger sensing and responsive behaviour. In this way one could imagine the components of a proto metabolism being distributed across many entities rather than being within one protocell and the production of communal cooperating behaviours could give rise to even more complex modes of communication that

could, in the manner of neural networks, be capable of storing information and processing information [8] [9] [10].

These pluralistic systems would be robust with respect to disruption on account of having multiple redundant units and would not need to be spatially confined within one cellular unit. Thus, these systems and their communication could provide the proto-tools in a modular system that moves synthetic biology towards a novel way of producing desired life-like schemes that could interface with natural cells or be integrated alongside natural cells and tissues [11].

6.4 References

[1] H. Oana, M. Morinaga, A. Kishimura, K. Kataoka and a. M. Washizu, "Direct formation of giant unilamellar vesicles from microparticles of polyion complexes and investigation of their properties using a microfluidic chamber," *Soft Matter,* vol. 9, no. 22, p. 5448, 2013.

[2] J. Dash, A. Patil, R. N. Das, F. L. Dowdall and S. Mann, "Supramolecular hydrogels derived from silver ion-mediated self-assembly of 5′-guanosine monophosphate," *Soft Matter,* vol. 7, no. 18, p. 8120, 2011.

[3] E. B. Dickerson, E. C. Dreaden, X. Huang, I. H. El-Sayed, H. Chu, S. Pushpanketh, J. F. McDonald and M. a. El-Sayed, "Gold nanorod assisted near-infrared plasmonic photothermal therapy (PPTT) of squamous cell carcinoma in mice," *Cancer Letters,* vol. 269, no. 1, pp. 57-66, 2008.

[4] C. Frantz, K. M. Stewart and V. M. Weaver, "The extracellular matrix at a glance.," *Journal of cell science,* vol. 123, pp. 4195-4200, 2010.

[5] J. L. Drury and D. J. Mooney, "Hydrogels for tissue engineering: Scaffold design variables and applications," *Biomaterials,* vol. 24, no. 24, pp. 4337-4351, 2003.

[6] B. Uygur, G. Craig, M. D. Mason and A. K. Ng, "Cytotoxicity and genotoxicity of silver nanomaterials," *Technical Proceedings of the 2009 NSTI Nanotechnology Conference and Expo, NSTI-Nanotech 2009,* vol. 2, no. 2, pp. 383-386, 2009.

[7] V. K. Sharma, R. a. Yngard and Y. Lin, "Silver nanoparticles: Green synthesis and their antimicrobial activities," *Advances in Colloid and Interface Science,* vol. 145, no. 1-2, pp. 83-96, 2009.

[8] E. Andrianantoandro, S. Basu, D. K. Karig and R. Weiss, "Synthetic biology: New engineering rules for an emerging discipline," *Molecular Systems Biology,* vol. 2, pp. 1-14, 2006.

[9] A. Tamsir, J. J. Tabor and C. A. Voigt, "Robust multicellular computing using genetically encoded NOR gates and chemical 'wiresg," *Nature,* vol. 469, no. 7329, p. 212–215, 2011.

[10] J. M. T. M. Kozaki and J. M. Seminario, "Molecular scale electronics: A synthetic/computational approach to digital computing," *Journal of the American Chemical Society,* vol. 120, no. 33, p. 8486–8493, 1998.

[11] P. E. M. Purnick and R. Weiss, "The second wave of synthetic biology: From modules to systems," *Nature Review Molecular Cell Biology,* vol. 10, no. 6, p. 410–422, 2009.